DEDICATED SOLUTIONS FOR STRUCTURAL HEALTH MONITORING OF AIRCRAFT COMPONENTS

Ioannis PITROPAKIS

Supervisors:
Prof. dr. ir. Martine Wevers
Dr. Helge Pfeiffer

Members of the Examination Committee:
Prof. dr. ir. Paul Sas
Prof. dr. Christ Glorieux
Prof. dr. Koen Van Den Abeele
Prof. dr. Vitalijs Pavelko
Dr. ir. Mark Winkelmans

Dissertation presented
in partial fulfillment of
the requirements for
the Degree of Doctor
in Engineering Sciences

June 2015

“ Γένοι' οἷος ἐσσὶ μαθών ”

Πίνδαρος 518 – 438 Π.Χ.

“ Learn what you are, and be such ”

Pindar 518 – 438 B.C.

Acknowledgements

The research carried out in the frame of this PhD thesis has received funding from the European Community's Seventh Framework Programme [FP7/2007-2013] under grant agreement n°212912. (Project: Aircraft Integrated Structural Health Assessment II - AISHA II). The consortium is coordinated by the KU Leuven and the further partners are MetaLogic (Belgium), DLR (German Aerospace Centre), Cedrat Technologies (France), Eurocopter-Marignane (France), Riga Technical University (Latvia), CTA (Spain), Meggit-Ferroperm (Denmark), ASCO (Belgium), Fraunhofer Institute IFAM (Germany), University of Leipzig (Germany), University of Basque Country (Spain), Free University of Brussels (Belgium) and Lufthansa Technik (Germany).

I want to give special thanks to my promoter Prof. Martine Wevers for giving me the opportunity to be a part of her team at KU Leuven and conduct this research but also for her valuable advices and guidance throughout my studies. Special thanks also to Dr. Helge Pfeiffer for his excellent supervision of my thesis and for his cooperation, patience and encouragement. He is a superb mentor and I strongly believe that if everyone had his exquisite moral the world would be a better place. Furthermore, I want to thank all my committee members for their support, Prof. Christ Glorieux, Prof. Vitalijs Pavelko, Prof. Koen Van Den Abeele, Prof. Paul Sas and Dr. Mark Winkelmans. I also want to thank Johan Vanhulst and all the technicians in MTM who make a brilliant job every day and always find solutions to our problems.

Finally, I want to thank everyone who believed in me and all my friends, colleagues and family for their support. I would need at least 10 pages to fill all the names here but you are all amazing and thank you endlessly for the unforgettable moments.

"I dedicate this thesis to my father Nikos, my mother Vasiliki and to my brother Sotiris as well as to those who keep trying and live with their own passion"

"Happiness is the meaning and the purpose of life, the whole aim and end of human existence."

Aristotle (384 – 322 B.C.)

Abstract

Aircraft structures, like any other mechanical structure, are subjected to various external factors that influence their lifetime. Mechanical loads and the environment are only some of the factors that can degrade the structure of aircraft components. Monitoring of these degradations by regular inspections or automated data recording is vital for the structural health of the critical components of an aircraft. This research proposes a number of dedicated solutions for structural health monitoring (SHM) of aircraft components helping the detection of structural degradation.

The dedicated solutions for SHM presented in this study include the following; 1. Flat coil sensors inspired by eddy current technology, 2. Electrical crack gauges for crack monitoring, 3. Optical fibres used for impact detection on composite materials, 4. SHM using ultrasonic Lamb waves testing with pseudo defects for signal validation as well as 5. Percolation sensors used for the detection of corrosion liquids in confined parts. The testing systems are applied in aircraft components made of aluminium, maraging steel and monolithic and sandwich carbon fibre reinforced polymers (CFRP).

The flat coil sensors are glued on aluminium 2024-T3 plates and are able to detect fatigue cracks in critical areas. The critical area is a hole in the middle of the plate since the lack of material consists of a stress concentrator point. The sensors are based on eddy currents that are induced into the material. Structural discontinuities under the surface of the material alter the electromagnetic properties of the coil showing an impedance change relevant to the crack size. It was found that a 2% increase of the relative difference of impedance corresponds to a crack size of 10 mm within the materials investigated.

The electrical crack gauges are glued on aluminium 2024-T3 plates and on an Airbus A320 slat-track. The crack gauges are made of an electrically conductive component and are connected to an ohmmeter. It was found that by exposing the plates to fatigue, simulating flight conditions, the electrical gauges, due to the loss of their electrical conductivity, can reveal the crack growth.

The optical fibres in a polarimetric setup are attached to monolithic and sandwich CFRC of floor panels and in an EC 135 tailboom. Lamb waves generated from a forced impact arrive at the optical fibres leading to an anisotropic refractive index, called birefringence. The pressure levels from the incident elastic waves result in a change of intensity due to a polarization rotation of the light propagating through the optical fibre. It was found that optical fibres offer various advantages compared to conventional piezoelectric transducers and the differentiation of the signal between input and output can reveal information on the impact force and on delaminations presence.

The pseudo defects are used for the validation of ultrasonic Lamb waves testing. It is well known that piezoelectric transducers can be used to excite and receive Lamb waves. These elastic waves can propagate through thin plates. Pseudo defects of different size and shape are placed on the plate in various angles and positions and the acoustic response with and without defect is compared and validated for SHM purposes. It was found that a correlation of the signals of the real defects and the pseudo defects is feasible and it can lead to a mapping for the probability of detection (POD) of real defects at different positions.

The percolation sensors are used in confined spaces in order to detect aqueous liquids or high humidity levels that can cause corrosion. The sensors are made of an organo-ceramic composite that consists of a conductive Titanium Carbonitride (TiCN) powder and Polyvinyl Alcohol (PVA). The concept of this sensor relies on the collapse of the percolation conductivity of the sensor due to swelling from aqueous absorption. This results in a sudden change in the electrical resistance of the conducting part. The sensor was validated concerning its temperature behaviour and its exposure in different levels of humidity with the aid of 10 salt solutions. It was found that the sensors can be used successfully, they were embedded now into three operational airplanes and due to their innovative function they have been patented.

The tests were conducted in the laboratories of the Department of Materials Engineering (MTM) and the Department of Physics and Astronomy (FYS) of KU Leuven, Belgium as well as in the German Aerospace Centre (DLR) in Braunschweig, Germany. The aircraft components were obtained from ASCO Industries, Belgium and Eurocopter (Airbus Helicopters), France. The research conducted for this PhD thesis was a part of the Aircraft Integrated Structural Health Assessment (AISHA II) European project from the 7th Framework Programme of the European Commission.

Korte samenvatting

Vliegtuigstructuren, zoals elke andere mechanische structuur, worden onderworpen aan verschillende externe factoren die hun levensduur beïnvloeden. Mechanische belastingen en het milieu zijn slechts enkele factoren die de structuur van vliegtuigonderdelen kunnen degraderen. Toezicht op deze degradaties door regelmatige inspecties of geautomatiseerde registratie van gegevens is van vitaal belang om de structurele gezondheid van de kritische onderdelen van een vliegtuig te kunnen opvolgen. Dit onderzoek stelt een aantal specifieke oplossingen voor structurele schade-monitoring (SHM) van vliegtuigonderdelen voor die kunnen helpen bij de opsporing van structurele degradaties.

De specifieke oplossingen voor SHM die in deze studie zijn de volgende; 1. Platte spoel sensoren geïnspireerd door wervelstroom technologie, 2. Elektrische strookjes voor scheurdetectie, 3. Optische vezels gebruikt voor de detectie van impact op composietmaterialen, 4 SHM met behulp van ultrasone Lamb golven gebruik makend van pseudo defecten voor signaalvalidatie alsmede 5. Percolatie sensoren voor de detectie van corrosieve vloeistoffen in afgesloten delen. Deze systemen worden uitgetest op vliegtuigonderdelen gemaakt van aluminium, maraging staal en monolithische en sandwich koolstofvezel versterkte polymeren (CFRP).

De platte spoel sensoren worden geplakt op aluminium 2024-T3 platen en kunnen scheuren detecteren op de kritieke plaatsen als gevolg van vermoeiing. De kritische zone is een gat in het midden van de plaat, die een spanningsconcentratie is. De sensoren worden gebruikt om wervelstromen te induceren in het materiaal. Structurele discontinuïteiten onder het oppervlak van het materiaal veranderen de elektromagnetische respons van de spoel en resulteren in een impedantieverandering die relevant is voor de lengte van de scheur. Er werd gevonden dat een toename van het relatieve verschil van impedantie met 2% overeenkomt met een scheur van 10 mm in de onderzochte materialen.

De elektrische strookjes worden geplakt op aluminium 2024-T3 platen en op een Airbus A320 slat-track. De strookjes die de scheur detecteren bestaan uit een elektrisch geleidende component en zijn verbonden met een ohmmeter. Gevonden werd dat door het blootstellen van de platen aan vermoeiing, vluchtomstandigheden simulerend, de elektrische strookjes de scheurgroei kunnen opmeten aan de hand van het verlies in elektrische geleidbaarheid.

De optische vezels worden op monolithische en sandwich CFRP vloerpanelen en op een EC 135 tailboom bevestigd. Lamb waves, opgewekt door een geforceerde impact, komen aan bij de optische vezels hetgeen aanleiding geeft tot een anisotrope brekingsindex, zogenaamd ‘birefringence’. De drukniveaus van de invallende elastische golven geven aanleiding tot een verandering van intensiteit

door een polarisatiedraaiing van het licht dat zich voortplant door de optische vezel. Het bleek dat optische vezels een aantal voordelen bieden ten opzichte van conventionele piëzo-elektrische transducers en de differentiatie van het signaal tussen ingang en uitgang informatie geeft over de impactbelasting en over de delaminaties die aanwezig zijn.

De pseudo defecten worden gebruikt voor de validatie van het testen met ultrasone Lamb golven. Het is bekend dat piëzo-elektrische transducers kunnen worden gebruikt om Lamb golven op te wekken en te ontvangen. Deze elastische golven kunnen zich voortplanten in dunne platen. Pseudo defecten van verschillende grootte en vorm worden geplaatst op de plaat in verschillende hoeken en posities en de akoestische respons met en zonder defect wordt vergeleken en gevalideerd voor SHM doeleinden. Gevonden werd dat een correlatie van de signalen van de werkelijke defecten en pseudo defecten haalbaar is en kan leiden tot een mapping van de waarschijnlijkheid van detectie (POD) van reële defecten op verschillende posities.

De percolatie sensoren worden gebruikt in beperkte ruimten om waterige vloeistoffen of hoge luchtvochtigheden, die corrosie veroorzaken, te detecteren. De sensoren zijn gemaakt van een organo-keramische composiet bestaande uit een geleidend titaniumcarbonitride (TiCN) poeder en polyvinylalcohol (PVA). Het concept van deze sensor berust op een ineenstorting van de percolatie geleidbaarheid van de sensor door zwelling ten gevolge van de absorptie van water. Hierdoor ontstaat een plotselinge verandering in de elektrische weerstand van de geleidende component. De sensor werd gevalideerd met betrekking tot zijn temperatuursverloop en de blootstelling in verschillende niveaus van vochtigheid met behulp van 10 zoutoplossingen. Gevonden werd dat de sensoren succesvol gebruikt kunnen worden, ze werden ingebed in drie operationele vliegtuigen en zijn door hun innovatieve functie gepatenteerd.

De testen werden uitgevoerd in de laboratoria van het Department Materiaalkunde (MTM) en het Departement Natuurkunde en Sterrenkunde (FYS) van de KU Leuven, België en in het Duitse Aerospace Center (DLR) in Braunschweig, Duitsland. De vliegtuigonderdelen werden verkregen van ASCO Industries, België en Eurocopter (Airbus Helikopters), Frankrijk. Het onderzoek voor dit proefschrift maakte deel uit van het Aircraft Integrated Structural Health Assessment (AISHA II) project uit het 7^{de} kaderprogramma van de Europese Commissie.

List of symbols

Greek	Explanation
α	Angle between laser beam and velocity factor
α_p	Unit laminate thickness parameter
δ	Effective depth for eddy currents
ε	Strain
ε_0	Dielectric permittivity in vacuum
θ_1	Angle of incidence for incoming light
θ_2	Angle of refraction for reflecting light
κ	Hooke's constant
λ	Wavelength
λ_i	Impact parameter
μ_0	Magnetic permeability in vacuum
ν	Frequency of light wave
π	Circle constant
σ	Conductivity or tensile stress
υ	Velocity of light in a medium
Φ_B	Magnetic flux
Φ_E	Electric flux
ω	Angular frequency

Latin	**Explanation**
A	Cross section area
Al	Aluminium
c	Velocity of light in vacuum (also elastic wave velocity)
c_l	Longitudinal wave velocity
c_t	Shear wave velocity
$E_{(x,y,z)}$	Electric field
$F_{(x,y,z)}$	Force
f	Frequency
f_D	Doppler frequency
$I_{(x,y,z)}$	Electric current
K	Hertz-Svelko factor
L	Length
m	Mass of impactor
n	Refractive index
P_2O_5	Phosphorus pentoxide
Q	Net electric charge within a volume
R	Electrical Resistance
V	Voltage
V_f	Volume fraction of fibres
v	Velocity of impactor
Y	Young's modulus
Z	Impedance

List of abbreviations

ACRO	Aircraft Crashes Record Office
AISHA	Aircraft Integrated Structural Health Assessment
AMOSS	Aircraft Management Operations Support System
BVID	Barely Visible Impact Damage
CAD	Computer Aided Design
CFRE	Carbon Fibre Reinforced Epoxy
CHOSeN	Cooperative Hybrid Objects Sensor Networks
CMC	Central Maintenance Computer
CT-Scan	Computer Tomography - Scan
ECFC	Eddy Current Flat Coil
ESAT	Department of Electrical Engineering
ESEM	Environmental Scanning Electron Microscope
FBG	Fibre Bragg Grating
HUMS	Health and Usage Monitoring System
KU Leuven	Katholieke Universiteit Leuven
LDV	Laser Doppler Vibrometer
MOSFET	Metal–Oxide–Semiconductor Field-Effect Transistor
MTM	Department of Metallurgy and Materials Engineering
NDT	Non-Destructive Testing
NTSB	National Transportation Safety Board
PM fibre	Polarization Maintenance fibre
PVA	Poly Vinyl Alcohol
PZT	Lead Zirconate Titanate
RH	Relative Humidity
RMS	Root Mean Square Value
SEM	Scanning Electron Microscope

SHM	Structural Health Monitoring
SM fibre	Single Mode fibre
TiCN	Titanium Carbon Nitride
TRL	Technology Readiness Level
USAF	United States Air Force
UV	Ultraviolet light

Table of contents

"In theory, there is no difference between theory and practice.
But in practice, there is."

Yogi Berra

CHAPTER 1

Introduction

December 17, 1903, the first powered airplane of the Wright brothers makes its appearance [1]. More than 100 years have passed since that successful moment and a remarkable development of this kind of transportation is witnessed today. Aircrafts are part of human's life and they are transporting millions of passengers daily. This massive fleet has to operate reliably and resiliently. To do so, modern engineering urges to find technical solutions in order to enhance the safety and reliability of aircraft structures and operations. Therefore, the safe use of aircrafts can only be guaranteed when appropriate damage assessment is in place.

Structural health monitoring (SHM) is a damage detection process in engineering structures e.g. by using automated sensor networks. Since the last two decades, the literature on SHM is exponentially growing [2-7]. The SHM system is considered as one of the most promising tools that can be used for early detection of structural damage and so to prevent critical damage [2]. Materials with implemented sensors belong to the group of "smart materials" as they are sensing the damage in a similar manner as the nerves in the human body.

The inspection of a material without damaging it is called Non-Destructive Testing (NDT). The last decades SHM as a kind of automated NDT is applied progressively in engineering structures such as buildings and bridges to trains and even aircrafts. SHM in the aerospace sector has begun to flourish the last decades with the development of higher standards of safety. It is notable that not until the late 1970s research started to investigate SHM of aircrafts in order to detect fatigue damage [8]. Therefore, this relatively new process of damage detection still has tremendous possibilities for development in the field of aeronautical engineering with a large variety of application areas today.

The last years there is a tendency for more efficient aircrafts with larger passenger capacity that can withstand the customer demands of the global market with an estimation of more than a total 17000 large passenger aircrafts manufactured by the year 2023 [9]. Some new types of aircrafts such as the Airbus A380, have become larger in order to carry more passengers utilizing new materials in order to be more durable and lighter. Except of the size, they also need to become faster to reach destinations in less time, less expensive due to the market needs and finally more environmental friendly. These parameters are taken into consideration by the aircraft manufactures who are trying to keep them in balance. An integrated SHM system in an aircraft is also affected by all the above parameters and should be as much economical as possible. However, since for every consumer or potential client in the global market the major concern is “safety first”, the future on SHM systems in aircrafts has been established and it is required to develop and standardize the respective systems.

An ageing aircraft is subjected to a range of different environmental conditions and stresses during flight and the SHM system must be able to give consistent and accurate measurements. The mechanical structure of an aircraft is designed to withstand a great amount of stresses and operate under harsh environmental conditions. However, the combination of high stresses and the degradation due to environmental conditions has a considerable impact on the aircraft’s life and its structural integrity and they influence radically the materials of the aircraft as well as the integrated SHM sensors networks. This impact on structural integrity is reflected in damages of the materials due to fatigue or corrosion. The majority of these problems are more significant in specific critical areas that are subjected to high fatigue loads. These critical areas can be found in various structural parts of an aircraft. They are characterized as high stress concentration areas and they need to be constantly monitored in order to prevent a possible structural damage. Thus, to enhance safety in aircrafts, a reliable SHM system is essential or becomes mandatory. Aircraft manufacturers, maintenance companies and research institutes are currently exploring which of the SHM technologies may have potential to be implemented into real aircraft structures [10,11].

An aircraft is a complex engineering structure that is made of a variety of dedicated materials such as aluminium alloys and composites that combine low weight with corrosion resistance.

Different kinds of SHM systems can be used today for the detection of cracks or delaminations. In order to locate damage in aircrafts components, we need a physically-based interaction of an instrument with that respective component. This can include direct optical observations with or without the use of penetrants or indirect observations with technologies such as eddy current testing for crack monitoring, optical fibre sensors for monitoring of impact damage or other acoustic techniques such as ultrasonic inspection for defect detection.

An important property of a SHM system is its reliability during the wide range of environmental and load conditions that are applied on an aircraft. Additionally, the precise method of integration of the network of sensors on the component under investigation is essential. Therefore, the adaptability of the SHM system plays also an important role. Due to the complex dimensions of the aircraft components, it is necessary that the SHM system is capable of monitoring areas that are difficult to access such as for example the confined spaces within the structural frame. In that way, maintenance will be able to reduce out of service times and re-organize their maintenance schedule resulting in time savings.

The target of this research is to create or develop techniques or methods that can be part of a sensor network similar to the human's nerve system, see figure 1.1. The human body has been described as one of the most unique non-destructive testing instruments ever created. The use of sophisticated electronic instrumentation, sensor network and other unique equipment for non-destructive testing can be considered as an extension of the human senses. Integrated sensors, optical, electromagnetic, piezoelectric but also electrochemical, can be used to enable continuous monitoring of the structural integrity of the aircraft components. The above structural health monitoring techniques that can reliably detect cracks at an early stage could reduce maintenance cost, enhance safety and at a developed stage, they could be used in the future as embedded sensors in the world's air-fleet.

Figure 1.1: SHM systems embedded in aircraft structures in analogy to the human's nervous system [12].

Until now, many SHM systems were proposed for aircrafts, there are however only a few certified SHM systems available today that are in service. An example of a certified SHM system is the Health and Usage Monitoring Systems (HUMS) that are installed in helicopters that can detect signs of possible failure on its components and specially on the rotor gearboxes [13]. Another example is the Honeywell's Central Maintenance Computer (CMC) first installed in a Boeing B777 aircraft and also the Aircraft Management Operations Support System (AMOSS) developed for the new Boeing B787 aircraft [14]. The best known "non-structural" health monitoring system that exists today is the flight recorder or "black box" that is constantly recording voice as well as digital information on electronic or electrical data [15]. The flight recorder is not a SHM system but more of an electronic failure reporting system. With a similar approach to the flight recorder, a reliable SHM system will be placed in an aircraft to record signals from sensor networks on the initiation of structural failure. In this way measurements can be taken by maintenance departments that will analyse the cause and the location of the failure as well as improve the structural integrity of the aircraft component that has been damaged.

This PhD thesis is conducted within the frame of the European project AISHA II (Aircraft Integrated Structural Health Assessment II) funded by the 7th Framework Programme of the European Commission. The target of the AISHA II project is the development of advanced solutions for structural health monitoring in aircrafts with a relatively high technology readiness level (TRL).

In this context, the close collaboration between our group and end-users, manufacturers as well as private and public research entities was essential. The full scale parts under investigation were aluminium alloy-based floor beams, slat-tracks made of maraging steel and helicopter tail booms consisting of monolithic and sandwich carbon fibre reinforced polymers (CFRP).

"We are what we repeatedly do. Excellence, then, is not a single act, but a habit."

Aristotle (384 – 322 B.C.)

CHAPTER 2

Problem statement

In this chapter there is a discussion regarding the importance of SHM in aircrafts along with a presentation of the problem statement. Also, a short reference to some examples of structural failures in aircrafts from the past years is given. Furthermore, the aim of study is presented and later on there is a section that refers to the advantages of SHM.

2.1 Preface

Structural Health Monitoring (SHM) is increasingly used in many different applications ranging from marine and wheeled vessels, such as fuel tankers and army vehicles, through to civil infrastructure applications, such as buildings, wind turbines and bridges [16]. It is desirable to use damage-detecting sensors on structures to prevent possible failure that can lead even to fatal disasters. If the onset of damage leading to major failure can be detected, action can be taken to limit or prevent the destruction of the structure, and repairs can be carried out. Therefore, implementing SHM solutions can lead to improved maintenance and in this way, besides safety, also positive economic effects can be obtained.

2.2 Importance of SHM in world aviation

2.2.1 Types of causes of structural failures in aircrafts

Figure 2.1 shows statistics on the different reasons for structural failures as reported by the United States Air Force (USAF). Related to the number of reported cases, the main reason for structural failures is fatigue damage arising from cyclic loading.

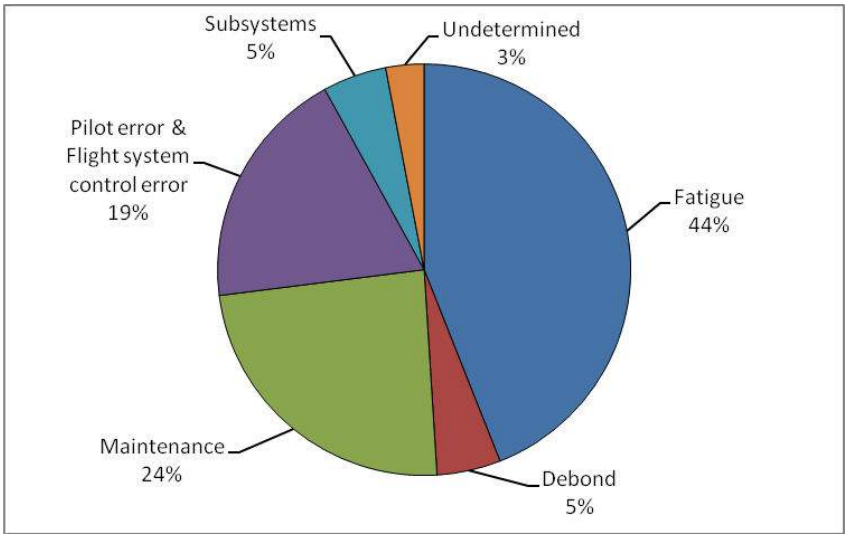

Figure 2.1: Example of percentages associated with types of causes on 37 USAF structural failures [17].

There are two categories describing the time evolution of fatigue stress; fatigue cycles or flight cycles. Fatigue cycles are characterized by the number of pressurizations and flight cycles that are defined by the number of complete take-

offs and landings. Most commonly, fatigue cycles are being used for the fatigue measurements in an ageing aircraft and a detailed fatigue rating method has been introduced from Boeing in the early 1980s [18].

2.2.2 Aircraft accidents statistics

The Aircraft Crashes Record Office (ACRO) in Geneva, Switzerland, registers the total number of deaths due to aircraft accidents. Up to today there are 131704 deaths from 20379 aircraft accidents [19]. These numbers include any kind of accident no matter if it was due to a structural failure or not. The mentioned numbers are significantly lower comparing to the number of fatal casualties by ground transportation, such as cars. Therefore, aircrafts still hold the position of the third safest transportation mode after the elevators and trains.

2.2.3 Notable cases of aircraft structural failures

Between 1927 and 1981, 1885 accidents including 2240 fatal casualties have been reported that are caused by fatigue failures [20]. There are many examples of structural failures that have been occurred in the past and some notable cases have been selected. One of the most notable cases of structural failure is the flight No. 243 from Aloha airlines operated on April 28, 1988, where a sudden decompression caused the separation of a large part of the fuselage from the aircraft while it was flying at an altitude of 24000 feet.

Figure 2.2: Photo of an extended structural failure to a Boeing B737-297 aircraft of Aloha airlines due to fatigue [21].

Investigations revealed that the fuselage suffered from “maritime corrosion” affecting rivets and lap joints connecting the fuselage to the other parts of the structure. According to the National Transportation Safety Board (NTSB) there were indications of pre-existing cracks that accelerated the process of fatigue fracture [22]. NTSB reported that the aircraft had accumulated 35496 flight hours and 89680 flight cycles.

Another notable accident occurred on August 12, 1985, when a Japan airlines Boeing B747-146SR aircraft crashed after take-off, 100 km outside Osaka international airport. Seven years before the accident, the aft pressure bulkhead was damaged during landing. The plane underwent a large scale repair but the company did not follow the necessary procedures [23]. As a result, fatigue cracks initiated from a number of rivets that propagated very fast through the whole structure. Eventually, few minutes after take-off the whole rear part of the plane started to break while pressurization problems were making the situation even more severe. The airplane was out of control losing altitude and it crashed on the mountains at an elevation point of 1565 m 12 minutes from take-off. This accident is the most fatal single flight accident ever occurred with 520 deaths and just 4 survivors.

Figure 2.3: Workers at the wreckage of Japan Air Lines flight 123, Aug. 12, 1985 [24].

A similar accident occurred on May 25, 2002, when a Boeing B747-209B aircraft from China airlines broke into four pieces in the air, shortly after take-off on the flight from Taiwan Taoyuan international airport to Hong Kong international airport. Again, fatigue was the main cause of the accident due to poor maintenance of the aircraft after a previous tail strike incident in 1980. The doubler repair that was attached after the tail strike did not cover an extended 30% of the length of the damaged area that would have been necessary.

Figure 2.4: The wreckage of the front part of the Boeing B747-209B aircraft from the accident of China airlines flight 611 [25].

Due to fatigue, the pre-existing cracks were steadily growing together with additional cracks initiating from the rivets. Poor maintenance of the aircraft had a consequence of the fracture of the metallic parts of the frame that finally the accident caused the death of all 206 passengers and 19 crew members.

A fourth notable case of a structural failure occurred during flight 578 from American Airlines. The Airbus A300 had a scheduled flight from John F. Kennedy International airport to Las Américas International airport in the Dominican Republic. Shortly after take-off, the plane's vertical stabilizer and rudder were separated from the body of the aircraft. Seconds later, the jet engines were also separated from the wings and the non-controlled airplane crashed on Belle Harbour, a residential area of New York City killing all 260 people on board and 5 on the ground.

Figure 2.5: Close up photo of the attachment point of the vertical stabilizer of Airbus A300 from American Airlines flight 587 directly on the crash site [26].

The reason of the accident was the delamination on the composite lugs that are used to attach the vertical stabilizer. The delaminations were a result of previous heavy turbulences and the poor maintenance of the aircraft did not consider the delamination problem. It was also found that the design of the composite lugs was not strong enough to withstand the high stresses that stretching the parts above their limits.

As a conclusion, as the number of aircrafts is constantly increasing, more accidents are likely to happen if no additional safety measures are taken. However, due to the rapid development of technology, air-safety has been increased and more intelligent SHM systems will further contribute to these improvements.

2.3 The need for dedicated SHM solutions on aircrafts

2.3.1 Aims of the study

This PhD study investigates the potential of SHM systems in aircrafts and presents dedicated solutions of SHM with proposals for on-line and off-line monitoring. Non-

Destructive Testing methods are applied for a selection of metallic and composite aircraft components in order to detect cracks, surface and internal damages on the structural materials that are caused by fatigue, high stresses and environmental changes.

2.3.2 Advantages of SHM

Billions of euros are spent every year in the commercial aviation sector to repair structural damages due to fatigue or corrosion. For this reason but also because safety issues have a very high priority in this sector, research is aiming to look for dedicated SHM solutions. Up to this moment, some SHM systems have been presented but only few of them have already been implemented for commercial use as an integrated system. Inspection of aircraft structures mainly involves visual inspection as well as NDT inspection serving as local monitoring systems of damage detection and mainly as external non-integrated solutions.

SHM is a strong tool for instantaneous inspection and it would be able to provide early alerts on structural problems to avoid future costs and improve safety factors. The dedicated SHM solutions that are discussed here can be used as embedded systems and are integrated into the aircraft components.

"There are no facts, only interpretations."

Friedrich Nietzsche (1844-1900)

CHAPTER 3

State of the art on structural health monitoring of aircraft components

A literature review of the proposed technologies for structural health monitoring that are used today on aircrafts is presented. At the beginning, there is an up-to-date SHM status on aircrafts followed by a research review of the non - destructive techniques that are used for SHM in this PhD thesis. Then, there is a literature review of the most common NDT methods that are used today for the inspection of aircraft components.

3.1 SHM review

3.1.1 Status today

To optimize the design of aircraft components, fatigue management programs were developed to monitor fatigue problems, and to estimate the fatigue life of an aircraft [27]. In addition to that, SHM for aircrafts are under development in order to have a reliable system that can be used for the early detection of cracks and delaminations as well as of corrosion problems. The ideal system would be integrated into the aircraft's structure and give instant measurements and data processing (online). A second but also prominent option is the creation of an implemented passive SHM system that only operates during maintenance, i.e. when the aircraft is out of service. In this context, the design of new aircraft is already now driven by "design for maintenance", i.e. the inspection capabilities of e.g. NDT methods are always considered [9].

To monitor the damage development in materials, a number of SHM techniques were proposed: acoustic emission [28-30], real-time micro-focus radiography [31], electrochemical noise measurements [32], ultrasound [33], optical fibre sensors etc [34,35]. New techniques to evaluate and characterize the extent of damage are also being developed or optimized (high-resolution X-ray computer tomography [36], optical fibres as smart materials).

3.1.2 Applicability of SHM

After basic and applied research, some applications came to the market and nowadays, they are on the way to be a standard in engineering structures, such as chemical plants, oil pipelines and bridges [16]. Finally, except of HUMS systems in helicopters, SHM applications in aircraft are still in an experimental phase. There are different reasons for this:

- Lack of technical maturity
  - → Solutions proposed only solved isolated problems
  - → Difficulties to match all natural environmental conditions
  - → Measured data are difficult to interpret due to the complex nature of aircraft parts
- Lack of acceptance by end-users
  - → Complicated and long-term certification process expected
  - → Scepticism against new technologies
  - → Pessimistic expectations concerning the return-on-investment

The lack of acceptance by end-users can be overcome by convincing technical solutions that respond to all the challenges inherent to aircraft operations. The major problem already mentioned in the list above is the difficulty to interpret the measured data obtained in complex aircraft components. This problem can in

principle be tackled by enhancing the number of sensors as well as improved data processing.

3.2 Literature review on SHM solutions

3.2.1 Eddy current technology

Eddy current testing covers 85% of NDT applications in commercial aviation [37]. It is already in use since many years and there is a variety of systems in the market, but they require an operator for performing local inspections and the sensors are not integrated into the structure. Therefore, they are not suitable to cover large parts of an aircraft and inspections are time-consuming. This has a negative impact from an economic point of view due to the fact that the aircraft has to stay on the ground for a long time in order to be inspected. The longer the aircraft stays on the ground, the higher the expenses are for the airline company.

The eddy current method is however also a promising inspection tool for SHM [38-44]. For this purposes the eddy current method is sometimes combined with other methods such as ultrasonic Lamb waves testing in order to obtain better results [45]. Some research groups as well as the USA Air Force have proposed “giant magneto-resistive” based eddy current systems that can be used in nonmagnetic metals and offer a high bandwidth and high sensitivity for inspection of multilayer structures [46-48]. Other similar flat eddy current sensors have been designed by the European Aeronautic Defence and Space Company (EADS) and they are proposed for utility in areas of aircrafts where joints or access points are present [49]. A related technique for crack growth monitoring includes meandering winding magnetometers mainly used on steel alloys [50,51].

3.2.2 Embedded electrical crack gauges

The use of embedded electrical crack gauges can be a simple and effective way detecting fatigue cracks in pre-selected areas where the damage is most likely to appear. These areas are called high-stress concentration areas. In an aircraft, the shape and the dimensions of the structural part varies according to the manufacturer. To determine the weakest points or the areas that the majority of load is expected, finite element analysis can be used that examines strains arising from load applied from any direction to any point on the material.

By pre-knowing the area where a crack is more likely to appear, crack gauges can be embedded on these specific areas of the material under investigation and monitor the fatigue crack growth. The gauges used in this study are electrical crack gauges. That means that the moment they are broken due to a crack, the electrical conductivity is interrupted. When the electrical conductivity is interrupted at the crack gauge, the monitoring system gives a warning that the crack has reached a critical size and the structural part needs to be replaced or repaired.

There are some proposed solutions in the literature so far concerning crack monitoring using strain gauges. For example, Martinez et al. propose a system with internal crack gauges that interrupts the electrical conductivity [52]. Also, the use of strain gauges has been proposed by many authors such as Tikka et al., while Baker et al. proposes a strain gauge system using a adhesively boron fibre reinforced plastic patch that is attached on top of the critical area and monitor cracks due to deformation [53,54].

There are already commercially available crack propagation gauges consisting of very thin flat metal stripes. When a crack propagates through the gauge, each time the crack breaks a stripe of the gauge, a stepwise increase of the electrical resistance is observed. In the figure below, the upper photo shows an example of this type of gauges. The middle and lower photo are taken using a Scanning Electron Microscope (SEM) at a scale of 200 µm and 20 µm respectively. The white stripes are part of the crack gauge and the dark area is the foil on which the gauge is deposited. At the right photo, the lateral view of one of the stripes of the crack gauge can be seen.

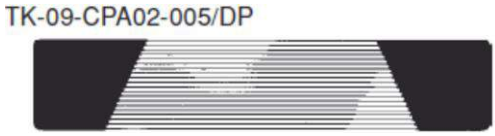

Drawing of crack propagation gauge

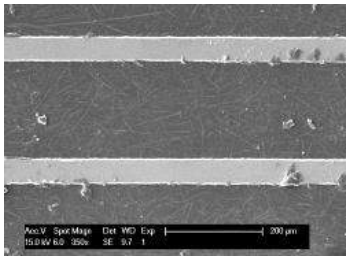

Top view (SEM)

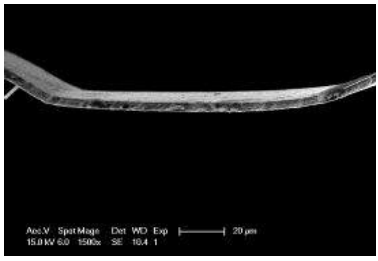

Side view (SEM)

Figure 3.1: Upper figure: A crack propagation gauge from VISHAY Electronic GmbH, Middle and lower figure: SEM photos with top and lateral view at 200 µm.

3.2.3 Ultrasonic Lamb waves

One of the most investigated SHM methods for aircrafts is the detection of damages by ultrasonic guided waves or so called Lamb waves. Numerous articles and books on this topic have been published the last years suggesting a variety of applications and confirming the potential of this method [55-59]. The method is based on the transmission of ultrasonic guided waves that are reflected from or transmitted through the defects or discontinuities of the material under inspection.

These Lamb waves have a long-range sensitivity and they might be ideal candidates for damage inspection of large plate-like areas that can be found in aircrafts. Their sensing ability is based on the change of their waveform when damage occurs along their propagation path. The alteration of their waveform takes place because their propagation properties are directly influenced by the mechanical properties of the inspected material.

3.2.4 Optical fibres for acoustic emission monitoring

Optical fibres have also been considered as SHM methodology in aircrafts [29,60,61]. Fibre optic sensor technologies are generally distributed in three categories of sensors. These are the inteferometric sensors, the distributed sensors and the grating-based sensors [34,62-64]. Interferometric sensors such as the Fabry-Pérot interferometer, are measuring very small deformations in the material's structure from the phase difference in the light that is distributed due to interference with an incoming acoustic wave. Distributed sensors are sensing fibres that are used for pressure, strain and temperature distribution measurements [65]. The grating-based fibre technology is an optical technology that is under continuous development is using Fibre Bragg Grating sensors (FBG). FBGs are immune to electromagnetic interferences and they already have been in operation for SHM in civil structures [66]. Another approach of optical fibres used as a sensing technology includes corrosion prevention by the detection of corrosive liquids [67].

3.2.5 Corrosion monitoring techniques

One of the most important problems today that aeronautical engineers have to deal with is the appearance of corrosion. Corrosion has a negative impact in any industrial application and results in very high costs as it reduces the lifetime and the performance of the material. Corrosion monitoring has been studied for centuries since it affects any kind of metallic material in any kind of application. The majority of research programs that can be found are mainly concentrated in the chemical or physical degradation of the protective coatings that can prevent corrosion on a metallic surface [68]. However, the coatings offer a good protection but they can be also damaged as a result of an intensive use of the aircraft [69].

Proposed methods that monitor corrosion in aircraft structures include ultrasonic testing (including Lamb wave testing), eddy current technology, optical fibre systems and other NDT techniques that are also discussed in this study [70-73]. Other metal corrosion sensors that have been studied include thin metal films that increase their resistance when they corrode or sensors that their function is based on galvanic corrosion [74]. Furthermore, since corrosion is a result of environmental changes, a common method to prevent corrosion is the use of sensors that acquire atmospheric measurements. These sensors are called sensing nodes and measure parameters such as relative humidity, temperature,

atmospheric pressure etc. Luna Innovations Incorporated has released environmental sensors on the market that suit for aerospace applications [75].

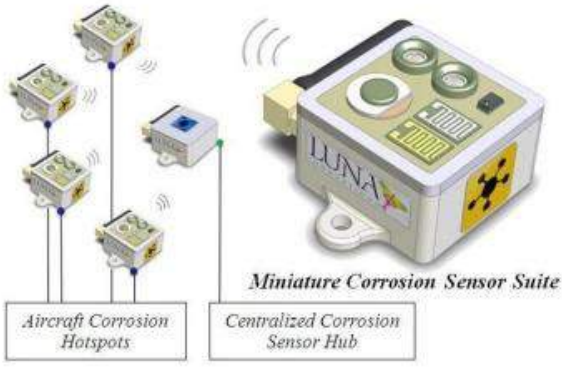

Figure 3.2: Environmental sensors for aerospace applications from Luna Innovations Inc. [75].

Most of the techniques that can be found in the literature are either applied for ground maintenance or the size and the function of the sensor is not appropriate for confined areas. More often the component under investigation needs to be removed in order to be inspected or the confined area is very small to host a sensor.

3.3 Literature review of other most common NDT methods

Below some of the most common NDT techniques, that are used today for SHM of aircrafts, are briefly discussed.

3.3.1 Visual inspection

A visual inspection is carried out by maintenance staff walking around the aircraft and inspecting specific areas that are vulnerable and can show wear, corrosion or cracks. The specialists check also for possible leaks and any unusual changes on the surface of the components. Almost 80 percent of the inspections that are taking place in an aircraft are visual [76]. This method has the disadvantages that it can detect only surface cracks and it is limited to the visual and observation capabilities of the inspector. However, this procedure is mainly used as a fast monitoring method for failures particularly when the aircraft has been just landed and it is ready to take off after few minutes or hours.

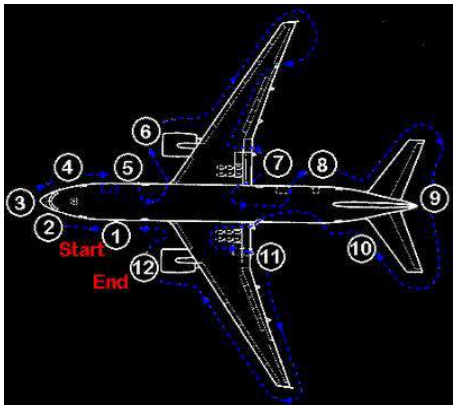

Figure 3.3: Scheme for visual inspections areas around a Boeing B777 aircraft [77].

3.3.2 Ultrasonic inspection

Ultrasonic testing is currently used as an NDT method for the detection of cracks and delaminations in aircraft components. It has been in practice for many decades offering technological advantages, and it follows a rapid development due to the smaller size and high processing speed of modern instrumentation as well as the contribution of robotics. Together with the visual inspection and the eddy current testing are the most common NDT methods used for crack detection.

The literature on ultrasonic testing applications for aircrafts is vast and in the last years many Lamb wave guided techniques are proposed [78-84]. Some interesting and novel methods of in-situ ultrasonic testing of aircraft parts have been presented but most of them are limited as external, non-integrated systems [85]. Also, ultrasonic testing has been introduced as a quality control test by many companies, for eg. NUTRONIK Gmbh and GE Inspection Technologies propose large, automated ultrasonic systems that are integrated into the aircraft composite production plants [86,87]. Furthermore, Olympus Corporation has produced a multimode ultrasonic adhesive bonding testing instruments for the inspection of the composite sandwich structures of aircrafts. However, those commercially available instruments are not integrated into the aircraft component itself but they are offered as external solutions that need to be operated manually by a technician or by a robot that scans the whole surface of the aircraft part.

State-of-the-art equipment is using computer scans (C-scans) able to automatically scan larger surfaces [88]. However, this technique requires extended instrumentation as well as a number of connections and cables establishing a significant drawback in the weight and the integration of the sensors into the aircraft components. This technique can be feasible for online monitoring, but it is necessary to use less cables and to find “hot spots” that require monitoring in order to minimize the number of sensors. Also wireless connections are under

development that helps minimizing the weight [89]. A drawback of the C-scan inspection is the accessibility of the aircraft component (robotised testing) or the need to remove it totally (water tank testing) in order to be inspected.

3.3.3 Magnetic particle inspection

This low-cost method is used on aircraft parts, and it is based on the magnetism of ferrous materials. The part under investigation is subjected to a magnetic field inside a large coil, where the surface of the part is magnetized almost up to its saturated flux density [90]. Then the part is covered with magnetic particles, usually iron fillings in a form of a powder or of a liquid suspension. The areas with discontinuities or defects at or near the surface of the material are detected due to the phenomenon of magnetic flux leakage. That means that the magnetic field appears to be stronger on the corroded or cracked areas showing different behaviour. The stronger magnetic field attracts more iron particles, which can be detected by another magnet or by appropriate lighting conditions [91]. By detecting the position of the iron particles, one can determine the location and the size of the damage. This method might be the most economical but it has the disadvantages that the part needs to be removed from the aircraft, it cannot inspect very large parts and it is suitable only for ferro-magnetic materials.

3.3.4 Liquid penetrant inspection

This relatively old NDT method can be used for the maintenance of aircraft parts [92]. It can be applied in non-porous materials and it can reveal surface breaking cracks. The liquid penetrant method is used on all ferrous and non-ferrous materials in contrary to the magnetic particle method that can be applied only on ferrous materials. The method is based on the capillary action of the liquid that penetrates in the crack at the surface of the material. The capillary action of a liquid occurs when the molecules of the liquid have the ability to move using the adhesion forces between the liquid and the sold material under inspection. In that way, the liquid can penetrate into the surface of the material without the aid of gravity and the molecules can be inserted in microscopic cracks. After the application of the coloured liquid penetrant, the surface is cleaned and a developer is applied on top. The developer attracts the molecules of the remaining coloured penetrant and reveals the areas of the cracks that can be visual to the inspectors. This NDT method has a fine performance and can have very accurate results [93]. However, similarly to the magnetic particle inspection method, the liquid penetrant method can monitor relatively small sizes of aircraft components and is more useful to investigate cracks that are located on the surface.

3.3.5 Radiography

Radiography is a widely known NDT method that has been employed in medicine and engineering for many years. Studies showed that X-ray, gamma-ray but also

neutron radiography are suitable for corrosion and flaw detection of materials and can be used for SHM in aircraft components [94-96]. In a similar manner to the human body, any object that consists of materials with different densities can be inspected with this method. When X-ray beams are excited and directed to the object, depending on the composition and thickness of the materials, the X-rays are absorbed or scattered. On the other side of the object an X-ray film or fluorescent screen will detect the remaining X-ray beams. In this way, a two-dimensional projection of the object can reveal damages inside the material. The last years it has been discussed that the radiography that uses film can be replaced with the digital radiology that uses digital detector arrays and can achieve even better visibility and shorter exposure time [97]. The method of radiography even effective is not convenient for continuous monitoring as the part usually needs to be removed in order to be inspected. Furthermore, the operating personnel can be subjected to radiation hazards and the chances for cancer development can be increased with the levels of exposure [98].

3.3.6 X-ray computer tomography (CT) Scan

Similar to X-ray radiography, X-ray computed tomography is used to obtain a three-dimensional image of the object under inspection. The X-ray beams are excited from multiple positions and with the aid of a computer processor, all the three dimensions together with the flaws inside the material can be detected. CT Scan is used for SHM for crack and defect detection and has the advantage that can give high resolution digital images [99]. However, it also has the disadvantage that the part needs to be removed and it is not applicable as an integrated system.

3.3.7 Thermography

This NDT method measures the surface temperatures of components and shows the level of heat dissipated in each area. For example, when the part is subjected to vibration, the areas that have been corroded or have flaws are more likely to heat up due to friction. These areas produce more thermal energy and they can be detected. There are two kinds of thermographic inspection; the passive and the active [100,101]. The passive depends on the material's ability to emit thermal energy and is mainly used when the materials are heterogeneous. During the active thermographic inspection , which is also called pulsed or transient thermography, the material is heated from an external source (it can be also be kinetic energy that is converted to heat) and the temperature difference on various areas of the material can be read by an infrared system [102].

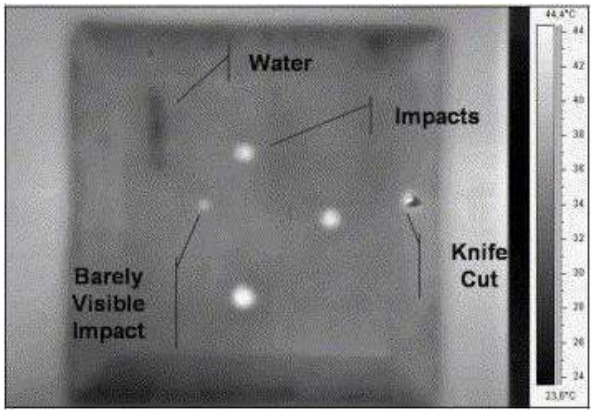

Figure 3.4: Various defects captured by thermographic imaging on a honeycomb composite plate [103].

Thermographic inspection as an NDT method becomes more and more popular to detect delaminations in composite aircraft components [104-106]. Interesting investigations have been also carried out using grating lock-in infrared thermography for the determination of the thermal properties of composite materials [107].

The NDT techniques discussed above have their own variations depending on their application. Below is an overview of all the NDT techniques that are used today according to the International Committee of Non-Destructive Testing (ICNDT) [108].

- Acoustic methods
  - Acoustic emission (AE)
  - Acoustic ranging
- Ultrasonic methods
  - Resonant inspection
  - Ultrasonic flaw detection
  - Ultrasonic thickness gauging
- Electromagnetic methods
  - Eddy current testing
  - Coating thickness measurement methods
  - Magnetic particle inspection (MPI)
  - Magnetic flux leakage methods
  - Alternating Field Current Measurement (ACFM) technique
- Optical methods
  - Laser-based inspection
  - Optical metrology and holography
  - IR Thermography
  - Electronic endoscopic inspection
- Potential drop flaw detection and sizing
- Erosion corrosion

- Leak testing methods
- Liquid penetrant inspection
- Visual inspection
- Radiography and radioscopy
- Neutron radiography (just experimental)
- Stress measurement using strain gauges etc.

"If you are going through hell, keep going."

Sir Winston Churchill (1874 - 1965)

CHAPTER 4

Materials selection and Structural Health Monitoring methods applied in this study

In this chapter, the selection of the proposed SHM methods that were investigated in KU Leuven on various structural parts of aircraft components is presented. A first tick point presentation of the SHM methods investigated in this study is given at the beginning of the chapter. Afterwards, a material selection of the aircraft components is discussed. Then, the evidence of the problem is shown and the theoretical background of each dedicated solution for SHM of aircraft components is discussed. The experimental details and results of each method are presented in the following chapters 5 to 9.

4.1 Applied SHM methods at a glance

In this thesis five main dedicated solutions for SHM of aircraft components are presented. These are:

- ✓ Flat coil sensors for SHM of aircraft components using eddy current technology
- ✓ Embedded electrical crack gauges for continuous crack growth monitoring
- ✓ Impact and impact damage detection on composite materials using optical fibres
- ✓ SHM using Lamb waves and the application of pseudo defects for signal validation
- ✓ Detection of corrosive liquids in confined parts using percolation sensors

Besides the proposed solutions above, some other methods and experimental results are presented in the appendices since they could not be explored to their full extent. At the end of the chapters 5 to 9, a table of the advantages versus the disadvantages for each solution is presented together with a brief description of the Probability of Detection (POD) that characterizes the effects and reliability of the SHM method.

4.2 Quantifying the defect prediction performance of SHM methods

4.2.1 Introduction

The last years, probability theory in Non-destructive Testing (NDT) has seen a rapid growth due to the necessity of selecting the best method for Structural Health Monitoring (SHM) that will efficiently and effectively identify the defect. Due to this need, probability theory in combination with mathematical modelling has created the concept of the Probability of Detection (POD). POD is a quantitative measurement that gives the probability of an accurate crack detection of an NDT method for SHM purposes and evaluates its capability for an effective measurement [109]. The POD depends on a number of parameters such as the defect's specifications and the testing environment. By knowing the POD, engineers can identify which method for SHM suits better to each unique case. The POD is high when the SHM method is almost certain that it will detect the defect in an instant measurement and low when the selected SHM method will not detect the defect instantly unless some parameters have been applied and a number of measurements are taken. For example, in the case of a strain gauge, for very small damages that have not cracked or elongated it, the POD is very low since the gauge

is still connected. On the other hand, when the crack breaks the strain gauge, there is a high probability of defect detection.

Today, various methods have been proposed for SHM of aircrafts that led to a variety of POD curves, which in turn their shape depends on a number of parameters. The challenge is to increase POD with the use of simplified sensors with an independent and direct sensitivity avoiding the complex responses of other SHM methods whose performance is limited on operation-dependent baseline variations as well as by signal interference within the intrinsically complicate airframe structures. In this study, an approach on POD related to the response of different kind of sensors for SHM is investigated.

4.2.2 Probablity of Detection (POD) and Probability of False Alarm (PFA)

To characterise the performance of an inspection technique and identify its inspection ability, POD together with Probability of False Alarms (PFA) are being used. In a simplified meaning, POD is the probability that shows a defect detection when the defect actually exists whereas PFA is the probability that shows defect detection when there is no real defect. For example, if POD is 0.95 then in 100 inspections, the defect will be found 95 times and if PFA is 0.01 then in 100 inspections of a clean part, there will be 1 false alarm.

4.2.3 Receiver Operating Characteristics (ROC)

The Receiver Operating Characteristics (ROC) curves are showing the performance of the selected NDT method for a pre-specified detection threshold [110]. In figure 1 below, there is a sample graph that shows a ROC curve, which is created from the POD and PFA. The best performance is given in the upper-left area of the graph where POD tends to 1 and PFA tends to 0. ROC curves are being used to display and compare simultaneously information on the POD and PFA [111].

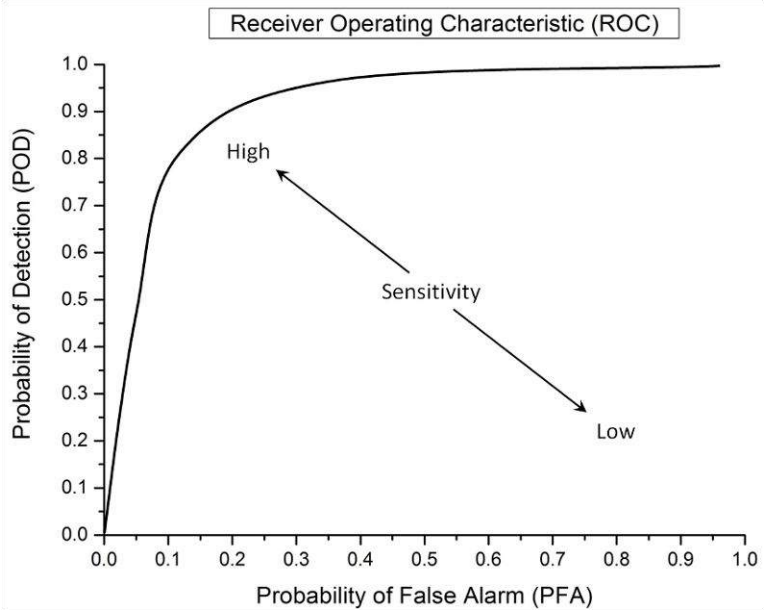

Figure 4.1: Example of ROC curve and direction of sensitivity.

From mathematics, any probability can reach a maximum numerical value of 1 or 100%. Therefore, as it can be presumed, when POD is near 1, then the detection of a defect is more certain than when it has a lower value. As a general rule, POD should always have larger values than PFA in order for the inspection technique to achieve better performance. The inspection of a defect is successful when the amplitude of the signal is over a certain threshold which indicates the discontinuity. If we have no idea whether a defect is apparent then the probability of measuring a signal that will reveal a defect is based on luck and it is assumed 50%. In figure below, high POD means low PFA and low POD means high PFA respectively. The straight line corresponds to a 50% probability of measuring the signal, meaning that at any point on the line the POD and the PFA have the same percentage. Above the straight line, the POD has always higher percentage than the PFA, for eg. at the point A, POD is 20% and PFA is 5%. The opposite behaviour is observed below the straight line where PFA is always larger than POD. For eg. at point B, POD is 85% but PFA is 95%. Therefore, the probability to have a correct measurement is higher than 50% at any point above the straight line and lower than 50% below it.

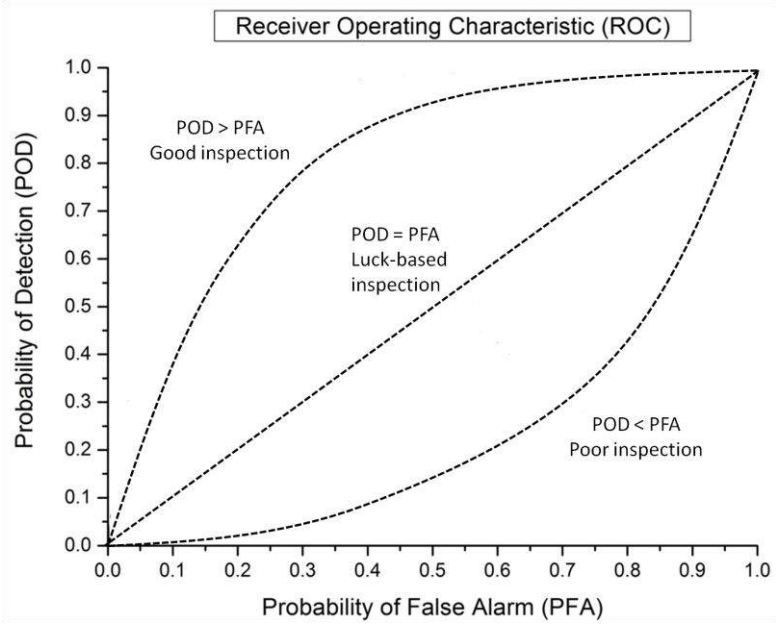

Figure 4.2: Likelihood of POD and PFA.

4.2.4 Understanding the POD

POD is following a hit-miss approach and has various models depending on the inspection method. These models include many parameters such as noise, geometry and defect visibility [112]. A standard definition of POD for the inspection of a defect with a size α can be as follows:

$$POD_a = \frac{C_D}{C_T} \qquad \text{Eq. 4.1}$$

Where C_D is the number of cracks that are detected and C_T is the total number of cracks from all the inspections. In order to create the POD curves from the inspection data some more complex modelling methods are required. One of the most common distribution methods used for plotting the POD curves has been described by Berens and Hovey with the following equation [113]:

$$POD_a = \left\{1 + \exp\left[-\frac{\pi}{\sqrt{3}}\left(\frac{\ln a - \mu}{\sigma}\right)\right]\right\}^{-1} \qquad \text{Eq. 4.2}$$

Where α is the size of the defect and μ and σ are mathematical parameters defined by Berens and Hovey [114]. The parameter μ is the natural logarithm of the size of the crack when there is 50% detectability, whereas σ is a scale parameter that

defines the trend of the POD curve. Both μ and σ parameters are defining the whole POD curve as a function of the crack length α.

Another common equation that describes POD curves for SHM methods and is frequently used for aircraft structures is the Palmberg equation that describes the probability of detection for a specific size of a crack or larger than that [115].

$$POD_a = \frac{\left(a/a_m\right)^{\beta}}{1+\left(a/a_m\right)^{\beta}} \qquad \text{Eq. 4.3}$$

Where a is the specific crack size, a_m is the crack size that gives a 50% probability of detection and β is a parameter of a random size. When the crack size a is 2 times the crack size of a_m and β is 3, then the POD is 88.89% and when β is 4, then the POD is 94.12%. In the equation above, only cracks that are bigger or equal to a_m can be detected.

Let's assume a case where we need to identify the performance of a random NDT method for a specific inspection of cracks with sizes larger than 5 mm. Ideally, a NDT method with a perfect accuracy will detect any crack larger than 5mm with POD value at 1. For cracks smaller than 5 mm POD value will be 0 [116]. In reality, due to noises and other signal disturbances, POD is usually changing progressively depending on the chosen NDT method. Figure 3 illustrates this example showing the difference between an ideal versus the real case of a POD curve for a crack threshold larger than 5 mm. This comparison is made with the purpose of understanding that a selection of NDT tools with the less baseline variations that interfere with the efficiency of detection are the best candidates that approximate the ideal case of POD.

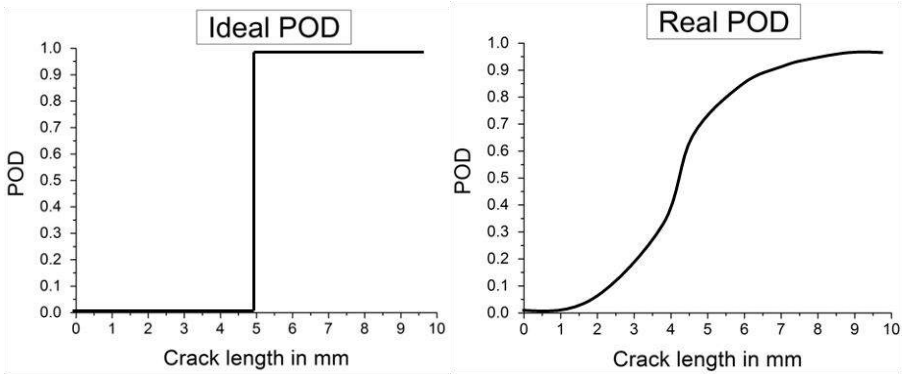

Figure 4.3: Ideal case of POD (left) and reality (right) for inspecting cracks equal and larger of 5 mm.

An example of POD curves on real NDT applications is illustrated in the figure below from Matzkanin and Yolken. Each one of the three POD curves corresponds to three different NDT methods, ultrasound, X-ray and Eddy current [109]. For the same material and parameters but also for a crack size bigger than 1.3 mm, it can be seen that the NDT method using ultrasound gives a better POD, making it more effective than the other two. In the graph below, NDT using ultrasound reaches 95% POD for cracks bigger than 5 mm.

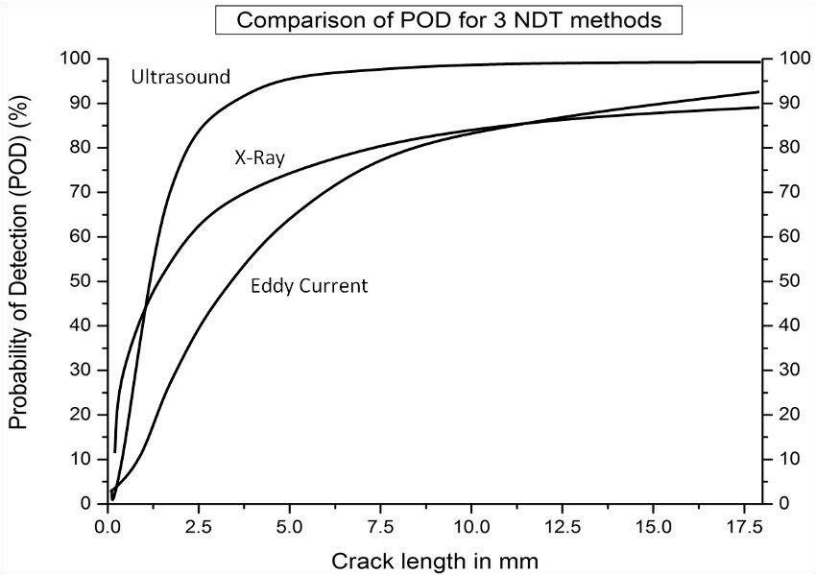

Figure 4.4: POD curves comparison for 3 NDT methods according to Matzkanin and Yolken [109].

4.2.5 Understanding the parameters of the POD curve

To accurately design these POD curves many parameters are taken into account. The performance of an SHM system and its ability of detection can be affected by the structural variability of the component such as surface interfaces, coatings but also by structural loading, unloading and thermal cycling. Internal load variations that are responsible for the component's degradation followed by bonding degradation of the transducers can also affect the performance of the SHM system during inspection [117].

The position, width and steepness of the POD curve show the effectiveness of the inspection method. For example, a very steep curve shows an immediate response with a high POD which in turn gives a better inspection performance. The steepness of the curve is directly related to the density of the data scatter from the data received after inspection. If the data are not spread all over the plot but are narrowed and follow a similar path after repetitive measurements (inspections),

then the data scatter is denser and this means that the inspection method is more effective giving more accurate results. Therefore, for a dense scatter of data, the POV curve turns anti-clockwise and the steepness of the curve becomes higher. In the figure below, a representation of the steepness of the POD curve according to the data scatter from the inspections is shown. It can be seen that for a denser data scatter the performance of an SHM system for detecting defects near 8 mm is better since the POD (%) becomes higher.

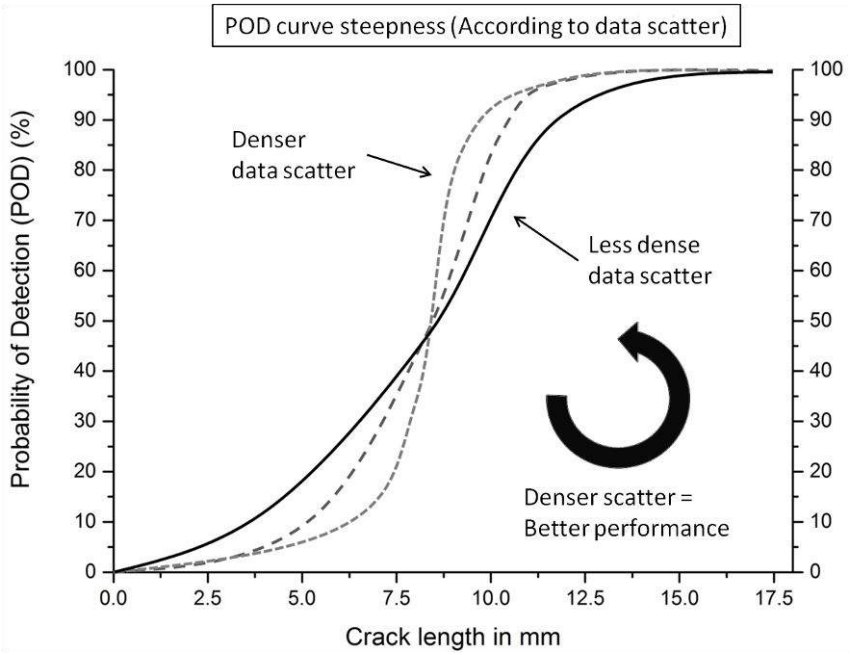

Figure 4.5: POD curve steepness according to data scatter.

The sensitivity of the SHM system for detecting smaller cracks is also related to the background noise. When the background noise is low, then the POD curve moves left on the graph and the steep comes earlier but when the background noise is high the POD curve moves further right on the graph showing a decent performance only for larger crack sizes.

The input parameters for each inspection method are different. POD is a result of the variability of the inspection data that is a product of many factors such as the operator's ability, material characteristics and morphology, equipment hardware and software, etc. Since noise is almost always apparent, there is a minimum threshold of intervention with the signal above which the POD takes effect. The figure below shows the correlation of noise with the signal and how the POD is increased according to signal's strength. The following method is known as Model-

Assisted Probability of Detection (MAPOD) that was established by the U.S. Air Force Research Laboratories, Federal Aviation Administration (FAA) and National Astronautics and Space Agency (NASA) [118].

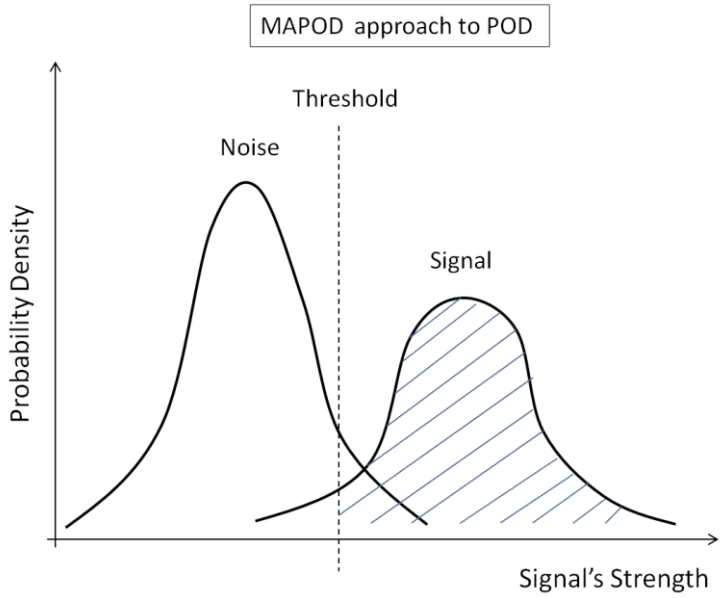

Figure 4.6: MAPOD approach to POD

MAPOD is the collection of approaches that use various inspection models whose inputs are used to estimate POD for SHM validation [119]. According to MAPOD, the point of threshold remains at a stable position starting a bit earlier from the end of the noise curve. The area where noise and signal join shows the Probability of False Alarm (PFA). When the signal curve moves left, the signal is weaker and the POD is low. Similarly, when the signal curve moves right, the signal is strong and the POD is high. The above method is using Physics-based models that predict the distribution of the noise and signal together with empirical knowledge from laboratory testing and gives an idea of the creation of the POD curves for different NDT methods.

Conventional acoustic or electromagnetic NDT methods are designed to have a linear acoustic response of materials from the generated signal and the non-linear material response is directly related to a change of frequencies, and noise. For the above reasons, a POD curve can be described as a convolution of signals that is made of the linear contribution of the NDT sensor and the non-linear response arriving from the frequency changes of the input signal [120]. For a smooth plotting of the response a normalization constant is used. Therefore, the POD function that gives the final curve can be rewritten as follows:

POD = normalisation constant x POD (linear sensor) x response curve (non-linear sensor)

4.2.6 POD for fuse-like non-linear sensors for SHM

For better results, the assessment of POD can be further deduced from inter-calibration of the NDT tools [121]. However, this inter-calibration requires elaborated data processing algorithms from additional hardware components. For online SHM and particularly in aircrafts, these high-end hardware components are required to be on-board and enfold a drawback regarding additional costs and weight. A proposed solution to this problem is the use of fuse-like non-linear sensors with less complex software.

From previous studies, fuse-like sensors such as embedded electrical crack gauges and percolation sensors have been used for SHM purposes on aircraft components showing prominent results [122,123]. For the case of embedded painted electrical crack gauges, the parameter is the electrical conductivity which is suddenly lost when the crack breaks them. Percolation sensors also have a sudden switch of their electrical conductivity when the environment inside the confined space reaches a specific amount of humidity that hydrates the sensor and causes the percolation effect.

Both painted electrical crack gauges and the percolation sensors are highly sensitive and are designed to give an instantaneous signal only when an adverse degree of damage in the material or change in the environment has emerged. The absence of a large number of baseline variations makes these solutions for SHM fairly efficient in defect prediction.

4.2.7 POD comparison – Example between painted electrical crack gauge and Eddy Current sensor

The painted crack gauges detection principle relies on the interruption of their electrical conductivity during fatigue loading. They are local sensors and are positioned exactly at the point where a crack is more likely to make an appearance. For the following example, the outer side of the painted crack gauge is positioned exactly 5 mm away from the stress concentration point that is investigated. When the crack reaches 5 mm, it starts breaking the gauge with a direction along its width that is 1.5 mm. At the moment where the crack penetrates the gauge, the painted electrical crack gauge indicates the problem and gives a warning. The POD for the electrical crack gauge starts to increase rapidly near the point of breakage and it becomes 100% very quickly. At that point the crack gauge is completely broken and even if it regains conductivity the alarm has already been recorded. The POD curve for the painted crack gauge takes effect from the point just before the crack

reaches the gauge until it is completely broken and it is estimated to follow a trend as illustrated below.

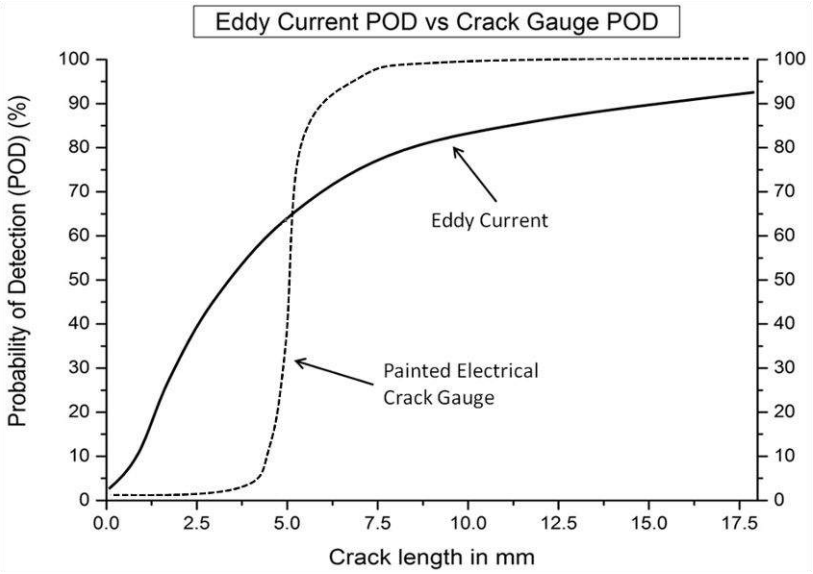

Figure 4.7: POD curve for Eddy Current and the estimated POD curve for the Electrical Crack Gauge

The POD curve of Eddy Current on the other hand does not have a close-to-binary value (0 or 1) but it fluctuates during an inspection. This sudden and ideal signal response for the electrical crack gauges can be explained by a deconvolution of the final signal. This difference in the steepness of the POD curves happens because the response of the electrical crack gauge is not affected by non-linear responses such as noise in contrary to the case of Eddy Current where noise influences its electromagnetic response. The recorded signal usually convolves noise that needs to be extracted in order to give this kind of response. However, inverse filtering is not recommended if there is no specific data for the noise signals. The POD curve of Eddy Current shown in the figure above is used as a random example and it can vary in shape but it almost never follows an ideal case.

The philosophy of POD for the fuse-like non-linear sensors finds explanation on the ground that a defect in order to be detected, the sensor itself has to be destroyed or change its physical properties. Therefore, the probability of detection for these sensors does not rely so much on baseline variations that make the detection more difficult (noise filtering, shape of defect or inspected material, etc.) rather than on their own structural integrity. This is the key for creating ideal cases of POD because there is no actual PFA. However, PFA can exist when the sensors themselves have been destroyed or malfunctioned, eg. impact on painted crack

gauges or a percolation sensor has been cut, but even in that case the alarm has already been recorded that the embedded system needs to be replaced.

4.3 Materials selection

Aircraft components are built from a variety of materials such as aluminium and titanium alloys, steel, composites, plastics etc. The main materials used for structural parts are the aluminium alloys Al 2024 or Al 6061 but the last years there is a high increase in the use of composite materials. Composite materials are much lighter than aluminium alloys and can withstand similar very high stresses. The percentage of the structural weight of composite materials for an aircraft has grown radically from less 1% to more than 50% over the last decades [124]. Composites can be used to manufacture important structural components such as the fuselage, wings, elevators, vertical stabilizers, rudders, ailerons, doors, rotors, and fuel tanks.

As a recent example, the new Boeing B787 Dreamliner aircraft is the first full-size, long range, commercial aircraft that is mainly produced by composite materials leaving the aluminium alloys in the second place. The materials used for the Boeing B787 Dreamliner are according to their weight 50% composite, 20% aluminium, 15% titanium, 10% steel and 5% others where on the other hand the Boeing B777 aircraft uses 12% composites and 50% aluminium [125].

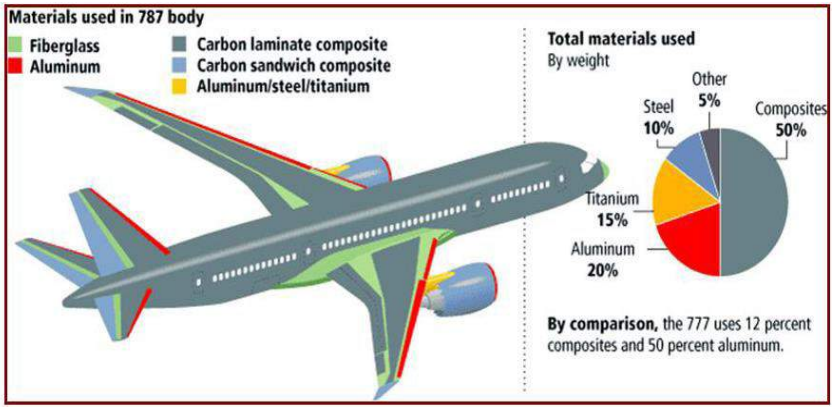

Figure 4.8: Materials selection for the structural body of the Boeing B787 Dreamliner [125].

4.4 Areas of implementation in this study

Prior to the sensor implementation, the areas that have the highest possibility to develop cracks or the components that are critical for the structural integrity need to be identified (hot spots). These critical areas of the aircraft components consist

of high stress concentration areas, joints or connections where rivets are apparent. Furthermore, areas that are vulnerable to impact by flying objects should also be included. In this PhD study, different approaches have been investigated for SHM of aircraft components. The figure below shows the dedicated solutions for SHM in aircraft components and the areas on the aircraft that they can be allocated. The main goal is to make an appropriate selection of these SHM methods that can be integrated in specific areas of the aircraft and monitor their structural integrity during their lifetime.

Figure 4.9: SHM solutions used in this study on critical areas of an Airbus A320 aircraft [9].

Every SHM solution that is applied to each aircraft component is selected carefully for optimum performance. There are many factors that need to be taken into consideration prior selecting the appropriate technique. These factors can be the following:

- Types of material under investigation and its properties
- Ease of sensor integration in the component
- Adaptability of sensor in the critical area
- General safety measures (fire protection, etc.)
- Weight and volume of sensor(s)
- Ease of data acquisition and analysis of results
- Reliability and performance in simulated flight conditions

Each SHM solution has advantages and disadvantages. It is often required that more than one technique can be used for the same component.

The aircraft components that are investigated in this PhD study are mainly manufactured from aluminium or steel alloys and composite materials. The next paragraphs give a short presentation of each aircraft component that has been used for the SHM purposes in this study.

4.5 Aircraft components investigated in this study

4.5.1 Aluminium plates

Aluminium alloys belong to the main materials used for the construction of the frame and most of the individual components of an aircraft. They are light materials with high stress level capabilities. In this study, unclad aluminium alloy 2024-T3 plates were tested under fatigue and varied temperature conditions. The NDT sensors used for these tests included an eddy current flat coil sensor, crack gauges and piezoelectric transducers. The dimensions of these plates are 300 mm (length), 80 mm (width) and 1 mm (thickness). Depending on requirements some plates were anodized prior to the sensor attachment. Furthermore, a square shaped aluminium plate of 1000 x 1000 x 1 mm (length x width x thickness) was used for the application of pseudo defects and Lamb wave testing. The aluminium plate components were investigated for crack and defect detection due to fatigue, impact, collision or destruction.

Figure 4.10: Al plate (left) for ultrasonic testing and Al 2024-T3 plates (right) for fatigue testing using various NDT methods.

4.5.2 Airbus A320 slat-track

An Airbus A320 slat-track manufactured by ASCO Industries was used for testing purposes. Slat-tracks are the components that confine and roll the slats on them during their operation. The slats are extensions that are used to increase the surface area of the wings during take-off and landing [126]. The slat-tracks expand the slats and transfer the stress between the slats and the wings of the aircraft. They are made of maraging steel as they need to be very strong and tough since they have to withstand a very high amount of stress [176].

Figure 4.11: Airbus A320 Slat-Track selected for NDT purposes [127].

4.5.3 Floor beams and panels

Floor panels attached to the floor beams were used for SHM monitoring and investigated in the NDT laboratory of the MTM department at KU Leuven. The floor panels are made of honeycomb composite material connected on an aluminium floor beam. Between the composite floor plates there are small linear gaps where the sensors are positioned. These unique humidity sensors are used to detect aqueous liquids in these areas that can cause corrosion.

Figure 4.12: Floor beams with floor panels in the NDT laboratory of the KU Leuven (left), floor beams inside an aircraft (right - Courtesy of Lufthansa).

4.5.4 Eurocopter (AIRBUS Helicopters) EC 135 tail boom

A tail boom from a Eurocopter EC 135 helicopter was used to investigate instant impact and impact damage together with delamination problems. The tail boom is about 4 meters in length and is made of honeycomb composite material. Piezoelectric transducers, a sonotrode and optical fibres have been attached in the inner side of the tail boom for NDT purposes. The full scale part had two rows of

single mode optical fibres protected in SMARTape and 32 piezoelectric transducers. The smaller part had also two smaller rows of SMARTape and 4 patches of PZT.

Figure 4.13: Full scale honeycomb composite tail boom (left) from an Eurocopter EC135 helicopter (right) [128].

4.5.5 Other composite plates

Square shaped honeycomb composite plates of sizes of 400 x 400 x 13 mm (length x width x thickness) as well as Carbon Fibre Reinforced Epoxy (CFRE) plates of smaller dimensions were used for ultrasonic testing and acoustic emission investigations. Piezoelectric transducers as well as single mode and multi-mode optical fibres were used for impact damage detection.

Figure 4.14: Composite plates used for NDT purposes at the KU Leuven.

4.6 SHM using eddy current technology

4.6.1 Damage evidence

Fatigue is the main reason of failure of materials of aircraft components [129,130]. The areas where the aircraft components are connected with lap joints or rivets are the most sensitive to fatigue. Most of the metallic parts in the frame of an aircraft are connected with rivets as they are very good permanent mechanical fasteners. Rivet connections have holes, where the rivet passes through. These holes are stress concentration areas and a crack is more likely to initiate from them. The

figure below shows a crack that has been initiated on a rivet connection due to fatigue.

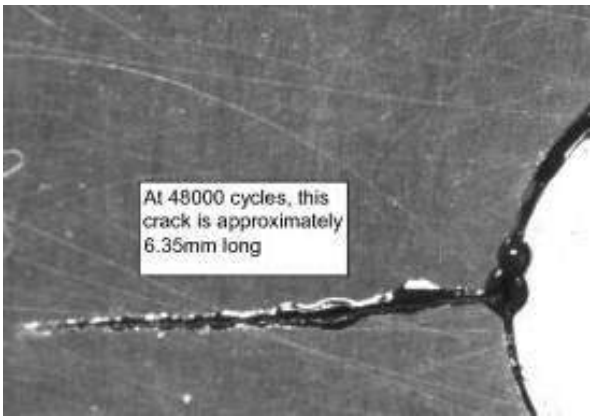

Figure 4.15: Crack growth from a rivet connection [131].

Thousands of rivets are used to connect the components for the assembly of a modern aircraft. Rivets are widely used in additional applications such as the connection of doubler repairs, which are attached usually on the outer skin of the aircrafts as protective patches in areas that have been slightly damaged since the replacement with a complete new part of the fuselage is very costly. In doubler repair, there are hundreds of rivet connections used. According to findings from previous incidents, the most critical area that is likely to initiate a crack in a doubler repair is the outer row of rivets since it is subjected to the larger amount of stress. However, sometimes, the doubler repair is not made of the same metallic material but is made of composite material that is bonded and coexists on the skin of the metallic components of the aircraft [132]. In that case the doubler repair is glued and there is no rivet connection. However this method is usually not allowed in operational practice.

4.6.2 Theoretical background

In 1824, the French physicist François Arago discovered an electrical phenomenon, known as the eddy current phenomenon, which occurs when a conductive material is near an alternating magnetic field [133]. Eddy current technology is thus based on electromagnetism. The word electromagnetism derives from the Greek words “ήλεκτρον” (electron), which was the name of amber and “μαγνήτης” (magnetis) from the ancient Greek city of Magnesia in Lydia, Asia Minor, where many magnetic stones were found and studied.

Electromagnetism was studied thoroughly and developed further by many renowned physicists such as Michael Faraday, Andrè Marie Ampère, Carl Friedrich Gauss, James Clerk Maxwell and later on by Heinrich Rudolf Hertz and Albert Einstein. The phenomenon is based on forces that appear on electrically charged

molecules surrounded by a magnetic and electric field. Maxwell's readings on Faraday's experiments in electromagnetism provided a solid feedback of this phenomenon. The most famous Maxwell's writings that discuss in depth about the electromagnetic field are his papers "On Faraday's Lines of Force", published in 1855, "On Physical Lines of Force", published in 1861 and "A Dynamical Theory of the Electromagnetic Field" published in 1865 [134]. Maxwell formulated equations that were previously studied from Gauss, Faraday and Ampère and added his own corrections. A younger physicist named Olivier Heaviside took Maxwell's equations and simplified them to the following ones that we use today [135].

The equations below describe all the classical electromagnetic phenomena.

Gauss' law for electricity $$\oint \vec{E}\, \vec{dA} = \frac{Q}{\varepsilon_0}$$ Eq. 4.4

Gauss' law for magnetism $$\oint \vec{B}\, \vec{dA} = 0$$ Eq. 4.5

Faraday's law $$\oint \vec{E}\, \vec{ds} = -\frac{d\Phi_B}{dt}$$ Eq. 4.6

Ampère – Maxwell law $$\oint \vec{B}\, \vec{ds} = \mu_0 (\varepsilon_0 \frac{d\Phi_E}{dt} + J)$$ Eq. 4.7

Gauss' law for electricity expresses the closed line integral of an electric field (E) through a closed surface (dA) is proportional to the total net charge (Q) inside of that surface. ε_0 is a constant which is called the absolute dielectric permittivity in vacuum.

The equation of Gauss's law for magnetism describes that the magnetic flux that is represented by the closed line integral of a magnetic field (B) through a closed surface (dA), is zero. This proves that there cannot be a point source of magnetic field but there are always two poles.

Faraday's law of induction describes that the closed line integral of an electric field (E) through a closed loop (ds) is opposite to the rate of change of magnetic flux (Φ_B) through the surface spanned by that loop.

The Ampère – Maxwell law describes that the closed line integral of magnetic field over a closed loop is proportional to the total electric flux (Φ_E) through a surface spanned by that loop. J is the current density and μ_0 is constant and is the magnetic permittivity in vacuum.

In Chapter 4, flat coil sensors are using the eddy current technology to detect flaws next to rivet holes and near the surface of aluminium plates. The process is based on the Faraday's law of induction. When a coil is fed with alternating current, an electromagnetic field will appear around the coil, which consists of an alternating electric and magnetic field. The alternating magnetic field, when it is near to a conductive material, it creates a new alternating electric field according to Faraday's law of induction as described above. This new electric field is inducing the eddy currents. The eddy currents in turn, create their own magnetic field which is opposing to the primary magnetic field of the coil. The opposing magnetic field causes impulsive changes in the apparent impedance of the coil of the sensor. Through the analysis of the change in the impedance of the coil sensor, eddy currents can give information on the homogeneity of the inspected surface of the material.

4.7 SHM using embedded electrical crack gauges

4.7.1 Damage evidence

Cracks due to fatigue are the most common damages that can occur in an aircraft during operation. The cracks can initiate from high stress concentration points or in areas where corrosion is apparent. In aviation industry and according to some manufacturers, small cracks are tolerant up to specific sizes. However, aircrafts should be 100% airworthy, they should have no flaws and should be in perfect structural health. Therefore, to prevent a rapid growth of a crack and to avoid a possibility of a large-scale damage, it is very important that the stress sensitive areas are regularly monitored. A recent example of fatigue damage was the appearance of multiple cracks in the brackets of the wings of a new Airbus A380 aircraft from Qantas Airways on January 2012.

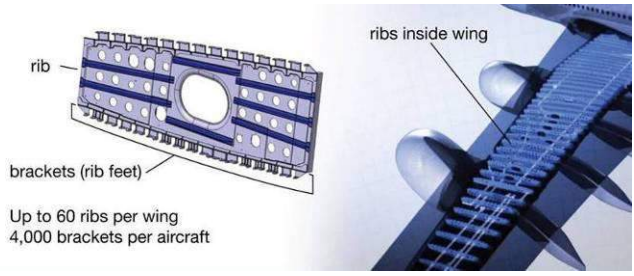

Figure 4.16: Drawings of components of the wing of an Airbus A380 aircraft from Qantas Airways where cracks have appeared [136].

In this PhD study, the crack gauges are conductive stripes that are embedded into the coatings of the metallic part under investigation. The crack gauges installation was performed in cooperation with the manufacturer of the aircraft components,

ASCO Industries N.V, Belgium. The SHM system is a proposed integrated system that can operate either as an online or an offline system.

4.7.2 Theoretical background

4.7.2.1 Methodology

Crack monitoring by crack gauges is based on the weakening or interruption of their electrical conductivity. The crack gauges are made of a conductive material that finally breaks together with the crack. An electric current is running through the conductive material of the gauges with a specific level of electrical resistance which depends on the kind of material used. The operation is as follows: Due to fatigue, cracks appear in the main material of the aircraft component that is under investigation. The crack passes through the crack gauge that is glued on the material and breaks it. When this happens, the resistance values of the conductive material of the crack gauges are reaching very high or infinite numbers. This occurs because the gauge has been cut and the electric current's flow has been interrupted. As it can be seen from the equation below, the resistance becomes infinite when the electric current is zero.

$$R = \frac{V}{I}, \quad I = 0, \quad R \rightarrow \infty \qquad \text{Eq. 4.8}$$

By monitoring the resistance values, it can be confirmed that the crack has reached the critical size and has cut the crack gauges. The technology makes use of resistance measurements with a relatively simple data analysis.

4.7.2.2 Closed crack issue

The fuselage and other structural components of an aircraft are constantly pressurized and depressurized due to stresses and pressure differences during take-off and landing. A crack in a component is likely to appear from fatigue. The crack will constantly stay open and close due to those cyclic pressurizations. When the aircraft is landed, the structural parts are subjected to less fatigue and due to the lack of pressurisation, cracks in the fuselage and other parts remain closed. These cracks might be macroscopically closed but they are microscopically open since they have altered the microstructure of the material. That means that they are difficult to be monitored since the material has been pressurized back in its original form in an atmospheric pressure and macroscopically look homogeneous. It is necessary that the crack gauges can detect the cracks instantly the moment that crack makes its appearance. Therefore, the electrical crack gauge should not regain its conductivity after the crack has penetrated through it. This is a great challenge since the crack gauge is re-attached and there is a chance of a regain of conductivity. In chapter 6, there is a proposal for an online monitoring solution that could be used to overcome this issue.

4.7.2.3 Material behaviour

Plasticity is also another factor that influences not only the resistance measurements using the crack gauge but also can result in the misjudgement of the critical break point. The physical theory of plastic deformation is quite difficult to be explained due to the complex geometries involved as well as the analysis of the non linear processes that occur [137]. However, it is important that any behaviour, elastic and plastic, prior the break point needs to be investigated in order to assure a reliable detection performance of the crack gauge. The figure below shows the different phases of the material's deformation when it is subjected to a gradually increasing tensile force.

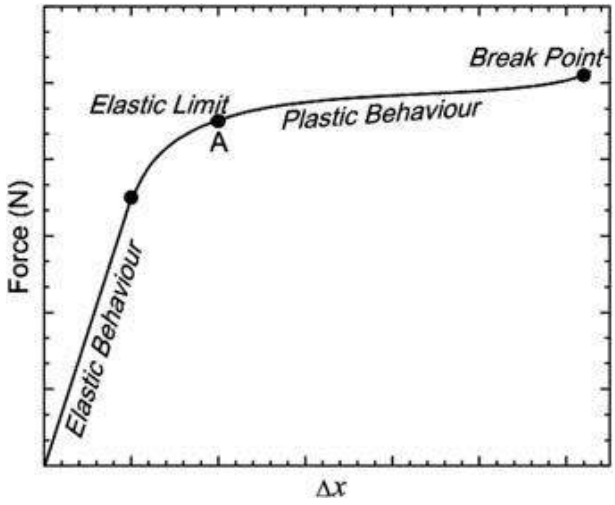

Figure 4.17: Elastic and plastic behaviour of a material indicated in the force-displacement Δx curve [138].

When the main material of the aircraft component is subjected to fatigue and the material can pass the elastic limit, local plastic deformation can occur. This plastic deformation is accompanied with void formation which is preceding the crack formation. This void formation is very important and needs to be taken into account when designing the crack gauge. This is because the crack gauge could malfunction during this plastic deformation of the material investigated and overlook the crack growth. Therefore, the crack gauge should be designed in order to have exactly the same or even less plastic deformation than the material under inspection. In that way, the crack gauge will break exactly at the point of the pre-appearance of the crack in the aircraft component.

Crack gauges can be made either of two or more constituent materials (composite) or of an isotropic material. Depending on the material that the crack gauge is made, it is very crucial that the gauge will break at the same moment as the component under investigation. In this study, in the test with the Airbus A320 slat-track, the attached crack gauge is made of aluminium and in the test with the aluminium 2024-T3 plates, the crack gauges were made of a conducting composite material. For the purpose of this study, a perfect bonding between the crack gauges and the main material is assumed.

4.7.2.4 Crack gauge made of an isotropic (uniform) material

In this study, only the tensile mode (opening mode I of the three fracture modes) has been taken into account since the fatigue tests performed were loaded in tension. The tensile mode distributes the stress in parallel to the length of the component. This stress distribution causes a crack which is perpendicular to the loading direction. Assuming that the load is applied uniformly on the material but also on the crack gauge then the tensile stress applied on the crack gauge is the following:

$$\sigma_g = \frac{F}{A_g} \qquad \text{Eq. 4.9}$$

where, σ_g is the tensile stress applied on the crack gauge, F is the load, and A_g is the cross sectional area of the crack gauge. For isotropic materials such as aluminium, the yield strength is known and it can be directly compared to another isotropic material. The yield strength is preferably used here as a limitation factor. This is because if the ultimate tensile strength is reached, it will cause permanent deformation in the material and the whole structure will fail.

4.7.2.5 Crack gauge made of a composite material

Composite materials are composed out of two or more different components and therefore have a more complex structure than isotropic materials. To examine the cracking of an underlying material in this study, a simple unidirectional fibre-reinforced composite material is investigated. Unidirectional fibre-reinforced composites have all fibres in one and parallel direction inside the matrix. It is assumed that the fibres and the matrix have a linear behaviour during loading. In the case of a crack gauge that is made out of this composite, then similar to the previous equation, the load that is applied on the material is the following:

$$F = \sigma_f A_f + \sigma_m A_m \qquad \text{Eq. 4.10}$$

where, σ_f and σ_m the tensile stress on the fibres and the matrix and A_f and A_m are the cross sectional area of the fibres altogether and the matrix respectively. If

A is the total cross sectional area of the composite, then a volume fraction of the fibres $V_f = \frac{A_f}{A}$ can be defined. The elastic modulus of a material can be described from the following equation:

$$Y = \frac{\sigma}{\varepsilon} \quad \text{Eq. 4.11}$$

where Y is the Young's modulus of a material, σ the tensile stress and ε the tensile strain. Hence, the maximum longitudinal tensile stress applied on the composite material is given by the following equation:

$$Y_C = V_f Y_f + (1 - V_f) Y_m \quad \text{Eq. 4.12}$$

where V_f and $1 - V_f$ are the volume fraction of the fibres and the remaining volume of the matrix respectively. Y_f and Y_m are the Young's moduli of the fibres and the matrix respectively. Y_C is longitudinal Young's modulus of the composite. The equation above represents the parallel combination of the mixing rule of composites. This approach assumes that there is perfect bonding between the fibre and the matrix. By knowing the material properties of the composite individual components, the behaviour during cracking can be quantified.

In a crack gauge made of a composite, usually one part is conductive and the other non-conductive. In order to have a reliable crack gauge, the conductive part should be the first that brakes together with the main material since it carries all the information. Therefore, it is important that the fibres will be those that break first and their ultimate tensile strength has to be the same as the main material under inspection.

The design of the crack gauge can be optimized by the appropriate selection of the materials that will comprise the composite. Therefore, the maximum amount of stress that is applied to the crack gauge before it breaks defines the Young modulus of the materials that are selected for the design of the composite. This is very important since the stress limits of the composite crack gauge should be compared with the stress limits of the aircraft component under investigation. It is necessary that the fracture behaviour and the stress limits of the crack gauge are known in order to follow the fracture behaviour of the main material in the critical places of the aircraft component that is monitored. It has to be noted that the role of the crack gauge is purely for crack monitoring and does not strengthen the aircraft component.

4.8 SHM using Lamb waves in ultrasonic testing

4.8.1 Damage evidence

It is vital that the structural materials of an aircraft are defect-free. However, in some cases, manufacturers allow a small damage tolerance that does not impair the structural integrity of the whole structure [139,140]. As it has been mentioned before, every metallic and composite part of an aircraft is subjected to fatigue, which along with corrosion in metallic parts, are the main reasons of cracking and failure of the structural materials. Small defects that can appear in the structural materials are not visible for the naked eye and can create a serious problem in the structural integrity of the aircraft. These defects can be cracks, inclusions, voids, small structural discontinuities, etc. in the metallic parts or a delamination, voids and cracks in the composite parts. Lambs waves in ultrasonic testing are used to propagate through the materials and reveal discontinuities cause by microscopic cracks.

As an example, the figure below shows cracks that have initiated near the surface of an aircraft part made from titanium [141].

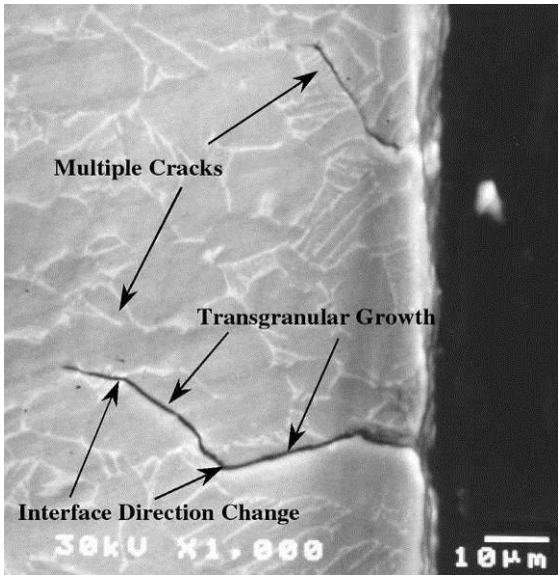

Figure 4.18: Multiple cracks due to fretting in titanium [141].

4.8.2 Theoretical background

SHM using Lamb waves is a technique that can detect cracks in the surface but also in the bulk of a material. The sensors that are mainly used for this application are probes or patches containing lead zirconate titanate (PZT) transducers as active

component. The principle of detection is based on the reflection or the decrease of the transmission of guided ultrasonic waves due to a defect inside the structure of the material. A PZT can be used either as an excitation source or as a receiver of acoustic waves. As a source, it excites acoustic waves in the material under investigation. As a receiver, it receives the acoustic waves that are reflected from the defect or that are transmitted through it.

This NDT technique is based on the phenomenon of piezoelectricity of the sensor material. When this material is subjected to external forces, the internal structure of the molecules is deformed and there is energy transformation from mechanical stress to an electric field and vice versa. The word piezoelectricity derives from the Greek words "πιέζω" (piezo), which means "pressurize" and "ήλεκτρον" (electron) which was the name for amber. Electron means "formed by the sun" and it was connected to the Greek god of sun "Ήλιος" (Helios). Amber was the first material that was studied for its electromagnetic properties by the Greek philosophers Thales and Theophrastus.

A piezoelectric material has the ability to generate voltage when it is subjected to force. This piezoelectric effect is a reversible process, which means that the material starts to deform when voltage is applied on it. This deformation generates the ultrasonic waves that propagate through the component under investigation. Ultrasonic is defined as the frequency beyond 20000 Hz, i.e. it represents the limit of sound that could be detected by humans. They are propagating through the material and interact with diverse boundaries of the material (edges, defects, voids) in a way that can be mathematically described [142].

As motivated above, when the PZTs are fed with alternating electric current in high frequency, they excite ultrasonic waves. Below is a sample table of the most common wave modes in solids.

Wave types in Solids	**Particle movement**
Longitudinal	Parallel to wave propagation
Transverse (Shear)	Perpendicular to wave propagation
Surface - Rayleigh	Elliptical orbit, single surfaces
Plate Wave - Lamb	Elliptical orbit, particle motion perpendicular to surface
Plate Wave - Love	Horizontal transverse (shear) waves
Stoneley wave	Wave guided along interface

Table 4.1: Types of acoustic waves in solids.

If the material under investigation is a thin plate, the sound waves propagate as guided plate waves (Lamb waves) in the case of lower frequencies. Since most of aircraft components are thin plate-like structures, Lamb waves are used in this study. Lamb waves have two main modes, the symmetric S_0 and the antisymmetric A_0 mode that are carrying most of the energy and are more convenient for practical

applications. Below is a representation of the particle movements of the solid in each mode respectively, where λ is the wavelength.

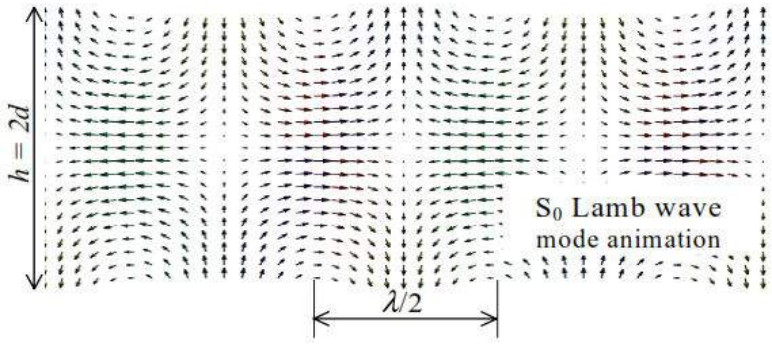

Figure 4.19: Symmetric mode of Lamb waves [143]

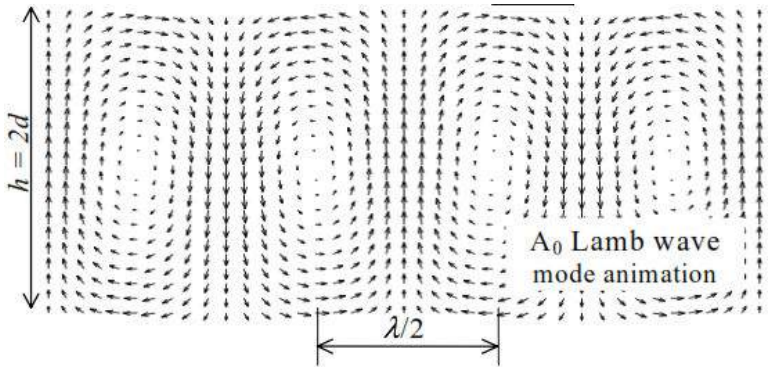

Figure 4.20: Antisymmetric mode of Lamb waves [143].

The Lamb waves are thus propagating in plate-like thin structures and in an infinite solid plate of thickness *d*, the wave (dispersion) equations are the following [144]:

$$\frac{\tan(\beta d/2)}{\tan(\alpha d/2)} = -\frac{4\alpha\beta k^2}{(k^2-\beta^2)^2} \qquad \text{Eq. 4.13}$$

$$\frac{\tan(\beta d/2)}{\tan(\alpha d/2)} = -\frac{(k^2-\beta^2)^2}{4\alpha\beta k^2} \qquad \text{Eq. 4.14}$$

where; $\alpha^2 = -\frac{\omega^2}{c_l^2} - k^2$ (Eq. 4.15) and $\beta^2 = -\frac{\omega^2}{c_t^2} - k^2$ (Eq. 4.16)

Letter k is the wave number of Lamb waves, ω is the angular frequency, c_l is the longitudinal wave velocity and c_t is the shear wave velocity. By finding the k, the phase velocity and the group velocity can be calculated.

4.9 SHM using optical fibres in acoustic emission testing

4.9.1 Damage evidence

Damages on aircrafts caused by impact are occurred often and the aviation industry is struggling to deal with that matter. Most commonly, aircrafts are subjected to impact with flying objects such as thick hail or birds that collide on them during flight at low altitudes and thus, most often during take-offs or landings. Bird strikes can cause significant damage on the aircraft and sometimes even fatal accidents if the birds are sucked by the jet engines [145-148]. The European Aeronautic Defence and Space Company (EADS) is highly concerned with the matter and is using computational methods to simulate bird strikes in order to optimize the bird-proof design of the jet engines [149]. One of the most well-known examples of bird strike incidents was the flight 1549 from US Airways operated on January 15, 2009. The Airbus A320 shortly after take-off had to proceed to an emergency landing on the Hudson River in New York after losing both engines due to bird strikes [150].

Figure 4.21: Photo of bird strike damage on the fuselage of a Boeing B767 aircraft [21].

Another cause of impact damage is the accidental collision of the ground support equipment vehicles with the parked aircraft. For example, the catering vehicles, belt loaders, fuel tanks, passenger stairs vehicles etc., are operating near the parked aircrafts and if they are not driven carefully, a collision can severely damage various aircraft components.

Figure 4.22: Photo of an aircraft's wing collision with a fuel tanker [151].

These examples are giving the wrong impression that these damages can easily be monitored just with a simple visual inspection. What is not often known is that the damage from impact, especially in the case of composites, even if it is not apparent visually, it could have destroyed the structure below the surface. This kind of damage is called Barely Visible Impact Damage (BVID) and even if it cannot be detected visually, it can create a significant amount of core damage and delamination in the composite structure [152]. As mentioned above, BVID is very likely to occur in sandwich-structured composite materials where the real damage from impact could be hidden below the outer surface. Many helicopter and airplane manufacturers are using this kind of composite material usually in a honeycomb structure for the construction of important structural parts such as tail booms, wings and others.

4.9.2 Theoretical background of acoustic emission

The first written records giving the fundamentals of acoustics are attributed to the philosopher Pythagoras of Samos from the 6^{th} century BC. Empedocles at 5^{th} century BC was the first who claimed that light has a limited velocity and Aristotle the first who studied the nature of acoustics at 4^{th} century BC [153]. The method of acoustic emission is based on the detection of acoustic waves that are produced due to an impact on the surface of a material or during internal redistribution of stresses throughout its structure. The acoustic waves, that are elastic waves, are propagating within the aircraft structure and cause micro-displacements that can be detected by appropriate sensors [154,155]. In contrast to ultrasonic testing, in the acoustic emission approach there is no need for external acoustic excitation into the material since the acoustic energy is generated from the impact or stresses. The acoustic emission method is analysing these acoustic waves propagating through the medium and picked up by the sensors [156]. The signals arriving at the sensors are giving important information regarding the cause of damage initiation and the progress of a structural discontinuity in a material.

Two kinds of sensors are used in this study for the detection of the acoustic waves created by the damage. The first NDT method utilizes PZTs and the second one uses single-mode (SM) optical fibres in a polarimetric setup. The theoretical part of the impact detection using SM fibres is discussed here.

An optical fibre consists usually of four parts, the core, which is pure glass, has the size of a human hair and carries the optical light, the cladding, the buffer coating and the protective jacket, as can be seen from the figure below.

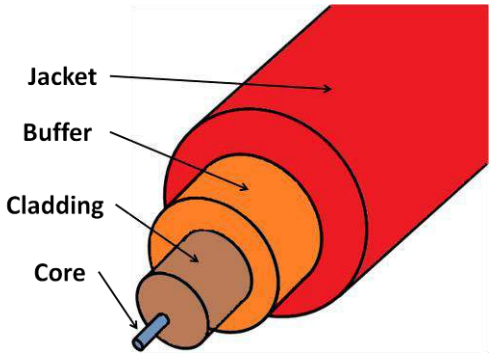

Figure 4.23: Parts of the single-mode optical fibre.

This study focuses on the acoustic waves caused by impact and the interference of these waves with SM optical fibres. The detection principle relies on theintensity modulation of the waveform of the light inside the optical fibre. The modulation is caused by the acoustic waves that hit the fibre and change the polarization of the light inside the SM fibre. Polarization is the orientation of the electric wave vector of the electromagnetic wave. The word polarization is derived from the Greek words “πόλος” (polos), which is the edge of the axis of a spinning sphere and “ίζειν” (izein), which means to employ.

Light is an electromagnetic wave that propagates through the core of an optical fibre starting from a laser light source. The wave velocity depends on the medium through which is travelling and it is given from the following equation.

$$c = \lambda \nu \quad \text{and} \quad \frac{c}{\upsilon} = n \qquad \text{Eq. 4.17}$$

where λ is the wavelength, ν the frequency of light wave, c the velocity of light in vacuum, υ the velocity of light in the medium and n the refractive index. The refractive index is different in each medium and is responsible for the change of the speed of light through it together with the change of its direction at an angle θ. The refractive indices, velocities of light and the angles of the direction of light are given from the following equation of Snell’s law.

$$\frac{\sin\theta_1}{\sin\theta_2} = \frac{\upsilon_1}{\upsilon_2} = \frac{n_2}{n_1} \qquad \text{Eq. 4.18}$$

where ϑ_1 and ϑ_2 are the angles of incidence and refraction respectively.

When there is an impact on the aircraft part under investigation, an acoustic wave is produced. The acoustic wave strikes the optical fibre and the sound pressure modulates the birefringence of the optical fibre leading to a change of the polarization properties of the two perpendicular modes (electric and magnetic) of the polarized travelling light inside the core of the fibre. This is related to a final mutual phase shift of the two perpendicular modes. The figure below, shows the phase shift of the wave inside and along the core of the SM optical fibre at an angle β° caused by the acoustic wave that is generated by impact or internal redistribution of stresses.

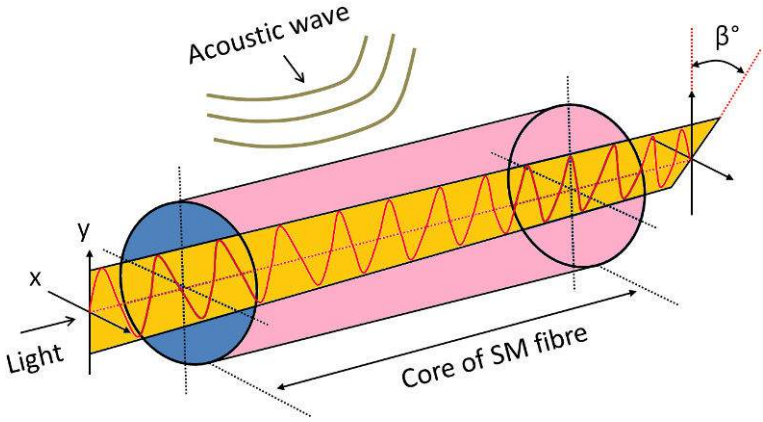

Figure 4.24: Phase shift at an angle β° at the output of the fibre.

Explanatory steps – how it works:

1. Acoustic wave (pressure wave) approaches the fibre after impact.
2. Pressure wave pressurizes optical fibre which is normally isotropic.
3. Optical fibre loses isotropy, optical properties get a gradient, anisotropy.
4. The optical property that casues anisotropy is called birefringency.
5. Birefringency makes both independent modes to propagate with different velocities changing finally the polarization.
6. At the polarization filter, the changed polarization appears as an intensity change (angle deviation in degrees).
7. Intensity change is detected by the light diode into a change in voltage.

8. The voltage signal is filtered to get a rid of unwanted frequency components.

The polarisation filter at the output of the sensing fibre isolates a particular polarization state that is analysed and compared to the reference polarization state of the light coming from the light source. The reference polarization state also minimizes the influence of the environmental disturbances to the signal. This difference in polarization is detected and analysed from the polarization analyser.

The intensity of the light that travels according to this polarization state varies due to the birefringence. The change in the light intensity is therefore an integrated response of all the phase dependent changes along the length of the active fibre sensor. By analyzing the intensity modulation of the light inside the fibre any external vibration that is caused by impact or stress redistribution can be detected.

Figure 4.25: AGILENT high speed polarization analyzer/controller (N7788B-400).

4.10 SHM for corrosive liquids

4.10.1 Damage evidence

Besides fatigue, corrosion is one of the most critical problems that interfere with the structural integrity of an aircraft. Fatigue itself can accelerate corrosion (stress corrosion) and corroded materials that are subjected to fatigue are exposed to a possible sudden failure. Every metallic part on the plane is likely to be subjected to corrosion, even in the case of proper maintenance. Corrosion can appear in any area and special attention is required in areas that are difficult to approach. These areas include confined spaces and parts that need to be disassembled in order to be inspected. For example, the floor beams inside a commercial aircraft's cabin are located below the floor panels and the seats of the passengers. During regular maintenance of this aircraft, the team has to disassembly all the seats and floor panels in order to reach the floor beams and do the inspection for damage detection. This procedure can be very costly since the aircraft needs to stay on the ground for a longer period. In the figure below, evidence of corrosion on the seat tracks that are attached on the floor beams is evident. The corrosion is in an advanced level and sometimes the passenger seat can be dislocated with a small amount of force.

Figure 4.26: Corrosion on seat tracks attached on floor beams from the cabin of an Airbus A320 aircraft.

In a cabin of a commercial aircraft, different kind of liquids can be spilled on the floor and absorbed through the carpet and reach metallic parts following narrow pathways of damaged sealings. The liquids can be either a variety of beverages that are served from the crew or even water that enter into the cabin during boarding on a raining day or from the lavatories. Aqueous liquids that are concentrated in confined spaces under the floor can increase the humidity levels and initiate or accelerate corrosion. The proposed sensors in this study can be positioned inside small pathways that exist on the floor beams between floor panels. They can detect aqueous liquids that are concentrated inside these pathways using the percolation effect. The theoretical background of the percolation effect is discussed in the following paragraphs.

4.10.2 Theoretical background

Percolation was originally the process of passing a fluid through a substance (needed for filtering). The theory behind this process is called the percolation theory and describes the connectivity of particles in materials with a randomised distribution. The probability of the movement of the liquid through the porous material can be explained mathematically. The liquid particles have a probability p to pass through the openings of the porous material and $(1-p)$ not to pass. The probability p creates a bond or a path that the liquid can move from one side to the other. The most common percolation model is the bond percolation model, where all bonds are independent. The bond percolation model can be illustrated as a lattice with bonds for the liquid particles that can be either connected (passage open) or not connected (passage closed). This kind of lattice is presented in the figure below.

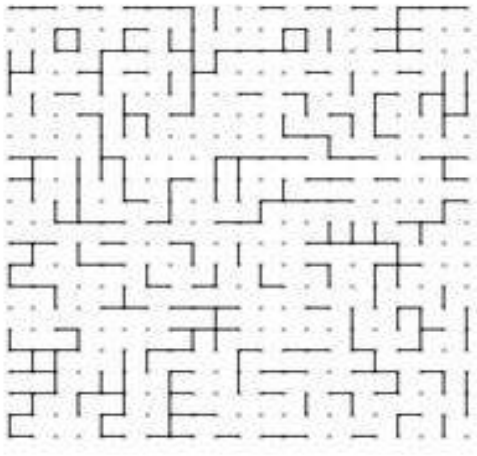

Figure 4.27: Lattice of a bond percolation model [157].

A unique sensor has been developed in the NDT group of the MTM department at KU Leuven, and it is used for the detection of aqueous liquids that can cause corrosion problems in confined areas of an aircraft. The sensor is made of an organo-ceramic composite. The ceramic part of the composite sensor is the conductive part consisting of titanium carbonitride (TiCN) particles. This conductive compound is embedded into a hydrophilic matrix (polyvinyl alcohol - PVA) that is exposed to spilled aqueous liquids. The concept of detection is based on the swelling of PVA particles that induce the collapse of percolation conductivity of the composite part when it is hydrated.

To enhance the compatibility of the two compounds and the stability of the composite, a reasonable contact between the TiCN and PVA is necessary during mixing. In general, PVA is used as a binder in the ceramic industry and it has excellent attribute of wettability [158]. The wettability factor is important since the distribution of PVA in the PVA-TiCN mixture affects its forming and handling and the strongly bonded hydroxyl group in PVA facilitates its adsorption ability. The adsorption of PVA is based on the hydrogen bonding of its hydroxyl group. Hydrogen bonding still remains a puzzle in the theoretical study of quantum chemistry but it can give an accurate description of thermophysical properties of such fluids. However, prediction of thermophysical properties of mixtures containing hydrogen bonding components is feasible by means of computational molecular simulation [159]. The hydrogen bonding of the hydroxyl group of PVA requires an acidic environment for adsorption. Hydrolysis of TiCN shows that the product is acidic giving H^+ ions. The chemical reaction for the hydrolysis of the TiCN is the following:

$$TiCN + H_2O = TiCNO + 2H^+ + 2e^-$$

The chemical relationship above confirms that PVA will wet TiCN due to hydrogen bonding. Therefore, the hydrophilic matrix absorbs the aqueous liquids that are mixed with the composite conductive compound.

In the case of the percolation sensor, the particles of the spilled aqueous liquid are absorbed by the hydrophilic matrix (PVA) of the composite mixture. Due to PVA's solubility in water, it will first swell and then dissolve. The presence of pores in the mixture will also facilitate the process of liquid absorption by capillary action, see figure below.

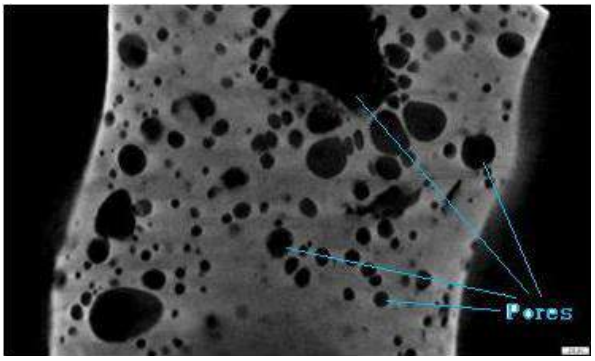

Figure 4.28: X-ray micro-CT picture of the pores present in a TiCN/PVA composite mixture [160].

After a small time period, the sensor will have taken up water from the aqueous liquid, and it will have caused swelling of the PVA particles, pushing away from each other the touching conductive particles of TiCN. There is a moment that the particles of TiCN cannot foreseen in the conductivity and the sensor will have a sudden "jump" in its resistance. The resistance of the sensor will increase dramatically of a factor of thousands or millions from the baseline. This point is referred as the percolation threshold and the material loses essential parts of its conductivity showing very large changes in resistance magnitude [161]. As a result, the sensor stops being conductive due to the collapse of the percolation threshold of the conductive compound (TiCN). This indicates the wetness of the area and which results in a warning. The composite part of the sensor can be dried again to reach the previous conductivity. Therefore, it is a reversible process and the sensor can be used again.

"I have not failed. I've just found 10,000 ways that won't work."

Thomas Alva Edison (1874 -1931)

CHAPTER 5

Flat coil sensors for SHM of aircraft components using eddy current technology

The aluminium skin of an aircraft is seriously loaded in fatigue especially during takeoffs, landing and turbulences. The repeated stresses can result in fatigue cracks, especially near stress concentrations such as edges, fillet transitions or connection areas where rivets are present. In some cases, the fatigue damage can lead to a fatal disaster when appropriate inspection techniques are not in place. The SHM method presented here is using an eddy current flat coil sensor made at the KU Leuven.

5.1 Motivation

In this PhD study the eddy current technology inspired a number of flexible small flat coil sensors that are attached to the aircraft component and that could even be connected together to form a sensor network. It is an attempt to create an integrated system that can continuously monitor cracks in aircraft components that are subjected to fatigue and save time and money from the scheduled maintenance programme. The NDT solution in this PhD study differentiates itself from the classical external eddy current equipment since it proposes integrated sensors in the aircraft component using simple impedance measurements and it is specifically designed in order to fit on top of the rivets in a doubler repair or in lap-joints all over the aircraft where microscopic surface cracks need to be monitored. Integrated solutions can be efficient and effective and with a combination of certain instrumentation they can be used during flight offering immediate measurements.

The proposed flat coil sensors use eddy currents induced in the material under investigation and they are mounted on the aircraft components at critical points that are more likely to fail due to fatigue conditions [162]. The integration process can be done in cooperation with the aircraft component manufacturer at an early stage of the production or assembly of the component or even during scheduled maintenance at the technical departments of the airline company. The sensors are positioned between the surface of the component under investigation and the protective coating layers. The protective coating layers on most of the metallic aircraft parts consist of a primer and a top-coating. The material of the sensor is flexible and has the ability to slightly bend. This makes the specific sensors applicable in areas with curved surfaces such as the fuselage or the wing of an aircraft.

A promising SHM technology that can monitor critical parts of an aircraft is thus based on eddy currents that make use of the alternating currents that are excited in the material under investigation and that create opposing magnetic fields to the magnetic field that causes them [163]. The defects in the specimen cause local interruptions of the induced eddy currents, which result in measurable impedance variations in a nearby search coil [164].

The eddy current technology has numerous advantages:

- It is a less complex damage detection technique than other detection systems providing simple data interpretation.
- It can give reliable measurements even if there is no direct contact between the material under investigation and the sensor.
- The weight of the sensors as well as the cost of equipment can be kept relatively low.

- It can be used in a large variety of frequencies determining penetration (detection) depth [165].

There are certainly some limitations to be considered.

- Scanning area of one eddy current sensor is relatively low.
- Eddy current only allows measurements on conductive materials.
- It has generally a relatively shallow depth of penetration (skin effect), therefore, is mostly used for plate structures.
- Very small discontinuities that are parallel to the field flow are difficult to detect [166].

5.2 Materials and methodology

5.2.1 Basic theoretical background

The basic principle is as follows, see also 3.2.1: when a coil is fed with an alternating current, it builds an alternating magnetic field (primary, magnetic field). This field is encircled by an electric field according to Faradays law of induction,

$$\oint \vec{E}\,\vec{ds} = -\frac{d\Phi_B}{dt} \qquad \text{Eq. 5.1}$$

Where E is the electric field through a closed loop and Φ_B is the magnetic flux through a surface encircled by the coil. In a conductive material, this alternating electrical field induces eddy currents. The eddy currents are confined to shallow depths near the conductive target surface. Their effective depth (δ) is given by,

$$\delta = \frac{1}{\sqrt{\pi f \mu_0 \sigma}} \qquad \text{Eq. 5.2}$$

In the formula above, *f* is the frequency, μ_0 is the magnetic permeability (H/mm) and σ is the electrical conductivity of the material under investigation. These eddy currents build up their own magnetic field (opposing magnetic field), which will be superimposed on the primary magnetic field. As a result, the impedance of the coil is changing. This impedance variation carries information of the electromagnetic properties of the material and the geometry of the system under inspection.

Figure 5.1, below, shows the formation of the eddy currents and how an opposing magnetic field is generated when the coil is approaching the conductive material.

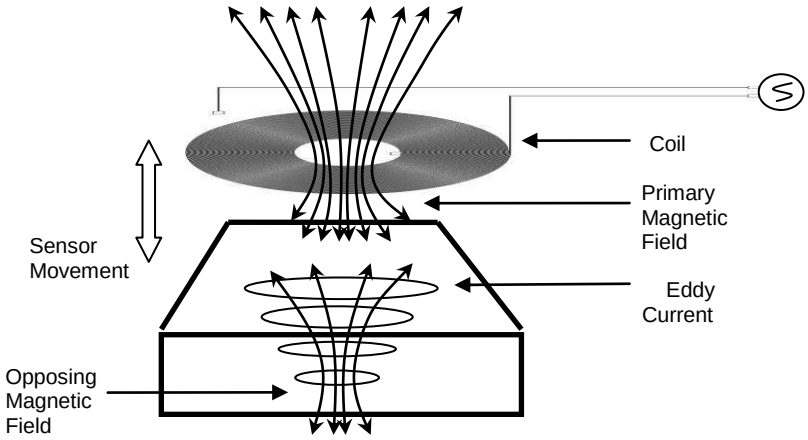

Figure 5.1: Eddy currents in a conductive material.

In this study a unique eddy current flat sensor is investigated for SHM of aircraft components. The sensors were made with the method of etching and printing copper on a Kapton foil.

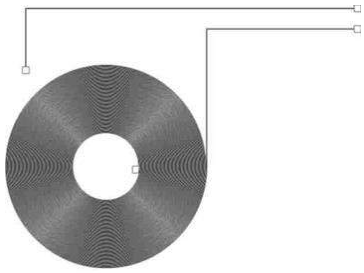

Figure 5.2: Eddy current flat coil sensor drawing.

Figure 5.2 shows the initial design of the flat coil sensor in AutoCAD. It is designed to fit exactly on top of a rivet that is used to connect two aluminium plates in an aircraft structure.

5.2.2 Design of the sensor

The sensor was tested on plates of the aluminium 2024-T3 alloy, which is a frequently used high strength aluminium alloy for aerospace applications. The coil has 50 windings and the width of each line as well as the pitch between them is 100 µm. The thickness of the Kapton foil is 25 µm, followed by an adhesive layer of 25 µm. The thickness of the copper that is printed on it is 35 µm. The material used for the coil is copper and the carrier material is made of a polyimide film (Kapton). Kapton has many advantages as it is flexible and almost transparent, which assists

to position the sensor on the plates with high accuracy. Furthermore, it can remain stable in a wide range of temperatures, from -273 to 400 °C. This is essential since an aircraft undergoes a variation of temperatures during its lifetime.

According to the "Handbook for Sound Engineers" [167], the normalized (divided by the magnetic constant μ) inductance of the spiral coil can be calculated with the Wheeler's equation shown below:

$$L = \frac{B^2 N^2}{8B + 11C} \qquad \text{Eq. 5.3}$$

Where, B is the radius of the windings, N is the number of windings and C is the thickness of the winding of the copper. Using this equation, a value of 28.88 μH is obtained for the flat coil sensor. The experimental inductance measurements with the flat coil sensor after several cycles of fatigue gave values of 19,5 – 23,9 μH.

5.2.3 Sensor integration in aerospace applications

Figure 5.3 below shows how the flat coil sensor can be attached directly on top of the rivets that connect two aluminium plates. Rivets are still the main method connecting most of the aluminium sheets within fuselage structures. The manufacturer or the airline company can provide the necessary information regarding the most critical areas for potential cracks or existing cracks that are allowed to propagate within a tolerance (e.g. after stop-drilling – a method to slow down the growth of an existing crack). In that way, the number of sensors, cables and total weight can be reduced. Such as mentioned above, these sensors can be used as a tool to follow the crack in areas where damage tolerance is accepted and where crack propagation is allowed to be monitored before the replacement of the part is needed.

In this study, also the reliability of the eddy current sensor to detect a fatigue crack in the aluminium 2024-T3 plates was investigated. In classic eddy current inspection techniques, the sensors are moved above and along the areas under investigation. The flat coil sensors tested in this study are embedded and attached on the areas under investigation. Therefore, in this SHM method, the impedance is determined at a fixed position and is related to the dimension of the crack.

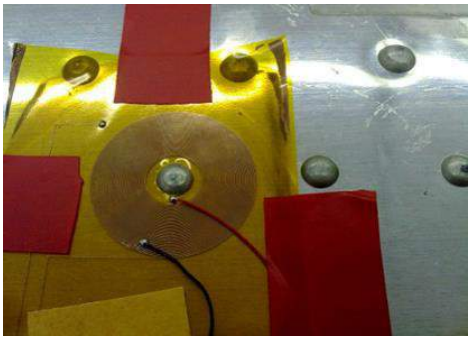

Figure 5.3: Flat coil sensor attached (the tape is used here for demonstrative purposes) on an aluminium sheet with rivet connections. The sensor fits exactly on top of a rivet and monitors a possible crack appearance.

5.3 Sensor integration and setup

5.3.1 Procedure of embedding the sensor

A streamlined integration of SHM sensors is important to ensure affordability of the whole SHM system. It is also essential that the sensor is able to operate efficiently at any time and loading condition. In this study, most of the aluminium parts provided and investigated had to be tested in relatively realistic in-flight conditions.

Prior installation, all aluminium parts of an aircraft have to be coated with two layers of an epoxy primer and a top-coating made of polyurethane. The first layer of the primer is directly applied on the anodised surface to maximize the protection towards corrosion. The top coating is applied for UV resistance, to colour and to resist fluids and chemicals. The flat coil sensor was embedded between the second layer of the primer and the finishing top-coating, see figure 5.4. The above procedure was followed to avoid the use of any additional adhesive for the sensor attachment. Only a small volume of epoxy glue was used on the sensor to attach it on the primer. Then, the sensor was painted with the top-coating together with the specimen under investigation. During the fatigue test, the sensor remained stable on the plate and was removed from the coating only when the plate was broken.

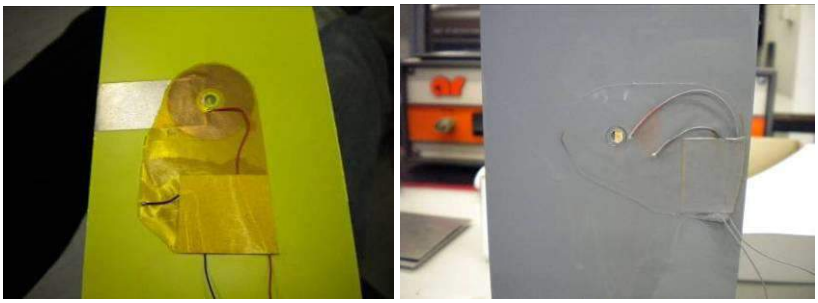

Figure 5.4: Foil sensor glued on the 2024 T3 Al plate, over the primer (left) and between layers (right).

5.3.2 Fatigue parameters

Fatigue cracks are the most common cracks that appear in the fuselage of an aircraft. The aluminium plates, 300 mm (length), 80 mm (width) and 1mm (thickness), were tested in a servo-hydraulic fatigue testing machine from Schenck AG (now Instron Schenck Testing Systems GmbH). This fatigue machine has a maximum load capacity of 160 kN. When simulating the cyclic loading, see figure 5.5, the sensor measurements would give information about the crack growth [168]. For all the tests carried out, the sinusoidal load had a maximum value of 12 kN and a minimum of 4 kN. The frequency of the cyclic load was 15 Hz.

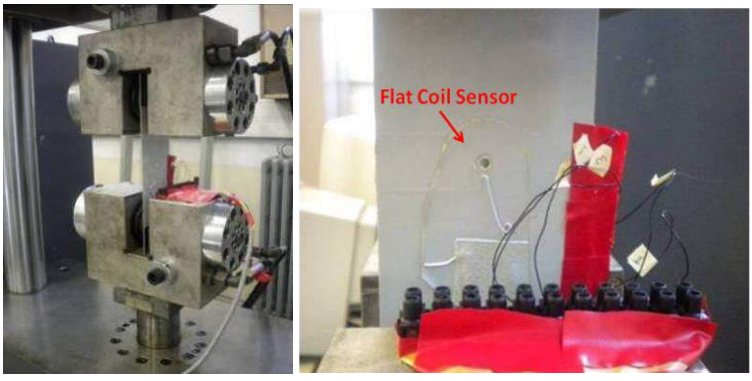

Figure 5.5: Final setup on Schenck Hydroplus fatigue machine.

5.3.3 Instrumentation

Electromagnetic impedance spectroscopy is used to collect the data. From the Cypher Instruments C-60, see figure 5.6, the electromagnetic frequency chosen for further analysis is 15 kHz. The analysis for electromagnetic frequencies of 5 kHz and 10 kHz provided the same general information.

Figure 5.6 shows both instruments used to measure and record the phase, impedance and inductance of the coil sensor during the fatigue experiment. The Cypher C-60 is an Impedance-Amplitude-Phase Analyser from Cypher Instruments Ltd, and it was used for the phase and impedance acquisition. The LCR Meter HM8018 from HAMEG Instruments GmbH was used for the inductance acquisition.

Figure 5.6: Cypher C-60 (left) for phase and impedance and the LCR HM8018 (right) for inductance acquisition.

5.4 Results and discussion

5.4.1 Phase and modulus of impedance

In figure 5.7, the phase and modulus of impedance of the sensor over the electromagnetic spectrum as recorded by the C-60 Cypher instrument is presented. The measurements were taken when the fatigue crack of the plate was open, therefore after 90,000 cycles the plate was held at the mean fatigue load (8 kN).

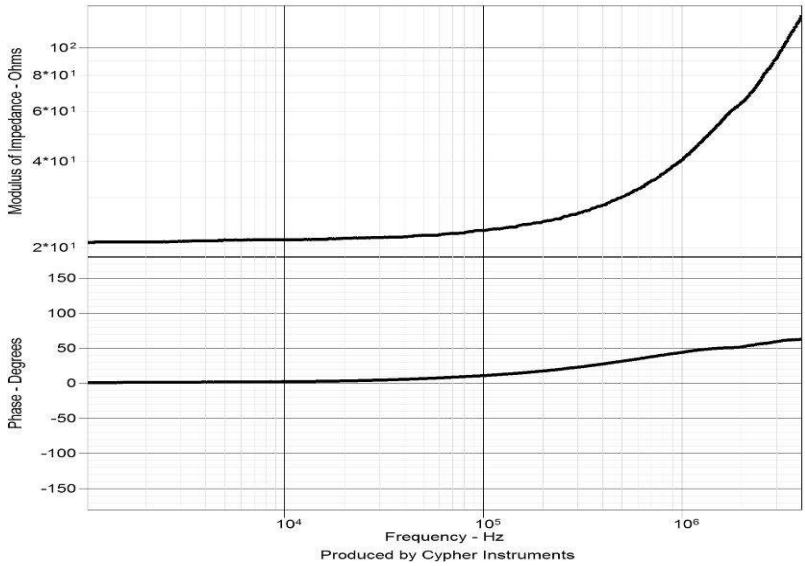

Figure 5.7: The phase and the modulus of the impedance spectrum for the plate with a hole recorded after 90,000 fatigue cycles and during static load of 8 kN.

5.4.2 Results of crack monitoring

The number of cycles generated in the tests went up to 120,000 cycles. This amount of cycles is enough to create a crack with a size of 12 mm in the plate. To introduce a stress concentration point from which the crack will initiate, a drill was used to create a hole of a 4 mm diameter before in the middle of the plate simulating the hole from a rivet. The crack initiated at both sides of the hole and propagated horizontally opposite to the load direction.

The crack growth was responsible for the change of impedance in the flat coil sensor. Figure 5.8 shows the size of the crack in millimetres, for both sides of the hole versus the number of cycles. This physical size of the crack in the plate was measured with a small ruler and a micrometer. The crack was not increasing equally at both sides of the hole. After several numbers of fatigue cycles, the fatigue machine was stopped in order to inspect the cracks. During the stop two static loading conditions were applied to the plate. In the first condition, the static mean load of 8 kN was applied to keep the crack open and in the second condition a minimum load (~ 0.4 kN) was applied and the crack was not visible with the naked eye. At 0.4 kN the crack microscopically is not closed. Figure below gives the average crack size on both plates during fatigue tests.

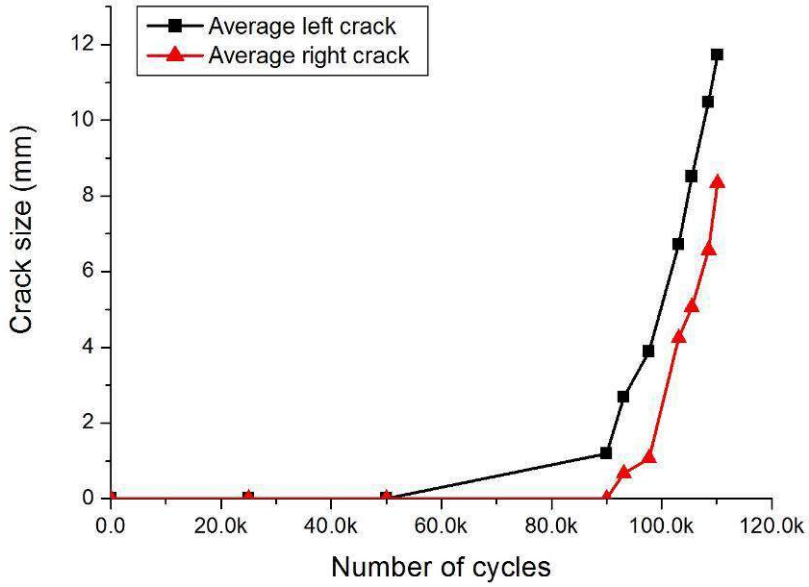

Figure 5.8: Average crack growth from both plates as a function of the number of cycles at load frequency: 15 Hz, mean fatigue load 8 kN, maximum fatigue load 12 kN and R= 0.3.

In figure 5.9, the line with the small black squares shows the impedance measured at a fatigue cycle of 15 Hz when the crack is closed (~ 0.4 kN) and the red triangles when the crack is open (8 kN) after several numbers of cycles. During fatigue testing at both plates, the crack started to grow at the hole after approximately 50,000 cycles. The impedance is increasing as the crack is growing below the surface of the flat coil sensor. When the number of cycles was around 100,000, the crack growth was fast. At the same time the instrument recorded very high impedances. After about 110,000 cycles, the plate broke and the impedance of the eddy current sensor gave an infinite value. The impedance measurements for the open and closed crack have a small deviation, especially up to 94,000 cycles, which is desirable for testing since the sensor should give almost the same measurements in open and closed conditions in order to detect the crack in both cases.

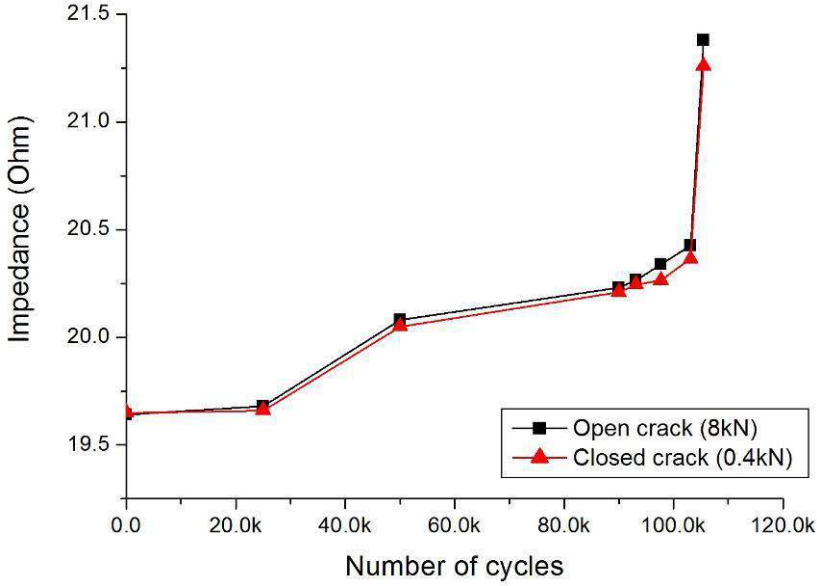

Figure 5.9: Arithmetic mean of impedance measurements (magnitude) from both plates when crack is open (8 kN) and closed (~ 0.4 kN) (at an electromagnetic frequency of 15 kHz).

In the first test series, two plates were subjected to the same fatigue conditions in order to test the repeatability. It is important for the flat coil sensor to give similar measurements in open and closed crack conditions. The reason is that while the crack is open (with load) or closed (no load), the sensor should always indicate the existence of the crack despite the loading conditions. A hole is created in the middle of the plate to assist the crack initiation on the plates. Before creating the hole, the plates were tested with the same fatigue load conditions to investigate the durability of the sensor during the full number of cycles. In figure 5.10, the open circles represent the relative difference of impedance ΔZ/Z (%) of the coil sensor on the plates without a hole or crack. The relative difference of the electrical impedance is the difference between the measured values at any point Z_n and the arithmetic mean value Z_0 over the arithmetic mean value Z_0. Z_0 is the average of all impedance measurements on the plate without hole before the crack initiation and is used as a reference for the tests. The results in figures 5.10 and 5.11 below are using this approach.

$$\Delta Z / Z(\%) = \frac{Z_n - Z_0}{Z_0} 100 \qquad \text{Eq. 5.4}$$

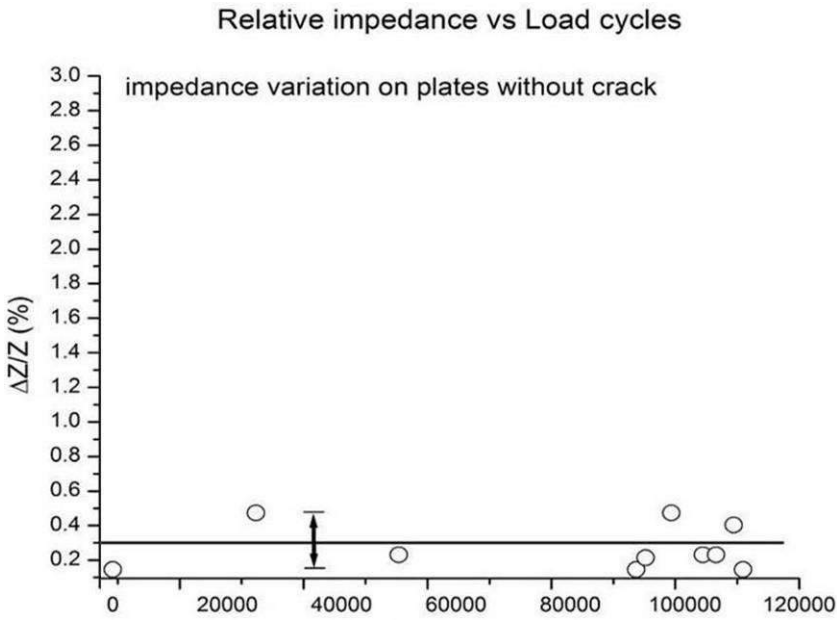

Figure 5.10: Impedance variation (magnitude) as a function of the number of load cycles on plates without crack.

Figure 5.10 presents the relative difference of impedance as a function of the number of load cycles at the plates with no hole and no crack. The impedances were recorded at two identical plates without any hole in fatigue load conditions typical for reliability testing. As mentioned above, the average of the first measurements was taken before crack initiation. The results show that the values follow a steady line and deviate from the initial value with a small uncertainty of 0.9 % during the total number of load cycles. Additional measurements were recorded after 80,000 cycles because that is the point where a crack starts to appear at the next test with the hole. Figure 5.11 below shows the relative difference of impedance measurements on the plates with the hole and when a crack is present. The relative difference of impedance is presented as a function of the crack growth in the plates with the hole. This graph shows that the relative difference of impedance is increasing at the same time as the crack size is also increasing. The black triangles show the relative difference of impedance measurements on each plate when the crack is closed and the white triangles when the crack is open. As the crack is growing, the impedance measurement thus shows a positive trend. Although small uncertainties are apparent, it can be seen that the relative difference of impedance on the flat coil sensor is increasing in proportion to the crack growth. In that way the damage caused by small cracks can be monitored.

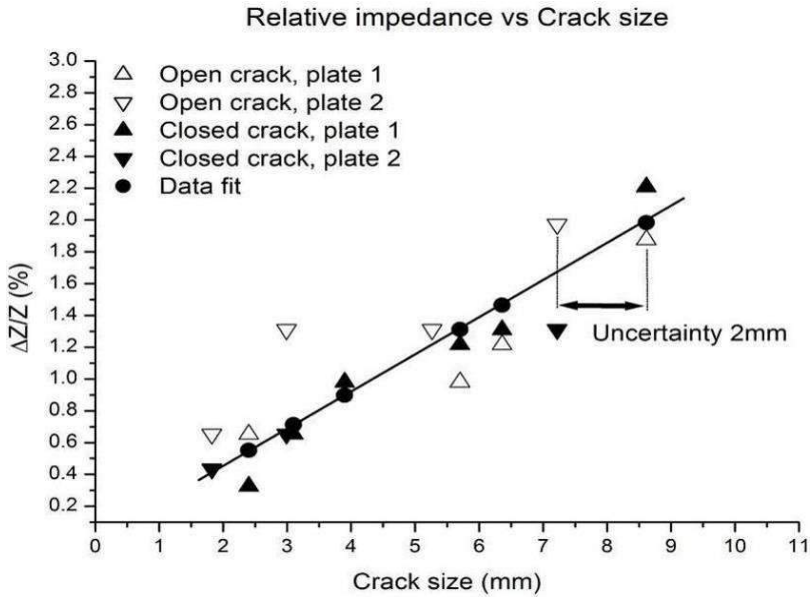

Figure 5.11: Impedance variation as a function of the crack size on plates with crack.

5.4.3 Temperature dependence of impedance measurements

In order to check the reliability of the results, another test series was performed simulating the temperature conditions during flight. The sensor was attached using the same procedure as described in paragraph 5.3.1. A usual range of temperature of an aircraft during flight is between -50°C to +80 °C. However, in the case that a component is placed next to heated areas such as the jet engines, the temperature can be even higher. The purpose of this test was first to test the durability of the flat coil sensor and second to investigate how the temperature influences the impedance measurements. In order to reach -50°C, the plate was positioned inside an insulated box filled with dry ice (solid form of carbon dioxide). To obtain higher temperatures, the plate was placed into an oven that was gradually heated up to +80 °C.

From -50°C to room conditions (~ 22 °C), the temperature was controlled by adding methanol, as it accelerates the temperature rise, and it was monitored by a thermocouple. The impedance measurements were obtained using the LCR HM8018 multimeter. The setup can be seen in the figure below.

Figure 5.12: Cooling system for the Al 2024-T3 plate using dry ice and methanol.

The plate with the embedded flat coil sensor was tested two times for reliability purposes in the respective temperature range. The first test (test 1) was performed before the plate was subjected to fatigue. The second test (test 2) was performed during a fatigue test but without the creation of a hole, thus no crack was present. During the fatigue test and after every 30,000 fatigue cycles (120,000 fatigue cycles in total), the plate was removed from the Schenck Hydroplus fatigue machine and was placed inside the insulated box as well as later on in the oven to cover the desired temperature range. Figure 5.13 on the next page shows how the temperature influences the impedance measurements.

A third test was performed in fatigue conditions but this time with a hole on the Al 2024-T3 plate for crack initiation. This test followed the same procedure with the previous ones and the relative difference of impedance was calculated in the mentioned range of temperature.

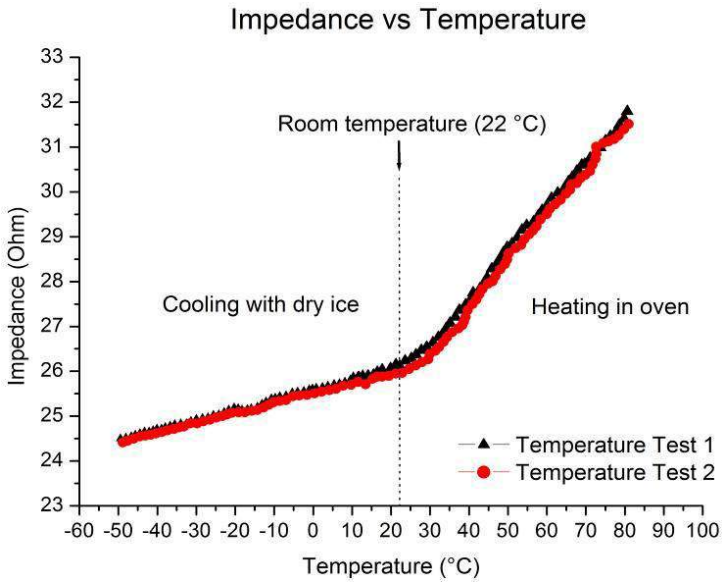

Figure 5.13: Impedance (magnitude) variation on the flat coil sensor as a function of the temperature. The plate is without a hole. At room temperature, the plate was placed inside the oven where the temperature incline after 22 °C was faster and showed higher relative differences of impedance. This indicates that the values do not represent equilibrium conditions at each temperature point.

According to figure 5.13 above, during the heating phase from -50 °C to room temperature (22 °C) the relative difference of impedance corresponds to roughly 1.0 %. It can also be seen that the relative difference of impedance has higher values during the heating phase from room temperature up to 80 °C. The results in figure 5.14 below show the relative difference of impedance on the flat coil sensor in the proposed range of temperature. From the graph below, it can be derived that in the beginning of the test and up to room temperature, for 1.0 % relative difference of impedance, the crack corresponds to 2 mm. The temperature dependence is coming from the temperature coefficient of the wires of the coil that are made of copper. The Impedance of the flat coil was measured both during heating and cooling but only the values at -50 °C, 22 °C and 80 °C where at equilibrium conditions and for these values the test is reversible.

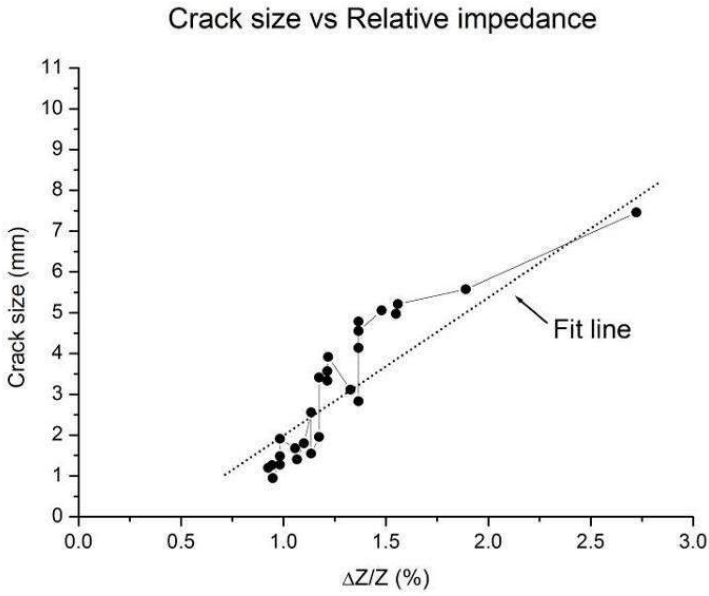

Figure 5.14: Impedance variation as a function of the crack size on plates with crack initiation from the hole.

It can be seen that there is an analogy to the previous tests performed at room temperature. From a crack initiated from a hole of a diameter of 1 mm, the relative difference of impedance (black dots) is following a positive trend. There are some deviations from the fit line possibly due to the sensor's higher sensitivity to temperatures higher than the room temperature and also from the small deformation of the sensor due to the crack. However, the relative difference of impedance is increasing with the crack growth.

5.5 Conclusions

The SHM method with the eddy current flat coil (ECFC) sensor is based on electromagnetic impedance spectroscopy using eddy currents. These flat coil sensors are embedded between the primer and the top-coating on aluminium sheets. An increase of the relative difference of impedance is observed for the flat coil sensors in proportion to the crack growth in the aluminium 2024-T3 plates tested in fatigue. According to the results, a crack size of 10 mm corresponds to a 2% change of relative difference of impedance.

The tests in the proposed temperature range showed that the sensors are durable but also that their performance can be affected by the temperature. In the previous tests, a simple thermocouple thermometer was used for the temperature measurements. The temperature dependence needs to be taken into consideration and therefore for practical use in operations temperature sensor is required.

The final target is to create an array of sensors that can even be embedded on the surface of the materials of the critical areas and can be used as an online crack detection system. The flexible design (eg. ability to bend and be attached on curves) of the ECFC sensor allows it to be used as an embedded sensor for various aluminium plate-like parts or for surfaces with rivets (e.g. doubler repair) in order to monitor small cracks that are created due to fatigue conditions.

There is still room for improvement concerning the design of the coil sensor as well as for the attachment of the sensor between the primer and the coating. Furthermore, the reproducibility tests in various environmental conditions (temperature-humidity during flight) can give a total overview on the sensor's reliability. Possibilities for other means of connection and data acquisition that will reduce the weight and the use of cables are under consideration, e.g. wireless connection.

The Probability of Detection (POD) using Eddy Current Flat Coil (ECFC) sensors as a SHM method depends on its electromagnetic signal boundaries. However, every change of the surrounding parameters will be considered as signal and this is a condition for quantifying the POD for this SHM method. The following table below shows the advantages and disadvantages using ECFC sensors as a SHM method.

Advantages	**Limitations**
Able to detect cracks below coatings	Temperature dependence
Suitable for riveted connections	Local measurement
Flexible and thin design, easy to install	Works only on conductive materials
Possibility of an array to cover larger areas	Wiring might be complicated
Ability to detect cracks in multi-layer structures	In the case of repair, aircraft component needs to be dissembled and re-painted

Table 5.1: Advantages and disadvantages of flat coil sensors as a SHM method.

Published papers and proceedings
"Crack detection in aluminium plates for aerospace applications by electromagnetic impedance spectroscopy using flat coil sensors", I. Pitropakis, H. Pfeiffer, M. Wevers, at Sensors & Actuators A: Physical, Vol. 176, April 2012, p. 57-63
"The use of flat coil sensors and impedance spectroscopy for fatigue crack monitoring of Al 2024-T3 plates", I. Pitropakis, H. Pfeiffer , M. Wevers, ISBN 978-0-415-62131-1, 5th International conference on Emerging Technologies in Non-Destructive Testing (ETNDT), Ioannina, Greece, 19-21 September 2011
AISHA II presentations
"Eddy current sensor", I. Pitropakis, AISHAI II meeting in Fraunhofer Institute for Manufacturing Technology and Advanced Materials (IFAM), Bremen, Germany, 17-18 September 2009
"Eddy current sensors in a realistic fatigue experiment", I. Pitropakis, AISHA II meeting in AIRBUS HELICOPTERS, Marignane, France, 27-28 January 2010

Table 5.2: Contributions.

"You miss 100% of the shots you never take."

Wayne Gretzky

CHAPTER 6

Embedded electrical crack gauges for continuous crack growth monitoring

In this chapter, tests using crack gauges made from conductive material are reported. The basic concept of crack detection is the interruption of electrical conductivity by fatigue cracks and other kind of mechanical damage. The gauges were mounted on aluminium 2024-T3 plates and on an Airbus A320 slat-track. The aluminium plates along with the A320 slat-track were consecutively painted with layers of primer and coating according to the manufacturer standards. The gauges were embedded between the layers of primer and coating in order to be protected and insulated. Results obtained from resistance measurements, show that these crack gauges could detect cracks at a relatively early stage.

6.1 Motivation

In this study, plates made of aluminium alloy 2024-T3 and a slat-track made of maraging steel (Airbus A320) were used for crack detection [123]. In general, slat-tracks in the form that they are manufactured today have not shown so far any significant problem that has been reported. Nevertheless, major slat-track and aircrafts manufacturers show a great interest in structural health monitoring of these components since the slat-track is a critical part of the wing during landing, take-off and manoeuvring. There are considerations on changing the material of the slat-track from steel to lighter metals or composites in the future but an appropriate SHM method should be applied in any case.

The last years, research has been conducted regarding SHM on slat-track related structural parts investigating the vibration properties that lead to the detection of structural damage [169-171]. Furthermore, a method for crack monitoring that could be applied on slat-tracks is using ultrasonic surface waves that are generated by wedged-shaped sensors [172-175]. Unfortunately, this method was not feasible due to the limited space at the position of the slat-track preventing attachment of the sensors when the racks inside the slat track were mounted. Another method used for crack detection on slat-tracks used flat piezoelectric transducers actuating different acoustic modes, including bulk waves and surface waves [176]. However, this method provides rather complex data requiring advanced data analysis. In this PhD work it is shown that crack gauges and the interruption of the electrical conductivity can be an efficient, simple and effective method for crack monitoring. Additionally, the equipment needed for data acquisition can be limited to a simple multimeter and the results obtained are instant and straightforward.

The target of the study is to create a system consisting of crack gauges placed on critical areas of aircrafts and to use simple multimeter technology to detect cracks. This system could be used on-line, when the aircraft is airborne or off-line, when the aircraft is on the ground. Offline monitoring has the advantage that no additional equipment is needed on-board the airplane, and the system can be monitored every time the plane is on the ground.

6.2 Materials and methodology

6.2.1 The working principle of the crack gauges and the explanation of open-closed crack conditions

Crack gauges are thin conductive stripes embedded on the material under investigation. The working principle of the crack gauges is the interruption of their electrical conductivity. The electrical resistance is monitored at certain time intervals using resistance measurements.

When the aircraft is operating, static and dynamic loads affect the integrity of the aircraft structure on long term. Under high stress, there is a potential for crack formation, and if a crack is present, it will open and close due to cycling loads. When the aircraft is on the ground, the fuselage is not pressurized and visual inspection is not always sufficient to detect closed cracks since the two sides of the crack have been microscopically re-attached. Furthermore, ultrasonic testing will not always be able to detect the crack because of lacking wave reflections.

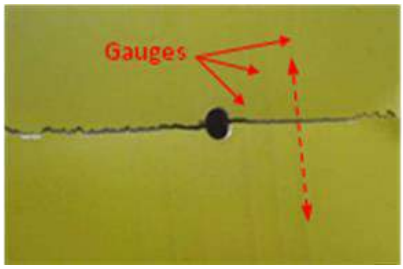

Figure 6.1: A large crack (30 mm each side) that interrupts the electrical conductivity on the embedded gauges.

Therefore, it is very important to continuously monitor and detect cracks even if the cracks are not detectible by classic NDT and visual inspections. The open and closed crack condition of the crack is vital to be taken into consideration.

6.2.2 Parts under investigation

In this study, the critical parts investigated are thin aluminium 2024-T3 alloy plates and an Airbus A320 slat-track. In the 2024-T3 plate, crack growth was monitored by crack gauges and in the A320 slat-track the performance of the electrical gauge was investigated with an existing artificial crack. Figure 6.2 shows the parts investigated under fatigue and compression load.

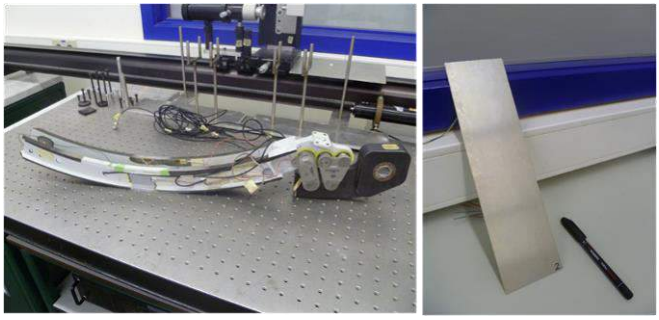

Figure 6.2: Parts tested: An Airbus A320 slat-track (left) and an aluminium alloy 2024-T3 plate (right).

The tested sheets with dimensions of 300 mm (length), 80 mm (width), 1 mm (thickness) are made of the aluminium alloy 2024-T3, which is widely used in

aerospace applications. Aluminium alloy 2024-T3 is a light material that has a high strength and fatigue resistance and it is used to manufacture aircraft structures such as wings and fuselage parts [177].

The A320 slat-track has a length of 64 cm and is made of maraging steel (grade 250) as it needs to be very strong to withstand the very high loads during take-off, landing and flight. The slat is the component of the aircraft located at the front edge of the wing and it is mounted on curved tracks, see figure 6.3. The whole mechanism is called a slat-track and its function is to keep the airplane from stalling when it is flying at high angles of attack [178].

Figure 6.3: Slat-track (Left side: position in airplane wing – Right side: dismounted) [176].

6.2.3 Painting procedure for the metallic aircraft parts

Many metallic aircraft components are coated by primers and finishing coatings. The same procedure was followed for the aluminium 2024-T3 plate and the Airbus A320 slat-track, see figure 6.4. The surface of the component was first coated with a layer of epoxy primer, usually of yellow or green colour, in order to insulate from electrical conductivity and maximize protection against corrosion. After the epoxy primer, a top coating made of polyurethane was applied on the component from the outside surface. It gives the decorative final colour for the product, and it provides chemical, stain and UV resistance. The painting procedure of the Airbus A320 slat-track was completed at the manufacturer of this component; ASCO Industries N.V., Zaventem, Belgium.

Figure 6.4: Painting procedure (Left side: Slat-tracks – Right side: finished Al 2024-T3 plate).

For the tests of this study, the A320 slat-track was painted with primer and the top-coating and the aluminium 2024-T3 plates were coated only with the epoxy primer.

6.2.4 Implementation of the crack gauges on the aluminium alloy 2024-T3 plate

For the plates made of the aluminium alloy 2024-T3, the crack gauges were conductive stripes made from an electrically conductive component (PC 3000 from Heraeus GmbH). The conductive component is a fast thermally-curing, solvent-free epoxy adhesive with silver particles. The plate was firstly coated with a layer of a two component epoxy primer (10P20-44 Akzo Nobel N.V.) in order to provide protection and electrical insulation. Then the conductive stripes were attached on the plate and afterwards the plate was painted again with the 10P20-44 primer for protection and electrical insulation of the conductive stripes.

For the creation of the electrical crack gauges, polyamide tapes (PPI 702) from PPI Adhesive products Corporation, Ireland, were used as guides. Between the tapes, conductive adhesive was applied with the aid of a spatula. The thickness of the conductive stripes was determining the height of the crack gauges (85 µm) and the width between the tapes was chosen to be 1.5 mm. The plate with the crack gauges was left in the oven for one hour at 60 °C. Then, the polyamide tapes were removed and the connection pads that are made of copper foil were glued on the plate using conductive adhesives. Next, the plates were placed again inside the oven for one hour at 60 °C for hardening. Finally, the plates were coated again with a layer of the epoxy primer and dried at room temperature.

For testing the suitability for crack monitoring, fatigue tests were performed (figure 6.5). Two different tests were carried out with the same parameters and number of fatigue cycles. One test without a hole in order to monitor the consistency of the measurements of the gauge during fatigue and another test with a hole that was responsible for the crack initiation.

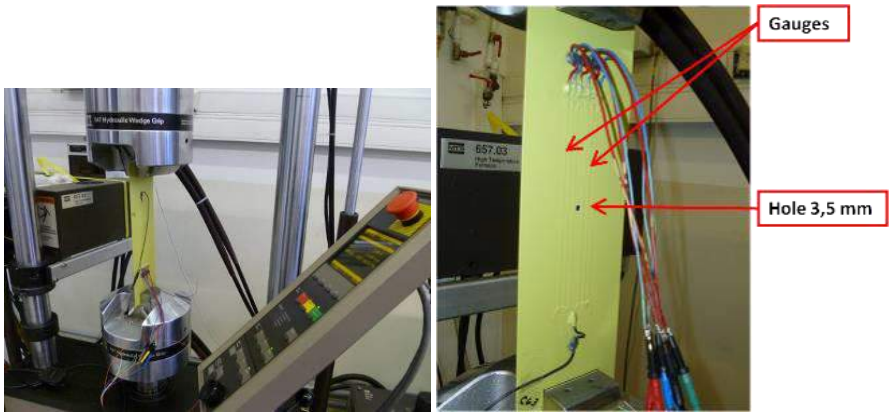

Figure 6.5: Al 2024-T3 plate set-up (Left: Fatigue test – Right: Embedded gauge).

The aluminium alloy 2024-T3 plates were subjected to a fatigue load of minimum 8 kN and maximum 12 kN. The fatigue test was performed on a servo-hydraulic 810

MTS testing machine by MTS Systems Corporation. The maximum dynamic load for this fatigue machine is 80 kN. The frequency of the cyclic loading was 15 Hz and 135,000 cycles were applied. To initiate the crack, a hole with a 3.5 mm diameter was drilled in the middle of the plate. 135,000 fatigue cycles are enough to create a significant crack size of ~12 mm on the plate at each side of the hole. Six crack gauges were embedded, three on the left and three on the right side of the plate, see figure 6.6.

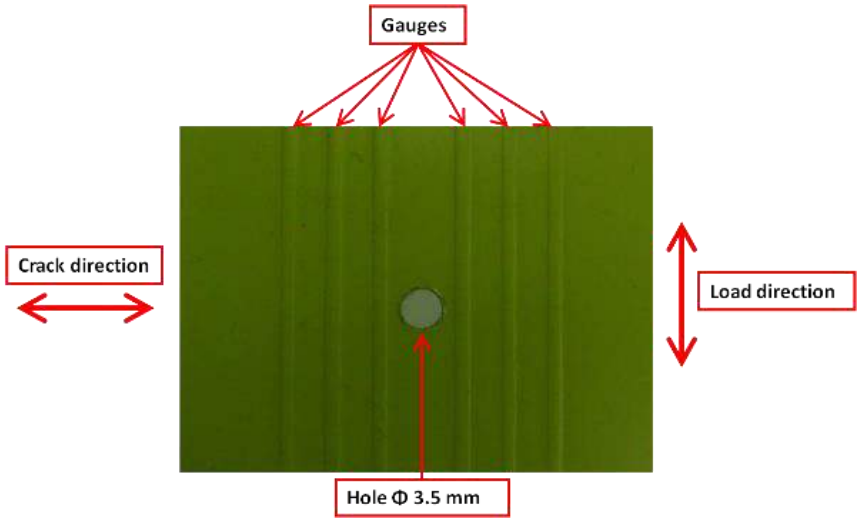

Figure 6.6: Crack gauges embedded on Al 2024-T3 plate.

The distance between the hole and the nearest gauges is 1 mm on each side and the distance between the gauges is 3 mm. The crack initiated at both sides and propagated perpendicular to the load direction.

A second test was also performed using stripes of aluminium foil as crack gauges for validity purposes.

6.2.5 Implementation of the electrical crack gauges on the Airbus A320 slat-track

To test the detection performance with respect to the closing crack problem, a crack gauge was mounted on the Airbus A320 slat-track and a 3 point bending test was performed. The crack gauge was a conductive stripe from aluminium foil that was embedded between the layer of the primer and the layer of top-coating. The dimensions of the aluminium stripe were 90 mm (length), 2.3 mm (width) and 18 µm (thickness).

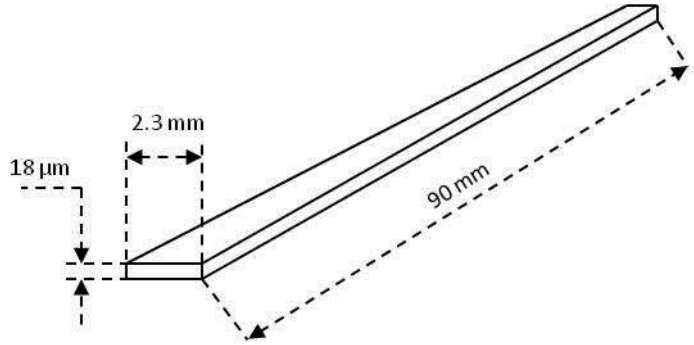

Figure 6.7: Drawing of an embedded Aluminium stripe.

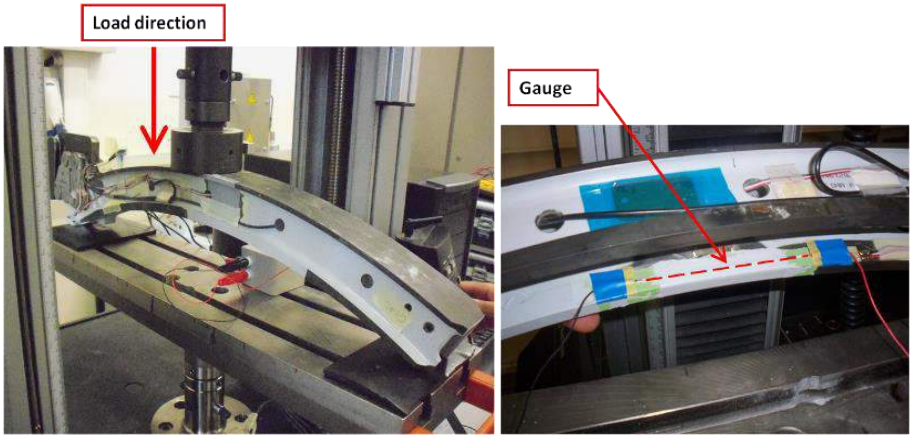

Figure 6.8: Slat-track set-up (Left side: 3 point bending test – Right side: Embedded gauge).

The 3-point bending test was performed on a 5567 Universal Testing Machine by INSTRON ®, see figure 6.8. In this test, the slat-track was pressed from 0 – 2 kN and then released from 2 – 0 kN for five times with a rate of 0.1 mm/min in order to obtain open and closed crack conditions. The maximum length of extension was at 3.54 mm. A pre-existing fatigue crack with a length of 42 mm was already present in the middle of the slat-track. Its purpose was to open during loading and close during unloading with the purpose of breaking and re-attaching the crack gauge. During bending, the instrument monitors the moment that the crack opened and broke the gauge and the electrical conductivity on the conductive stripe was interrupted. During load-release (unloading), the instrument monitored the moment that the crack closed and the conductive stripe regained conductivity. The test was repeated five times for reproducibility purposes. The crack gauge was in a position that does not interfere with the rolling of the slat-track during operational movements.

6.3 Results and discussion

6.3.1 Crack propagation in the 2024-T3 plate

Initially, a durability test was performed on the plate without a hole in order to verify that the resistance measurements on the gauges will remain relatively stable if a crack is not present. Figure 6.9 shows the resistance measurements during the durability test. There was no significant alteration on the resistance values of each crack gauge.

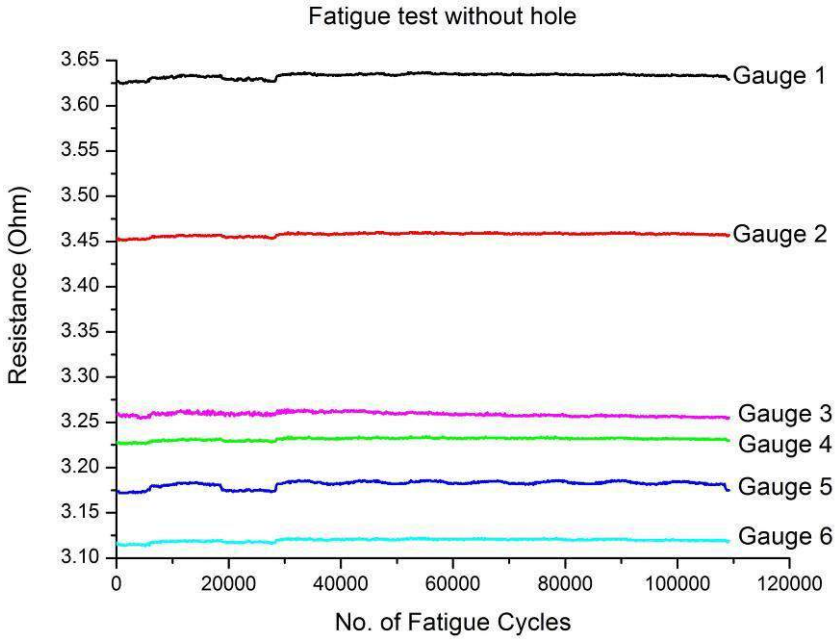

Figure 6.9: Resistances of the crack gauges on the plate without a hole (120 000 cycles is approximately the lifetime of an airplane).

After the durability test, a hole of 3.5 mm diameter was drilled and a second fatigue test was performed. The plate was subjected to the fatigue load and the crack propagated horizontally and passed through all six gauges before the fatigue test was stopped at 135,000 cycles, see figure 6.10.

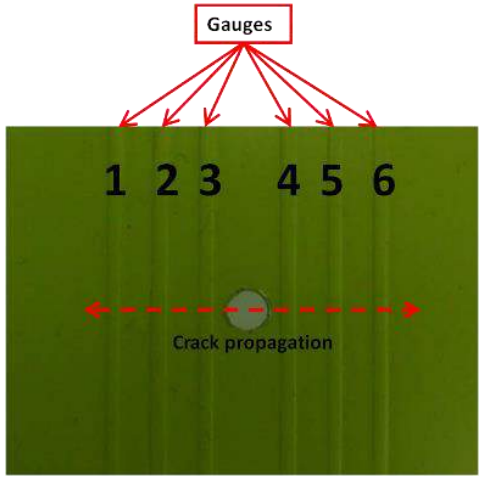

Figure 6.10: Six embedded gauges and direction of crack propagation.

Figure 6.11 depicts the moments at which the electrical conductivity of each gauge is interrupted during the fatigue test. As the crack was growing, it was consequently breaking the gauges. At the moment they broke, they showed infinite values of resistance, thus no conductivity. As expected, the gauges 3 and 4 were the first to lose conductivity.

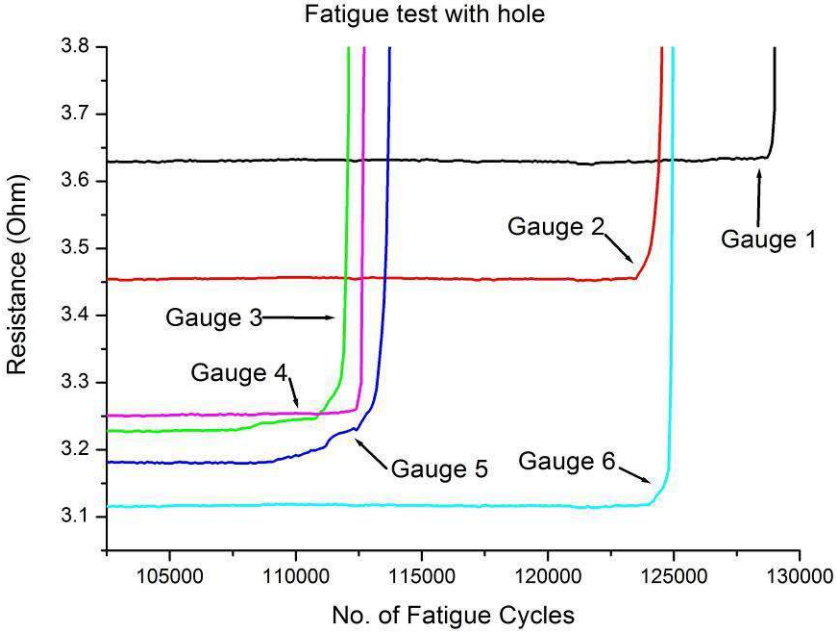

Figure 6.11: Interruption of electrical resistance on the 6 gauges on the aluminium alloy 2024-T3 plate.

The crack appeared after 105,000 cycles and Figure 6.12 shows the crack growth on the left and the right hand side of the hole as a function of the number of fatigue cycles. The crack length was measured with the use of a simple micrometer. It can be seen that the crack grew up to a length of 10 mm at each side after an additional 26,000 fatigue cycles. At this point, the crack had passed through all six embedded gauges. This means that the crack had broken all six of them, and when the crack was open, all gauges have resistance values that are out of range.

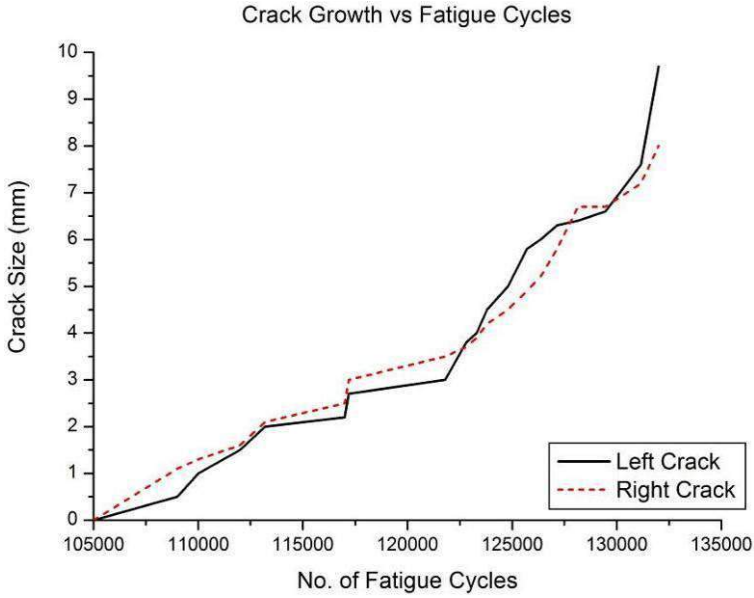

Figure 6.12: Crack growth starting at 105,000 cycles (first appearance of crack). The crack growth initially is linear and shortly before cracking is following a parabolic curve.

At the end of the fatigue test, the crack had interrupted the electrical conductivity in all six gauges. To monitor the possibility of regaining conductivity when the crack was closed another test was performed. The plate was subjected to a static load of 10 kN keeping the crack open. When the crack was open, all gauges (1-6) lost conductivity showing infinite values of resistance. Then, the static load was slowly reduced to zero and the crack was closing again. The results showed that gauges 2, 3, 4 and 5 did not regain conductivity after the completion of the test. However, crack gauges 1 and 6, that positioned far away from the hole and near the end of the crack, initially regained conductivity for a few minutes but after that the resistance was increasing until it showed values out of range.

Gauge No.	Resistance before fatigue (Ohm)	Resistance after fatigue (Ohm)	Conductivity regained
1	3.6 ± 0,01	5.9 ± 0,01 then Out of range (-> ∞)	Yes at 6 kN
2	3.4 ± 0,01	Out of range (-> ∞)	No
3	3.2 ± 0,01	Out of range (-> ∞)	No
4	3.1 ± 0,01	Out of range (-> ∞)	No
5	3.1 ± 0,01	Out of range (-> ∞)	No
6	3.2 ± 0,01	5.1 ± 0,05 then Out of range (-> ∞)	Yes at 0 kN

Table 6.1: Conductivity on each crack gauge after cracking.

Table 6.1 summarises the results. The results confirm that when these gauges are monitored, they can detect crack propagation through them due to the interruption of their electrical conductivity. Nevertheless, further tests need to be performed in order to optimize the crack propagation gauges in a way that the material of the gauge when broken it will not regain conductivity under any circumstances. This can be achieved with a careful materials selection and the design of the structural properties of the crack gauges, regarding their stiffness (Young modulus), in order for the crack gauges to break together with the material of the aircraft component under investigation.

6.3.2 Microscopic investigation at crack point

The cross section of the broken plates at the point of the crack gauges was investigated in an environmental scanning electron microscope Philips XL30 ESEM FEG, see figure below.

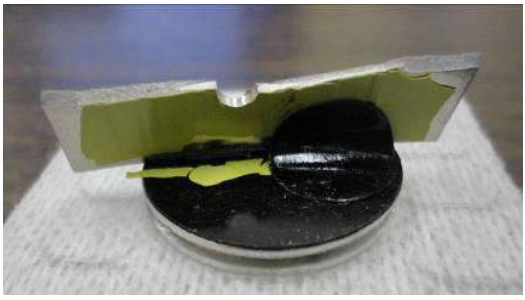

Figure 6.13: Part of the broken Al 2024-T3 plate scanned in ESEM. The crack propagated in both directions from the hole in the middle.

Figure 6.14 below shows the cross section of the crack gauge and its dimensions. It has an average thickness of 85 μm, which can locally reach a thickness of 144 μm at its peak, while it is 1.25 mm in width.

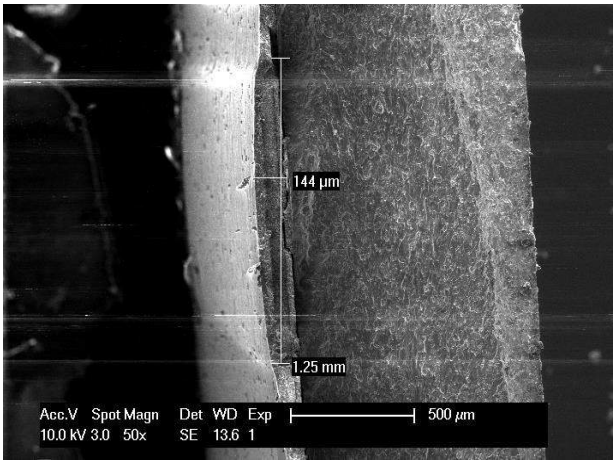

Figure 6.14: Photo taken by an environmental scanning electron microscope Philips XL30 ESEM FEG showing the cross section of the crack gauge and its dimensions (width and height at peak). The gauge is embedded between the top primer (left) and the aluminium plate (right).

The crack gauge can be seen between the dimension lines. The light coloured layer on the left is the epoxy primer component (10P20-44 Akzo Nobel N.V.) and the thick material on the right is the aluminium alloy 2024-T3. In the following photo, the layers of each component as referred in section 6.2.4 can be seen.

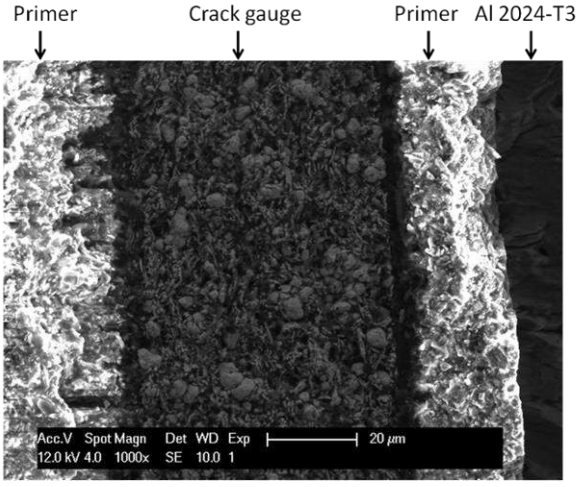

Figure 6.15: Cross section of plate at the location of the crack gauge showing the different layers of materials.

With the Philips XL30 ESEM microscope the energy-dispersive X-ray spectroscopy tool was used to give an approximation of the chemical composition of the

materials. The following table shows the results of the elemental analysis as provided by the Philips XL30 ESEM microscope.

Layer	Elements	Weight Ratio (%)
Primer	C	59.7
	O	30.9
	Al	0.3
	Si	5.0
	Ti	1.3
	Cr	2.5
Crack Gauge	C	33.9
	O	9.3
	Mg	1.6
	Si	0.4
	Mo	1.1
	Ag	53.3
Aluminium alloy 2024-T3	Cu	3.4
	Mg	13.8
	Al	82.8

Table 6.2: Elemental analysis of the tested sample at the crack point.

The elemental analysis reveals the presence of silver that was used to enhance the conductivity of the crack gauge. Titanium and silicium were used in the primer to achieve a high oxidation and wear resistance and, together with chromium, offer corrosion protection while giving the preferable decorative colour for the coating [179]. The following photo shows further microstructural details of the crack gauge made of a polymer silver conductive adhesive.

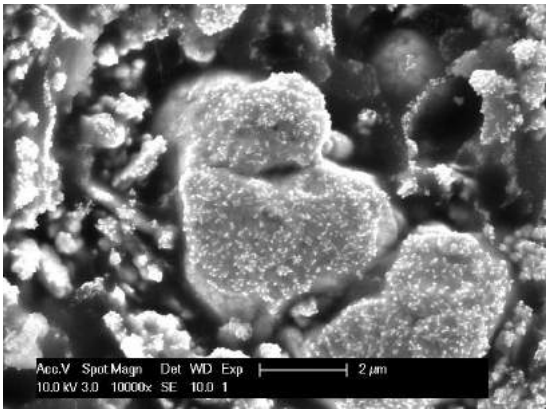

Figure 6.16: SEM photo of the PC 3000 polymer silver conductive adhesive from Heraeus GmbH that is used for the production of the crack gauges. The zoom is selected to be at 10000x. It shows the grains of Chromium mixed with Silver which is responsible for the conductivity on the crack gauge.

From the microscopic investigation at the crack point, it can be seen that the crack created a detachment of the coating with the embedded gauges, see figure below.

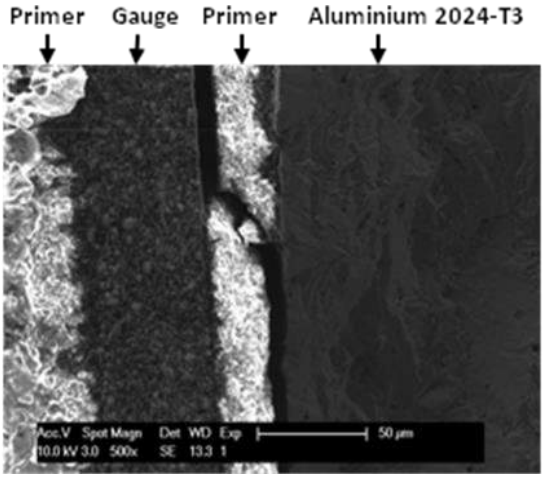

Figure 6.17: The layer of primer coating that is located between gauge and aluminium has been detached due to the crack.

The detachment was mostly apparent at the surface side of the aluminium and in some cases it penetrated the first layer of the primer and separated it with the gauge.

By observing the surfaces of the three different layers of the cross section and creating a backscattered image, information on the surface morphology within each layer of the laminated structure can be obtained, see figure below.

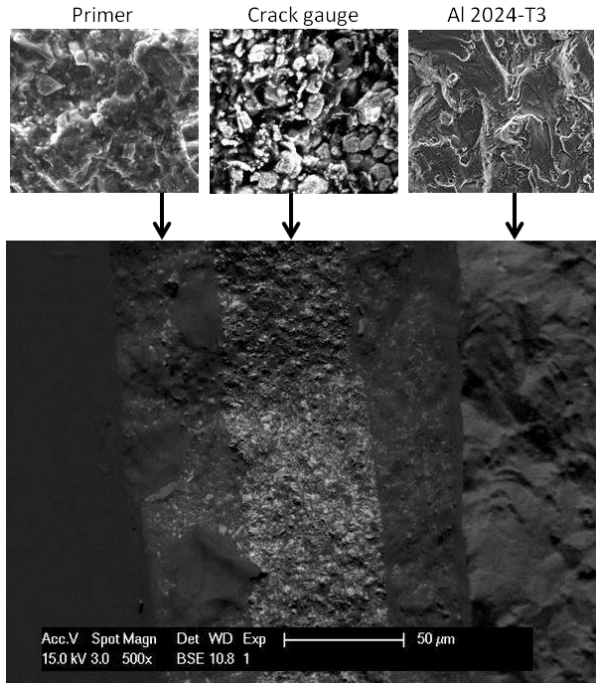

Figure 6.18: Backscattered X-ray image (scale 500x) of the cross section of the broken aluminium 2024-T3 plate with the embedded crack gauge on top (photo below) and the microstructures of each layer (three photos above in scale 5000x).

The microscopic images presented in figure 6.18 show that there were no signs of large ductility neither in the crack gauges nor in the aluminium 2024-T3.

6.3.3 Investigation on the conductivity on the crack gauges during loading and unloading

Another plate with embedded conductive stripes made from aluminium foil as crack gauges was tested in a 5567 Universal Testing Machine by INSTRON ®. On the plate there was a pre-existing crack that had cut the aluminium stripes as the plate was already subjected to fatigue in a servo-hydraulic fatigue testing machine from Schenck AG (now Instron Schenck Testing Systems GmbH).

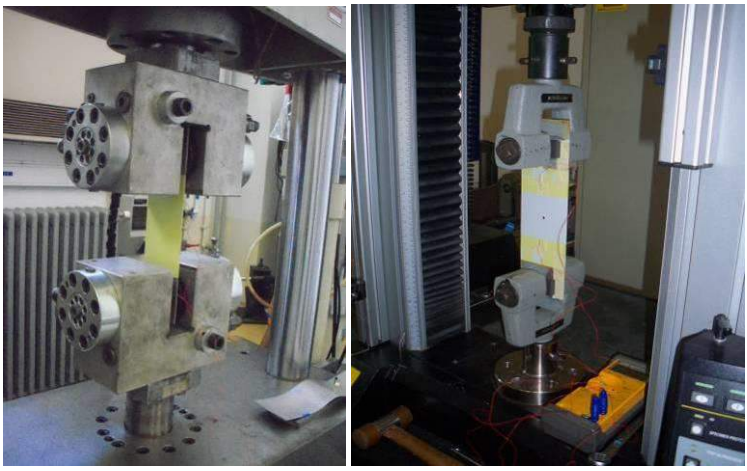

Figure 6.19: Plate with embedded crack gauges (Al stripes) placed on the fatigue machine (left) and on the tensile machine (right).

The fatigue test on that plate was performed at up to 100,000 cycles with a cyclic frequency of 10 Hz. This number of fatigue cycles was sufficient to create a crack length that overpassed the crack gauges that were positioned 3 mm away from the hole with a diameter of 4 mm. The fatigue test showed also here that as the crack was passing through the aluminium stripes, they were losing their conductivity and this was an indication of the crack growth.

However, the goal of this test was to investigate the loss or regain of conductivity the moment that the crack was open or closed when tensile force was applied and released. Therefore, the aluminium plate was placed in a tensile machine in order to create open and closed crack conditions when the load was applied and released. The load for the tensile test ranged from 0 to 3 kN. The rate of displacement was chosen to be 0.1 mm per second.

The load was applied on the aluminium plate with embedded aluminium stripes and it was slowly increasing up to 3 kN. The graph below shows 3 typical cycles during the test. The load was increased and at a load value of 1.739 kN, characterized by point 1, the resistance on the aluminium stripe became infinite. After reaching the peak of 3 kN, the load was slowly released with the same rate. The resistance on the Al stripes was regained at a load value of 0.242 kN, at the characterized point 2.

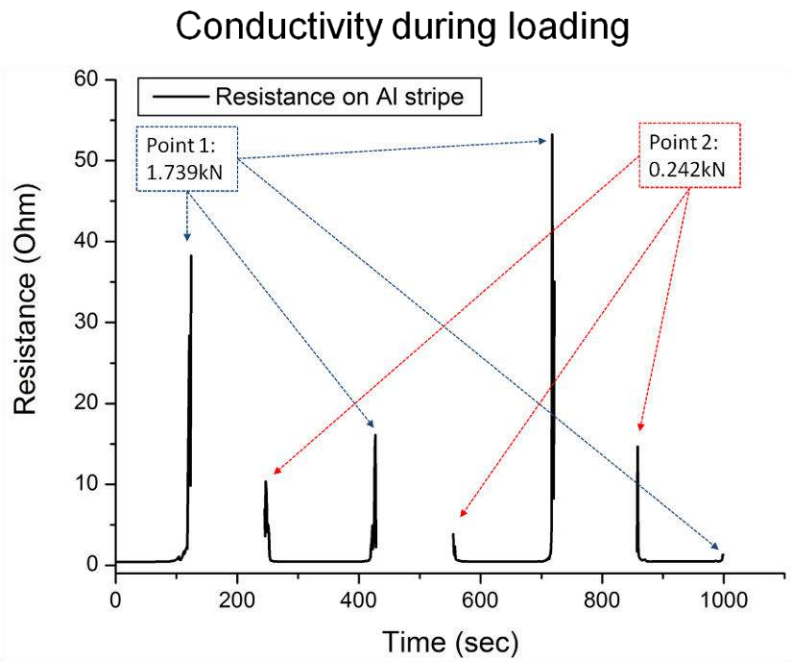

Figure 6.20: Conductivity of Al stripes when crack is open and closed due to loading and unloading.

The same observation occurred in all the cycles of the test and also at the same load values. Therefore, it can be concluded that the conductive stripes regain their conductivity when the crack is closed even if they break due to fatigue. However, at least for the open cracks, the sensors detected the problem at a relevant low value of load (1.739 kN) and at a small crack size undetected with the naked eye.

6.3.4 Airbus A320 slat-track

The Airbus A320 slat-track was subjected to a 3 point bending test with a load up to 2 kN and then it was released. The main purpose of the test was to investigate the reliability of the crack gauge when the crack was open and closed again. When the slat-track was compressed, the crack on the slat-track opened and the crack gauge broke. In the release mode, the crack was closed and the gauge was reattached. Table 6.3 shows the vertical extension of the slat-track with respect to the compressive load applied.

Load	Compressive extension (mm)	Compressive load (kN)
Minimum	0.09	0.014
Maximum	3.54	2.049

Table 6.3: Compressive extension and load on A320 slat-track.

The slat-track was compressed five times to test the reproducibility. The instruments monitored the exact point where the resistance becomes infinite, indicating an interruption of the electrical conductivity.

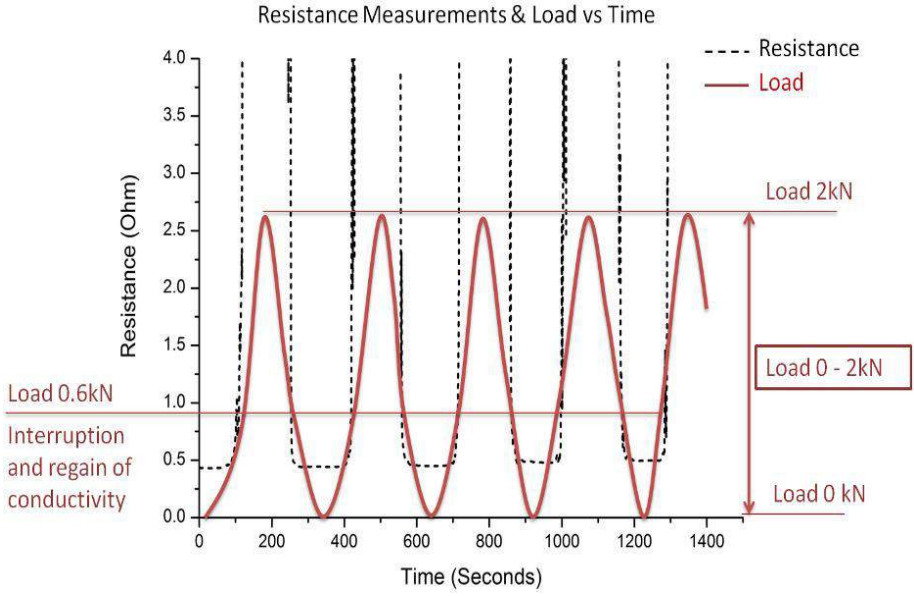

Figure 6.21: Resistance measurements and load (dashed line: Electrical resistance, dark line: Load).

The loss of conductivity occurred at 0.6 kN during compression. At the same time, when the load on the slat-track was released, the crack gauge regained conductivity when the crack was closing. This occurred again almost at the same compressive load of 0.6 kN. The result presented in figure 6.21 shows that the crack gauge used on the A320 slat-track can monitor cracks by the interruption of electrical conductivity with a straightforward data interpretation.

Figure 6.22 below shows however that the electrical resistance of the crack gauge is increasing after each cycle. The bending test was performed only with 5 cycles but other results show that it is possible that in some cases after many fatigue cycles the conductivity on the crack gauge drifts.

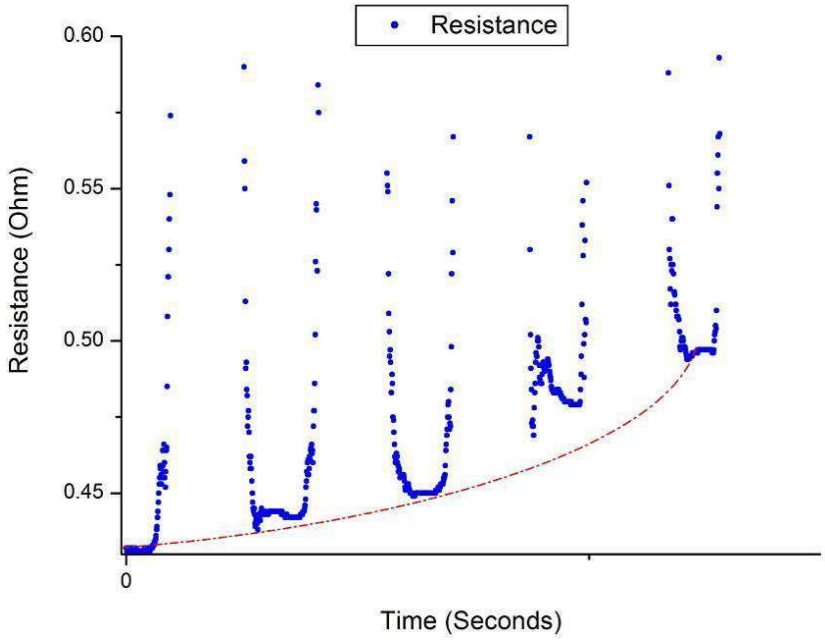

Figure 6.22: Resistance on crack gauge after each cycle. Each cycle lasted 1h and 10 minutes.

The change in resistance is caused by deformation of the crack gauge after each cycle or even possibly introduced by oxidation of the newly created surface. The resistance of the crack gauge was increased and it was measured after few weeks showing eventually a very large value. Future tests will be repeated in order to investigate more in depth this phenomenon.

6.4 A possible solution for the "closed crack problem"

For off-line monitoring and reliable crack detection, the following issues have to be taken into account. Due to cyclic loading, cracks constantly open and close during flight. Off-line monitoring can take place during scheduled maintenance when the aircraft is on the ground and at that moment, cracks can be closed. In that case, the crack propagation gauges are re-attached even if the crack has passed through it. Therefore, the conductivity can be regained and, consequently, it cannot be seen if the crack has reached the critical size since the gauge gives no indication of electrical interruption. A solution to this important issue is presented below.

In order to find the first moment that the crack breaks the electrical crack gauge, a simple and effective solution for off-line monitoring can be employed by implementing the principle of an electrical fuse. The fuse is located inside a small box and is connected to a Metal–Oxide–Semiconductor Field-Effect transistor (MOSFET) and the embedded electrical crack gauge. The first moment that the

open crack reaches a size that breaks the gauge, the electrical conductivity at the electrical crack gauge is interrupted. When the electrical crack gauge loses conductivity, high voltage is applied on the MOSFET. This voltage induces a conductive channel that goes to the electrical fuse and burns it. During off-line monitoring, a simple push button test indicates if the crack propagation gauge is broken or not, see figure 6.23. In that way even closed cracks that could resume the electrical conductivity can be detected during inspections.

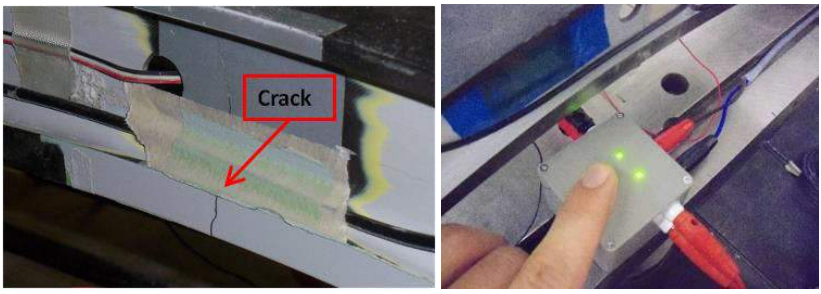

Figure 6.23: Crack on A320 slat-track (left) and push-button test for crack indication (right)**.**

In a fuse system, when the button is pressed, the test lamp can indicate that the crack propagation gauge has never been broken and the crack has not reached the critical point. The critical point is the point where the crack propagation gauge is placed as it indicates a crack size that is outside damage tolerance. If the button is pressed and there is no light, then the crack must have passed through and broken the gauge. That means that the crack has exceeded the critical size and the component needs to be replaced. To be able to utilize this method, a small permanent electrical current is needed in order to flow though the conductive crack gauge and the parallel circuit with the fuse. However, having permanent electrical current in a SHM system can be a disadvantage for some applications. Therefore, the current should be kept as small as possible and appropriate electrical insulation materials should be used.

6.5 Illustration of a possible SHM system

Figure 6.24 below shows a possible concept for implementation of crack gauges on e.g. slat-tracks using crack propagation gauges. The same concept can for sure also be applied for aluminium alloy 2024-T3 structural parts. The idea is to have an integrated and lightweight network of crack propagation gauges embedded on critical areas of the aircraft that can easily detect cracks, do not interfere with other electrical devices and be simple in philosophy and data interpretation.

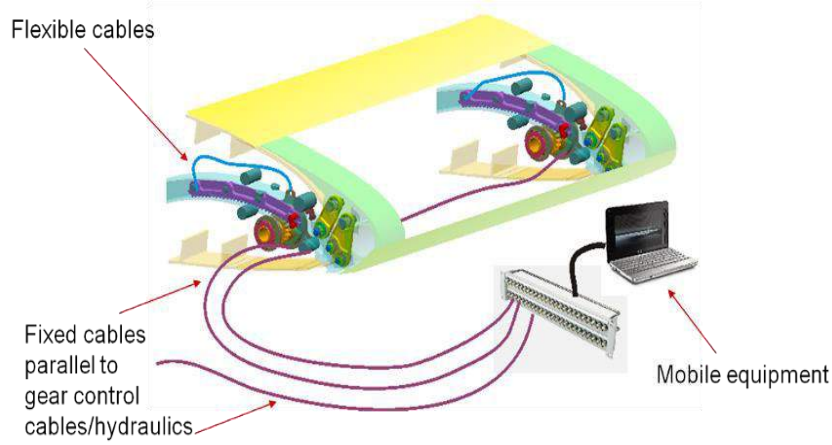

Figure 6.24: Example of final implementation concept.

6.6 Conclusions

Electrical crack gauges have been tested on aluminium 2024-T3 plates and on an Airbus A320 slat-track. The results show that the interruption of the electrical conductivity due to the crack growth can be easily monitored. These electrical crack gauges can detect cracks when they reach a critical size and monitor them even if sometimes they seem microscopically closed. In that way, they give an added value to safety and offer options to reduce or eventually focus the scheduled maintenance of an aircraft. Additionally, with appropriate equipment they can be used either as an off-line or an on-line SHM system. Due to their design, they can be used to follow various linear paths and cover medium to large areas of aircraft components. The embedded gauges are glued on the primer layer to ensure insulation and they can work as integrated systems on critical aircraft components.

Because conductive crack gauges contain metallic parts, there is always a possibility for galvanic corrosion between crack gauge and the metallic parts under investigation. Therefore, proper material selection and embedment of the crack gauges are necessary. A possible solution would be a crack gauge made of zinc, which is conductive and at the same time can offer galvanic protection of the cracked area that is exposed.

The Probability of Detection (POD) using embedded electrical crack gauges depends on its conductivity when broken. The following table below shows the advantages and disadvantages using embedded electrical crack gauges as a SHM method.

Advantages	Limitations
Suitable for on-line and off-line monitoring	Detects cracks but not internal delaminations in composites
Can offer galvanic protection	Each gauge can record one crack at a time
Flexible design using a CNC tool	Needs many gauges to cover multiple areas
Does not affect mechanical properties when appropriate tailored	Two different metals come into contact when an crack exists, not an issue due to stochiometry
Small temperature dependence	

Table 6.4: Advantages and disadvantages of embedded electrical crack gauges as a SHM method.

Published proceedings
"Crack detection in aluminium 2024-T3 plates and in Airbus A320 slat-track using electrical crack gauges", I. Pitropakis, H. Pfeiffer, T. Gesang, S. Janssens, M. Wevers, 18th World Conference for Non-Destructive Testing (WCNDT 2012), Durban, South Africa, 16-20 April 2012
AISHA II presentations
"Extended crack propagation gauges - progress achieved by fatigue measurements", I. Pitropakis, AISHA II meeting in AIRBUS HELICOPTERS, Marignane, France, 27-28 January 2010
"Fatigue crack detection using implemented crack wires", I. Pitropakis, AISHA II meeting in Aeronautical Technologies Centre (CTA), Vitoria, Spain, 18-19 October 2010
"Fatigue crack determination using painted crack gauges in aluminium sheets", I. Pitropakis, AISHA II meeting in KU LEUVEN, Leuven, Belgium, 27 October 2011

Table 6.5: Contributions.

"How strangely do we diminish a thing as soon as we try to express it in words."

Maurice Maeterlinck (1862 – 1949)

CHAPTER 7

Detection of acoustic impact in composite materials using optical fibres

This chapter presents how optical polarimetric fibre sensors can be used as line-integrating sensors to detect impact events. The aircraft materials investigated in this study are simple composite plates as well the tail boom of a helicopter. Optical fibre sensors were mounted on the composite material by appropriate adhesives. The change in light propagation caused by the elastic pressure waves arising from the impact were detected along the whole length of the active fibre sensor. The results from the optical fibres are very similar to those obtained using piezo-electric sensors and show the potential for further development as an NDT technique for aerospace applications when non-electric sensors for online impact detection are needed.

7.1 Motivation

One possibility to detect "barely visible impact damage (BVID)" after impacts on aircraft materials is non-destructive testing (NDT) technology using ultrasound [180]. The ultrasonic waves are usually excited and received by piezoceramic transducers. Some modern SHM applications intend to use optical fibres as receiving elements. There are many reasons why the application of optical methods for acoustic sensing can be more advantageous compared to the widespread use of traditional piezoceramics. Optical fibre sensors can be used to detect acoustic emission with the advantage of being relatively cheap and insensitive to electromagnetic interferences. They can work as line-integrating sensors and could in some cases monitor larger areas without the need to cover the structure with an enormous amount of point sensors. For long structural parts, one line of an SM optical fibre can replace many smaller piezoelectric transducers that are only appropriate for small areas of inspection. In combination with PZTs that act as sources of wave excitation, SM optical fibres can offer an advantage to detect large areas for possible defects inside the structure of the aircraft component. In previous studies, they have already been used successfully to monitor impact damage in helicopter tail-boom using active ultrasonic excitation [4-6].

Of all the technologies, the use of a single-mode fibre in a polarimetric set-up is the most promising method. However, the number of studies performed so far is limited, and this is in contrast to the high potential of this technology. Additional efforts are required to fully explore the potential of the technology (stable baseline conditions, advanced data analysis, adaption for aircraft operations).

7.2 Materials and methodology

In this study the in-situ detection of impact using a polarimetric approach is presented. The extent of impact that can cause a possible damage can approximately be derived from the magnitude of the acoustic signals. The principle of detection is as follows. By means of a stabilized laser source (wavelength 1310 nm) polarized light (continuous-wave) is propagating through the core of the optical fibre. When not subjected to external influences, the material is approximately isotropic and two linear orthogonal modes propagate through the Single Mode (SM) fibre at the same velocity. However, when Lamb waves arising from a physical impact on the material upon which the optical fibre is mounted, then the material becomes more anisotropic due to its elastic optic effects resulting to birefringence [181]. The periodic ultrasonic pressure on the fibre thus causes the two polarization modes to travel at different velocities resulting in a polarization change. When both modes have passed a polarization filter, the magnitude that shows the light intensity change can be read out by a light diode.

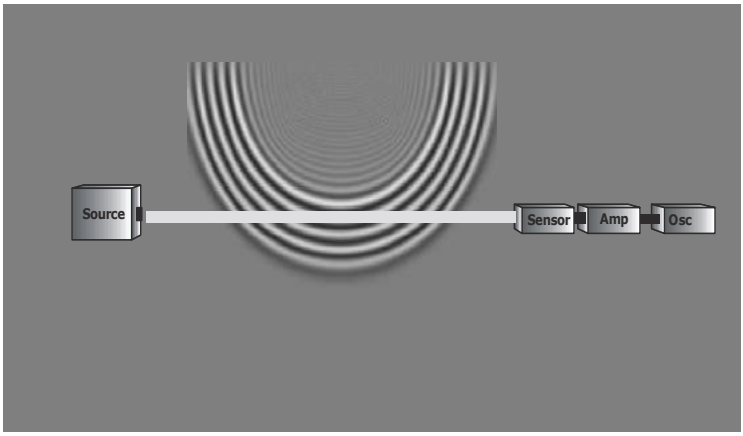

Figure 7.1: Simplified scheme for detection of impact in a polarimetric set-up of a Single Mode (SM) optical fibre.

Figure 7.1 shows the schematic set-up that is used for the detection of immediate impact on flat lab-scale specimens. As mentioned above, in contrast to previous studies, no active ultrasonic source was applied but the impact was directly measured in-situ. This will have consequences for the sound propagation to be expected because a broad acoustic frequency spectrum will be excited with time-dependent behaviour. The resulting change of polarization was measured and controlled by an AGILENT polarization analyser/controller (N7788B-400).

7.3 Test on carbon fibre reinforced plates

7.3.1 Test set-up

The laboratory-scale parts were made of carbon-fibre reinforced epoxy (CFRE) composites. On the plate, two different optical fibres were attached by appropriate adhesives: a Single-Mode (SM) optical fibre and a Single-Mode Polarization-Maintaining (PM) optical fibre, as well as piezoelectric patches that served as a reference. Figure 7.2 shows the impact-testing set-up that was designed to introduce a non-destructive low-velocity impact on the CFRE plates. An impactor, in this case a sphere of 18.9 grams made of steel, was allowed to fall from a pre-determined height to strike the test specimen attached on a horizontal plate.

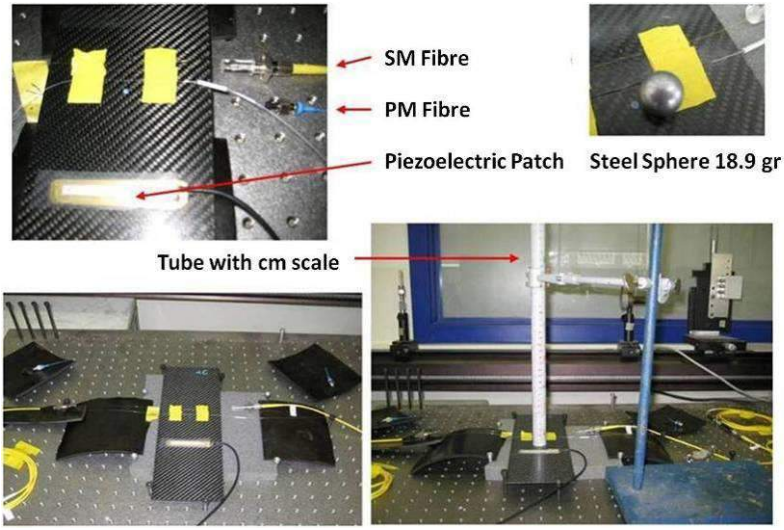

Figure 7.2: Impact testing set-up

7.3.2 Results and discussion

Impact-generated vibration signals were recorded due to the impact of the metallic sphere on the plates. For the initial height of the impactor (metallic sphere) at 10 cm, the signals received from each sensor can be seen in figure 7.3. There is a clear difference between the signals obtained by the two types of optical fibres, the Single-Mode (SM) and the Single-Mode Polarization-Maintaining (PM) optical fibre, and the piezoelectric patch (PZT).

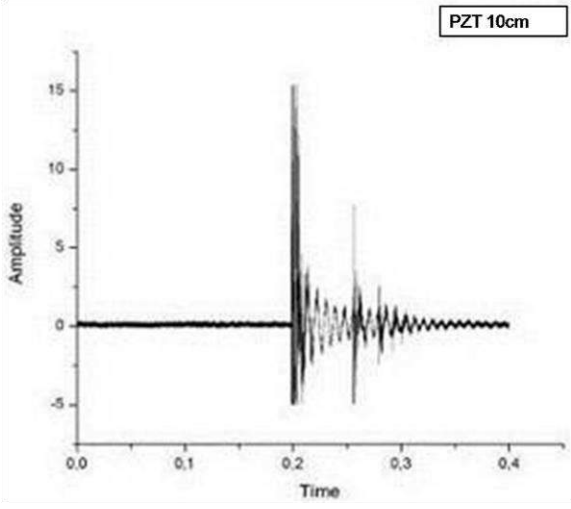

Acoustic response of a PZT

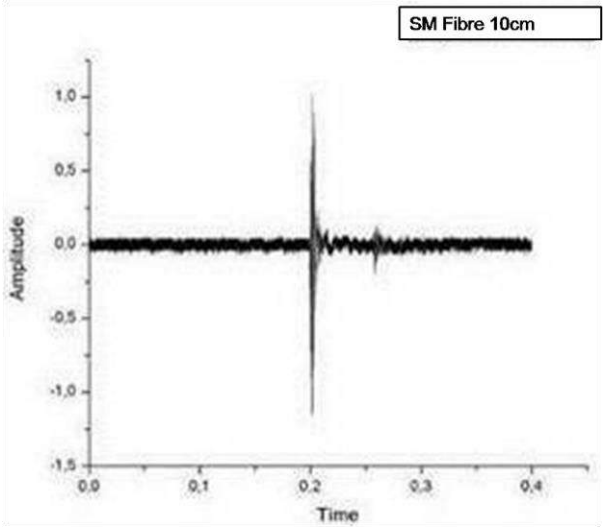

Acoustic response of a Single-Mode fibre

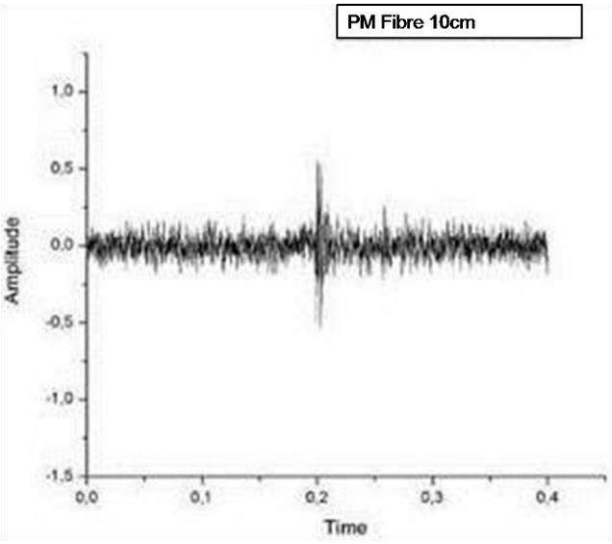

Acoustic response of a Polarization-Maintaining optical fibre

Figure 7.3: Vibration signals from an impact when the metallic sphere was dropped from 10 cm height: Piezoelectric Patch (PZT) (up), Single-Mode (SM) optical fibre (centre), Polarization-Maintaining (PM) optical fibre (down).

Single-mode fibres have a higher sensitivity than PZTs when used in the polarimetric set-up which is caused by the change of the polarization state as a

result of the shear waves. PM fibres can also be used to detect impact, but the signal-to-noise ratio is less. PM fibres maintain the polarization of the light inside the fibre along its length due to the reduction of internal reflections. The signal of the PM fibre is similar to the SM fibre when the SM fibre is used without a polarization filter. This shows that the received signal at PM fibres and of SM fibres without polarization filters arises from intensity modulation due to effects like micro-bending.

Figures 7.4 and 7.5 below show the impact-generated vibration signal detected by the single-mode optical fibre by when the metallic sphere is dropped from a height of 6 and 10 cm respectively. It is clear the more intense the impact, the higher the amplitude of the optical signal. This can be explained by the equation of the potential energy (E_p):

$$E_p = mgh \qquad \text{Eq. 7.1}$$

Where *m* is the mass, *g* is the gravitational acceleration and *h* is the height from which the metallic sphere is dropped.

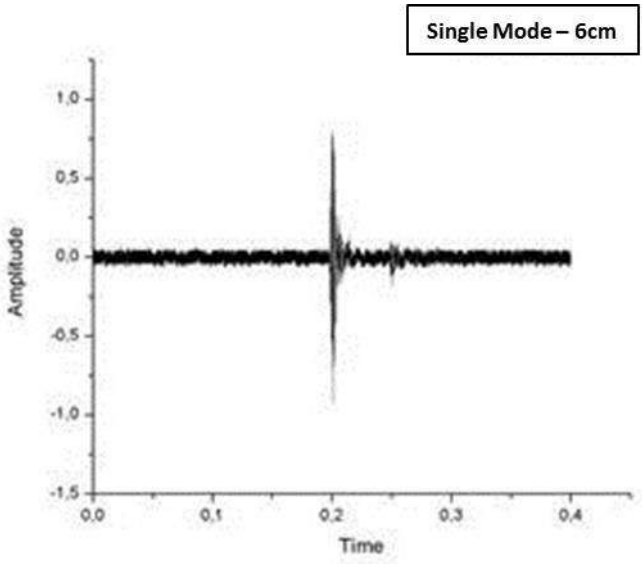

Figure 7.4: Impact test from distance 6 cm and signal received from the Single Mode optical fibre.

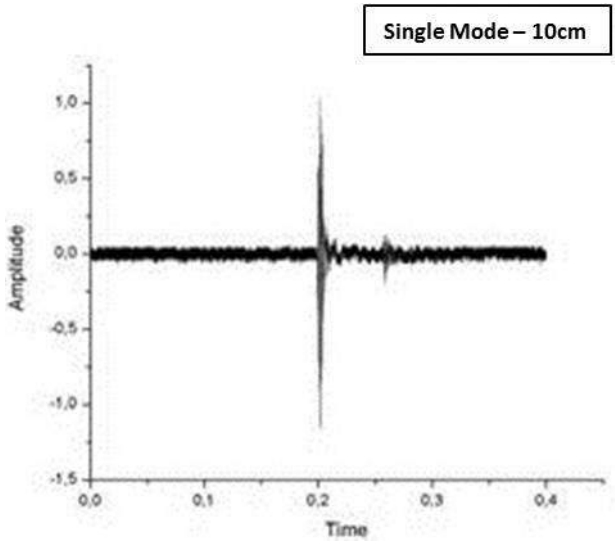

Figure 7.5: Impact test from distance 10 cm and signal received from the Single Mode optical fibre.

7.4 Test on Eurocopter EC135 tail boom

7.4.1 Test set-up

For the feasibility test on a helicopter composite tail boom, a SMARTape® optical fibre sensor (fig. 7.6) was used to assist the handling of the fragile and brittle optical fibres during the sample preparation. It is manufactured by the company SMARTEC from Manno, Switzerland. It is a PPS/glass fibre composite tape with an embedded Single-Mode optical fibre. This thermoplastic composite tape also protects the optical fibre from external mechanical or chemical influences.

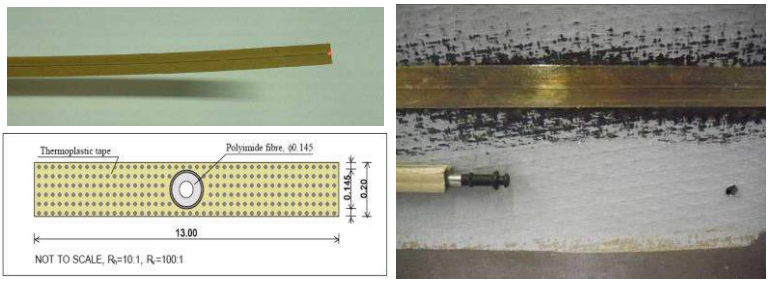

Figure 7.6: Single Mode fibre in SMARTape®.

Figure 7.7 shows the set-up of a part of the tail boom used for the experiments.

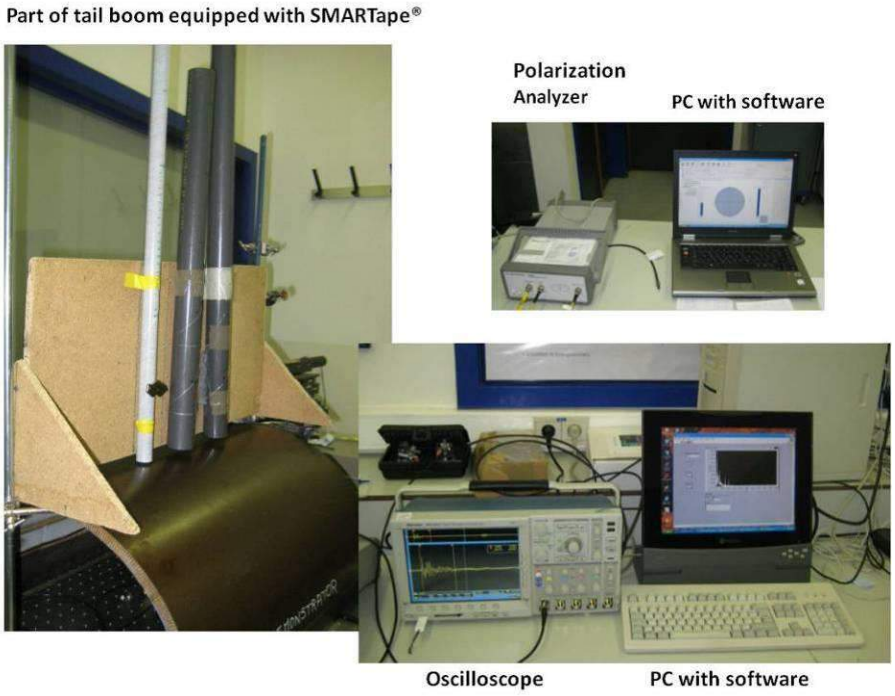

Figure 7.7: The set-up for the impact test on a part of the tail boom from EC 135 equipped with a SMARTape® and the instruments to read out the Single Mode optical fibre.

Figure 7.8 shows the full scale part used for the impact test.

Figure 7.8: Part of EC-135 Tail-boom (left), Piezoelectric patch & SMARTape® (right).

7.4.2 Results and discussion

The following results show the response that can be expected when using optical fibre sensors. As shown in the pictures below, the RMS value from the signal of the acoustic response is increasing as impact energy exerted by the impactor becomes higher. This trend is measured for the PZT as well as the SM optical fibre. Additionally, a reproducibility test performed 10 times (see top axis) for impacts at 10 cm (white squares) shows that the results follow relatively a steady trend. The black squares represent RMS values for the main impact test dropping the sphere from 0 to 30 cm height (bottom axis). It must be mentioned that this impact is non-destructive.

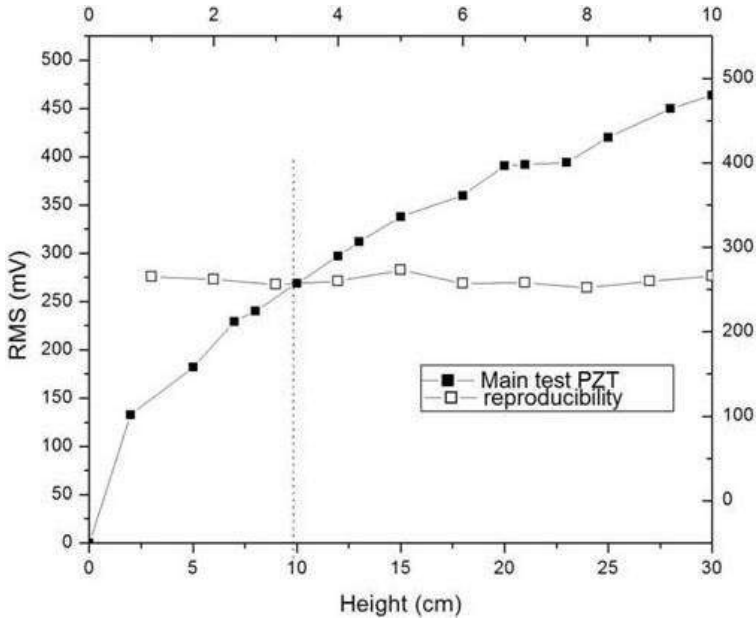

Figure 7.9: The acoustic response (RMS of electrical signal) as a function of the dropping height measured values for the reproducibility test at 10 cm for the PZT sensor.

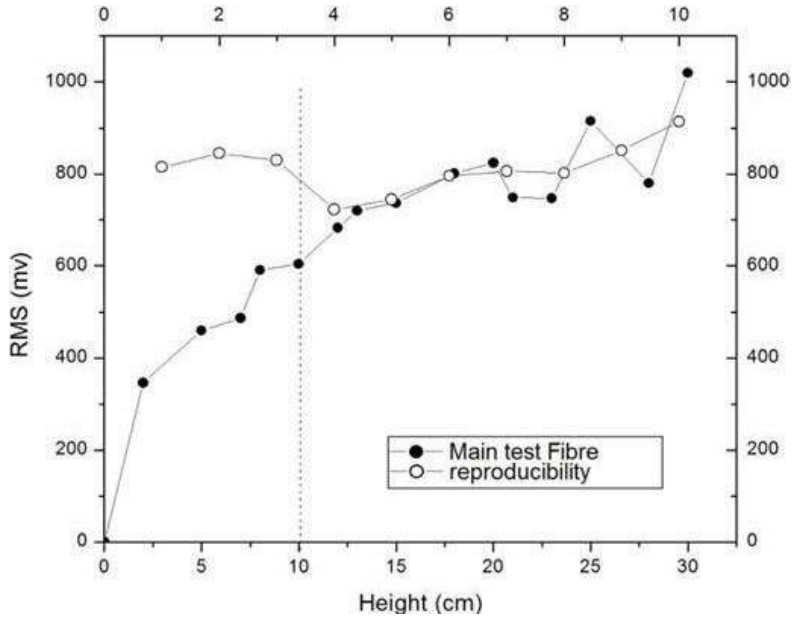

Figure 7.10: The acoustic response (RMS of electrical signal) as a function of the dropping height measured values for the reproducibility test at 10 cm for SM optical fibre sensor.

In a comparative experiment, the same impact was detected by the Single-Mode optical fibre in the SMARTape® and the piezoceramic patch (PZT). The graph in the next page shows the amplitude of the measured signals versus time (Figure 7.11). The voltage amplitude is measured in Root-Mean-Squared (RMS) values since they give an average of the amplitude values at each point of the waveform. The acoustic response shown by the fibres gave a relevant clear signal with no main interferences. It can be seen that the acoustic response by PZT is similar to the acoustic response of the SM optical fibre showing its potential as an acoustic sensor. Acoustic emission waveforms (2^{nd} burst is a second impact) and frequency distribution recorded by piezoelectric crystals (black line) and by optical fibres (green line), obtained from impact in monolithic carbon fibre reinforced epoxy plates.

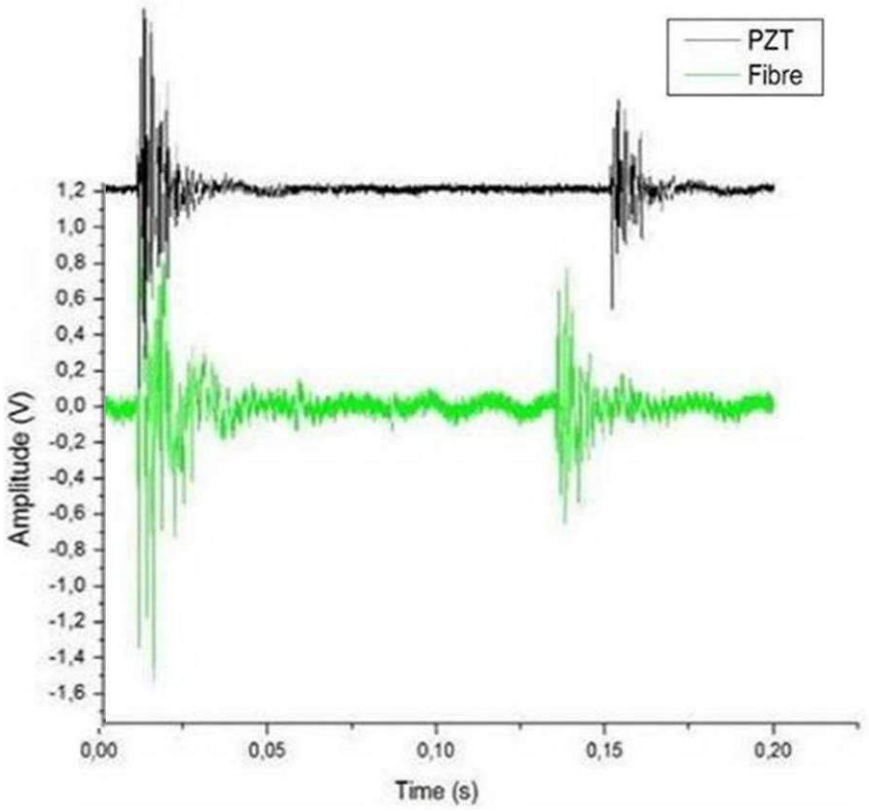

Figure 7.11: Optical fibre and PZT arriving acoustic signals (amplitude versus time) [198]. The SM fibre is more sensitive in acoustic interferences and its acoustic response has very small deviations compared to the acoustic response of the PZT which is almost flat between the two peaks. The second peak in the graph is from the second bounce of the impactor. The second signal arrives slightly earlier to the SM fibre since the impactor did not land on the same point.

The graph in the next page shows the comparison between the piezoelectric patches and the embedded optical fibre in the SMARTape on amplitude versus frequency (Figure 7.12). The graph shows the amplitude of the acoustic response in a range of frequencies up to 6 kHz.

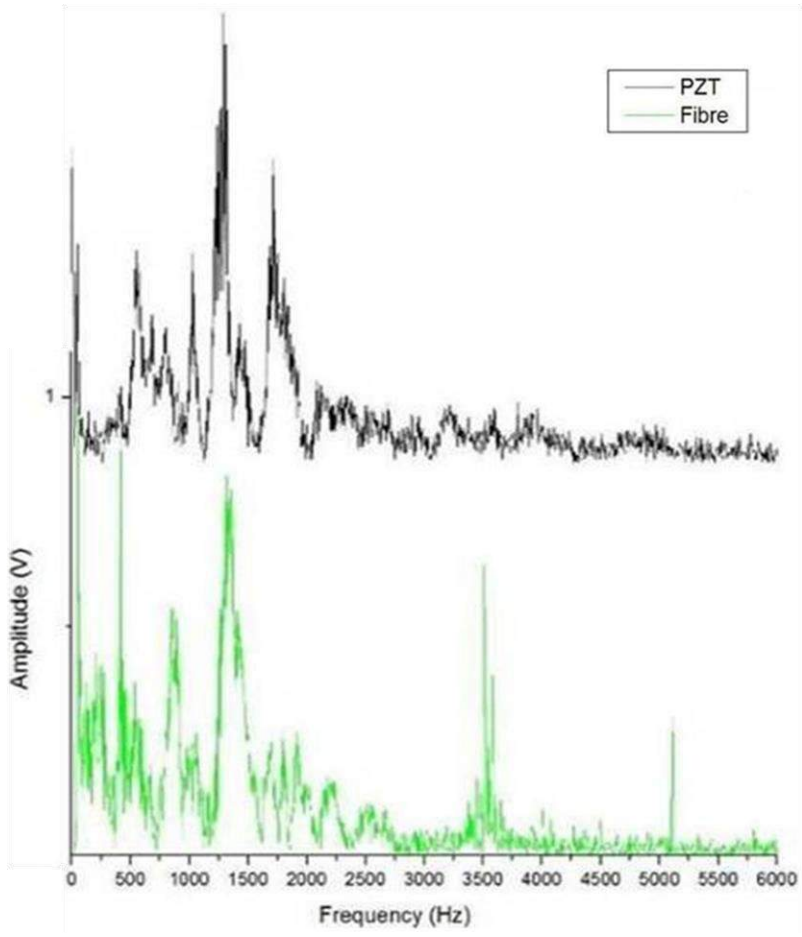

Figure 7.12: Optical fibre and PZT signals (amplitude versus frequency). The frequency response of the SM fibre has some noise artefacts due to the eigenfrequency of the fibre and its higher acoustic sensitivity than the PZT.

Optical fibre sensors even if they have lower RMS values, they show similar acoustic response to impact with the piezoceramic patches in such model situations. The graph shows noise artefacts that are represented by the multiple peaks

Optical fibre sensors of this type are line-integrating sensors while piezoceramic patches are point sensors [182]. Therefore, when the sensing area of the optical fibre is clearly larger than the wavelengths, the signal obtained by fibre sensor will nevertheless have a different acoustic response with respect to a point sensor. This phenomenon can be understood if one considers the optical fibre as a kind of acoustic interferometer.

Signals arriving from the acoustic source arrive at the fibre at different times (time-of-flight), according to their increasing distance from the source. The detector itself registers all incoming signals, thus adding-up all the incoming waves (see also [183]). Depending on the acoustic energy from the impact, there will be a phase shift of the light inside the fibre and a resulting waveform will be measured. Furthermore, the sensitivity for the detection of the Lamb modes, S_0 and A_0 depends on the polarization of the light propagating in the sensing fibre [184]. Lamb mode selection could therefore be achieved by corresponding polarizer settings using the polarization controller presented in the following paragraph.

7.5 Polarization analysis of optical fibres

In the literature, it has already been mentioned that the polarization of the light modes in the single-mode optical fibre has an influence on the sensitivity towards specific Lamb modes to be detected [184]. Therefore, a series of impact tests was performed at different degrees of polarization. Figure 7.13, shows a screenshot of the software used from the AGILENT polarization analyser/controller (N7788B-400).

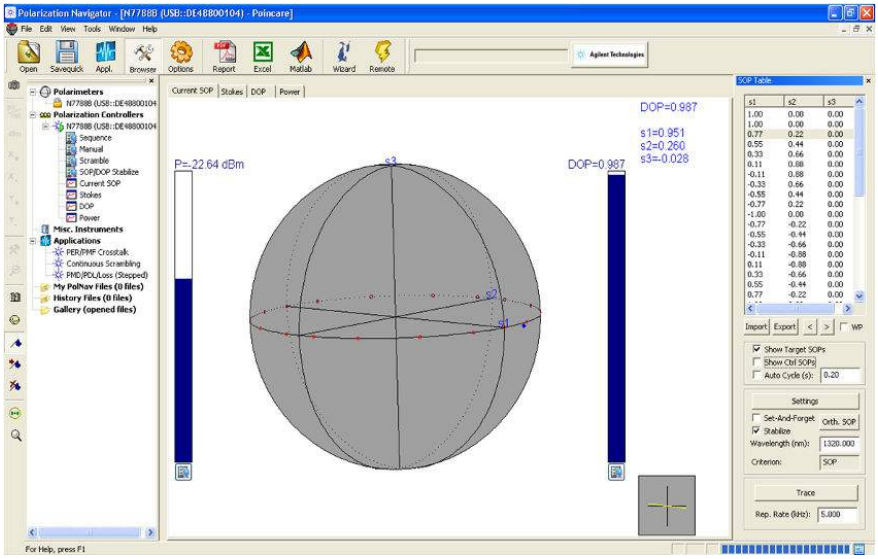

Figure 7.13: Screenshot of the polarization controller

The results below show the waveforms and the corresponding RMS values for different polarization angles (Figure 7.14).

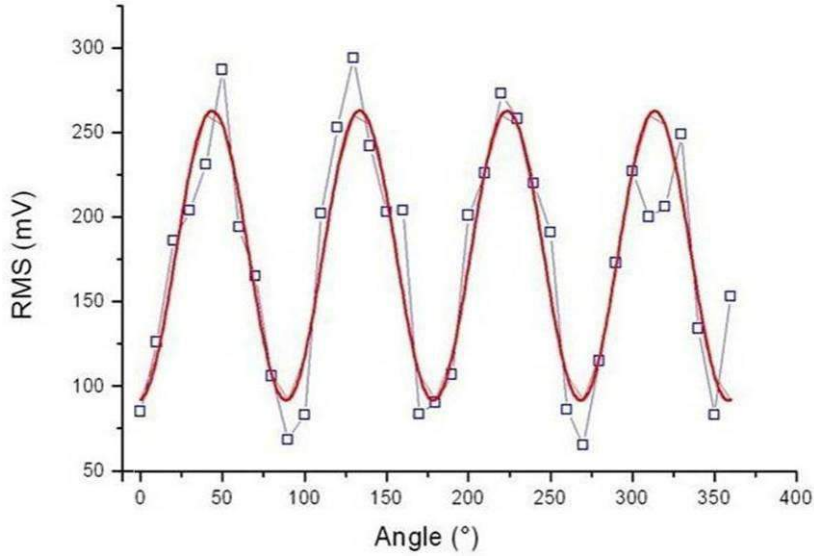

Figure 7.14: RMS for a non-destructive impact event (12 mJ) as a function of the polarization, the data were fitted by a sinusoidal function.

The results above also show that the polarization should be controlled when the instrument is used for damage detection. Otherwise, the amplitude could be underestimated by a factor of more than 3. Finally, a point to be mentioned is that polarisation control of optical fibres can have further operating restrictions such as temperature dependence, complex configuration and relatively high costs.

7.6 Impact energy and the square root law

The relationship between the impact energy and RMS values measured was determined for different impact energies and set-ups. For all cases investigated, the RMS values show a square-root behaviour versus the initial impact energy (see figure 7.13). Models on impact energies are analysed to account for this behaviour and, interestingly, this behaviour only holds for non-destructive impact. If the impact energies are higher, additional energy is consumed for the structural destruction of the material resulting in an acoustic energy lower than expected since a large part of the energy becomes thermal. For the case of non-destructive impact, the following considerations were made. According to the conservation of energy equation below, the kinetic energy (E_k) is equal to the potential energy (E_p) of the sphere at a height *h*:

$$E_k = E_p \Rightarrow \frac{1}{2} m v^2 = mgh \qquad \text{Eq. 7.2}$$

And the velocity becomes

$$v = \sqrt{2gh} \qquad \text{Eq. 7.3}$$

In non-destructive or elastic impacts, a part of the kinetic energy becomes acoustic forming elastic waves that propagate through the material. This acoustic energy is proportional to the time duration of impact of the sphere on the composite plate. In turn, the impact duration that is responsible for the generation of the acoustic wave depends on the velocity of the sphere at the time of impact. A study on the impact behaviour of glass/epoxy composite plates was performed by F. Mili and B. Necib showed that the deflections on the plate due to impact forces are directly proportional to the impact velocity [185]. Consequently, the height from which the sphere is dropped affects the voltage amplitude on the PZT that follows the square root of the height *h* according to equation 7.3. Correspondingly, J. Lee et al, showed that the velocity of impact material is directly affecting the voltage amplitude of the piezoelectric sensor [186]. Thus, the piezo-response follows linearly on the initial impact velocity and the deviation from this square root law directly shows when destructive processes occur.

The composite material of the EC 135 tail boom has a sandwich structure (honeycomb) with carbon-epoxy layers on the outer surface. The square-root law behaviour of the amplitude of the acoustic signal that can be seen in the graphs below is expected until the material reaches its elastic limit. After that point, the honeycomb material will deform plastically and inner damage will be induced. At that moment the total absorbing energy will be directly proportional with the incident impact energy and the deviation of above graphs can reveal the discontinuity of the material's structure [187]. Composite materials have complex failure mechanisms where the matrix is deformed from the dissipated energy that causes the plastic deformation [188]. Delaminations can appear between the core and the skin of the composite even if the surface might seem intact but they contribute to the structural integrity of the composite.

Heinrich Hertz was one of the first who thoroughly studied contact mechanics back in 1882 with his publication "Über die Berührung fester elastischer Körper" – "On the contact of elastic solids". Hertz's study was for isotropic materials, however, Svelko's contact theory that was based on Hertz's theory developed even further the distribution of contact stresses between two bodies of anisotropic materials [189]. According to contact theory when the impact velocity is increased, the contact duration between the impactor and the plate is also increasing. Therefore, the contact duration of the impactor with the plate is directly proportional with the amount of elastic energy that is transferred to the plate and increases the internal fibre failure stress. A parameter λ_i gives the response of fibre reinforced composite during impact according to the following equation [190]

$$\lambda_i = \frac{\left(\alpha_p K^{2/5}\right)\left(vm^3\right)^{1/5}}{h^2} \qquad \text{Eq. 7.4}$$

Where α_p is the unit laminate thickness parameter, K is the Hertz-Svelko factor, v the impact velocity, m the mass of the impactor and h is the height from which the impactor is dropped. The coefficient of restitution which reveals when the non-elastic impact occurs can therefore be determined in terms of the above parameter λ_i.

Figure 7.15 below shows the RMS values of the acoustic waves resulting from the non-destructive impact of the metallic sphere on the composite plate with respect to its drop height.

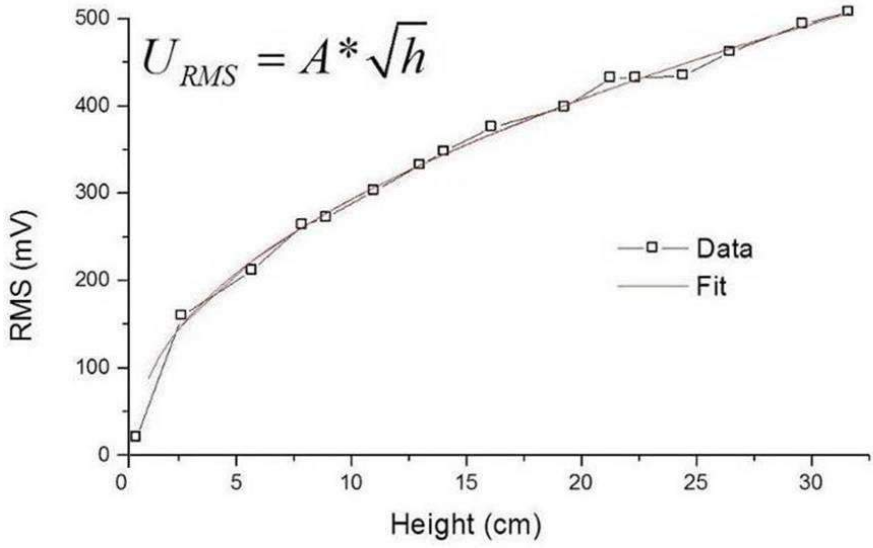

Figure 7.15: RMS value of acoustic waves versus non-destructive impact energy, the fit-curve is modelled by a simple square-root law.

A sphere made of plasticine with the same dimensions as the metallic sphere, thus with less weight, was used for reliability testing purposes in order to confirm the results in case the impact was not elastic but plastic and the material was stuck on the surface of EC 135 tail boom.

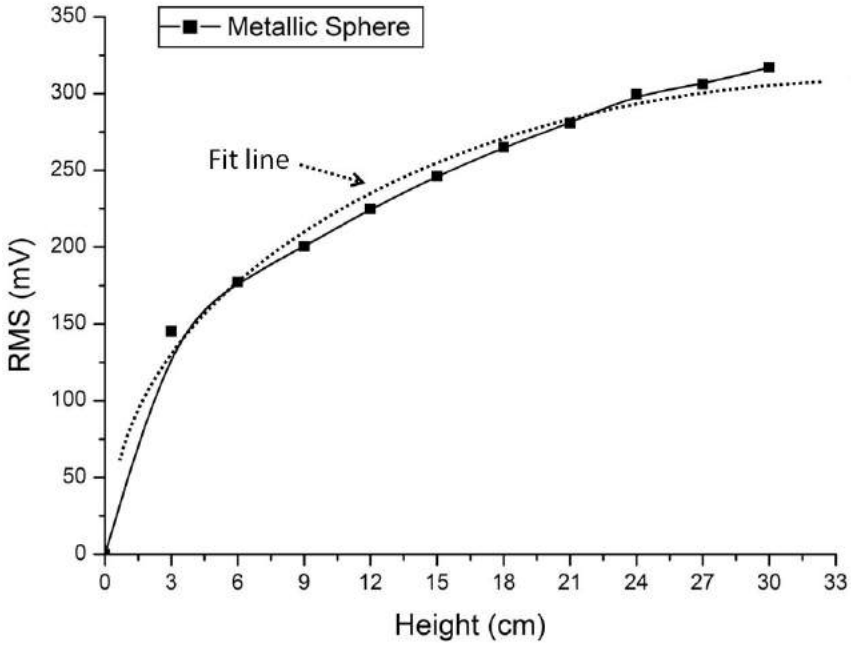

Figure 7.16: RMS value of acoustic waves versus height that corresponds to higher impact energy from a sphere made of plasticine. The dashed line follows the square root law and shows the data fit with the RMS values.

The following picture shows a screenshot of a Labview programme illustrating a possible steering programme for an impact detection system that shows the essential features of a final impact detection system (Figure 7.17). Two different thresholds can be defined in this programme, one for the amplitude of the impact pulse and one for its energy content. If an impact of certain intensity occurs, an alarm signal is given. Impacts from hazardous external parameters such as birds etc., that can hit an aircraft's critical part during flight, can be instantly be monitored by the optical sensors and give a direct signal on the material condition.

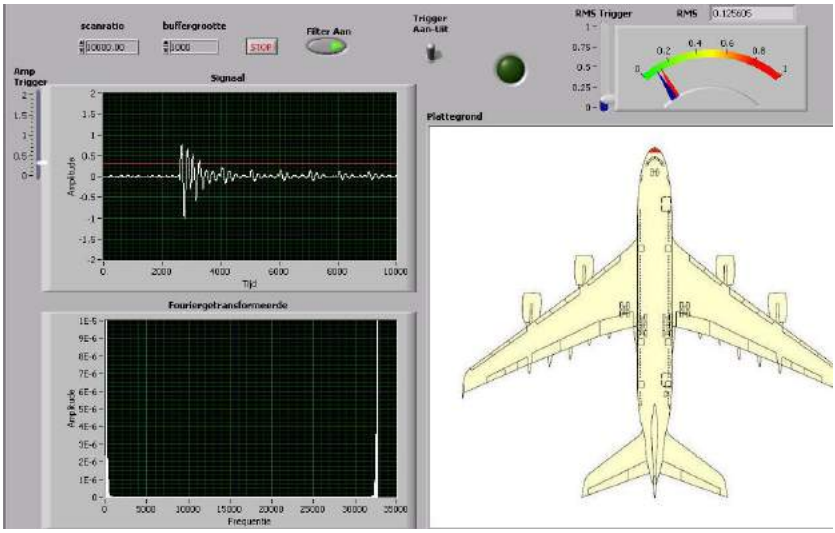

Figure 7.17: Screenshot of a Labview-programme showing essential features of an impact detection system, such as localization of impact on the aircraft and the range of impact energy by monitoring the RMS values of voltage amplitude. The graphs on the left side show the acoustic responses after an impact (top) and its frequency response (bottom). By using a range of frequencies, it is possible to choose the appropriate one for better damage detection.

7.7 Conclusions

The acoustic emission techniques mentioned in chapter 7 reveal some advantages such as the fast and accurate indication of a possible structural damage and the direct mounting of the sensors on the component under investigation. The acoustic emission method can be used for SHM while the component is subjected to vibrations and stresses in real operating conditions. The disadvantage of acoustic emission is that it usually gives an indication of the appearance of the damage but it does not always offer quantitative results of the size and the depth of it. However, the quantitative results can be obtained with a combination with other methods, such as ultrasonics, thermography or shearography.

This study shows that optical fibres in the polarimetric set-up can be used as appropriate sensors for the in-situ monitoring of impact. When compared with the conventional piezoceramic patches, the performance when regarding the signal-to-noise ratio of the acoustic response is similar. Comparing to PZTs, SM optical fibres have the advantage that they can detect larger areas with fewer sensors and less volume of cables.

Furthermore, the Probability of Detection (POD) using SM optical fibres and PZTs depends on the signal quality and the amount of acoustic inferences. The following

table below shows the advantages and disadvantages using SM optical fibres as a SHM method.

Advantages	Limitations
Independent from electromagnetic interferences	No indication of size and depth of damage
Similar acoustic response with PZTs	Complex data acquisition
Can cover larger areas than PZTs	Relative high cost of instrumentation
Less volume of cables than PZTs	Initial Polarisation state depends on temperature and other environmental variables
Cheap sensors with high sensitivity and potential in SHM	Automated polarisation controller still expensive
	Additional equipment is needed for noise filtering that adds some cost and weight

Table 7.1: Advantages and disadvantages of optical fibres as a SHM method.

Published proceedings
"Impact damage detection in composite materials of aircrafts by optical fibre sensors", I. Pitropakis, H. Pfeiffer, M. Wevers, 10th European Conference for Non-Destructive Testing (ECNDT 2010), Moscow, Russia, 7-11 June 2010
"The use of a polarimetric fibre sensor to detect impact damage in aircraft composites", I. Pitropakis, H. Pfeiffer , M. Wevers, ISBN 978-0-415-62131-1, 5th International conference on Emerging Technologies in Non-Destructive Testing (ETNDT), Ioannina, Greece, 19-21 September 2011
AISHA II presentations
"Damage detection with optical fibres in EC 135 Tailboom", I. Pitropakis, AISHA II meeting in EUROCOPTER, Marignane, France, 27-28 January 2010
"Damage detection in EC 135 Helicopter Tailboom", I. Pitropakis, AISHA II meeting in MEGGIT SA, Helsingor, Denmark, 31 May - 1 June 2010

Table 7.2: Contributions.

"Not everything that is counted counts and not everything that counts can be counted."

Albert Einstein (1879 - 1955)

CHAPTER 8

SHM using Lamb waves and the application of pseudo defects for signal validation

A common NDT technique that is applied for damage detection is using Lamb waves. To initiate Lamb waves, lead zirconate titanate transducers (PZTs) were used in this study. PZTs excite and receive acoustic signals that are carrying information regarding the structural continuity of the medium. Pseudo defects of various shapes and size were attached on the surface of an aluminium plate in different angles simulating damage conditions of real defects. The acoustic signals received on the PZTs were investigated and compared with a reference signal when there was no defect. The main purpose of this approach was to investigate the acoustic responses of the pseudo defects and compare them to those of real defects.

8.1 Motivation

One prominent possibility to detect damage in aircraft materials is non-destructive testing (NDT) using ultrasound [191]. Ultrasonic waves are usually excited and sensed by piezoelectric crystals that offer excellent possibilities in non-destructive testing since many decades. However, these are essentially point sensors, implying a number of disadvantages, such as the vulnerability to interferences. A possible solution is the application of ultrasonic array sensors, but these arrays are usually costly high-tech devices, difficult to wire and integrate. Nevertheless, the ultrasonic wave technology it still under development and has a great potential. Therefore, its further investigation has a positive value for SHM in plate-like structures.

In this study, ultrasonic Lamb wave technology is used as the basic physical damage detection principle for developing an aircraft damage monitoring system. Lamb waves were firstly described in theory by Horace Lamb in 1917 [192]. They are essentially ultrasonic waves that propagate in a solid plate with free boundaries [193]. Lamb waves differ from classic bulk ultrasonic waves in their propagation properties:

- Lamb waves propagate in plate-like structures
- Lamb waves can propagate over longer ranges (up to tens or even hundreds of metres) and they are therefore well-suited for global and long range inspections

Many components of an aircraft's structure are flat, curved and plate-like. Due to the dominance of these plate-like structures, the use of Lamb waves is beneficiary to be exploited as a non-destructive technique for SHM. The detection of material damage with Lamb waves is based on the fact that the propagation of these wave types is affected by the presence of phenomena like corrosion, cracks, pits or delamination. The signals that are obtained from samples with pre-defined natural defects, such as cracks, flaws or other artificial defects such as notches or boreholes are compared with signals obtained from undamaged samples. In that way Lamb wave testing is assessed towards its reliability and accuracy [194].

8.1.1 Lamb wave modes

One important basic property of Lamb waves is their inherent dispersive nature: the velocity of propagation of a Lamb wave depends on the frequency and the thickness of the plate. In Lamb wave testing applications the symmetric mode (S-mode) and anti-symmetric mode (A-mode) are most frequently used. These modes require frequencies that are below 1 MHz [195]. Figure 8.1 shows Lamb wave dispersion curves for the basic S-modes and A-modes in an aluminium plate with respect to the frequency-thickness fraction.

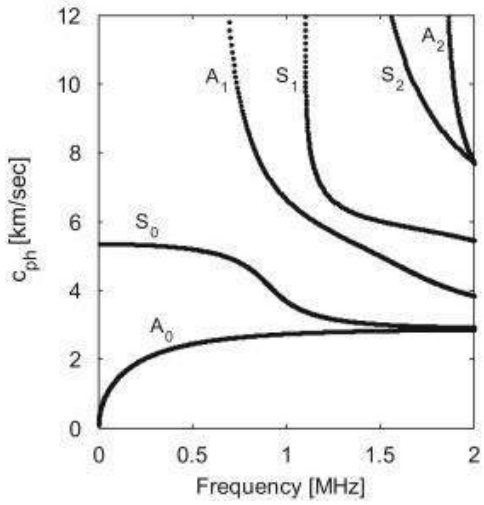

Figure 8.1: Lamb wave dispersion curves in an aluminium plate (phase velocity for symmetric and anti-symmetric modes) [196]

Lamb wave modes partially reflect at defects, but a part of their energy is also transmitted, so both configurations (transmission and reflection) can be used for detection. Therefore, the influence of different sizes and depths of various defects but also pseudo-defects on the Lamb wave modes is monitored. For fixed low frequencies, the symmetric (S) and anti-symmetric (A) modes have different velocities when they propagate through the medium. The symmetric and anti-symmetric zero modes (S0 & A0) are existing for the whole frequency spectrum from the lowest to very high frequencies. Figure 8.2 in the next page shows a B-scan presenting the phase difference of the velocities for the two modes when propagating on the aluminium plate. The excitation frequency on the PZT was 400 kHz. The B-scan is generated in Matlab. The dark blue colour is the baseline of zero amplitude, while the brighter colours are representing an increase in amplitude with the red colour being the highest peak. The amplitude changes that are apparent below the two modes are the acoustic reflections. The B-Scan was obtained from a 1 mm thick aluminium plate using PZTs for excitation and acoustic receipt purposes. Paraffin was used as a coupling medium between PZTs and the plate. Paraffin's advantages are that it can be reused when heated; it provides better coupling ability than grease and offers also better vibration transmissions.

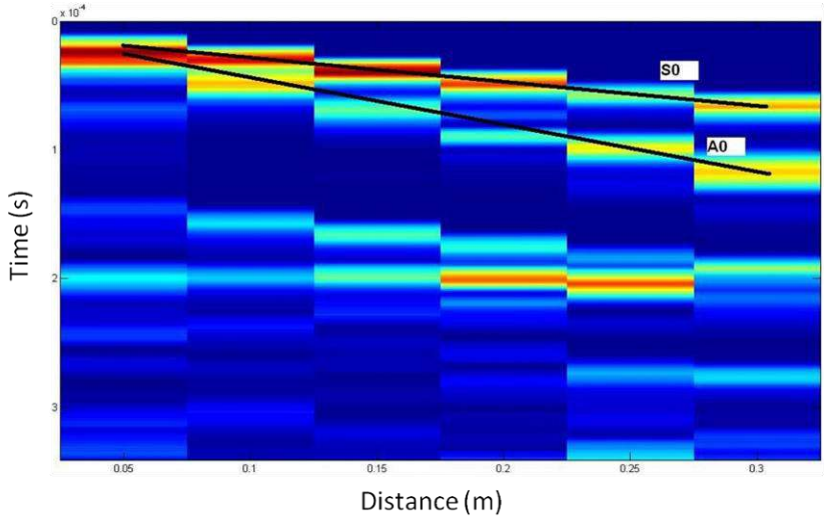

Figure 8.2: B-scan showing the time delay of the S0 and A0 modes with excitation frequency of 400 kHz on the aluminium plate.

By analogy with Thursby et al. [184], the location of a defect is identified by investigating the different pathways of a signal. When multiple sensors are placed in different positions, the path of the acoustic waves from the actuator to the receivers will also be different. However, when the receivers are positioned in multiple locations, then the combination of the received signals can give a better indication of the possible location of the defect than using one receiver positioned at a single point. A second method is to measure delay in the arrival time of the Lamb waves (or the difference in velocity). If there is a presence of a defect in the pathway of the wave, the amplitude of the wave is affected. Using a sensor network in this way it is possible to identify the location of the defect [197, 198]. In composite materials, the arrival times of the waves are heavily dependent on the orientation of the fibre reinforcement since the internal structure affects the propagation velocities of the acoustic waves.

8.1.2 Application of Lamb waves in this study

Aircraft structures have a diversity of shapes, are built by different kind of materials and are subject to various kinds of damages. For a reliable SHM system, it is important that the appropriate parameters for each application are well defined. The tests in this study were performed on aluminium plate-like samples with a thickness of 1mm. It is important to select an appropriate driving frequency in order to define an appropriate SHM system based on Lamb waves [199]. From literature but also from experimental observation, for given thickness and material, the most appropriate frequency for Lamb waves is between 300 to 400 kHz [200,201]. In general, acoustic waves that propagate in aluminium plates with low

thickness need smaller wavelengths and therefore, they require a higher frequency range since for all waves the following equation applies:

$$c = f * \lambda \qquad \text{Eq. 8.1}$$

Where c is the wave velocity, f is the frequency and λ is the wavelength. In frequency of 400 kHz, the S_0 mode is giving a group velocity of 5,400 m/s according to the dispersion curve in figure 8.3 below. Thus, following the equation above, the corresponding wavelength is 13.5 mm.

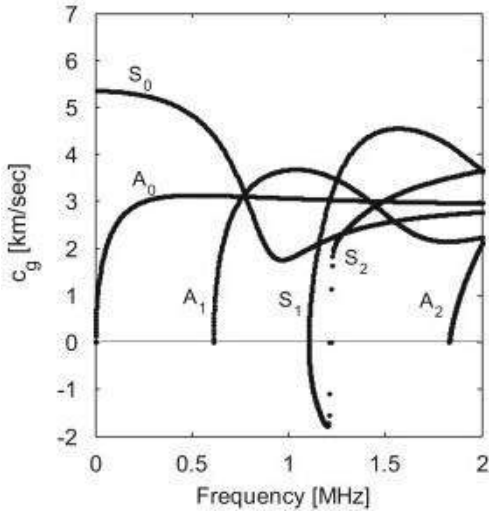

Figure 8.3: Lamb wave dispersion curves in an aluminium plate (group velocity for symmetric and anti-symmetric modes) [196]

Figure 8.3, below shows a piezoelectric transducer attached on an aluminium plate and shows in a schematic way how reflected or transmitted Lamb waves are used for the detection of a defect.

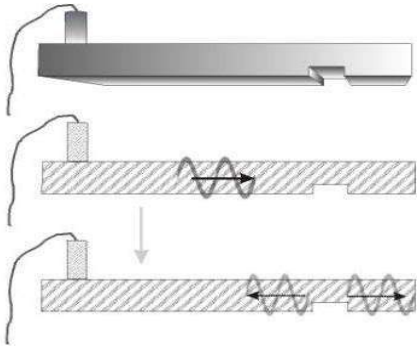

Figure 8.4: Representation of defect detection using Lamb waves [194].

Most of the aircraft structures are made from materials such as aluminium alloys and carbon fibres composites. The last years there is a tendency that composite materials are replacing aluminium due to their very good strength to weight ratios. Although the Lamb wave propagation in anisotropic composite materials is more complex than in isotropic, Lamb waves can be used in both types of materials and provide solutions in SHM [202].

8.2 Materials and methodology

8.2.1 Piezoelectric transducers

The piezoelectric transducers that generate and detect the Lamb waves were made of lead zirconate titanate (PZT). The PZTs were positioned in specific areas on the sample under investigation in order to enable optimised "probability of detection" (POD). These surface acoustic Lamb waves that are excited on the surface of a solid material are also called Rayleigh waves named by the John William Strutt, 3rd Baron Rayleigh, who was the first who discussed about their existence [203].

The whole concept of generation and detection of ultrasonics in technical applications is mostly based on piezoelectricity. Piezoelectricity is a phenomenon where mechanical stress is transformed into an electric field and vice versa. It can be found on the surfaces of specific materials. When they are subjected to a vibration or stress, the internal structure of the molecules, that form the material's crystal, is deformed. It is observed that this deformation of the molecules creates positive and negative charges and therefore an electrical polarity is generated [204].

Figure 8.5 below, shows a round PZT attached near a pseudo-defect on the aluminium plate as well as the variety of pseudo-defects that were used for the tests. The height of the round pseudo defects was 15 mm and the height of the rectangular pseudo defects was 10 mm while their length and width varied between 5 mm and 40 mm.

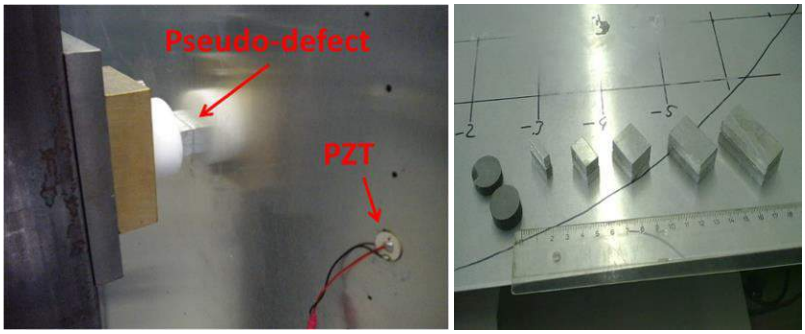

Figure 8.5: PZT and pseudo-defect attached on the plate (left) and different shapes and sizes of pseudo-defects (right).

PZTs are acting here as transducers that excite and receive acoustic vibrations. In order to attach them but also to remove and re-attach them for the test purposes, grease or paraffin was used as a coupling agent between the PZTs and the surface of the aluminium plate. This technique has been previously proved successful in order to achieve low noise and clear wave signals from the PZTs [205]. The PZTs were provided from Meggit PLC, Helsingør, Denmark. Meggit PLC is one of the industrial partners of the AISHA II European project.

8.2.2 Set-up for the aluminium plate 1x1m

In order to hold the 1x1m plate and to press the pseudo-defects on both sides a metallic frame with adjustable clamps was used. Figure 8.6 below, shows the design of the frame and the two clamps that are used to press the pseudo-defects against the plate. The plate was placed inside the frame using four non-conductive holders at each edge.

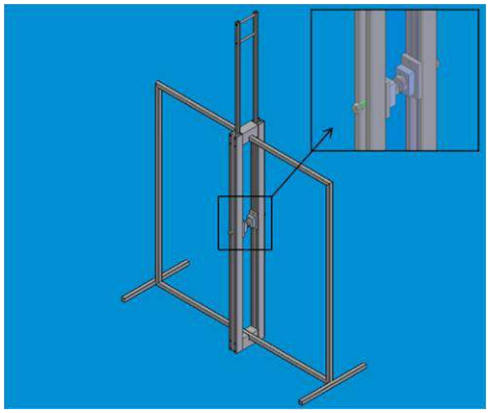

Figure 8.6: Holding equipment for 1x1m plates and pseudo-defects.

The pseudo defects were positioned between the clamps at various positions on the surface of the plate. An illustration of the set-up using a rectangular pseudo defect and 2 PZTs for the investigation of the acoustic signal is presented in the figure 8.7 below.

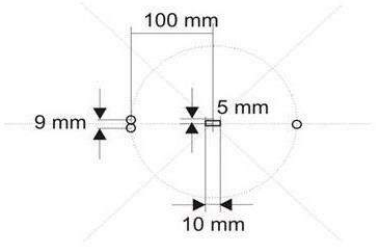

Figure 8.7: Layout and position of sensors and pseudo defect. The circles are the PZTs and the rectangular is the pseudo defect.

In the previous figure, when the source and receiver are located next to each other and opposite the pseudo defect, then the reflection of the Lamb wave is investigated. In contrary, when the pseudo defect is located between the source and the receiver, the transmission of the Lamb wave is investigated.

8.2.3 Application of pseudo defects

A point that needed to be investigated was the amount of pressure that had to be applied on the pseudo defects in order to get the best measurements possible in point of acoustic reflection or transmission. The more force was applied on the pseudo defect, the more it was pressed on the aluminium plate and therefore, it was affecting the reflection or transmission of the acoustic signals from the PZTs. A screwdriver with adjustable torque settings was used for the above reason. The investigation of this behaviour within the AISHA II research was first studied by Professor Vitalij Pavelko from the Riga Technical University (RTU), Latvia. The results in Riga but also in Leuven showed that above a specific value of torque and further, the amplitude of the acoustic signals was not changing. This value of torque was adequate to rely on and it was used to press the pseudo defects on the plate. Table 8.1 below, shows the amount of force applied on the pseudo defects and figure 8.8 shows how the acoustic signal stays stable above 400 N.

Torque	Force	Peak-to-Peak	RMS
Nm	N	mV	mV
0	0	3.46	1.16
2	235.3	2.66	1.15
2.5	294.2	2.64	1.12
3	352.9	2.58	1.07
3.5	411.8	2.54	0.864
4	470.6	2.54	0.86
4.5	529.4	2.54	0.861

Table 8.1: Peak-to-Peak and RMS values for different values of force.

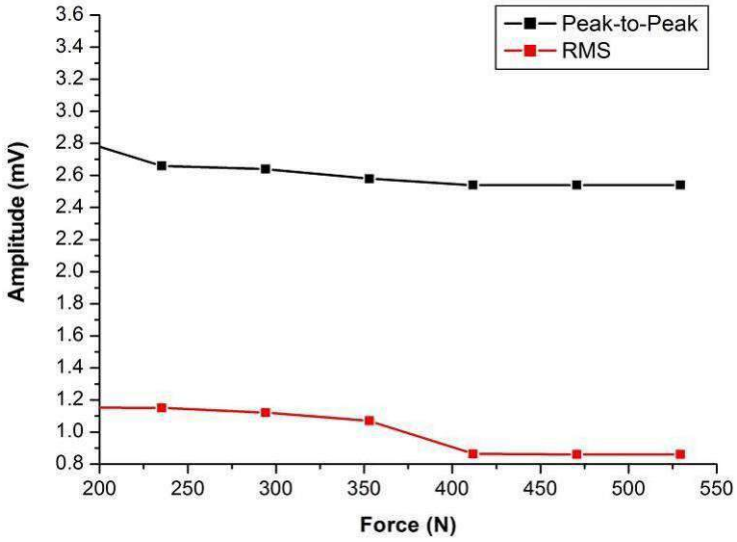

Figure 8.8: Acoustic signal remains relatively stable after an amount of force applied on the pseudo defect. The arriving acoustic signal is transmitted through the pseudo defect from the actuator to the receiver

The investigation on the reflection and transmission of the Lamb waves by the pseudo defects was performed through a series of tests. Different shapes of pseudo defects were used and they were positioned in different angles in order to examine their influence on the acoustic response. Usually, the pseudo defect was positioned in the centre of the plate and the PZTs were allocated around it. One PZT was the source exciting guided waves and another PZT was the receiver, receiving the acoustic signal. The acoustic signal from the wave generator was at a frequency of 350 kHz with 5 counts of burst at an output voltage of 10 V_{pp}. It was initiated from an Iwatsu Pulse/Function Generator and it was finally analyzed in a Tektronik DPO 4034 Digital Phosphor Oscilloscope, which was generating the relevant waveforms showing the amplitude on the Y axis versus time on the X axis.

8.3 Results and discussion

8.3.1 Reproducibility tests

Prior Lamb wave testing using pseudo defects, reproducibility tests were performed to confirm the consistency of the results from the acoustic measurements when the PZTs were attached on the aluminium plate. Two PZTs were used. The first PZT was used as a receiver at a steady point and the other was the excitation source which was re-attached 10 times for reproducibility purposes. The distance between the PZTs was 30 cm and the coupling medium was paraffin. Paraffin is melting at a temperature of 70 °C. The sensor is touching the paraffin

while it is in the liquid phase. After seconds it cools down and creates a small solid layer on the sensor. Then, the sensor is attached on the aluminium plate by holding it at the point of preference and at the same time the aluminium plate is heated on the other side using a steamer. The heat melts the layer of paraffin and the attachment on the plate is successful. To remove the sensor, the plate is heated using the steamer at the point where the sensor is attached and then the process is repeated 10 times for reliability purposes. Table 8.2 below shows the root mean square (RMS) values of the amplitude of the acoustic response in millivolts. The test showed that the acoustic deviation was less than 10% which was within the reasonable limits. Figure 8.9 shows the sender and receiver positioned opposite each other.

No. of attachments	RMS value (mV)	Mean (mV)
1	7.3	7.9 ± 0.6
2	7.7	
3	7.8	
4	7.5	
5	7.7	
6	8.5	
7	7.9	
8	8.2	
9	8	
10	8.3	

Table 8.2: RMS values of the acoustic signal on the PZT when attached 10 times.

Figure 8.9: Sensors attached on the aluminium plate by paraffin in a set-up to test the reproducibility. The left PZT is used as an excitation source on the aluminium plate and the excited signal is coming from the waveform generator at 350 kHz with 5 bursts at 10 V_{pp}

8.3.2 Acoustic responses

As stated above, the main purpose of the use of the pseudo defects was to investigate the acoustic response with respect to a comparison of pseudo and real

defects. As motivated above, the advantage compared to real defects, is that the pseudo defects that give a clear echo can be removed from the plate without damaging the material (Figure 8.10 [194]).

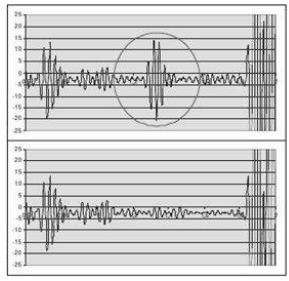

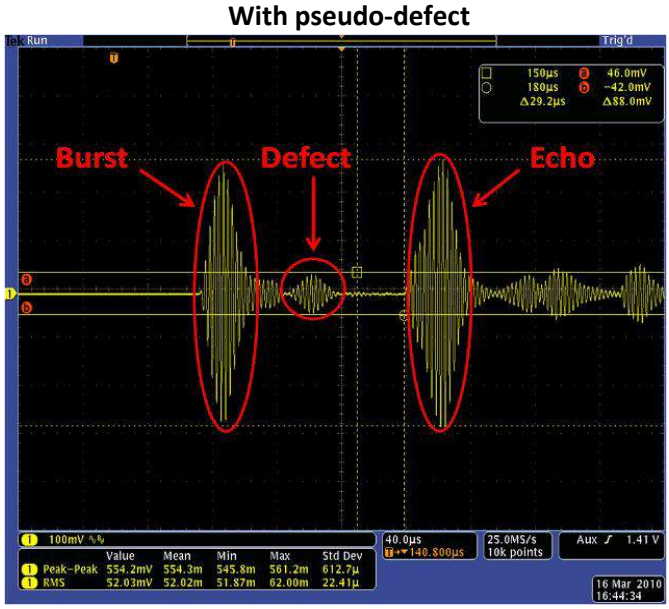

Figure 8.10: Upper figure: Received waveforms with and without pseudo defect. Lower figure: Waveform generated from a Tektronik DPO 4034 Digital Phosphor Oscilloscope. The amplitude change caused by the pseudo defect is apparent next to the first burst.

The main difference between a real defect and a pseudo defect is the amplitude of the reflected acoustic signal. The pseudo defects are pressed against the material and this gives them a reduced acoustic contact with the sample under investigation compared to a real defect where part of material is missing. Taking this factor into account we can prejudge that in case of a real defect, the acoustic response will be much stronger. Furthermore, in this study, the influence of the size and position of the pseudo defects on the reflected acoustic signals is investigated together with the comparison of the acoustic response for the pseudo defect and for a real

defect. Figure 8.11, shows how the RMS value is changing when a rectangular pseudo defect is positioned in different angles.

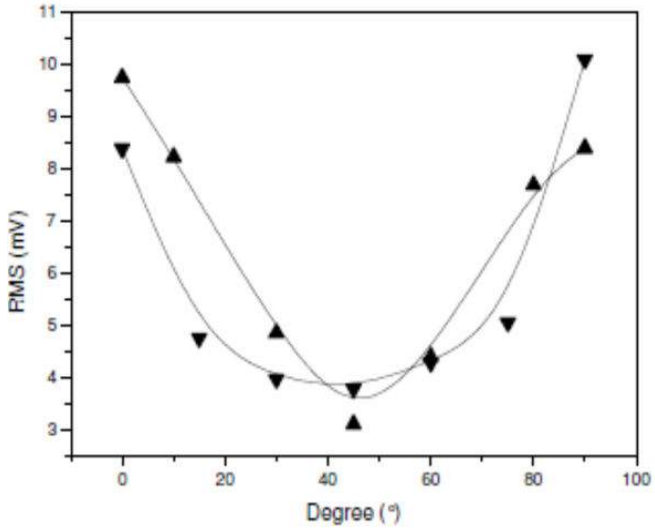

Figure 8.11: RMS of acoustic responses reflected at square-cut pseudo-defects as a function of the angle towards the wave front. The two curves represent slightly different positions with respect to the source.

The orientation of the pseudo defect alters the direction of the acoustic reflection. Thus, the reflected signal that is recorded from the PZT has different amplitude with respect to the angle. The results are given by the Root Mean Square (RMS) values and peak-to-peak values taken from the given waveforms that were obtained representing the acoustic response at a specific time gate. This can be easier understood by using a rectangular pseudo defect. In figure 8.12, below, a square pseudo defect is positioned at 15, 25, 45, 60, 75 and 90 degrees with respect to the direction of the excited acoustic wave from the PZT. The graph shows how the position of the pseudo defect influences the amplitude of the acoustic response due to the different angles of signal reflection.

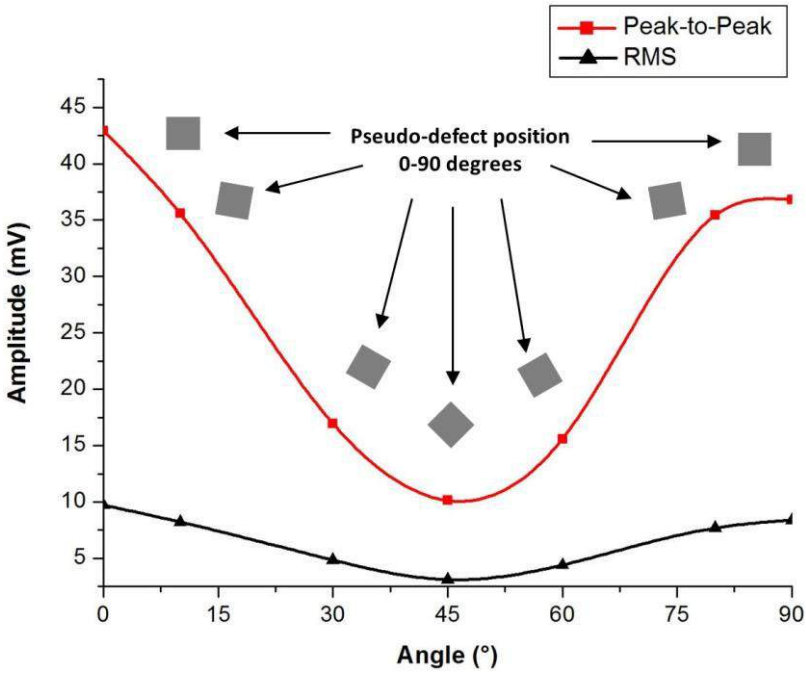

Figure 8.12: RMS and Peak to Peak values of the reflected acoustic signal at the PZT in relation to the different angles of the pseudo defect.

8.3.3 Comparison between defects and pseudo defects

Relationships of the amplitudes of the acoustic response between defects and pseudo defects are necessary to be analogous to each other and stable in order for the system to be validated. The pseudo defects can be applied with different sizes and orientations, and the reflected signal is influenced by it. The amplitude of the reflected signal is e.g. directly proportional to the size of the pseudo defect. This is expected since the larger the area of the pseudo defect, the more signal is reflected back. However, the amplitude values of the reflected signal from the pseudo defects are systematically lower than the signal arriving from real defects since there is no absence of material. Additionally, it has to be taken into account that the reflected signal could also show high amplitude values due to the superimposing of two waves that causes interference and not due to the size of pseudo defect. By knowing the RMS ratio, a calculation and prediction of the RMS values expected from a defect is feasible. In that way, the size and the location of the defect can be estimated. Figure 8.13 below illustrates a comparison of the acoustic response between a pseudo defect and a real defect. When a pseudo defect is applied, the RMS amplitude of the acoustic response is significantly lower than the amplitude when a real defect is apparent. In this experiment, the pseudo-defects were rectangular with 5 mm in width and from 5 mm to 40 mm in length.

Excitation frequency was at 350 kHz and the pseudo-defects were positioned perpendicular to the direction of wave propagation.

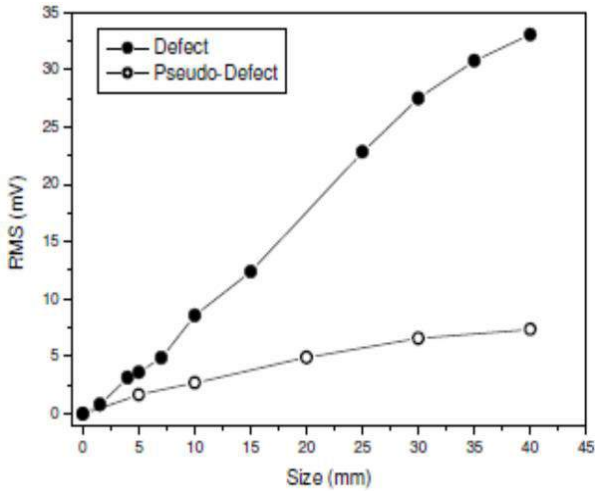

Figure 8.13: RMS of waveforms reflected at pseudo-defects and artificial defects as a function of the length of the reflector being in line with the wave front.

Figure 8.14 below presents a nomogram that shows the RMS factor that can be calculated for a given size of a pseudo defect. The nomogram can thus predict the amplitude of the RMS value the real defect would have.

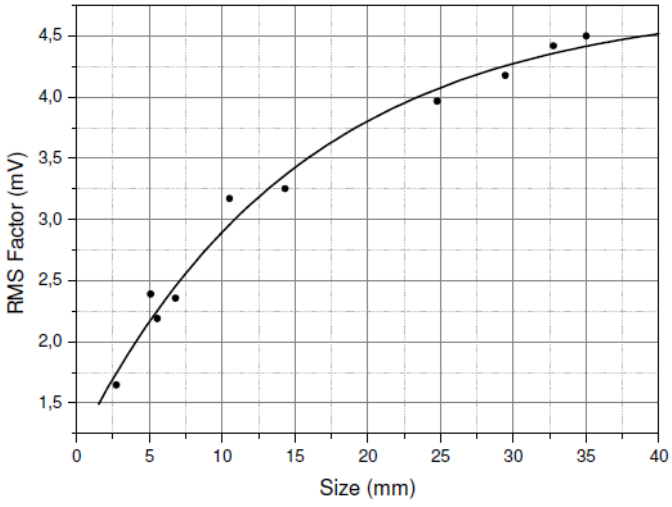

Figure 8.14: Nomogram presenting a conversion RMS factor for a given size of a pseudo defect that reflects the acoustic signal. From the above data, the RMS value of a real defect can be estimated, eg. 2,3 mV correspond to 5 mm.

The above graph can also be used vice versa in order to estimate the size of a real defect from the measured RMS value. The dots are the experimental results of the RMS values that follow a specific trend.

8.4 Conclusions

The results above indicate a clear comparison and relationship of the signals between real defects and pseudo defects. The pseudo defect setup can therefore be used as a tool for the validation of defect detection systems in plate-like structures providing analogous acoustic values of reflection and transmission. An important advantage of pseudo defects is that they offer flexibility for signal comparison since they can easily be removed and afterwards moved to another position. In the case of real defects, the magnitude of the signals is higher. However, the incremental change of the dimensional parameters in each case is related between the two types of defects. Therefore, a correlation of the signals of the real defects and the pseudo defects is feasible and can be filed in a database. This can enable a mapping for the probability of the detection of real defects at different positions.

The Probability of Detection (POD) using Lamb waves clearly depends on the size and the orientation of the defect as well as on the shape of the inspected material. The following table below shows the advantages and disadvantages using Lamb waves as a SHM method.

Advantages	**Limitations**
Lamb waves can cover large areas	Dispersive characteristics
Easy installation of PZTs	Multiple waveforms in single frequency – thickness dependent
Localization of defect using multiple sensors	Volume of cables for array of sensors – added weight
Cost effective and efficient method	Guided waves require active driving mechanism - voltage supply
Can be used in both metallic and composite materials	Difficult signal interpretation when multiple reflections at boundaries occur.
Can easily be removed and repositioned	Not very thin cracks can be simulated, no non-linear behaviour can be tested
	Performance is subjected to noise interference and for the noise filtering additional equipment is needed that adds weight and cost

Table 8.3: Advantages and disadvantages of the use of Lamb waves as a SHM method

Published proceedings
"The use of pseudo-defects in validation of ultrasonic structural-health-monitoring technologies", H. Pfeiffer, I. Pitropakis, M. Wevers, 10th European Conference for Non-Destructive Testing (ECNDT 2010), Moscow, Russia, 7-11 June 2010
AISHA II presentations
"Pseudo defects", I. Pitropakis, AISHA II meeting in Fraunhofer Institute for Manufacturing Technology and Advanced Materials (IFAM), Bremen, Germany, 17-18 September 2009
"Imaging of defects using air-coupled Lamb wave detectors", I. Pitropakis, AISHA II meeting in LUFTHANSA TECHNIK, Frankfurt, Germany, 26-27 January 2011

Table 8.4: Contributions.

"If you only do what you know you can do then you never do very much."

Tom Krause (1934 - 2013)

CHAPTER 9

Detection of aqueous corrosive liquids in confined parts using percolation sensors

Corrosion is a major problem for the durability of metallic structures. A prerequisite for corrosion is the presence of electrolytes in the respective structural parts of the aircraft. The performance of a sensor that is able to detect aqueous liquids is presented in this chapter. The principle of detection is based on the collapse of the percolation conductivity on the conductive part of the sensor. These sensors can be placed on the floor beams below the cabin of the aircraft and a few have been already installed in 3 airplanes of Lufthansa that are in operation and so far they give promising results.

9.1 Motivation

Corrosion problems in the aerospace sector are very costly, as an example, only the United States Defence department spends about $ 10 billion annually for corrosion maintenance in aviation equipment [206]. Aircraft structural parts are designed and built to be corrosion resistive. They are carefully coated and protected against possible means of corrosion. Therefore, the right material selection and the use of corrosion resistive materials for finishing can reduce the rate of corrosion. Nevertheless, the presence of corrosion depends on the existence of aqueous liquids and in the long run it is very difficult to be avoided. Consequently, one of the most important means for SHM in confined areas should be obtaining information on the presence of wetness. By knowing the presence of wetness, we can predict the possibility of corrosion in that area.

Figure 9.1: Floor beams inside an Airbus A320 after removal of the floor panels (photo courtesy of Lufthansa).

Due to their complex design, confined parts can frequently be found in aircraft structures and such spaces are more difficult to monitor because of the restricted access. Moreover, they are also not always designed to host workers for maintenance purposes [207]. Examples of such parts are the beams that are located below the floor of the cabin of an aircraft. They run across the aircraft along its length and support the floor composite plate of the cabin. Airlines have a scheduled maintenance program but usually the time interval between these maintenances is very long (4-6 years) so that the corrosion can usually not be detected in an early stage.

9.2 Materials and methodology

9.2.1 Materials selection for the sensor

The sensor in this study is made of an organo-ceramic composite that consists of a conductive Titanium Carbonitride (TiCN) powder and Polyvinyl Alcohol (PVA) [208]. PVA can be found commercially as a product of polyvinyl acetate (PVAc). During production phase, PVA can be either partially hydrolyzed or fully hydrolyzed that affects its solubility. It is a water soluble polymer with a broad range of applications. It has very good adhesive properties and good resistance to oil and solvents. Additionally, it has good mechanical properties being flexible withstanding high tensile stress. Depending on the grade of hydrolysis, its melting point can reach up to 230 °C. The Polyvinyl alcohol (PVA – CAS 9002-89-5) was 95 % hydrolyzed (M_w = 95.000) and was obtained from Acros Organics, Geel, Belgium.

The other compound of the mixture, TiCN, is conductive ceramic consisting of titanium nitride (TiN) and titanium carbide (TiC) in a ratio of 70/30 respectively. TiCN is a variant of TiN but it has better hardness and a high melting point together with good thermal and chemical stability. It also has excellent electrical and thermal conductive abilities, which makes it a perfect candidate for the conductive part of the sensor. TiCN was obtained from HC Starck, Lautenburg, Germany and the mean grain size was 1.2-2.0 micrometers.

The two compounds were mixed in an appropriate volume fraction (x_v =0.46). The figure below shows the concentration correlation of the components when there is water ingress. Depending on the concentrations of the PVA and TiCN, the composite is behaving as either as an insulator or a conductor.

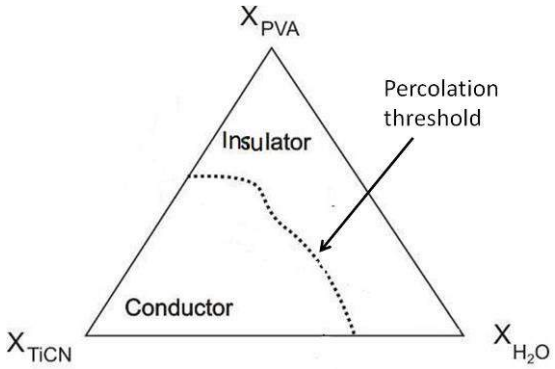

Figure 9.2: Principal scheme of a three component (PVA – TiCN – H_2O) phase diagram indicating the conductivity area as a function of mole fractions. The dotted line shows the point of the percolation threshold. TiCN and H_2O are the conductive elements while PVA is the insulator.

The microstructure of the composite can be seen in the figure below using scanning electron microscopy (SEM Philips XL30 FEG). The TiCN particles are embedded in the hydrophilic PVA matrix. The volume fraction of TiCN for this sample was x_v = 0.46. This volume fraction has been selected for the final sensor design. The size of TiCN particles is given in micrometers in the following photo.

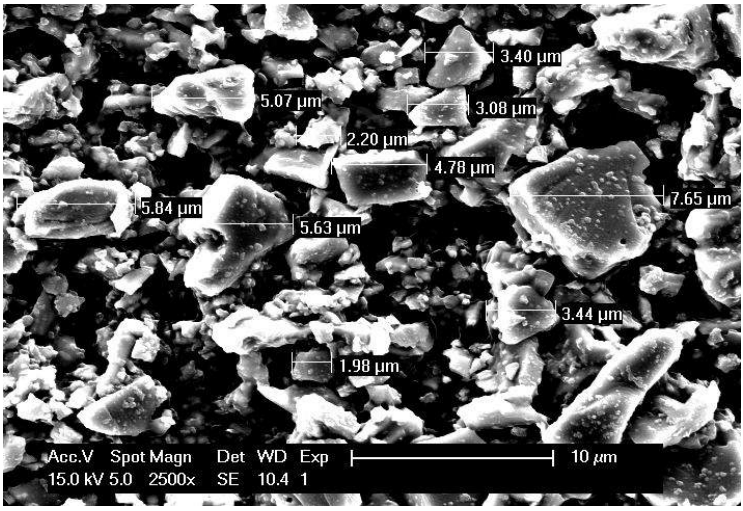

Figure 9.3: SEM (Philips XL30 FEG) photo of TiCN particles embedded in a PVA matrix.

9.2.2 Relative humidity and the percolation threshold

Inside the aircrafts that fly at altitudes up to approximately 10 km, the relative humidity is in the range of RH = 10-20% [209]. During boarding the humidity can increase up to RH = 40%. This value of humidity can be used as a baseline for the sensor response. Therefore, the composite part of the sensor should be designed with appropriate concentrations of its compounds in order for the percolation conductivity to collapse at a relative humidity of approximately RH = 80%. In that way, even if the relative humidity inside the aircraft, and especially in confined spaces, fluctuates and increases up to RH = 60%, the percolation threshold will not appear until higher values of humidity are apparent. The graph below shows the percolation threshold at RH = 80 % and two range areas, A and B. Range A stands for normal operational conditions in an aircraft and range B stands for humidity values of RH = 100 % that indicate the spilled aqueous liquid case.

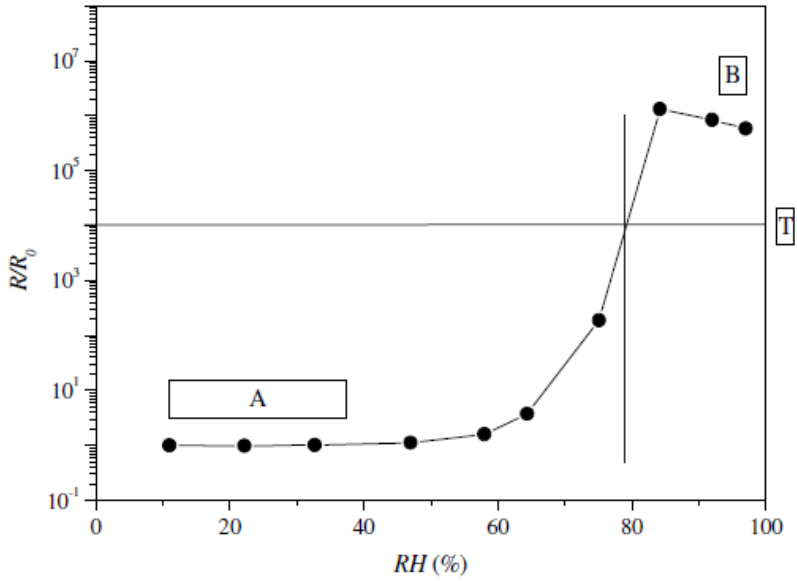

Figure 9.4: Percolation threshold for TiCN/PVA mixture (x_v = 0.45) and the areas of operational conditions in an aircraft (A) and the damage case (water ingress) (B) [210]

9.2.3 Preparation of the mixture and sensor design

The compounds were mixed using appropriate weights of TiCN and PVA together with a specified amount (approximately 16 gr) of Milli-Q water (ultrapure water) in an electric mixer. While mixing, the mixture was heated at a temperature slightly below 100 °C. In that way, part of the water evaporated and after one hour, the remaining mixture had a form of a viscous fluid that could be poured. The remaining mixture was then passed through a sieve in order to remove any hydrolyzed PVA that had not been dissolved completely. After sieving, the mixture was ready and it was stored in plastic syringes. To make the sensor, a polyamide cord was used that is impregnated with the above hydrophilic TiCN/PVA composite mixture, see figure below. The cord had a diameter of approximately 1 mm and contained an electric wire from which the resistance measurements were acquired. The electric wire was insulated and connected to a Kethley 2000 digital multimeter for measurements recording. The electric wire was connected with the conductive coating at the edges of the cord in order to make a closed circuit.

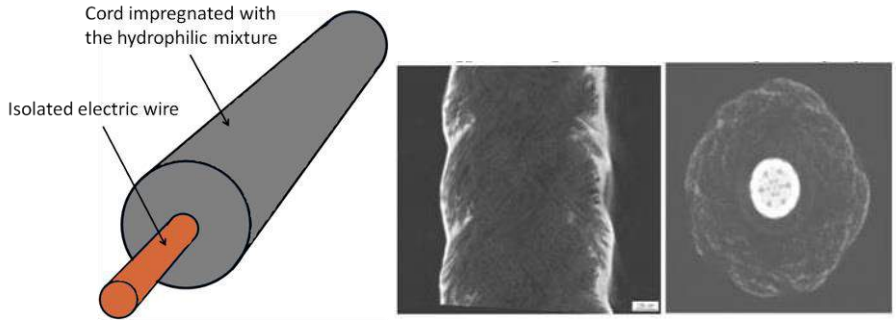

Figure 9.5: Design of the percolation sensor (left), microfocus X-ray imaging photo of the sensor with 1 mm diameter (right) [211]

9.2.4 Sensor implementation

The floor of a cabin of an aircraft usually consists of a number of floor panels made of composite that are attached on the floor beams that are made of aluminium. Between the two composite plates that are attached on one floor beam there is a small gap that separates them (Figure 9.6).

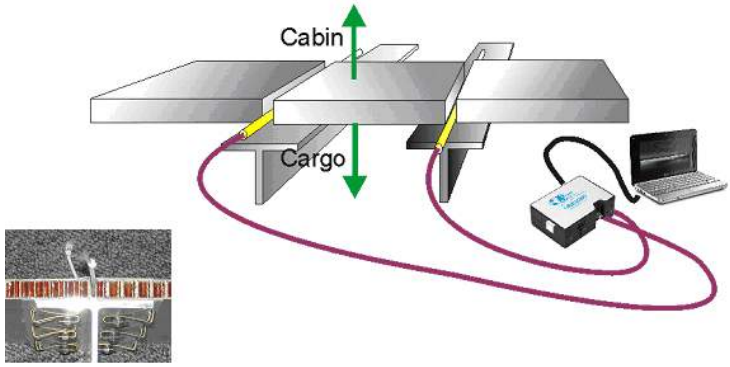

Figure 9.6: Illustration of the percolation sensors installed between the floor panels and on top of the floor beams inside a cabin of a passenger aircraft.

This gap is large enough to fit the proposed sensors and it can work as a pathway that can be many meters in length depending on the size of the aircraft. In case of bad floor insulation, the spilled liquids are concentrated in those gaps and can cause severe damage if not detected. Therefore, the sensors are positioned along these gaps between the floor panels and exactly on top of the aluminium floor beams. Figure below is a photo of an installed sensor in the galley area of a Boeing B737. The sensor should be flexible enough to bend and follow the curves of the pathways between the floor-panels.

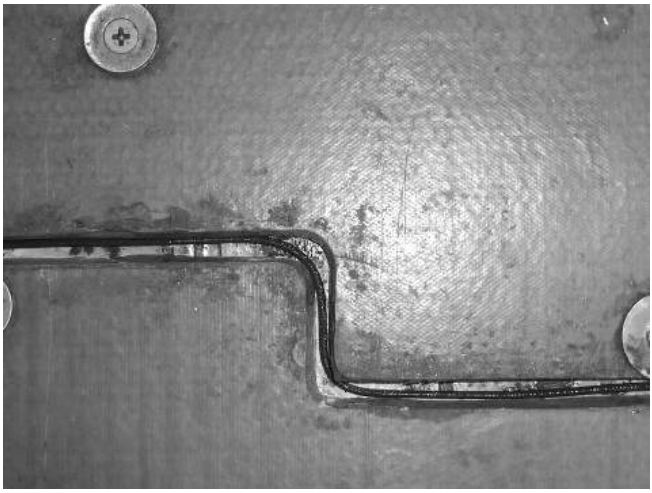

Figure 9.7: Percolation sensor installed between floor-panels in a Boeing B737.

The length of each sensor can be up to many meters and can be produced on demand depending on the requirements. The measurements are resistance values of the sensors that give information of the level of conductivity and the percolation threshold. This in turn can give an early indication of the wetness and warns for liquid concentration at these points that can create corrosion problems. The method is simple but effective and at the moment is under continuous assessment installed in operational passenger aircrafts from Lufthansa.

9.3 Results on percolation activity in different conditions

9.3.1 Test setup and methodology

In order to monitor the percolation activity of the sensors in different temperature and humidity conditions the following setup as presented from the figure below was used.

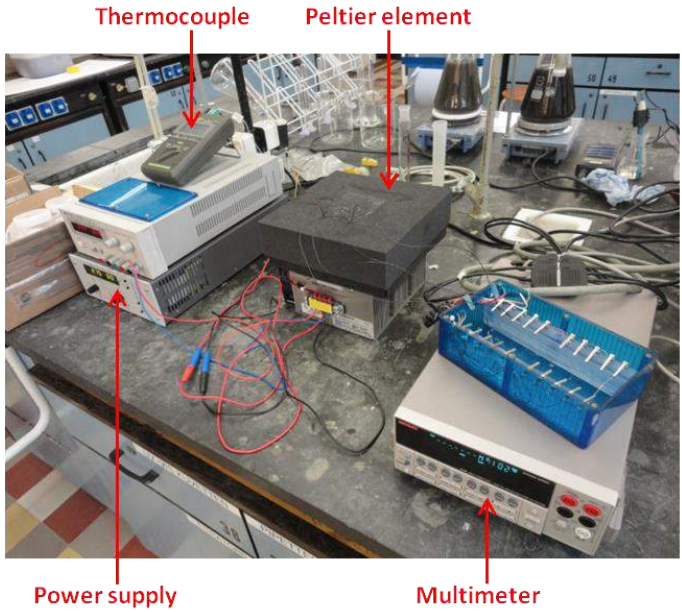

Figure 9.8: Setup for the salt tests using thermoelectric cooling to obtain the desired temperatures.

In order to achieve different temperature conditions for the tests, a Peltier element was used that was transferring heat through a conductive surface to a closed chamber insulated in all the other directions. The voltage power supply of the Peltier element was adjusted every time to obtain the desired temperature. Inside the closed chamber the percolation sensors were placed. The sensors were connected to a Kethley 2000 multimeter that was measuring the resistances. The multimeter was connected to a PC that kept the data files. The thermocouple was not touching the conductive surface of the Peltier element measuring the exact air temperature inside the closed chamber.

Two percolation sensors were positioned inside the closed chamber. One sensor was covered with an extra layer of PVA and the other was exposed without PVA. The PVA with the layer of PVA is exactly the same with the ones installed in the aircrafts. The sensors were positioned and attached on a plastic non-conductive holder in order to avoid the contact with the conductive surface of the Peltier element.

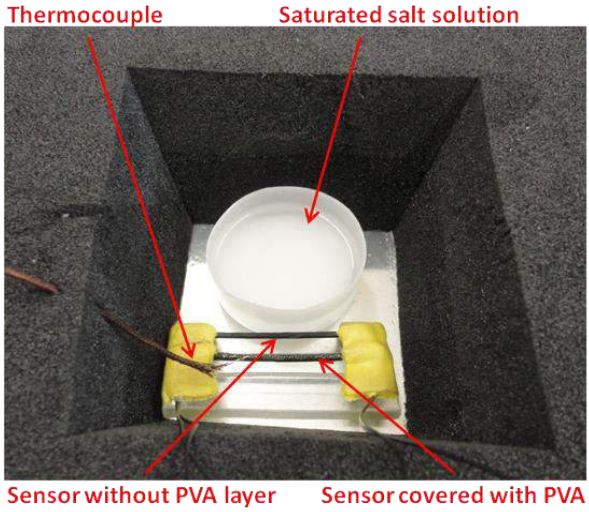

Figure 9.9: Percolation sensors inside the closed chamber with a saturated salt solution for temperature and humidity adjustment.

The sensors were tested in different temperature conditions using 10 salt solutions. Each salt solution had a different relative humidity that was measured at 25 °C and the humidity values were taken from literature, see table 9.1 below. The phosphorous pentoxide (P_2O_5) was used as a dehydrating agent. The other salts with the higher relative humidity were dissolved in Milli-Q water to make saturated solutions. Milli-Q water is high quality ultrapure water that is produced from Millipore Corporation, Massachusetts, United States of America.

Dehydrating agent	**RH %**
P_2O_5	0
Salts	**RH %**
LiCl	11.3
CH_3COOK	22.2
$MgCl_2$	32.7
KSCN	47.0
NaBr	58.2
$NaNO_2$	64.4
NaCl	75.1
KCl	84.2
KNO_3	92.0
K_2SO_4	97.0

Table 9.1: Relative humidities of salts at 25 °C [212].

When the resistance value of the sensors was becoming steady then each salt was replaced inside the chamber with the next one with higher relative humidity. The

relative humidity of the salts was increasing up to RH = 97 % (K_2SO_4) in order to hydrate the sensor. After K_2SO_4 the sensors were dehydrated again with P_2O_5 and the process was repeated for 5 °C, 15 °C and 25 °C.

9.3.2 Conditions with P_2O_5

Phosphorus pentoxide is a dehydrating agent with a relative humidity of approximately RH = 0 % and is therefore not used in a solution with Milli-Q water. Therefore, at the beginning of each test, the P_2O_5 removed any water molecule from the sensors and dried them completely. In that way, a nominal resistance (baseline) for the sensor could be obtained after each test for a complete dry condition. However, from the results it was observed that the resistance measurements were dropping until the sensor was completely dry before it was hydrated again. In some cases, the dehydration process on the sensor could continue even with the salts of low relative humidity. This occurred possibly because in some cases the sensors needed a quite long time to be dehydrated with just P_2O_5 and dehydration continued until the sensor got wet gain. In order to accelerate the drying process, the sensors can be put in an oven with high temperature.

The sensors after multiple hydrations and dehydration from the tests, they returned to a resistance value that was much lower than when they were hydrated since they become conductors again. That makes them ideal sensors to be used multiple times. Below is a table of the initial resistance values when exposed to room conditions and the change of resistance after three tests and complete dehydrations.

Sensors	**Room 22 °C**	**5** °C	**15** °C	**30** °C
With PVA	1717 ±1 Ω	999 ±1 Ω	3742 ±1.79 Ω	1436 ±1 Ω
Without PVA	347 ±1 Ω	312 ±1 Ω	196 ±1 Ω	160 ±1 Ω

Table 9.2: Resistance values of the dried sensors at various temperatures.

After hydration the sensors had very high values of resistance, i.e. they were almost non-conductive, as explained in the theory at paragraph 4.8.2. Dehydration with P_2O_5 dropped the resistance of the sensors and they became conductive again. Below are the graphs that show the dehydration of the sensors while its resistance dropped from large magnitudes to lower ones. The resistance data were recorded up to 5 hours. At that time the resistances had not reached a complete equilibrium but the resistance drop was significantly small enough to stop the measurements.

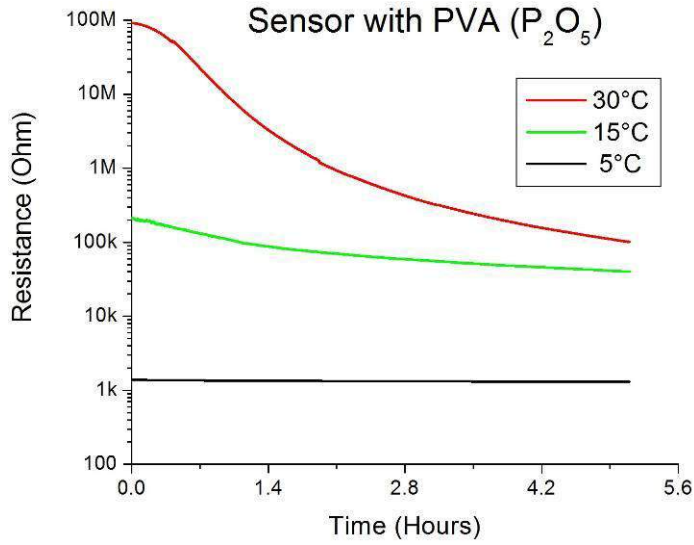

Figure 9.10: Resistance drop with dehydrating agent P_2O_5 for sensor with PVA coating. Horizontal axis is in logarithmic scale since the drop of resistance is very high.

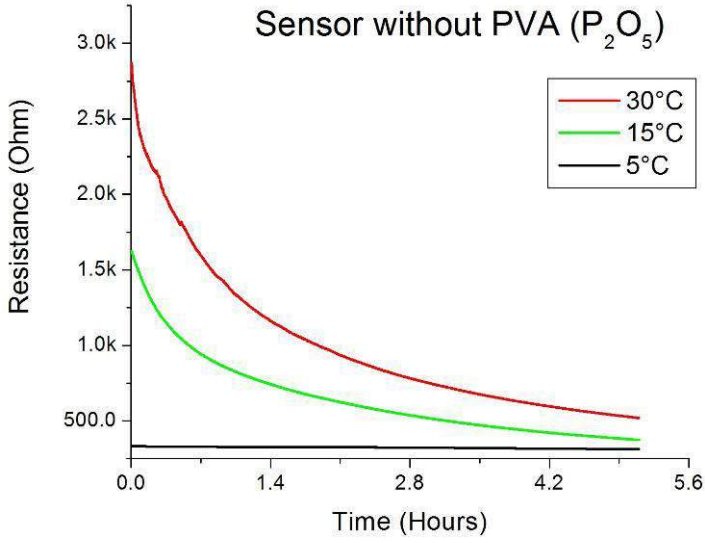

Figure 9.11: Resistance drop with dehydrating agent P_2O_5 for sensor without PVA coating.

From the graphs above, it can be seen that one important factor for the dehydration rate is the temperature. At 5 °C, the resistances of both sensors were already at the baseline values before their complete dehydration and that is why the resistance drop is almost negligible. It is obvious that the sensor with PVA coating hydrates and dehydrates easier than the one without PVA. This can be

explained that as the temperature increases in an environment of 0 RH%, it is easier for the hydrophilic PVA inside and around the composite compound to react with water molecules as they become more active.

9.3.3 Conditions with the saturated salt solutions

The sensors were exposed to relative humidities from 11.3 RH% to 97.0 RH% that were adjusted from the eleven salts found in table 9.1. The following graph shows the change in resistances of the sensor with PVA as the relative humidity inside the chamber is increasing up to 97 RH%. The horizontal axes are in logarithmic scale since the change in magnitude is very large.

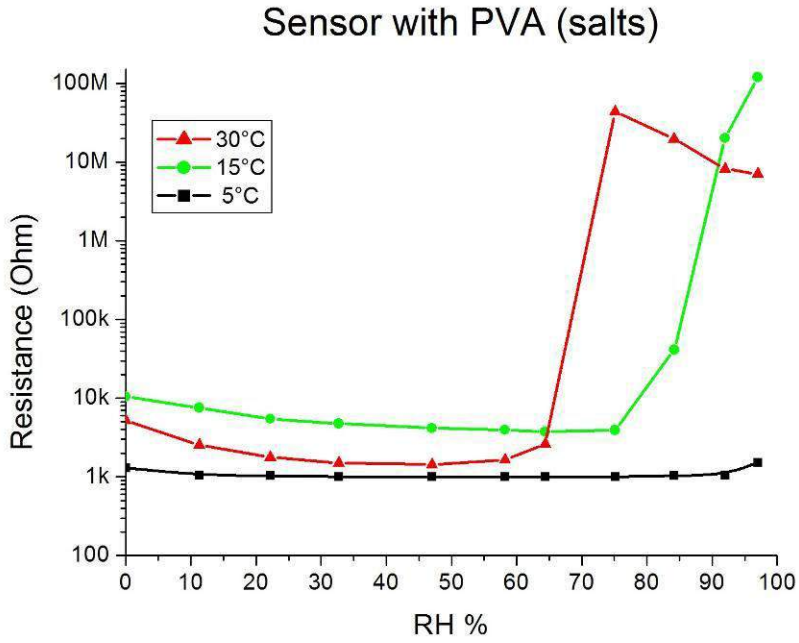

Figure 9.12: Sensor with PVA coating exposed to different relative humitidies at three different temperatures [equilibrium conditions].

It can be observed that the hydration process starts earlier at higher temperatures since the water molecules gain thermal energy and become more active. The resistances are decreasing, even after the sensor has been exposed to the dehydrating agent P_2O_5, therefore, it needs to be mentioned that the sensors were still dehydrating at lower values of relative humitidies until the process starts to become reversible. The graph below shows the change in resistances of the sensor without the extra PVA layer as the relative humidity inside the chamber is increasing. It can be observed in lower temperatures that the sensor with the PVA layer remains conductive, meaning that the resistance remains in low values.

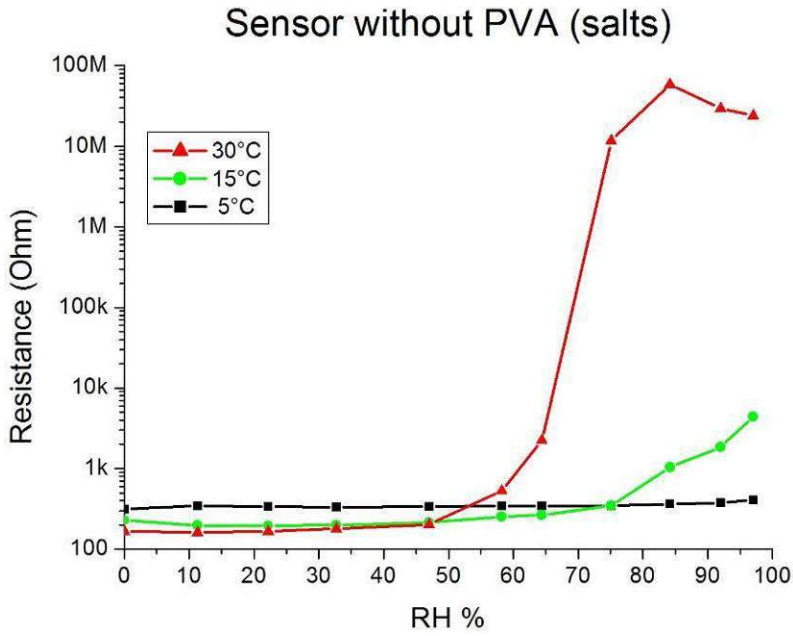

Figure 9.13: Sensor without PVA coating exposed to different relative humidities at three different temperatures.

At 5 °C the change of resistance is negligible and in 15 °C the increase in resistance magnitude is starting to become noticeable. At 30 °C, the collapse of the percolation threshold is more apparent and starts at about 58.8 RH%, when the sodium bromide is inserted into the chamber. It can be seen thought, that the sensor with the PVA layer behaves well similar to the sensor without PVA. Nevertheless, it seems that the sensor without PVA has a better performance in a wider range of temperatures.

In order to observe more in detail the sudden change in resistance of the conductive compound of the sensor with the PVA layer, the following graph in figure 9.14 was developed. It shows the resistance change at the point of the collapse of the percolation threshold, which occurred between 64.4 RH% and 84.2 RH%. The peak on the graph is very steep and the critical point represents the average point when the percolation collapses and the sensor becomes from conductor to an isolator.

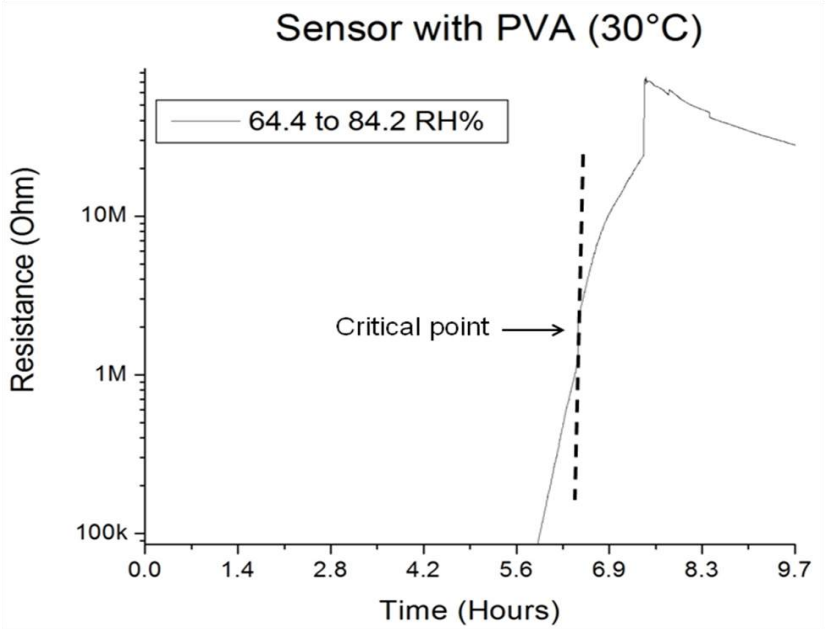

Figure 9.14: Sensor with PVA coating exposed between 64.4 and 84.2 RH% at 30 °C.

The critical point in this case is near 70 RH%. It can also be observed that after the highest peak, the resistance drops again. This can be explained by the increase in water amount that is also conductive. However, the magnitude remains in relatively very high levels compared to the baseline.

Finally, the results are very promising since the large difference of electrical resistance of the sensor before and after the collapse of the percolation conductivity can give valuable information regarding the presence of aqueous liquids that can cause corrosion problems.

9.4 Reliability test

Another test for reliability purposes was performed using the same procedure as described above with a sensor covered in PVA layer. The test was performed with all the previous salts at three different temperatures. This sensor was chosen because the layer of PVA is necessary for protection and speeds up the sorption process. The sensors that are provided from KU Leuven to some companies for testing are also covered with the layer of PVA. The reliability test results can be seen in the graph below.

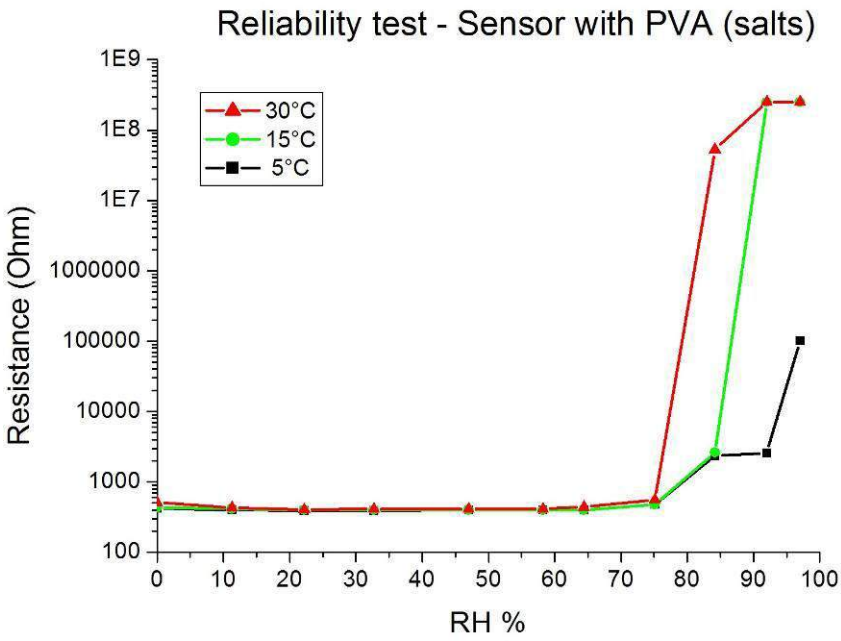

Figure 9.15: Reliability test on the sensor with PVA that is exposed to different relative humidities at three different temperatures.

The reliability test above confirms the percolation threshold behaviour on the sensor. It can be seen that at a relative humidity of 70%, the resistance is increasing and the sensor from a conductor becomes an insulator. The process of this phenomenon is even more apparent at higher temperatures where the water molecules are more energetically active.

9.5 Additional durability tests

A series of tests were performed to test the durability of the sensor in fatigue and tensile stress. The sensor was connected to a Keithley multimeter 2700 for resistance measurements. The length of the sensor was 20 cm. The two edges of the sensor were hold by cast aluminium in order to be easier to clamp it into the machine.

9.5.1 Fatigue test

The setup of the fatigue test can be seen from the figure below. The test was performed in a SCHENCK DU 312 fatigue machine. The number of fatigue cycles was up to 120 000. The static load was at 33 N and the cyclic load was at 27 N. The oscillation frequency was kept at 1 Hz.

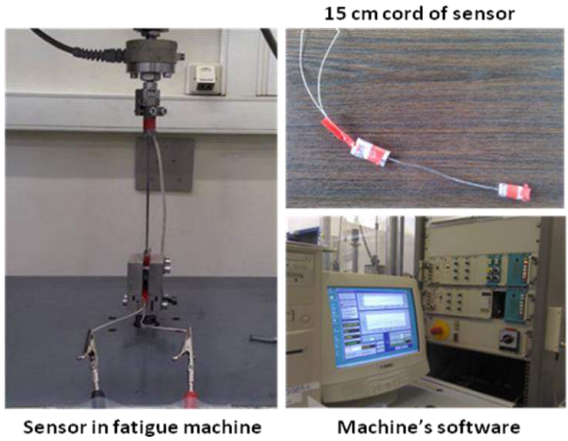

Figure 9.16: Setup for the durability tests of the percolation sensor subjected to fatigue and tensile stress.

The graph below shows the resistance measurements versus time. Since the oscillation frequency is 1 Hz, every second corresponds to 1 cycle.

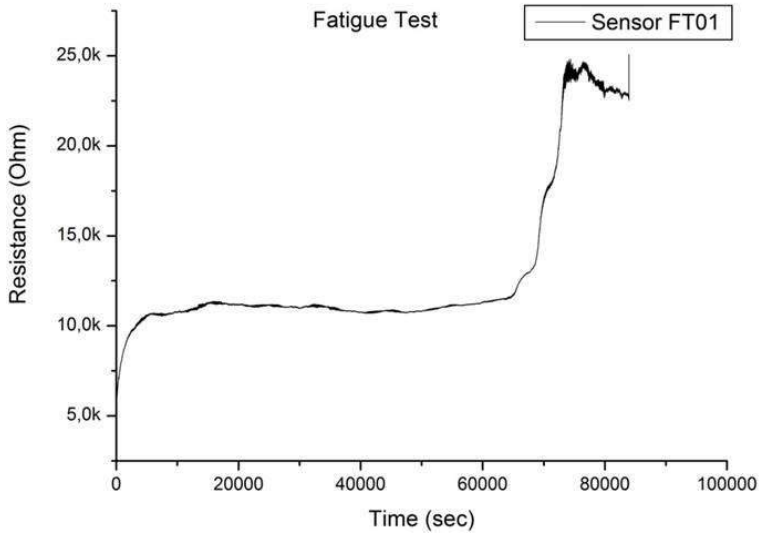

Figure 9.17: Resistance measurements of the percolation sensor subjected to fatigue

The resistance of the sensor prior the test is 5.82 kOhm. From the graph, it is apparent that during fatigue load the resistance is increasing and reaches the highest peak at 25 kOhm at about 83 000 seconds. After 87 000 cycles the sensor loses conductivity. The sensor is relatively durable since it remains conductive for a large number of cycles under fatigue load. Also, in real operating conditions, the sensor is not receiving the same amount of load as the material of the area that is

inspecting since it is not permanently attached on it. This is a positive factor since the sensor that is installed in the floor panels has adequate fatigue limits and it can be used for the whole lifespan of an aircraft.

9.5.2 Tensile test

The tensile test was also performed in the same machine as the fatigue test. The maximum extension was 10 mm and the velocity of the extension was kept at 0.5 mm per minute. The graph below shows the resistance values versus the extension through time. The resistance of the sensor prior the test was 485 kOhm. The resistance initially increases, then drops up to 1091 seconds where it becomes infinite and the sensor loses conductivity. The tensile load is stopped and the resistance drops at 1.5 MOhm.

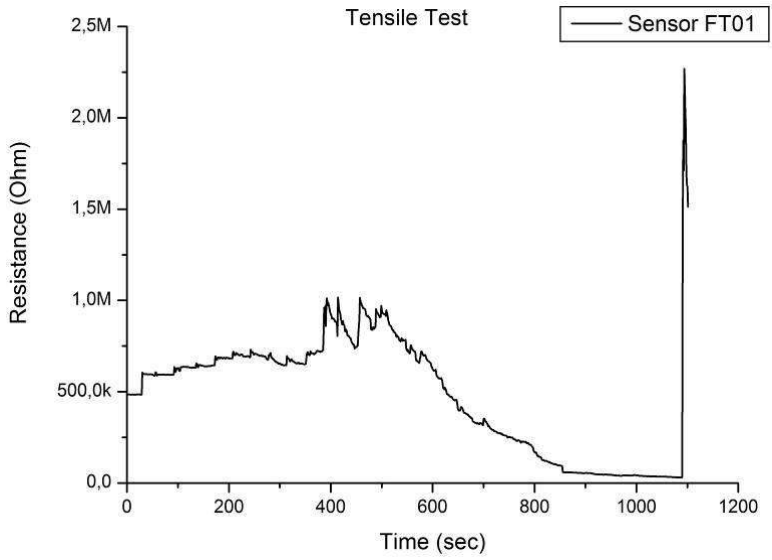

Figure 9.18: Resistance measurements of the percolation sensor subjected to tensile stress.

The sensor lost conductivity at 1091 seconds which corresponds to an extension of 9.09 mm. Therefore, for a total sensor length of 20 cm (200 mm), the test showed that the sensor can be stretched almost for 5% of its length before it stops being conductive.

9.6 Conclusions

The percolation sensor presented in this study can monitor wetness concentration points throughout the whole floor panel of the aircraft. The floor panel consists of

hundreds of square meters and the sensors could follow the lines between the floor panels and the floor beams. Most of the commercial humidity sensors are using physical or chemical adsorption by activating ionic conduction or by transferring electron from the water [213]. The percolation sensor in this study works entirely on percolation particles and the use of a ceramic powder for the production of electrical conducting polymer in this kind of sensors is innovative. The sensor has been patented under the publication number WO2012006692 and international application number PCT/BE2011/000046 with the name: SENSOR FOR DETECTING LIQUID SPILLING.

The dedicated solution for corrosion prevention in confined aircraft parts has been so far successful. The sensor is installed between the floor panels and is active while the aircraft is airborne. The regular maintenance of the floor beams normally takes relatively long time periods, between four to six months [214]. The application of this sensor has the advantage to monitor the whole area of the floor beams in regular time intervals reducing the time and cost of inspection. Therefore, it is a great tool for SHM of the floor beams of aircrafts. These sensors are already on-board on three aircrafts of Lufthansa Airlines. They have been implemented in one Boeing 737-530 and two Boeing 747-400 of Lufthansa. Just inside the two Boeing 747-400, there are 20 sensors with integral length of approximately 50 meters that are located in three different areas of the cabin. The percolation sensors are constantly tested for their reliability and for purposed of future certification. If the sensors get certified from the airlines and the European Aviation Safety Agency (EASA), they could offer a high return of investment concerning maintenance expenses.

The sensors' capabilities can also be exploited in a variety of other applications. They can be used as a tool for aqueous liquids detection in a variety of engineering structures such as under the roof of buildings or in other confined areas found in industry.

The Probability of Detection (POD) using percolation sensors is directly relative to the temperature and the humidity levels of the inspected confined space. The following table below shows the advantages and disadvantages using percolation sensors as a SHM method.

Advantages	Limitations
Can detect high levels of humidity in confined parts	Temperature dependent
Unique and flexible design appropriate for floor-panels in aircrafts	
Easy to produce, install and collect data	
Can prolong the maintenance intervals	
Sensor takes up water (buffering effect)	
Durable sensor with high sensitivity	
Can cover large areas	
No electromagnetic or mechanical interference with other materials	
Instant online measurements possible	
Can be re-used many times	

Table 9.3: Advantages and disadvantages of percolation sensors as a SHM method.

Published papers and proceedings
"Liquid detection in confined aircraft structures based on lyotropic percolation thresholds", H. Pfeiffer, P. Heer, I. Pitropakis, G. Pyka, G. Kerckhofs, M. Patitsa, M. Wevers, at Sensors & Actuators B: Chemical, Vol. 161, Issue 1, January 2012, p. 791-798
"Leakage monitoring using percolation sensors for revealing structural damage in engineering structures", H. Pfeiffer, P. Heer, M. Winkelmans, W.Taza, I. Pitropakis, M. Wevers, Structural Control and Health Monitoring (International Journal), December 2013
"Structural Health Monitoring in an operational airliner: results on the implementation of percolation sensors achieved within the European Project: Aircraft Integrated Structural Health Assessment II (AISHAII)", H. Pfeiffer , M. Patitsa, I. Pitropakis, M. Wevers, ISBN 978-0-415-62131-1, 5th International conference on Emerging Technologies in Non-Destructive Testing (ETNDT), Ioannina, Greece, 19-21 September 2011
"Leakage detection in aircraft by percolation sensors for the prevention of floor beam corrosion and detection of pinhole cracks in hydraulic tubes", H. Pfeiffer, I. Pitropakis, M. Patitsa, M. Wevers, 6th International Conference "Supply on the wings", Frankfurt/M, Germany, 2-4 November 2011
"Structural health monitoring in an operational airliner: an intermediate report on leakage monitoring with percolation sensors", H. Pfeiffer, P. Heer, H. Sekler, M. Patitsa, I. Pitropakis, M. Wevers, 6th European Workshop on Structural Health Monitoring, Dresden Germany, 6-12 July 2012
"Fuse-like devices replacing linear sensors – working examples of percolation sensors in operational airliners and chemical installations", H. Pfeiffer, I. Pitropakis, M. Wevers, H. Sekler, M. Schoonacker, 6th International conference on Emerging Technologies in Non-Destructive Testing (ETNDT 2015), Brussels, Belgium, 27-29 May 2015.

Table 9.4: Contributions.

"Know thyself."

Thales (624 – 546 B.C.)

CHAPTER 10

Summary and outlook

This chapter formulates general conclusions regarding the dedicated solutions for SHM of aircraft components that are discussed in this PhD thesis. It also gives a short review on the AISHA II research project and the research partners. Furthermore, it presents general thoughts on the output and applicability of the results that were produced in the previous chapters.

This PhD research covered a part of the field of automated non-destructive testing with advanced sensors, with a focus on sensor implementation and data analysis used for SHM of aircraft components. SHM is a technology where integrated sensors are used to enable continuous monitoring of the structural integrity. Therefore, it is evident that the safe use of aircrafts can only be guaranteed when efficient means of damage assessment are in place.

However, besides the expected enhancement of safety and maintenance performance, also economic aspects play an important role. Together with project partners Eurocopter (France), Lufthansa Technik (Germany), German Aerospace Centre - DLR Braunschweig (Germany), Fraunhofer Institute - IFAM (Germany), ASCO (Belgium), Metalogic (Belgium), Cedrat (France), CTA (Spain), Meggit SA (Denmark), University of Bask countries (SPAIN), Technical University of Riga (Latvia) University of Leipzig (Germany) the NDT research group of the department MTM in KU Leuven had the opportunity to develop dedicated SHM solutions for automated inspection systems in aircrafts.

In this PhD thesis, various SHM methods on aircraft components were investigated using different approaches from electromagnetic techniques to acoustic excitation methods with a variety of sensors from thin flat coils, electrical crack gauges, optical fibres, PZTs to unique percolation sensors. The experimental results showed successful ways to detect cracks, small structural discontinuities or delaminations. In the following short paragraphs, each sensor that was discussed in the previous chapters is presented together with its applicability, functionality and effectiveness.

The flat coil sensors are designed to monitor cracks and flaws mainly (but not limited there) around a rivet connection using electromagnetism. Rivets can be found all over the aircraft structural body and are considered stress concentration points. Impedance spectroscopy allowed the identification of a crack using eddy currents determined for a fixed frequency.

The electrical crack gauges are designed to monitor cracks and flaws on plate-like structural parts on an aircraft. Their detection principle is based on resistance spectroscopy and the interruption of their conductivity. The experimental results revealed that they can detect cracks at an early stage of their growth and give a warning of the problem.

The single mode optical fibres as well as the piezoelectric transducers offered an exclusive understanding on the acoustic emission technique. Theses sensors can be placed almost in any point of the aircraft body that is relatively wide that could be subjected to impact damage. Optical fibre sensors with their acoustic sensitivity showed that they can replace a number of PZTs in large longitudinal aircraft components offering a number of advantages in acoustic emission.

The use of piezoelectric transducers as excitation sources and receivers led to the exploration of the acoustic reflection and transmission of Lamb waves on

aluminium plates utilizing pseudo defects. The application of pseudo defects as artificial damages was a first step to simulate real damages that can appear in plate-like structural parts. The goal is to have a database of acoustic responses that can be used as a comparable reference for the detection of the size and location of real defects.

The percolation sensors offered a distinctive approach for the detection of aqueous liquids in confined areas of structural parts of the cabin floor in aircrafts. Their unique design and functionality based on the percolation effect manages to prevent possible corrosion problems and comprises a great asset for the re-schedule of maintenance procedures that can be financially very beneficial.

Five other NDT methods that are presented in the appendices can be suitable candidates for inspection of the structural continuity of aircraft components. These methods are often using equipment that is more suitable for monitoring structural parts after they have been removed from the aircraft. There are some interesting approaches and efforts but their study is limited and they need further development.

The main target of this research was to find systems that can be embedded on the aircraft and monitor its structural health in a similar function as the flight data recorder (black box) monitors and records changes in the electronic data systems and avionics. A complete and efficient nervous system of the above concept that will cover the whole areas on an aircraft might take several years from now to appear. However, all the previous methods analysed in this study and their promising experimental results can comprise an added-value in the exploration of new ideas that can lead to the technological development and enhancement of advanced SHM systems of aircrafts.

Solution	Methodology - Innovation	Application	Achievement
Flat Coil Sensors	Designed at MTM, KULeuven	On top of rivets, holes or screws, surface points of stress concentration on aircraft components	Correlation of crack depth with relative difference of impedance
	Produced at ESAT, KULeuven		
	Similar sensors made by AIRBUS but no major publications on such sensors		
Crack Gauges	Designed and produced at IFAM & MTM, KULeuven	Any point on an aircraft where cracks are likely to appear (stress concentration points)	Crack length monitoring with instant measurement and warning alert
	Unique fuse solution for monitoring closed crack issue		
	State of the art small blue electrical crack gauges		
SM Optical Fibres	Acoustic emission technique	In longitudinal plate-like aircraft components (eg. Helicopter tailboom)	Exploration of their potential on damage detection for SHM on aircraft components
	Comparison between SM & PM optical fibres and PZTs		
	SMARTape application on aircraft components		
Pseudo Defects	Signal correlation of acoustic response to real defects	In metallic and composite plate-like components of aircrafts	Relationship of the acoustic response between real defects and pseudo defects for signal validation
	Easy attachment and detachment method		
	Association of position (angle) and geometry of defect with acoustic reflections		
Percolation Sensors	State of the art innovative design, sensors produced at MTM, KULeuven	In various confined spaces in the aircraft, ideally on floor beams between floor panels and seat tracks	Detection of humidity levels from aqueous liquids preventing corrosion problems
	Patent: WO2012048390 A2		
	Patent: US20130113505 A1		

Table 10.1: Overview of the dedicated solutions presented in this thesis.

"Be yourself, everyone else is already taken."

Oscar Wilde (1854 – 1900)

Appendix A

Additional experimental results

Besides the techniques on SHM on aircraft components that were discussed in the previous chapters, an overview of some additional approaches is presented here. They have a strong link to the previous ones but due to the limited investigation and results, they are placed in a separate chapter. Each technique has a different approach but the same target; to monitor and detect cracks or delaminations in the composite or metallic material of the aircraft components. The Laser Doppler Vibrometer tests were performed in cooperation with the Laboratory of Acoustics and Thermal Physics of the KU Leuven.

A.1 Investigation on a sonotrode application

A.1.1 Theoretical background

A sonotrode is a coaxial tool that is used as a mean of piezoelectric vibration exciter [215]. An ultrasonic sonotrode (resonator) made of steel was used as an additional tool for wave excitation to cover a larger area. The sonotrode, upon which the PZT material is attached, resonates with the same frequency as the PZT and transfers the acoustic energy to the desired area.

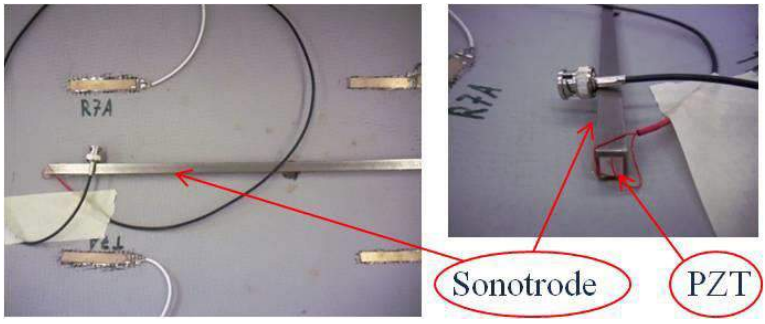

Figure A.1: Steel sonotrode with a PZT attached on its edge

The ultrasonic sonotrode is an extension of the active part of an ultrasonic unit and excites ultrasonic waves along a longitudinal surface. The sonotrode was attached with epoxy glue on the inner surface of the tail boom of an EC 135 helicopter by Eurocopter. At each edge of the steel rod PZTs are attached to transmit the acoustic energy. In this study, the excited acoustic waves are detected by other PZTs attached alongside the tail boom. The sonotrode method enhances ultrasonic wave propagation and its philosophy is based on the ultrasonic testing technique as it is discussed in paragraph 4.6.2.

A.1.2 Applications in aircraft components

There is not much in the literature today regarding the application of an ultrasonic sonotrode for defect detection in aircraft components using Lamb waves. However, when combined with other techniques such as the laser scanning vibrometry, delaminations or small cracks can be revealed in thermoplastic materials during vibration and heating up of the component [216]. Another application of the ultrasonic sonotrode on aircraft components that has been discussed in the literature is the ultrasonic impact treatment for surface hardening of the materials of the aero-engines [217]. Other kinds of sonotrodes are popular in welding industry. These sonotrodes are mainly used in ultrasonic welding machines as assisting the welding process of materials by giving energy to the welding area for better results. Furthermore, sonotrodes are also popular as ultrasonic homogenizers for mixing or as ultrasonic cleaners for separating contaminants from vessels.

A.1.3 Materials and methodology

Piezoelectric transducers usually have small size and surface area but a sonotrode can be used to amplify and transport vibrations to a larger and usually longitudinal area by making Mach waves.

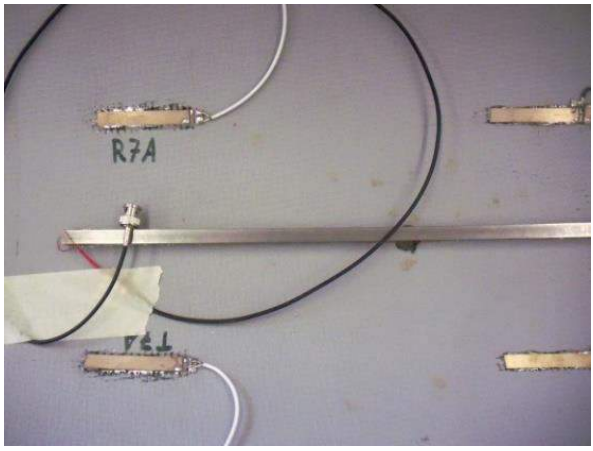

Figure A.2: A sonotrode surrounded by four flat PZTs and attached on the inner surface of an EC 135 tail boom.

In this study a sonotrode made of steel was attached in the inner side of a tail boom from a Eurocopter EC 135. Two square piezoelectric transducers (PZTs) were attached on the top and the bottom edge of the sonotrode. The PZTs are made from MEGGiTT systems PLC, Denmark. The sonotrode was mainly used as an excitation source and two rows (upper and lower) of PZTs as well as an embedded single mode optical fibre in SMARTape were used as receivers of the acoustic signal, see figure A.3. A pseudo defect of a diameter of 6 cm was attached on the tail boom and was used to investigate the sensibility of the acoustic waves that are generated from the sonotrode and the PZTs. The test gave some interesting results and in the future this method can be optimized with further analysis of the acoustic signal. The main target is the optimization of acoustic measurements from the optical and acoustic sensors. Figure below shows the three different kinds of sensors used for the acoustic measurements on the EC 135 tail boom.

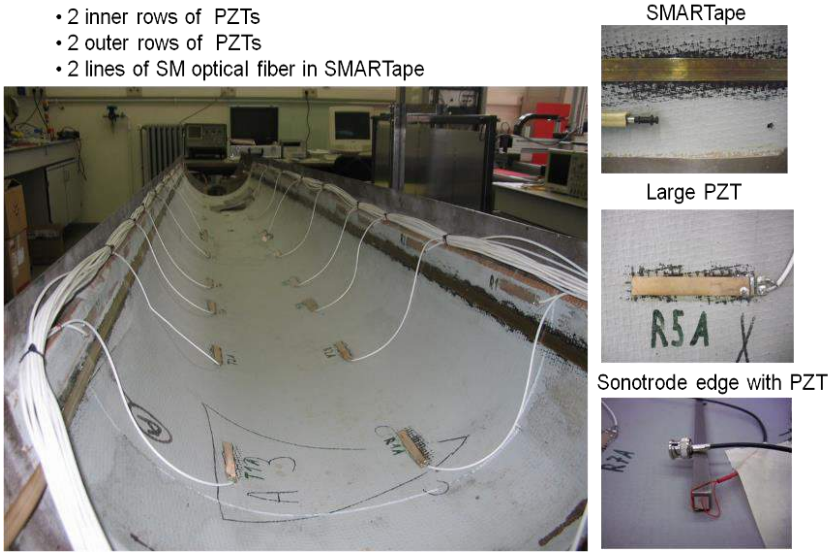

Figure A.3: Inner surface of EC 135 tail boom showing the PZT rows and SM optical fibres in the SMARTapes (left), SMARTape, PZT and Sonotrode with an attached PZT on its edge for acoustic exhitation (right).

A.1.4 Results and discussion

The results below show the acoustic response from the eight PZTs that are positioned in parallel to the sonotrode. In the following case the sonotrode is the excitation source and the PZts are acting as receivers. The tail boom is equipped with eight PZTs that are located in parallel direction to the sonotrode. The graphs below are generated from MatLab. The left graph shows the acoustic response in all eight PZTs when the pseudo defect is attached. The graph on the right shows the

difference of the acoustic response when subtracting the reference signal without any defect with the signal with the defect.

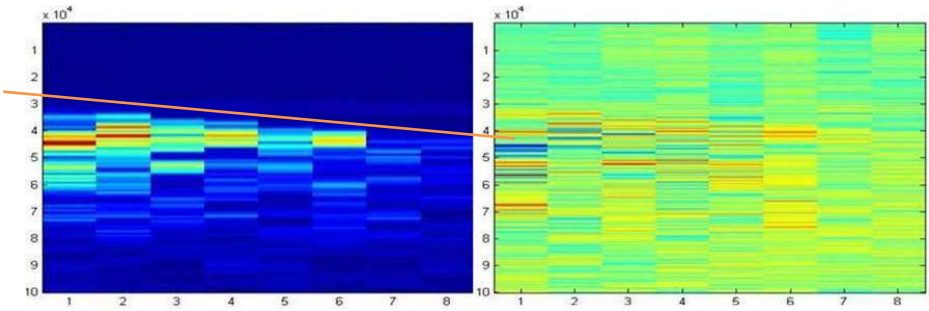

Figure A.4: Arriving acoustic signal using a pseudo defect (left), difference between the acoustic signal using a pseudo-defect and the acoustic signal with no defect (right).

The sonotrode increases the oscillation displacement amplitude of the PZT that is attached on it and it creates Mach waves making the acoustic waves to move faster. It can be seen that the application with a sonotrode can successfully increase the wave excitation in a large longitude aircraft component and can reduce the number of PZTs that are used for excitation purposes. This can result to less cables and costs and to a large excitation coverage.

A.2 Investigation on damage detection by C-Scan

A.2.1 Theoretical background

High frequency ultrasonic top view C-Scans were performed by a C-Scan equipment available in the NDT laboratory of KU Leuven. This NDT technique examines defects, porosities and strong differences in acoustic impedance inside the material and permits their identification. The figure below shows the C-Scan robotized instrument that is used for the experiments.

Figure A.5: Ultrasonic C-Scan equipment in NDT laboratory, MTM, KU Leuven.

The C-Scan consists of a very high frequency (up to 50 MHz) pulse-echo ultrasonic microscope that is positioned above the component under investigation. A transducer is scanning the component at a pre-defined speed and the computer generates the scanned images at the screen. The coupling medium can be water or air and in our case, the transducer is positioned slightly under the surface of the water which is used as a couplant. The transducer has both the role of a generator of the pulses and receiver of the echo. Depending on the discontinuities inside the material under investigation, the return times of the echo to the transducer is changing. By knowing the distance of the transducer from the component as well as the thickness of the component, the return times can give an estimation of the size of the defect together with its location in depth [218]. The computer is synchronized with the transducer and the peak amplitudes of the returning signal are stored in the computer database. From this database the computer generates an echo pattern of the scanned area. The echo pattern that is displayed on the screen is known as the A-Scan.

A.2.2 Applications in aircraft components

C-Scan is used for the detection of defects in aircraft components but it is considered a more time consuming SHM method than others since the transducer is inspecting the area in small pieces usually by millimeters [219]. Furthermore, depending on the shape of the component, it is sometimes necessary to remove it from the aircraft and put it in the tank of water in order to inspect it. However, for large flat and curved areas, there are mobile systems that can scan the component without removing it. In both cases, even though it is a time consuming method, it can offer reliable results when there is an evident discontinuity in the core of the material but it is not very suitable for the bare visible impact defects (BVID) identification [220]. In the following experiments, the visualization of the Lamb wave propagation was investigated with the aid of C-Scans. The key point was to create a movie that shows how the Lamb waves are propagating through the sample plates and also the reflection of the waves on defects or pseudo-defects.

A.2.3 Materials, methodology and results in KU Leuven

Ultrasonic C-scans are also used to verify among other things, the extent of the damage. In composite materials, various damage mechanisms occur. Defects such as matrix cracks, fibre breakage, delaminations and debonding influence each one in a different way the propagation of the plate waves through the structure.

The C-scan equipment available in the NDT laboratory of MTM, KU Leuven, is a HFUS (Ingenierbüro dr Hillger) with a frequency range of 1-120 MHz and the low frequency system is an Olympus 5077PR with a frequency range of 1kHz to 35 MHz. The data acquisition system is the National Instruments PCI-5114 with a sampling rate of 250 MS/sec.

The scan area follows three dimensional axes. 1200 mm in X axis, 1600 mm in Y axis and 300 mm in Z axis. The C-scan equipment utilizes a high and a low frequency system.

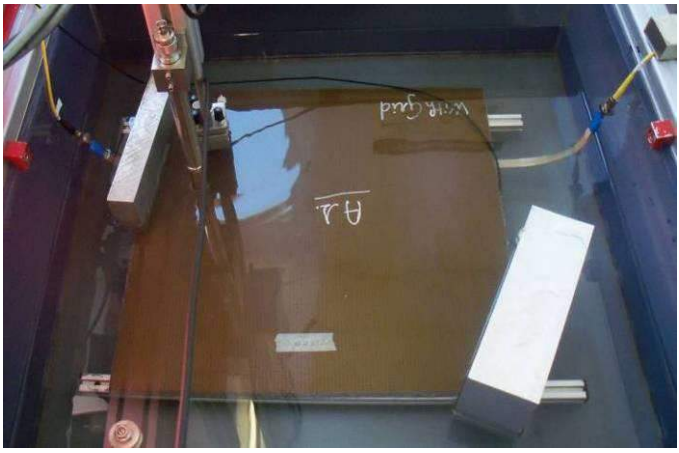

Figure A.6: A honeycomb composite plate submerged into water and monitored for structural flaws using a C-Scan equipment.

A pseudo defect was attached few centimetres above the centre of the honeycomb composite plate. C-scan revealed the wave formation on the composite plate. Due to acoustic reflection, the location of the pseudo defect can be seen as a white spot that doesn't follow the cyclic-linear reflections.

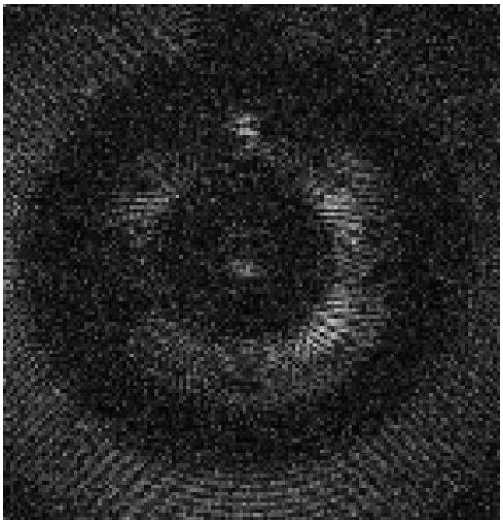

Figure A.7: C-scan reflections and reveal of the pseudo defect few centimetres above the centre of the plate.

A.2.4 Tests partially performed in cooperation with the German Aerospace Centre (DLR)

A C-Scan was performed on an aluminium 2024-T3 plate of the same size and material as the plates used for the fatigue tests in Chapters 5 and 6. A PZT was attached in the middle of the plate as an excitation source and a pseudo defect was placed in a short distance above the PZT. Figure below, shows the aluminium plate on a top view and on a side view, the position of the PZT and the formation of the Lamb waves that propagate through the plate. The wave discontinuities on the left and right side of the PZT are the reflections of the acoustic signal from the edges of the aluminium plate.

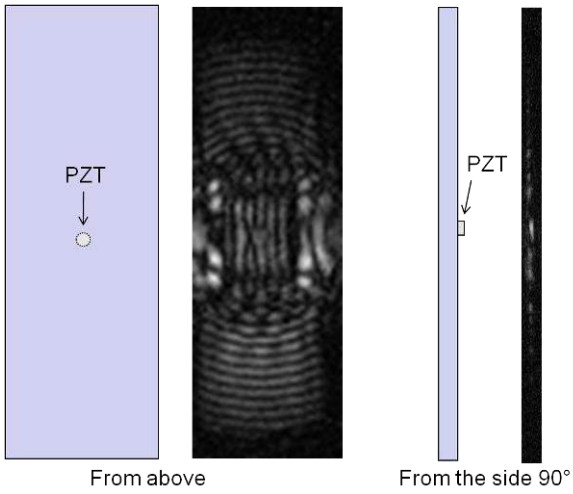

Figure A.8: Top and side view of the Al 2024-T3 plate and the wave propagation on it.

The C-Scan shows the wave formation on the plate. The pseudo defect that was placed near the PZT can be clearly seen. Below, a screenshot of the waves produced from the PZT and the detection of the pseudo defect due to reflection similar to the tests performed in KU Leuven.

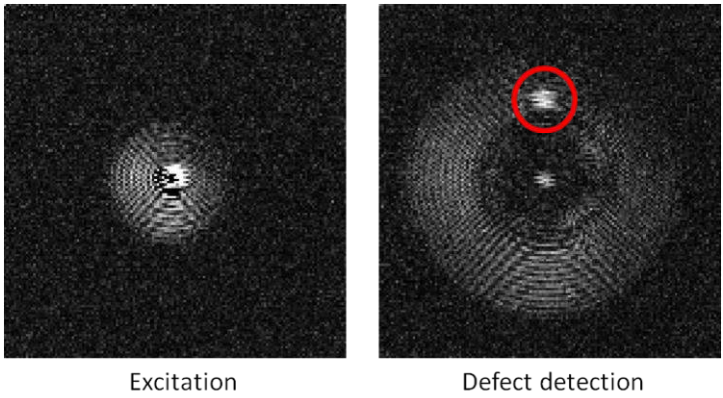

Figure A.9: Lamb waves excited from a PZT positioned in the centre of an Al 2024-T3 plate and on the right photo a defect detection due its acoustic interference.

The elastic waves are excited in homocentric circles around the PZT and are travelling through the plate until they are reflected from a structural discontinuity that can be either a defect or the edges of the sample under investigation. This wave propagation method is proved successful and can detect defects around the surface of an aluminium plate-like structure.

A honeycomb composite plate, made of the same material as the EC 135 tail boom, was also tested in order to obtain a simulation of the acoustic waves and its modes when they interact with a defect. The composite plate has a rectangular PZT attached that serves as an excitation source for Lamb waves. On the other side of the composite plate a single mode (SM) optical fibre is glued to be used as an optical monitoring method. Unfortunately, the SM fibre was broken and the defect detection test was completed only by wave propagation methods using the PZT. In the middle of the plate (where the 2 euro coin is apparent) there is a delamination caused by an impact with a hummer. Figure below (A.10) shows the setup.

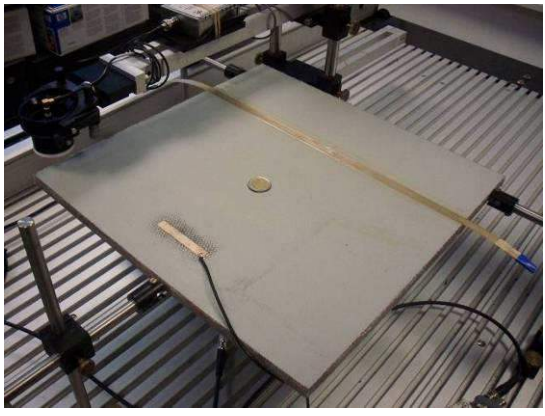

Figure A.10: Honeycomb composite plate for C-Scan testing in DLR.

An evaluation of the Lamb wave propagation method through the composite plate is investigated together with the damage detection by monitoring the acoustic reflection on the defects. The PZT has a rectangular shape with 5 cm in length and 1 cm width.

After the first impulse, the faster symmetric mode is the first that is reflected at the edges of the composite plate. The anti-symmetric mode that follows gives a clear echo on the defect that is positioned few centimetres above the PZT. At the point where the Lamb waves are interacting with defects, mode conversion is apparent where the S0 mode is converted to A0 mode [221].

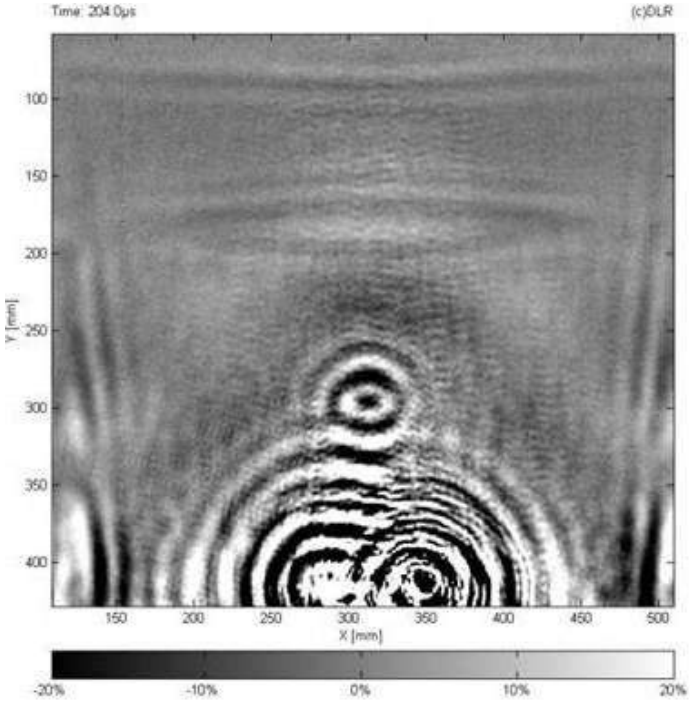

Figure A.11: C-Scan performed at DLR showing the reflection of the acoustic signal on the defect.

A.2.5 Conclusions

From the above experiments, it can be seen that the C-Scan can offer a clear mapping of the formation of the acoustic waves on the aluminium plate. Each time there is a reflection, a structural discontinuity but also the exact position of the defect can be revealed. However, this method is not appropriate for SHM since the aircraft part needs to be removed completely in order to be monitored.

A.3 Characterisation of dispersion characteristics using a Laser Doppler Vibrometer

A.3.1 Theoretical background

A Laser Doppler Vibrometer (LDV) was used for the investigation of impact damage at a composite part of a tail boom of a Eurocopter EC135 helicopter. Small PZT patches are exciting waves through the composite material and the LDV monitors the vibrations. Therefore, it is used for non-contact vibration measurements and it gives information of the structural condition from the signal that arrives from the reflected light. The Laser Doppler Vibrometer extracts the vibration amplitude and frequency by calculating the shift of the laser beam that is reflected from the vibrating material. The principle is as follows; there are two laser beams that initiate from the source and then are split with a beam splitter. One of the beams is used as a reference and the other is hitting the target after it passes through a Bragg cell that adds a frequency shift. The vibrating component under investigation (in this case the EC 135 tail boom) is introducing a Doppler shift to the hitting laser beam. The beam is then reflected back to the vibrometer after having changed its frequency two times from the Bragg cell and the vibrating component. The beam with the shifted frequency and the beam with the initial frequency are combined and compared from a photo detector. The equation that gives the Doppler frequency shift on the beam when it hits the vibrating component is the following:

$$f_D = \frac{2v_{(t)}\cos(a)}{\lambda} \qquad \text{Eq.10.1}$$

Where f is the Doppler frequency shift, $v_{(t)}$ is the function of velocity of the beam with time, α is the angle between the laser direction and the velocity vector and λ is the wavelength of the laser beam.

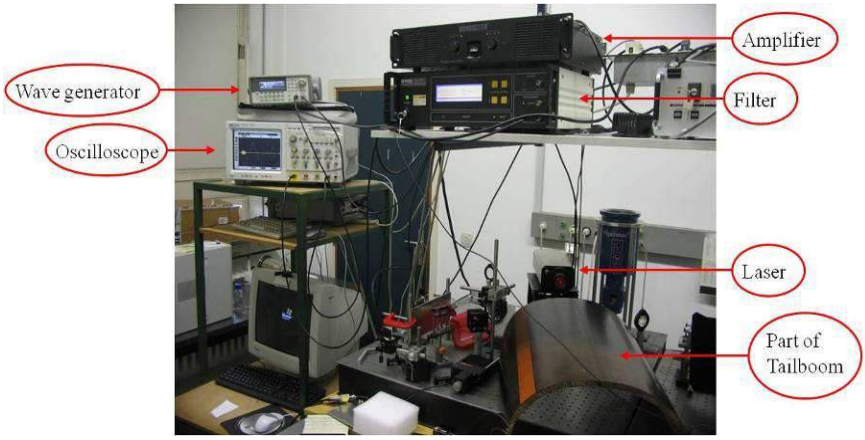

Figure A.12: Setup of the test with the Laser Dobbler Vibrometer performed at the laboratory of Acoustics, Physics Department, KU Leuven, in cooperation with Prof. Dr. Christ Glorieux.

A.3.2 Applications in aircraft components

Laser Doppler Vibrometry is already applied for damage detection and localization in aircraft components such as panels and fuselages [222,223]. In literature, LDV is mostly used for the investigation of acoustic nonlinearity in delaminations of composite materials of aircrafts but also for modal testing and analysis [224-227]. Laser Doppler Vibrometry is capable for obtaining reliable scanning images and if combined with full-field shearographic vibrometry, it can give even better results for the detection of sub-surface delamination [228]. The LDV technique has also been used from the department of Mechanical Engineering at the Vrije Universiteit Brussels in a damaged Airbus A320 slat-track that showed that it can detect the presence and the depth of the crack [229].

A.3.3 Materials and methodology

This study was performed at the laboratory of Acoustics and Thermal Physics at the department of Physics and Astronomy of KU Leuven. A part of a tail boom from a Eurocopter EC 135 was used as the component of investigation. The core of the composite tail boom was previously damaged due to an impact. The target of this study is to determine the degree of symmetry of the acoustic displacements at both sides (inner and outer) of the tail boom [230]. Also the vibration displacements of the edges of the tail boom where detected and investigated.

A Laser Doppler Vibrometer (LDV) is an optical instrument that its operation is based on the Doppler Effect. It uses a laser beam that continuously measures frequency changes due to vibrations on the reflecting surfaces [231]. The LDV was a Polytec OFV 353 as can be seen from the figure below. The LDV was equipped with a Polytec OFV 3001 vibrometer controller.

Figure A.13: A Polytec OFV 353 Laser Doppler vibrometer.

Figure A.14: Laser Doppler vibrometer monitoring structural flaws on the surface and in the core of an EC 135 tail boom.

Figure A.14 above shows target points of the laser beam. The laser beam can be seen with the red dot on the part of the EC 135 tail boom. In order to have a light reflection to the LDV exactly at the same direction, a small piece of retro-reflective tape was used on the target point, see figure A.14, left image. The signal generator used was an Agilent 332550A, the oscilloscope for the signal plotting was a Hewlett-Packard Infinium 500 MHz and the signal amplifier was from HQ Power Professional Audio. A rectangular PZT with 5 cm in length and 1 cm width that was obtained from PIEZOCERAM, S.R.O., Czech Republic, served as an excitation source for Lamb waves.

The EC 135 Tail Boom was placed in 3 different ways in order to achieve vibration measurements of the acoustic waves that were propagated from one piezoelectric patch. Signal was boosted from the amplifier and the measurements were recorded from the Oscilloscope. It was carefully selected that the point in the inner surface is exactly opposite the point on the outer surface, in order to have a much better comparison of the results at the same area. The structure of the tail boom was made of carbon fibre reinforced plastic (CFRP) sandwich composite with a monolithic skin of 1 mm only on the outer surface. The vibration amplitude and the frequencies were extracted from the Laser Doppler Vibrometer due to the motion of the surface. The range of frequencies recorded were 8 – 30 kHz with a step of 1 kHz. The burst period was 10 ms and the signal was averaged 4096 times.

A.3.4 Results and discussion

The tests obtained non-contact vibration measurements of the surface (inner and outer) and the core of a part of a Eurocopter EC 135 tail boom. Every 1 kHz, the waveforms of the reflected signals were recorded and compared. Figure A.15 shows all the 23 waveforms versus time when the laser beam is targeting from the side the core of the honeycomb material of the EC 135 tail boom. Figure A.16 below shows a contour graph indicating the highest peaks of amplitude of the reflected light.

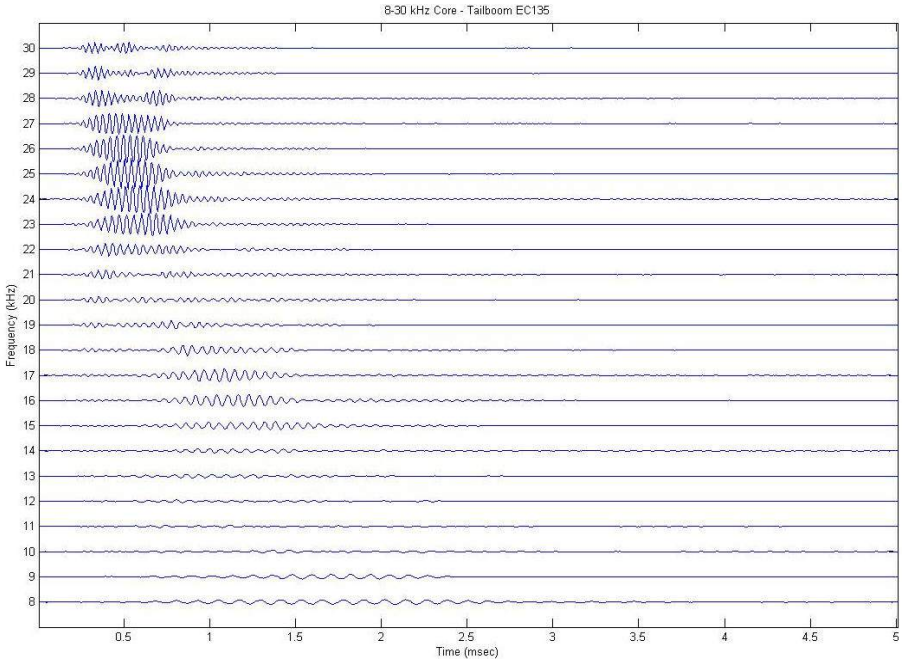

Figure A.15: Waveforms for each frequency (8-30 kHz) versus time when laser is targeting the core of the tail boom from the side. The waveform at 25 kHz has the highest amplitude and peak

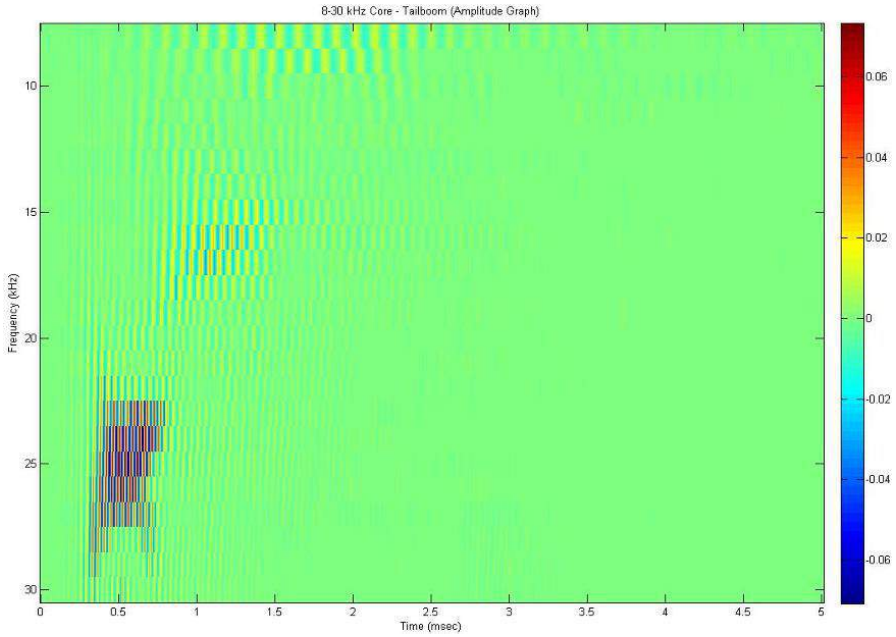

Figure A.16: Contour plot from Matlab for the frequency spectrum (8-30 kHz) versus time. The start of Y axis is at the top of the graph. At ~ 25 kHz, the amplitude reaches its highest peak.

From the figures above it can be observed that at around 25 kHz, the amplitude of the signal is higher compared to the other ones. In the cases where the laser was targeting the inner and the outer surface of the EC 135 tail boom, the highest amplitude of the signal was observed at 16 kHz for both sides.

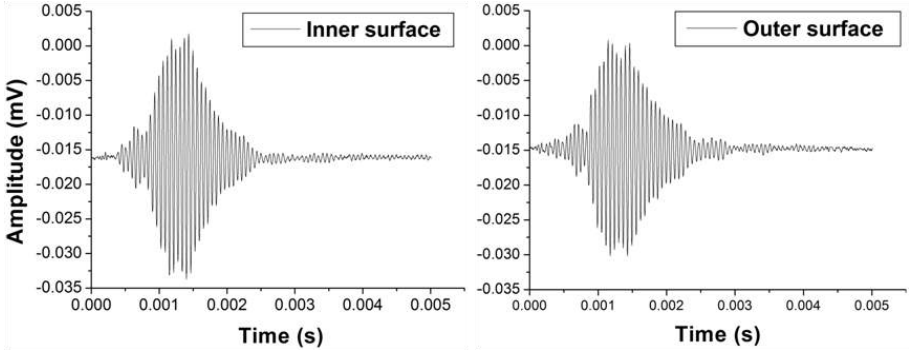

Figure A.17: Waveforms from the signals reflected from the inner and the outer surface of the EC 135 tail boom at a frequency of 16 kHz.

A.3.5 Preliminary conclusions

The key point of this experiment was to investigate at which frequencies the composite structure of the EC 135 tail boom shows symmetric waves at both sides. The waveforms on the inner and outer side of the tail boom were determined exactly at the same axis position and all the results together proved that up to a frequency of approximately 30 kHz, the waveforms were propagating symmetrically on each side. Finally, it was also observed that the burst becomes faster as the frequency is increasing that indicates a dominating A_0 mode.

A.4 Damage detection by an air-coupled electrets array transducer

A.4.1 Theoretical background

An air-coupled electrets array transducer was developed and tested for damage detection in the NDT laboratory, MTM, KU Leuven. It consists of eight electrets microphones that can be selected individually to act as an excitation source or a receiver. The transducers are made from an electret dielectric material that has high resistance and chemical stability and it is able to offer very good operational reliability without a sensitivity loss even if they are stored for a long period in conditions of high temperature and humidity [232]. Electrets are charge-polarized dielectrics that they do not require external polarizing voltage [233].

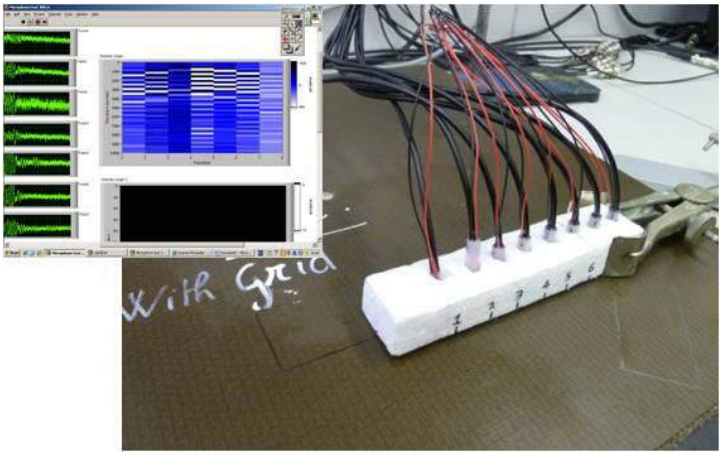

Figure A.18: Photo of the air-coupled Lamb wave array performing a test on a honeycomb composite plate.

A.4.2 Applications in aircraft components

Electret microphones have been studied so far for a variety of applications in the aviation industry. Most of the studies though that can be found in the literature are dealing with the reduction of the noise of aircraft parts such as the jet engines [234,]. The National Aeronautics and Space Administration (NASA) of the United States of America, has proposed an electrets microphone arrays for the measurements of the airframe noise flight but also noise source localization measurements of jet engines [235,236]. In this study the proposed electrets array transducer is offering a possibility for real-time measurements for the detection and localization of a defect on a honeycomb composite plate.

A.4.3 Materials and methodology

An array of sensors for flaw detection has a higher potential than point sensors standing alone. Having many sensors working together can result to more accurate measurements for the localization of the possible damage. In this study, an eight channel air-coupled array transducer has been tested and investigated on a composite honeycomb plate as well as on a composite part from the tail boom of the Eurocopter EC 135 helicopter. The air-coupled ultrasonic technique is combined with Lamb wave excitation from an actuator. The goal is to visualize how the Lamb waves interact with the defect and read the incoming acoustic signal from receivers that are placed in different locations. In that way, not only the existence of the defect can be monitored but with further analysis of the incoming signals, it is possible to predict the possible location of the defect on the sample under investigation. In this study the air-coupled array that is used for the test purposes is equipped with eight electrets microphones at distance of 15mm from each other. The electrets microphones are generating electric field in the air gap [237]. The array was positioned in different locations and the arriving signal was analyzed. The array was connected to a National Instruments NI PXI-1033 data analyzer, see figure A.19.

Figure A.19: An array of air-coupled electrets microphones used for defect detection on composite plates (left), NI PXI-1033 analyzer (right).

On the composite samples under investigation, a piezoelectric transducer (d = 7mm) has been attached in order to act as a source of wave excitation. The air-coupled array transducer receives the acoustic signals from the source and the data are collected from the National Instruments NI PXI-1033 and finally analysed with the aid of LabVIEW software. Figure A.20, below, shows a top view drawing of the setup.

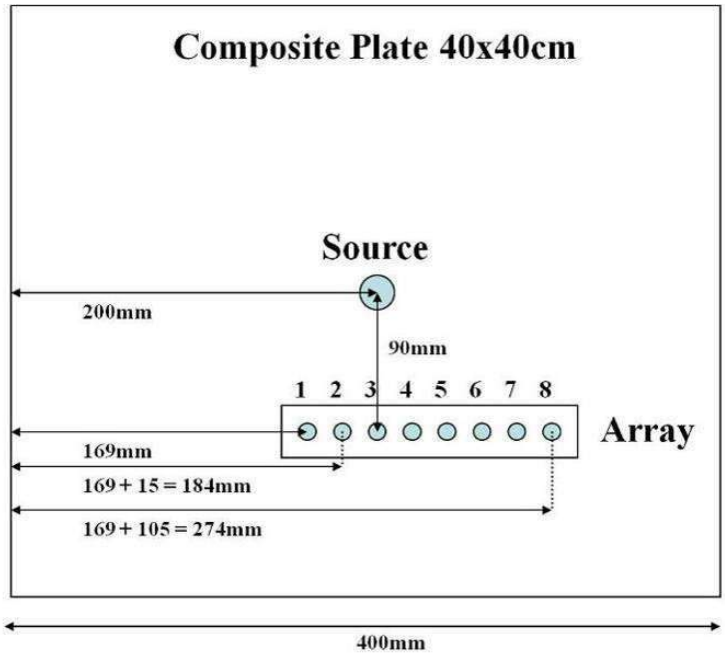

Figure A.20: Drawing of a top view of the array of sensors and the PZT (source) in the middle of the composite plate.

The above array technique has been also used with PZTs in previous investigations as a passive phased-array mode [238, 239]. The difference in this study is that an air-coupled array can be used as an adjustable and removable tool in contrast to an array of PZTs that they would need to be attached on the sample with the use of a special ultrasonic couplant.

The NI PXI-1033 data analyzer has a burst output to connect the active pseudo defect for wave excitation and 8 connectors for electrets microphones to receive the acoustic waves. The software used for getting the data from the signals is LABVIEW. In LABVIEW, a block diagram that analyses the signals from the microphones and builds up the graphs had to be developed. The block diagram has various inputs, parameters and options such as filters and Hilbert transformation equations that are used to obtain the required data. These graphs give the waveform that is obtained by the eight electrets microphones.

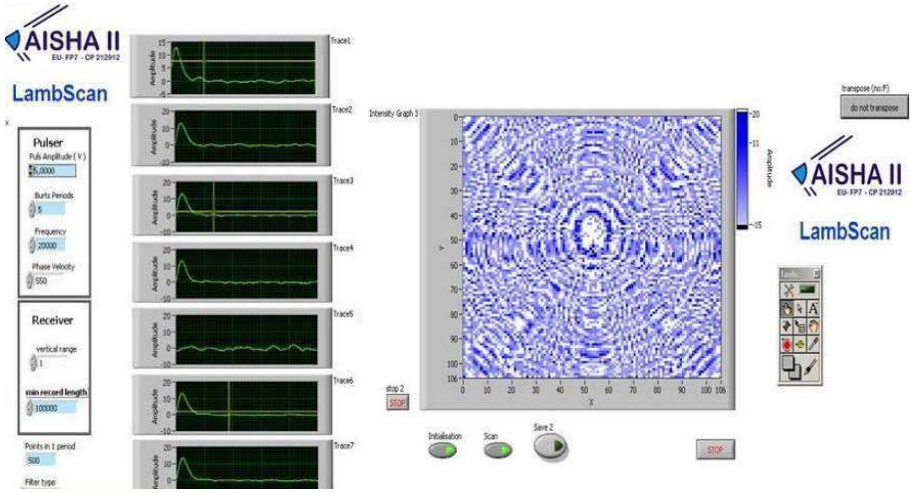

Figure A.21: Screenshot from an example of the proposed software showing the signal on electrets microphones after Hibert transform (left), scanning result of the whole area without defect (right).

In figure A.21 above, the signal of each sensor is shown on the left after the Hilbert transform has been applied to it. The graph on the right shows the image that has been obtained after scanning. The scanning is without a pseudo-defect, just to see the function of the electric microphones. The time interval to get an image during scanning was 2-3 minutes.

A.4.4 Results and discussion

During the tests, one of the eight electrets microphones was malfunctioning and therefore, the results that are presented below are obtained from seven microphones. As a first test, the seven electrets microphones were positioned directly in the middle of the plate on top of the PZT that was acting as a source of excitation. As a second test, the seven electrets microphones were positioned on the bottom right corner of the composite plate with an angle of 45 degrees to each side. In figure A.22, below, the 7 electric microphones are presented with the black circles. On the bottom image of figure A.22, seven different eclipses are appearing between the active pseudo-defect (in this case PZT) and the electric microphones. It could be seen that in a case of impact damage, the air-coupled array could spot the location since the signal will be interrupted by the defect. Nevertheless, the software as well as the parameters of the test are in a primary stage and need further development.

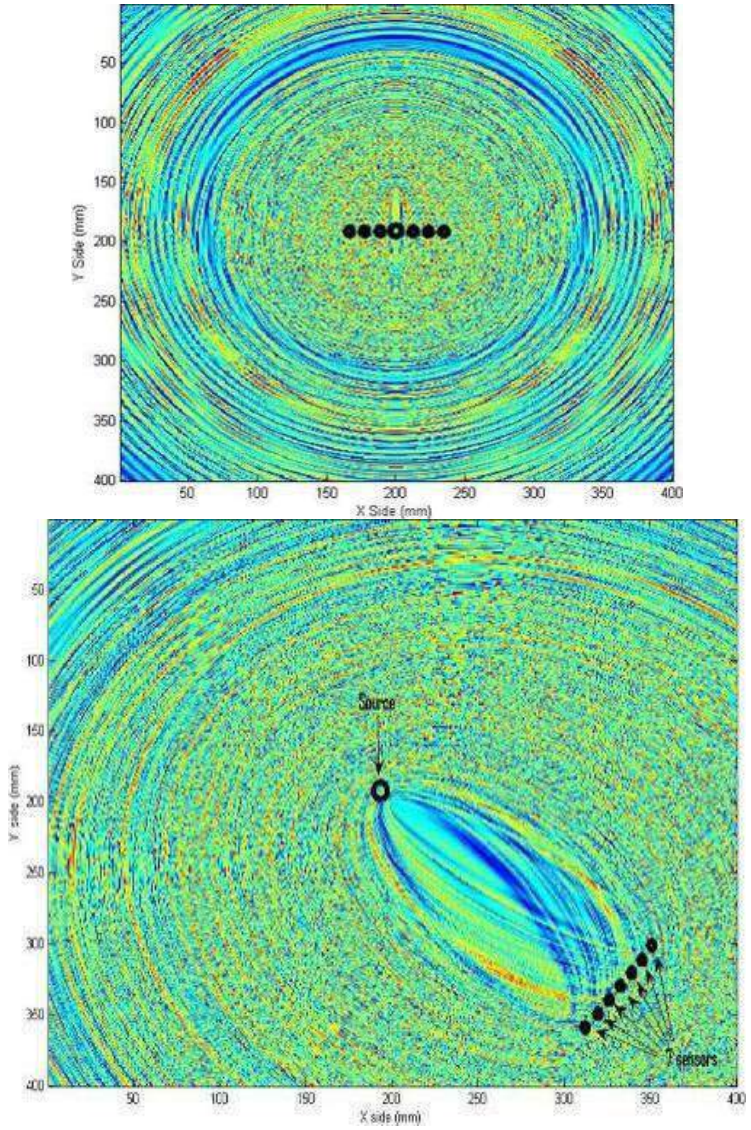

Figure A.22: Array in central position and on top of PZT (up), array positioned on bottom right corner with 45 degrees angle – seven eclipses are appearing (down). Plates are without defects and the screenshots are showing the signals between the sensors.

On the composite part of the Eurocopter EC 135 tail boom, the array of sensors is attached on the inner curved surface with the aid of a small clamp. In that case, the excitation source is a large rectangular PZT that is positioned near the edge of the part of the tail boom, see figure A.23.

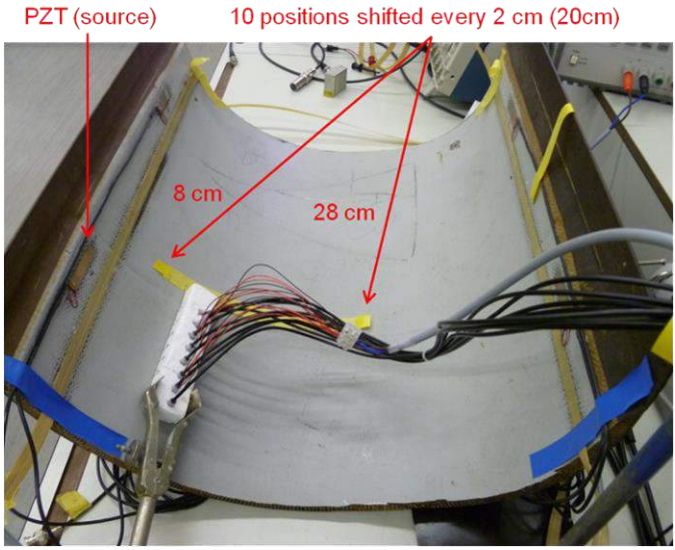

Figure A.23: Air-coupled array positioned in the inner area of a part of a tail boom EC 135.

Figure below, shows the time delay of the waves each time the distance from the piezoelectric source is increased. The phase velocity is obtained from the slope. After a linear regression for the equation, the value of the phase velocity was calculated about 530m/s.

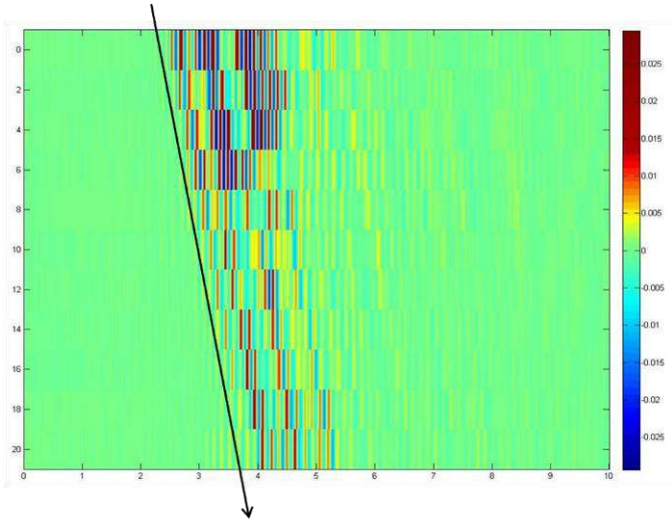

Figure A.24: Acoustic response on the electrets microphones every 2 cm for 10 times from the reference position. With linear regression on the signal obtained in each position the phase velocity is calculated.

A.4.5 Summary

The 8-electret microphone air-coupled lamp wave detector was used for an attempt to give a 2-dimensional defect imaging in composite plates and gave some promising results. Further development of the detection system and the optimization of the necessary parameters on the software are feasible. The main purpose was to create an easy hand-scanner for NDT applications with the ability to receive on-time images for defect detection on composite components.

A.5 Crack monitoring using optical interruption

A.5.1 Theoretical background

Single Mode (SM) optical fibres were embedded in thin aluminium 2027-T3 plates and tested under fatigue conditions. The concept of crack monitoring using optical interruption is quite simple. SM fibres are fed with light that is transmitted from a laser source. The optical signal from the fibre is interrupted after it has been broken due to a crack that had initiated from a hole in the middle of the plate. The hole has the role of a stress concentration point that initiates the crack. The plate was subjected to fatigue until the fibres are broken. Then a simple tensile-release test showed the reliability of the fibre to carry light after its breakage. The optical interruption on the SM fibres took place every time the crack was open. The results showed that the optical fibre had the ability to transmit light when the crack was closed.

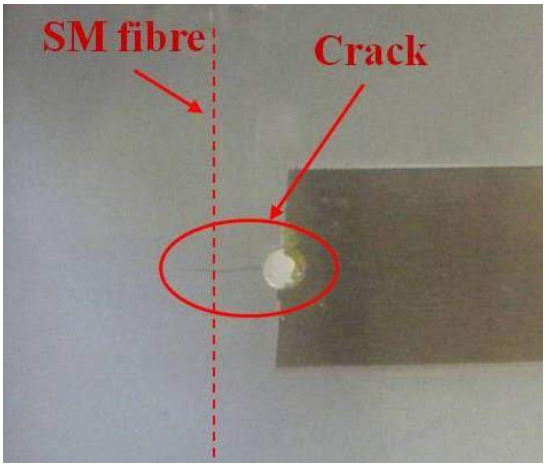

Figure A.25: A crack that has been created due to fatigue and breaks an embedded SM optical fibre interrupting the signal.

A.5.2 Application in aircrafts

At the moment there is no application of optical interruption as described above in SHM of aircrafts. The test was performed in MTM, KU Leuven to investigate the ability of the SM fibre to behave as a crack gauge. With the use of fibres as crack gauges, corrosion problems as well the use of electric current on the areas under investigation can be avoided.

A.5.3 Materials and methodology

A short study was accomplished for the investigation on crack detection using optical fibers as crack gauges. Single mode optical fibers are connected with a laser source and light is transmitted through them. They are embedded between the layers of primer and top coating as it was explained in chapter 5. The setup that appears in figure A.26 shows the servo-hydraulic fatigue testing machine from Schenck AG (now Instron Schenck Testing Systems GmbH) together with the other instruments necessary for data analysis. The instruments include a laser source, a filter, a polarization controller and an oscilloscope.

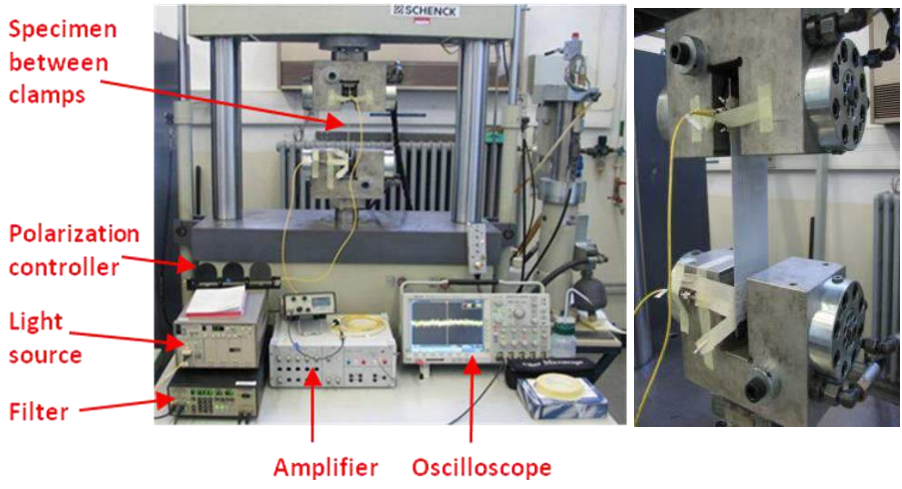

Figure A.26: Setup for crack detection using optical interruption (left) and aluminium 2024-T3 plate installed in the fatigue machine (right)

The fatigue parameters are similar to those discussed in chapter 3. The sinusoidal load had a maximum value of 12 kN and a minimum of 4 kN. The frequency of the cyclic load was 15 Hz. The number of cycles generated in the test went up to 100 000 cycles. This amount of cycles is enough to create a considerable crack ~10 mm in the plate. A hole of 4 mm diameter had been created in the middle of the plate in order to initiate a crack. Therefore, the crack propagation was horizontal opposite to the load direction. Due to fatigue, the growing crack broke the optical fibre. When a static load was applied that stretched the plate, the crack remained

open. At that point, the optical fibre lost signal and there was no transmission of light.

A.5.4 Results and discussion

The concept of the study was to investigate whether the optical fibre would regain the signal if the load was released and the crack was closed. It can be seen in figure A.27 that from the preliminary tests that were performed, the optical fibre was regaining signal every time the crack was closed. Therefore, the optical fibre even if it was broken, it was collimated to the initial position and the light could go through with almost no loses.

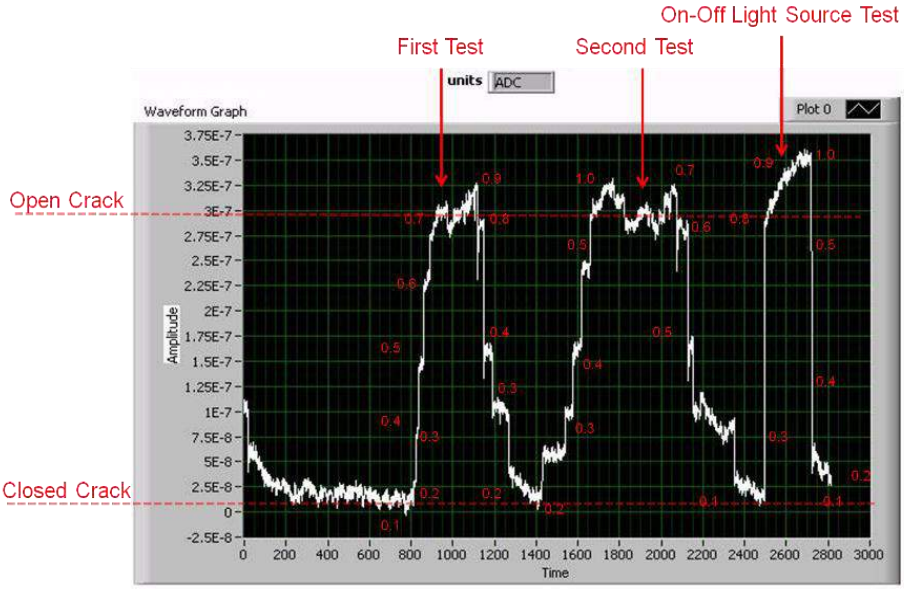

Figure A.27: Optical interruption and reinstatement

Figure above illustrates the light signal on the single mode optical fibre. The numbers 0 to 1.0 correspond to load values expressed in volts. The value of 0 Volt is translated to no load (0 kN), thus a closed crack. 1.0 Volts corresponds to a maximum load (8 kN), thus open crack. At open crack, the amplitude is very high and is translated to loss of signal on the optical fibre. Two short tests were performed together with a reliability test. At the reliability test, the light source was turned off and on in order to confirm the changes of the amplitude on the broken fibre. In real applications, the optical interruption would inform for the presence of a crack but it would not be appropriate for off-line monitoring since the signal in the broken fibres is recaptured.

Bibliography

[1] G. Bill, *World encyclopaedia of aero engines: All major aircraft power plants, from the Wright brothers to the present day*, ISBN 1852605979, P. Stephens publishing Ltd, 4th edition, 1998.

[2] H. Pfeiffer and M. Wevers. *Aircraft Integrated Structural Health Assessment – Structural Health Monitoring and its implementation within the European project AISHA* in EU Project Meeting on Aircraft Integrated Structural Health Assessment (AISHA), Vol. 13 (10), www.ndt.net, Leuven, Belgium 2008.

[3] S.W., Doebling, et al., (1996), *Damage Identification and Health Monitoring of Structural and Mechanical Systems From Changes in their Vibration Characteristics: A literature Review*, Los Alamos National Laboratory report LA-13070-MS.

[4] S.W., Doebling, et al., (1998), *A Review of Damage Identification Methods that Examine Changes in Dynamic Properties*, Shock and Vibration Digest 30 (2), pp. 91-10

[5] H. Soon , et al., (2001), *A Review of Structural Health Monitoring Literature 1996-2001*, Los Alamos National Laboratory report LA-UR-02-2095.

[6] W. J. Staszewski, C. Boller and G. R. Tomlinson, *Health Monitoring of Aerospace Structures: Smart Sensor Technologies and Signal Processing*, John Wiley & Sons Ltd., ISBN: 0-470-84340-3, 2004.

[7] X. Tao and C. Lu, *Analysis of Aircraft Composite Structural Health Monitoring and Life Prediction Technology*, Applied Mechanics & Materials, Vol. 88-89, 2011, p. 515-523.

[8] C. R. Farrar and K. Worden, *An introduction to structural health monitoring*, Phil. Trans. R. Soc. A(2007), Vol. 365, p. 303-315.

[9] H.Assler, *Design of Aircraft Structures under Special Consideration of NDT*, Presented by J. Telgkamp, 9th ECNDT, Berlin, Germany, 25-29 September 2009.

[10] H. Speckmann and R. Henrich. *Structural Health Monitoring (SHM) – Overview on Technologies under Development;* 16th World Conference on NDT, Montreal/CDN, 2004.

[11] S. Bo-lin, S. Bi-feng and C. Fei, *New Sensor Technologies in Aircraft Structral Health Monitoring*, 2008 International Conference on Condition Monitoring and Diagnosis Proceedings, Beijing, China, April 21-24, 2008

[12] H. Speckmann and H. Roesner, *Structural Health Monitoring: A contribution to the intelligent Aircraft Structure,* European Conference in Non-Destructive Testing, 25-29 Sep., Berlin, 2006.

[13] D. Jensen, *HUMS*, Article online on Aviation Today, Oct. 2006.

[14] D. Gorinevsky, *Design of Integrated SHM system for Commercial Aircraft Applications*, Proc. of the 5th International Workshop on Structural Health Monitoring, Stanford, United States, Sep. 2005.

[15] K. M. Kavi, *Beyond the black box*, IEEE Spectrum, Aug. 2010, Vol 47(8), p. 46-51.

[16] C. Boller, F.K. Chang and Y. Fujino, *Encyclopedia of Structural Health Monitoring*, Wiley 2009.

[17] C.A. Babish IV, "*USAF ASIP: Protecting Safety for 50 Years*," 2008 ASIP conference, San Antonio, TX, 2 Dec 2008.

[18] W. Huang, T.-J. Wang, Y. Garbatov and C. Guedes Soares, *Fatigue reliability assessment of riveted lap joint of aircraft structures*, International Journal of Fatigue, Vol. 43, Oct. 2012, p. 54-61.

[19] *Various Statistics*, Aircraft Crashes Record Office Online. http://www.baaa-acro.com/Statistiques%20diverses.htm

[20] G.S. Campbell and R. Lahey, *A survey of serious aircraft accidents involving fatigue fracture*, International Journal of Fatigue, Vol. 6, Issue 1, Jan. 1984, p. 25-30.

[21] C. F. Tiffany, J.P. Gallagher and C.A. Babish, *Threats to aircraft structural safety, including a compendium of selected structural accidents/incidents*, Engineering Directorate (ASC/EN), Final Report, Mar. 2010.

[22] National Transportation Safety Board. (1989). *Aircraft Accident Report: AAR89-03*, Washington D.C., United States of America Government.

[23] H. Kobayashi and H. Terada, *Crash of Japan Airlines B-747 at Mt. Osutaka*, Hatamura Institute for the Advancement of Technology, Failure Knowledge database, Mr. 25, 2011.

[24] *Mount Osutaka airline disaster: Workers at the wreckage of Japan airline flight 123*, August 1985, Photograph: Encyclopedia Britannica Online, Web. 26 Jun. 2012.

http://www.britannica.com/EBchecked/media/146046/Workers-at-the-wreckage-of-Japan-Air-Lines-flight-123

[25] *Wreckage part of Boeing 747-209Bfrom China airlines flight 611*, Photo courtesy of www.airdisaster.com, http://www.airdisaster.com/photos/ci611/6.shtml

[26] *Vertical Stabilizer and components of aircraft recovered from the water*, Photo courtesy of www.thewebfairy.com, http://thewebfairy.com/911/587/index.htm

[27] B. Aktepe and L. Molent, *Management of Airframe Fatigue through Individual Aircraft Loads Monitoring Programs*, International Aerospace Congress, Adelaide, Australia, Sept. 1999.

[28] M. Wevers, S. Van Huffel, S. Vandenplas and J.M. Papy, *Acoustic emission monitoring using a polarimetric Single Mode optical fibre sensor* Int. J. Materials and Structural Integrity 1 (2007) 148-160.

[29] R. D. Finlayson, M. Friesel, M. Carlos, P. Cole and J. C. Lenain, *Health monitoring of aerospace structures with acoustic emission and acousto-ultrasonics*, 15th World Conference on NDT, Rome, October 200..

[30] S. Vandenplas, J.M. Papy, M. Wevers and S. Van Huffel, *Acoustic emission monitoring using a multimode optical fibre sensor*, Insight 46 (2004), p. 203-209.

[31] R. D. Bowman, B. A. Bennet and M. E. Stevenson, *Radiographic inspection in failure investigations, Journal of failure analysis & prevention*, Vol. 3, Numner 3 (2003), 73-77.

[32] L. B. Reynolds, R. Twite, M. Khobaib, M. S. Donley and G. P. Bierwagen, *Preliminary evaluation of the anticorrosive properties of aircraft coatings by electrochemical methods*, Progress in Organic Coating, Vol. 32, Issues 1-4, Dec. 1997, p. 31-34.

[33] W.-L. Liu, C.-K. Jen, K.-T. Wu, M. Kobayashi and N. Mrad, *Flexible ultrasonic transducer arrays for health monitoring of an aircraft component*, Insight-Non-Destructive Testing and Condition Monitoring, Vol. 53, Number 6, June 2011, p. 316-320 (5).

[34] H. Guo, G. Xiao, N. Mrad and J. Yao, *Fiber Optic Sensors for Structural Health Monitoring of Air Platforms*, Sensors 2011, Volume 11, Issue 4, P. 3687-3705.

[35] J. M. Lopez-Higuera, L. R. Cobo, A. Q. Incera and A. Cobo, *Fiber Optic Sensors in Structural Health Monitoring*, Journal of Lightwave Technology (2011), Vol. 29, Issue 4, pp. 587-608.

[36] S. P. Knight, M. Salagaras and A.R. Trueman, *The study of intergranular corrosion in aircraft aluminium alloys using X-ray tomography*, Corrosion Science, Vol. 53, Issue 2, Feb. 2001, p. 727-734.

[37] H. Weber, *Role of nondestructive testing evaluation in civil aviation: historical development, current status, future challenges*, SPIE, 2455, 1995, p. 45-53.

[38] A. Sophian, G. Y. Tian, D. Taylor and J. Rudlin, *Design of a pulsed eddy current sensor for detection of defects in aircraft lap-joints*, Sensors and Actuators A: Physical, Vol. 101, Issues 1-2, Sep. 2002, p. 92-98.

[39] Y. He, F. Luo, M. Pan, F. Weng, X. Hu, J. Gao and B. Liu, *Pulsed eddy current technique for defect detection in aircraft riveted structures*, NDT & E International, Vo. 43, Issue 2, Mar. 2012, p. 176-181.

[40] N. Goldfine, V. Zilberstein, A. Washabaugh, D. Schlicker, I. Shay and D. Grundy, *Eddy Current Sensor Network for Aircraft Monitoring*, Aerospace Health Monitoring, Vol. 61, Issue 7, July 2003.

[41] E. Pelletier, M.Grenier, A. Chahbaz and T. Bourgelas, *Array Eddy Current for Fatigue Crack Detection of Aircraft Skin Structures*, Proceedings from 5th International Workshop, Advances in Signal Processing for Non-Destructive Evaluation of Materials, Quebec, Canada, 2-4 Aug. 2005.

[42] H. Lemire, P. R. Underhill, T. W. Krause, M. Bunn and D. J. Butcher, *Improving Probability of Detection of Bolt Hole Eddy Current Inspection*, Research in Nondestructive Evaluation, Vol. 21, Issue 3, Aug. 2001, p. 141-156.

[43] J. Schreiber, U. Cikalova, S. Hillmann, J. Hoffmann and N. Meyendorf, *A Fatigue Life Assessment of Aircraft Alloys Using Fractal Analysis in Combination with Eddy Current Testing*, Proceeding form 18th World Conference in Nondestructive Testing, South Africa, 16-20 April 2012.

[44] U. Godbole and A. Gokhale, *Eddy Current Inspection in Aircraft Industry*, Proceedings from National Seminar on Non-Destructive Evaluation, Hyderabad, India, Dec. 7-9, 2006.

[45] J. Schreiber, U. Cikalova, S. Hillmann, J. Hoffmann and N. Meyendorf, *A Fatigue Life Assessment of Aircraft Alloys Using Fractal Analysis in Combination with Eddy Current Testing*, Proceddings from the 18th World Conference in Nondestructive Testing, Durban, South Africa, 16-20 Apil, 2012.

[46] T. Dogaru and S. T. Smith, *Giant Magnetoresistance-Based Eddy-Current Sensor*, IEEE Transactions on Magnetics, Vol. 37, No. 5, September 2001.

[47] A. Jander, C. Smith and R. Schneider, *Magnetoresistive Sensors for Nondestructive Evaluation*, 10th SPIE International Symposium, Nondestructive Evaluation for Health Monitoring and Diagnostics, San Diego, California, USA, 6-10 March, 2005.

[48] N. V. Nair, V. R. Melapudi, H. R. Jimenez, X. Liu, Y. Deng, Z. Zeng, L. Udpa, T. J. Moran and S. S. Udpa, *A GMR-Based Eddy Current System for NDE of Aircraft Structures*, IEEE Transactions on Magnetics, Vol. 42, No. 10, October 2006.

[49] B. Petitjean, S. Barut, S. Rolet and D. Simonet. *Damage Detection on Aerospace structures:Last Development at EADS.* Proceedings of the Third European Workshop on Structural Health Monitoring, ISBN 1-932078-63-0. DEStech Publications, Inc., 2006, p.159-166.

[50] A. Washabaugh, B. Zilberstein, R. Lyons, K. Walrath, N. Goldfine and E. Abramovici, *Fatigue and Stress Monitoring Using Scanning and Permanently Mounted MWM-Arrays,* AIP Conference proceedings, 2003, Vol. 20, p.1598-1605.

[51] B. Zilberstein, D. Grundy, V. Weiss, N. Goldfine, E. Abramovici, J. Newman and T. Yentzer, *Early detection and monitoring of fatigue in high strength steels with MWM-Arrays,* International Journal of Fatigue 27, 2005, p.1644–1652.

[52] M. Martinez, L. Gang, D. Backman, A. Oudovikine and N. Bellinger, *Crack Detection on Composite and Metallic Aerospace Structures*, ISG Preventive Technology Inc., Nov. 2008.

[53] J. Tikka, R. Hedman and A. Siljander, *Strain gauges capabilities in crack detection*, from the proceedings of the 4th International Workshop on Structural Health Monitoring, Stanford, 15-17 September 2003.

[54] A. A. Baker, R. J. Callinan, M. J. Davis, R. Jones and J. G. Williams, *Repair of Mirage III Aircraft using the BFRP Crack-Patching Technique*, Theoretical and Applied Fracture Mechanics, Vol.2, Issue 1, Oct. 1984, p. 1-15.

[55] H.-S. Yoon, D. Jung and J.-H. Kim, *Lamb wave generation and detection using piezoceramic stack transducers for structural health monitoring applications*, Smart Materials and Structures, Vol. 21, Issue 5, May 2012.

[56] H. Cho, C. J. Lissenden, *Structural health monitoring of fatigue crack growth in plate structures with ultrasonic guide waves,* Sage Publications, Doi: 10.1177/1475921711430439, Feb. 2012.

[57] J. E. Michaels, T. E. Michaels, S. J. Lee, X. Chen, N. Gandhi and F. Shi, *Understanding and exploiting the effects of loading on ultrasonic sensing*

systems for structural health monitoring, Georgia Institute of Technology, Atlanta, Accession number: ADA559972, Feb. 2012.

[58] G. J. Qi, H. Lei, P. Jeng, G. Q. Fu and R. S. Geng, *Health Monitoring during Aircraft Vertical Empennage Fatigue Test by Acoustic Emission Method*, Proceedings from 18th World Conference in Nondestructive Testing, Durban, South Africa, 16-20 April, 2012.

[59] W. J. McGonnagle, *International Advances in Nondestructive Testing*, Routledge Publishing, ISBN-10: 2881243274, Jan. 1, 1989.

[60] N. Fourier, F. Santos, C. Brousset, J.L. Arnaud and J.A. Quiroga, *Optical Tool for Impact Damage Characterization on Aircraft Fuselage*, Proceeding from 16th World Conference in Nondestructive Testing, Montreal, 30 Aug. – 3 Sep. 2004.

[61] M. Khan, *Applications of Optical Device During Maintenance of Aircraft*, Proceeding from 16th World Conference in Nondestructive Testing, Montreal, 30 Aug. – 3 Sep. 2004.

[62] T. Yoshino, K. Kurosawa, K. Itoh and T. Ose, *Fiber-Optic Fabry-Perot Inteferometer and its sensor applications*, IEEE Journal of Quantum Electronics, Vol. 18, Issue 10, October 1982, p. 1624-1633.

[63] D. Philen, I. White, J. Khul and S. Mettler, *Single-mode fiber OTDR: Experiment and Theory*, IEEE Journal of Quantum Electronics, Vol. 18, Issue 10, October 1982, p. 1499-1508

[64] T. Gangopadhyay, *Prospects for fibre Bragg gratings and Fabry-Perot interferometers in fibre-optic vibration sensing*, Sensors & Actuators A, Vol. 113, 2004, p. 20-38.

[65] A. J. Rogers, *Distributed optical-fibre sensors for the measurement of pressure, strain and temperature*, Physics Reports, Vol. 169, No. 2, 1988, p. 99-143.

[66] M. Majumber, T.K. Gangopadhyay, A. K. Chakraborty, K. Dasgupta and D. K. Bhattacharya, *Fibre Bragg gratings in structural health monitoring – Present status and applications*, Sensors and Actuators A: Physical, Vol. 147, Issue 1, 15 Sep. 2008, p.150-164.

[67] M. Patitsa, H. Pfeiffer and M. Wevers, *Corrosion Prevention by Detection of Corrosive Liquids using Optical Fibre Sensors*, Proceeding from the 10th European Conference in Nondestructive Testing, Moscow, Russia, 7-11 June 2010.

[68] A. Jaya, U. H. Tiong and G. Clark, *The interaction between corrosion management and structural integrity of aging aircraft*, Fatigue & Fracture of Engineering Materials & Structures, Vol. 35, Issue 1, January 2012, p. 64-73.

[69] J. F. O'Connell and G. Williams, *Passengers' perceptions of low cost airlines and full service carriers: A case study involving Ryanair, Aer Lingus, Air Asia and Malaysia Airlines*, Journal of Air Transport Management, Vol. 11, 2005, p. 259-272.

[70] M. Z. Silva, R. Gouyon and F. Lepoutre, *Hidden corrosion detection in aircraft aluminium structures using laser ultrasonics and wavelet transform signal analysis*, Ultrasonics, Vol. 41, Issue 4, June 2003, p. 301-305.

[71] M. N. Libin, K. Balasubramaniam, C. V. Krishnamurthy and R. Engelbart, *Tone burst eddy current thermography for estimation of corrosion defects in aircraft components*, AIP Conference Proceedings, American Institute of Physics, Vol. 1430, Issue 1, 2012, p. 425-432.

[72] J. F. Martins-Filho and E. Fontana, *Optical Fibre Sensor System for Multipoint Corrosion Detection*, Optical Fibre, New Developments, Edition 1, Chapter 3, In-Tech Publishing, January 2009, ISBN 9789537619503.

[73] V. T. Rathod and D. Roy Mahapatra, *Ultrasonic Lamb wave based monitoring of corrosion type of damage in plate using a circular array of piezoelectric transducers*, NDT & E International, Vol. 44, Issue 7, November 2011, p. 628-636.

[74] T. J. Garosshen, *Corrosion Sensor Systems for Aircraft Applications*, Materials Selection & Design, Vol. 51, No. 3, March 2012, p. 56-60.

[75] J. Demo, *Smart Environmental Corrosivity Sensor Suite for Aircraft Applications*, NAVAIR public release, N073-171-0494, 2009.

[76] NDT Resource Centre Online, Nondestructive Testing in the Aerospace Industry,http://www.ndt-ed.org/AboutNDT/SelectedApplications/AircraftInspection/Aircraft%20Inspection.htm

[77] Technical Diagnostics and NDT-Review Blogspot, *Aicraft Visual Inspection*, 24 Feb., 2010, http://ndt-review.blogspot.be/2010/04/aircraft-visual-inspection.html

[78] D.C Worlton, *Ultrasonic testing with Lamb waves*, Nondestructive Testing, Vol. 15, 1957, p.218-222.

[79] T.L. Mansfield, *Lamb wave inspection of aluminium sheet*, Materials Evaluation, Vol. 33, 1975, p.96-100.

[80] K. Diamanti and C. Soutis, *Structural health monitoring techniques for aircraft composite structures*, Progress in Aerospace Sciences, Vol. 46, Issue 8, Nov. 2010, p. 342-352.

[81] I. A. Viktorov, *Rayleigh and Lamb Waves*, Physical Theory and Applications, Plenum Press, New York, 1967.

[82] J. B. Ihn and F. K. Chang, *Pitch-catch active sensing methods in structural health monitoring for aircraft structures*, Structural Health Monitoring, Vol. 7, p.5-19.

[83] S. Kuznetsov, E. Ozolinsh, I. Ozolinsh, V. Pavelko, M. Wevers and H. Pfeiffer, *Lamb Wave Interaction with a Fatigue Crack in a Thin Sheet of Al2024-T3*, EU Project AISHA Meeting, Leuven, Belgium, June 2007.

[84] V. Pavelko, I. Pavelko, E. Ozolinsh and S. Kuznetsov, *Application of Fatigue Crack Open Effect for Aircraft Structural Health Monitoring*, Proceedings from the 6th International Workshop of NDT Experts, Prague, Czech Republic, 10-12 Oct., 2011.

[85] Z. Li and F. Luo, *Novel Method of In-situ Ultrasonic Test of Aircraft Parts*, Proceedings from the 9th International Conference on Electronic Measurements & Instruments, Beijing, China, 16-19 Aug, 2009.

[86] W. Haase and A. Mauer, *Latest developments on industrial ultrasonic testing of aircraft components*, Proceedings from the 16th World Conference on Nondestructive Testing, Montreal, Canada, Aug. 30 – Sep. 3, 2004.

[87] A. Maurer, W. Deodorico, R. Huber and T. Laffont, *Aerospace Composite Testing Solutions using Industrial Robots*, Proceedings from the 18th World Conference in Nondestructive Testing, Durban, South Africa, 16-20 April, 2012.

[88] J. H. Gieske, *Evaluation of Scanners for C-Scan Imaging for Nondestructive Inspection of Aircraft*, Final Report, U.S. Department of Transportation, Federal Aviation Administration, Vol. 2, Issue 11, Oct. 1994.

[89] J. Demo, F. Friederdsdorf, C. Andrews and M. Putic, *Wireless corrosion monitoring for evaluation of aircraft structural health*, Aerospace Conference Proceedings, IEEE, 3-10 March 2012.

[90] K. Mandal and D. L. Atherton, *A study of magnetic flux-leakage signals*, Journal of Physics D: Applied Physics, Vol. 31, Issue 22, Nov. 1998.

[91] Md. Alahi Uddin Khan, *Non-destructive Testing Applications in Commercial Aircraft Maintenance*, www.ndt.net , Vol. 4, Issue 6, June 1999.

[92] L. R. Hall, R. W. Finger and W. F. Spurr, *Corrosion Fatigue Crack Growth in Aircraft Structural Materials*, Boeing Aerospace, Accession Number: AD0916695, Sep. 1973.

[93] C. A. Harding and G. R. Hugo, *Review of Literature on Probability of Detection for Liquid Penetrant Nondestructive Testing*, Defence Science and Technology Organization, Victoria, Australia, Technical Report, Accession Number: ADA560011, Nov. 2011.

[94] W. L. Dunn and A. M. Yacout, *Corrosion detection in aircraft by X-ray backscatter methods*, Applied Radiation and Isotopes, Vol. 53, Issues 4-5, Nov. 2000, p.625-632.

[95] W. J. Lewis, L. G. I. Bennett, T. R. Chalovich and O. Francescone, *Neutron radiography of Aircraft composite Flight control Surfaces*, Proceedings from 15th World Conference in Nondestructive Testing, Rome, Italy, 15-21 Oct. 2000.

[96] X. Wang, B. S. Wong, C. G. Tui, K. P. Khoo and F. Foo, *Real-time Radiographic Non-destructive Inspection for Aircraft Maintenance*, Proceedings from 17th World Conference on Nondestructive Testing, Shanghai, China, 25-28 Oct. 2008.

[97] U. Ewert, U. Zscherpel and M. Jechow, *Essential Parameters and Conditions for Optimum Image Quality in Digital Radiology*, Proceedings from 12th World Conference in Nondestructive Testing, Durban, South Africa, 16-20 April, 2012.

[98] P. Van Rooijen, *PREDICT, an alternative approach to radiation protection in industrial radiography*, Proceedings from 7th European Conference in Nondestructive Testing, Copenhagen, Denmark, 26-29 May 1998.

[99] C. Hao, X. Zhou and L. Ming, *The application and development of radiography technology based on X-ray*, Procceding from the International Symposium on Photoelectronic Detection and Imaging, ISBN: 9780819476623, Aug. 21, 2009.

[100] S. M. Shepard, *Introduction to active thermography for non-destructive evaluation*, AntiCorrossion Methods and Materials, Vol. 44, Issue 4, Emerald Publishing, Aug. 1997.

[101] J. A. Charles and D. W. Wilson, *Passive Thermal Nondestructive Flaw Detection in Composites*, Newark Centre for Composite Materials, Accession Number: ADA303236, Aug. 1979.

[102] N. P. Avdelidis and D. P. Almond, *Transient thermography as a through skin imaging technique for aircraft assembly: modelling and experimental results*, Infrared Physics & Technology, Vol. 45, Issue 2, Mar. 2004, p. 103-114.

[103] T. D. Orazio, C. Guaragnella, M. Leo and P. Spagnolo, *Defect detection in aircraft composites by using a neural approach in the analysis of thermographic images*, NDT & E International, Vol. 38, Issue 8, Dec. 2008, p.665-673.

[104] N. P. Avdelidis, B. C. Hawtin and D. P. Almond, *Transient thermography in the assessment of defects of aircraft composites*, NDT & E International, Vol. 36, Issue 6, Sep. 2003, p. 433-439.

[105] T. Zweschper, A. Dillenz, G. Riegert and G. Busse, *Lockin Thermography Methods for the NDT of CFRP Aircraft Components*, Proccedings from 8th European Conference in Nondestructive Testing, Barcelona, Spain, June 2002.

[106] C. Ibarra-Castanedo, M. Susa, M. Klein, M. Grenier, J.-M. Piau, W. Ben Larby, A. Abdelhakim and X. Maldague, *Infrared Thermography: Principle and Applications to Aircraft Materials*, Proceedings from International Symposium on NDT in Aerospace, Fürth, Germany, Dec. 3-5, 2008.

[107] G. Kalogiannakis, H. Zhang and C. Glorieux, *The use of Grating Lock-in IR thermography for the determination of thermal properties,* Proceedings from the 4th International Conference on NDT, Chania, Greece, 11-14 Oct., 2007.

[108] Most widely used NDT techniques, ICNDT, 2006, http://www.icndt.org/Home/WhatisNDT.aspx

[109] G. A. Matzkanin and H. T. Yolken, *Probability of Detection (POD) for Nondestructive Evaluation (NDE)*, Nondestructive Testing Information Analysis Centre, Texas, August 2001.

[110] F. Schoefs, A. Clement, J. Boero and B.Capra, *Expert judgement for combining NDT tools in RBI context: Application to Marine Structures, ASRANet Conference, Edinburgh, United Kingdom, 14-16 June 2010.*

[111] F. Jenson, E. Iakovleva and C. Reboud, *Evaluation of POD curves Based on Simulation Results*, 7th International Conference on NDE in Relation to Structural Integrity for Nuclear and Pressurized Components, Yokohama, Japan, 12-15 May 2009.

[112] R. B. Mabuza, *Numerical Analysis of Probability of Detecting Defects in Engineering Materials*, 18th World Conference on Nondestructive Testing, 16-20 April 2012, Durban, South Africa.

[113] A. P. Berens and P. W. Hovey, *Evaluation of NDE reliability characterization*, USAF Report No. AFWAL-TR-81-4160, 1981.

[114] A. P. Berens and P. W. Hovey, *Characterization of NDE Reliability*, Review of Progress in Quantitative NDE, I, New York, Plenum Press, 1982.

[115] B. Palmberg, A. F. Blom and S. Eggwertz, *Probabilistic Damage Tolerance Analysis of Aircraft Structures*, Probabilistic Fracture Mechanics and Reliability, M. Nijhoff, Dordrecht, The Netherlands, 1987.

[116] F. Van den Abeele and P. Goes, *Non Destructive Techniques for Risk Based Inspections*, Proceedings from the 5th International Conference *on* Sustainable Construction *&* Design*:* Ghent *U*niversity, Belgium

[117] L.E. Pado, J. B. IHN and J. P. Dunne, *Understanding Probability of Detection (POD) in Structure Health Monitoring Systems*, The 9th International Workshop on Structural Health Monitoring, Stanford University, 2013.

[118] R. B. Thomson, L. H. Brasche, D. Forsyth, E. Lindgren, P. Swindell and W. Winfree, *Recent advances in model-assisted probability of detection*, Centre for Nondestructive Testing Evaluation, Iowa State University, 6 Jan 2009.

[119] John C. Aldrin, David S. Forsyth, Harold A. Sabbagh, Eric A. Lindgren, Jeremy S. Knopp, Charles F. Buynak, Enrique A. Medina, Demonstrations of Model-assisted Probability of Detection (MAPOD) Evaluation, Iowa State University, NDE Centre, Feb. 2012.

[120] I. Solodov, *Nonlinear acoustic NDT: Approaches, methods, and applications*, NDT in progress proceedings, Prague, 2009.

[121] J. R. Rudli, *Reliability of inspection for fatigue cracks in offshore structures*, Institution of Electrical Engineers, Savoy Place, London WC2R OBL, UK. 6/1-6/3, 1996.

[122] H. Pfeiffer, P. Heer, M. Winkelmans, W.Taza, I. Pitropakis, M. Wevers, *Leakage monitoring using percolation sensors for revealing structural damage in engineering structures*, Structural Control and Health Monitoring (International Journal), 17 December 2013.

[123] I. Pitropakis, H. Pfeiffer, T. Gesang, S. Janssens, M. Wevers, *Crack detection on aluminium 2024-T3 plates and on an Airbus A320 slat-track using electrical crack gauges*, 18th World Conference for Non Destructive Testing (WCNDT 2012), Durban, South Africa, 16-20 April 2012.

[124] D. R. Tenney, J. G. Jr. Davis, N. J. Johnston, R. B. Pipes and J. F. McGuire, *Structural Framework for Flight: NASA's Role in Development of Advanced Composite Materials for Aircraft and Space Structures*, ID: 20110012179, NASA report, May 2011.

[125] Boeing 787/7E7 Dreamliner, *Specifications and materials*, http://bintang.site11.com/Boeing_787/Boeing787_files/Specifications.html

[126] K. Deckers, P. Guillaume, D. Lefeber and D. De Baere, *Turning Point Based Fatigue Test Using Amplitute Adapted Time Waveform Replication*, Proceedings of the SEM Annual Conference, June 1-4, 2009, Albuquerque, New Mexico, USA.

[127] R. Longo, S. Vanlanduit and P. Guillaume, *Laser vibrometer measures surface acoustic waves for nondestructive testing*, International Society for Optical Engineering, Sensing and Measurement, 29 November 2006, SPIE Newsroom. DOI: 10.1117/2.1200611.0377.

[128] J. Kaletka, H. Kurscheid and U. Butter, *FHS, the new research helicopter: Ready for service*, Aerospace Science and Technology, Vol. 9, 2005, p.456-467.

[129] J. Schijve, *Fatigue of aircraft materials and structures, International Journal of Fatigue*, Vol. 16, Issue 1, January 1994, p. 21-32.

[130] R. A. Smith, *Fatigue in Transport: Problems, Solutions and Future Threats*, Trans IChemE, Vol. 76, Part B, August 1998.

[131] R. Jones, K. Cairns, J. Baker, K. Krishnapillai and B. Hinton, *A study of the effect of CPCs on fatigue crack propagation in a representative fuselage lap joint specimen*, Engineering Fracture Mechanics, Vol. 87, June 2012, p. 1-15.

[132] A.A. Baker, *Advances in the Bonded Composite Repair of Metallic Aircraft Structure*, Vol. 1, Elsevier Science Ltd., ISBN:0-08-042699-9, 2002.

[133] F. P. Miller, A. F. Vandome, J. McBrewster. *Eddy Current.* ISBN 6130233590. VDM Publishing House Ltd., 2009.

[134] T. K. Simpson, *Maxwell on the Electromagnetic Field: A Guided Study*, Rutgers University Press, ISBN-10: 081352363X, Feb. 1997.

[135] M. Hansen, *Maxwell's Equations*, Art of Problem Solving, http://www.artofproblemsolving.com/LaTeX/Examples/Maxwell's%20Equations.pdf, May 2004.

[136] M. Ciavarella, *Cracks in A380? Every plane now in the air is an experiment by itself...*, 10 February 2012, http://imechanica.org/node/11898

[137] E. C. Aifantis, *The Physics of Plastic Deformation*, International Journal of Plasticity, Vol. 3, p. 211-247, 1987.

[138] C. A. Triana and F. Fajardo, *Dependence of some mechanical properties of elastic bands on the length and load time*, European Journal of Physics, Vol. 33, Issue 4, April 2012.

[139] R. C. Alderliesten, *Damage tolerance of bonded aircraft structures*, International Journal of Fatigue, Vol. 31, Issue 6, June 2009, p. 1024-1030.

[140] Al. Th. Kermanidis, P. V. Petroyiannis, Sp. G. Pantelakis, *Fatigue and damage tolerance behaviour of corroded 2024 T351 aircraft aluminium alloy*, Theoretical and Applied Fracture Mechanics, Vol. 43, Issue 1, March 2005, p. 121-132.

[141] T. Farris and A. Grandt, *Discovering a Better World Today - Healthy Aircraft*, Engineering Edge, Purdue University Publications, 2002.

[142] P. J. Shull, *Nondestructive Evaluation: Theory, Techniques, and Applications*, Marcel Dekker AG, ISBN: 0-8247-8872-9, 2002.

[143] V. Giurgiutiu, *Lamb Wave Generation Wafer Active Sensors for Structural Health Monitoring*, Proceeding from the 10th Annual International Symposium on Smart Structures and Materials and 8th Annual International Symposium on NDE for Health Monitoring and Diagnostics, San Diego, 2-6 March 2002.

[144] L. Zhenqing, *Lamb Wave Analysis of Acousto-Ultrasonic Signals in Plate*, Proceedings of the 15th World Congress on Nondestructive Testing, Rome, 2000.

[145] J. Thorpe, *Fatalities and destroyed civil aircraft due to bird strikes 1912-2002*, IBSC26/WP-SA1, Warsaw, 5-9 May, 2003.

[146] H. Blokpoel, *Bird hazards to aircraft: Problem and prevention of bird/aircraft collisions*, Clarke, Irwin & Co. Publishing, ISBN 10: 0772010870, 1976.

[147] S. Georgiadis, A. J. Gunnion, R. S. Thomson and B.K. Cartwright, *Bird-strike simulation for certification of the Boeing 787 composite moveable trailing edge*, 14th ICCS, Composite Structures, Vol. 86, Nov. 2008, p.258-268.

[148] I. Smojver and D. Ivancevic, *Numerical simulation of bird strike damage prediction in airplane flap structure*, 5th ICCS, Composite Structures, Vol. 92, Issue 9, Aug. 2010, p. 2016-2026.

[149] S. Heimbs, *Computational methods for bird strike simulations: A review*, Computers & Structures, Vol. 89, Issue 23-24, Dec. 2011, p. 2093-2112.

[150] R. A. Dolbeer, *Birds and aircraft – fighting for airspace in even more crowded skies*, Human – Wildlife Conflicts, Vol. 3, Issue 2, p. 165-166.

[151] *Aircraft vs. Fuel Track*, Now public crowd powered media. http://www.nowpublic.com/aircraft_vs_fuel_truck_0

[152] U. Polimeno and M. Meo, *Detecting barely visible damage detection on aircraft composite structures*, 6th ICCST, Composite Structures, Vol. 91, Issue 4, Dec. 2009, p. 398-402.

[153] G. Sarton, *Ancient Science through the golden age of Greece*, Courier Dover, ISBN: 0-486-27495-0, 1993, p.248.

[154] M. Wevers, *Listening to the sound of materials: acoustic emission for the analysis of material behaviour*, NDT & E International, Vol. 30, No. 2, 1997, p. 99-106.

[155] T. M. Morton, R. M. Harrington and J. G. Bjeletich, *Acoustic emissions of fatigue crack growth*, Engineering Fracture Mechanics, Vol. 5, Issue 3, Sep. 1973, p. 691-692.

[156] R. Geng, *Modern acoustic emission technique and its application in aviation industry*, Proceedings of Ultrasonics International and World Congress on Ultrasonics, Vol. 44, 22 Dec. 2006, p. 1025-1029.

[157] O. Semar, *Exemplary simulation of internal erosion phenomena with bond percolation model*, Bauhaus-Universitat Weimar, http://www.suffos.bam.de/en/projektschwerpunkte/simulation/index.htm

[158] K. Ando, Z. Kato, N. Uchida, K. Uematsu and K. Saito, *Wetting of aqueous solutions of organic binder (PVA) on sapphire and fused quartz*, Journal of Material Science, 1989, p 4048-4051.

[159] I. Pitropakis, *Molecular Modelling & Simulation of Binary Vapour-Liquid Equilibria of Hydrogen Bonding Fluids*, Master of Engineering Thesis, Institute of Thermodynamics and Thermal Process Engineering, University of Stuttgart, Germany, January 2007.

[160] W. T. Taza, *Performance of Percolation-Threshold Based Sensors for Detecting Aqueous Liquids*, MTM, KU Leuven, Belgium, June 2012.

[161] H. Pfeiffer, P. Heer and M. Wevers, *Corrosion Prevention by Detection of Aqueous Liquids Using Sensors with a Percolation Threshold Transition*, Proceeding from the 2nd International Symposium on Nondestructive Testing, Hamburg, Germany, 22-24 Nov. 2010.

[162] I. Pitropakis, H. Pfeiffer and M. Wvers, *Crack detection in aluminium plates for aerospace applications by electromagnetic impedance spectroscopy using flat coil sensors*, Sensors & Actuators A: Physical, Vol. 176, April 2012, p. 57-63.

[163] A. S. M. Algarni, *Image fusion based enhancement of electromagnetic nondestructive evaluation,* Part of Doctoral Thesis, Electrical Engineering department, King Saud University, Riyadh, Saudi Arabia, 2009.

[164] W. Lord and R. Palanisamy. *Development of theoretical models for Non-Destructive Testing Eddy-Current Phenomena.* Eddy-Current Characterization of Materials and Structures, ASTM STP 722, George Birnbaum and George Free, Eds., American Society for Testing and Materials, U.S.A. 1981, pp. 6.

[165] V. Uchanin, G. Lutsenko, À. Dzhaganian, V. Buga, V. Derecha. *Technical Paper–Universal eddy current flaw detectors & their application for the detection of hidden flaws*, www.ndt.org.

[166] Charles J. Hellier. *Handbook of non-destructive evaluation*, ISBN 0-07-028121-1. McGraw-Hill Co., 2001, p.8.18-8.20.

[167] G. M. Ballou, *Hanbook for Sound Engineers third edition,* ISBN-10: 0-240-80758-8, Elsevier Inc., Focal Press publications, 2005, UK, chapter 10, p.226.

[168] J. M. Papazian, J. Nardiello, R. P. Silberstein, G. Welsh, D. Grundy, C. Craven, L. Evans, N. Goldfine, J. E. Michaels, T. E. Michaels, Y. Li and C. Laird, *Sensors for monitoring early stage fatigue cracking,* International Journal of Fatigue 29, 2007, p.1668-1680.

[169] S. Vanlanduit, E. Parloo and P. Guillaume, *An on-line combined linear-nonlinear fatigue crack detection technique*, NDT E Int. 37 (2004) 41-45.

[170] S. Vanlanduit, E. Parloo and P. Guillaume, *Combined damage detection techniques*, J. Sound Vibr. 266 (2003) 815-831.

[171] P. Verboven, P. Guillaume, B. Cauberghe, S. Vanlanduit and E. Parloo, *A comparison of frequency-domain transfer function model estimator formulations for structural dynamics modelling*, J. Sound Vibr. 279 (2005) 775-798.

[172] J. Pohl, *Risstiefenmessung mit Ultraschall-Rayleighwellen*, ZfP in Anwendung, Entwicklung und Forschung, www.ndt.net, Berlin, 21-23 May 2001.

[173] R. Longo, S. Vanlanduit and P. Guillaume, *Laser vibrometer measures surface acoustic waves for nondestructive testing,* SPIE Newsroom (2006).

[174] S. Vanlanduit, P. Guillaume and G. Van der Linden, *On-line monitoring of fatigue cracks using ultrasonic surface waves,* NDT E Int. 36 (2003) 601-607.

[175] S. Vanlanduit, P. Guillaume, J. Vermeulen and K. Harri. *Damage Assessment of Structures Vi*, Trans Tech Publications Ltd, Zurich-Uetikon 2005, pp. 549-556.

[176] H. Pfeiffer, D. De Baere, F. Fransens, G. Van der Linden and M. Wevers, *Structural Health Monitoring of Slat Tracks using transient ultrasonic waves*, EU Project Meeting on Aircraft Integrated Structural Health Assessment (AISHA), Leuven, Belgium, June 2007.

[177] R. Shevell, *Fundamentals of flight*, ISBN 0133390608, Englewood Cliffs, Prentice Hall 1989, Ch. 18, pp 373-386.

[178] D. Crane, *ASAS Dictionary of Aeronautical Terms*, ISBN 0940732610, Aviation Supplies & Academics Incorporated, 1987.

[179] H. A. Jehn, F. Thiergarten, E. Ebersbach and D. Fabian, *Characterization of PVD (Ti, Cr) N_x hard coatings*, Surface and Coating Technology, Vol. 50, 1991, p. 45-52.

[180] M. Wevers, L. Rippert and S. Van Huffel, *Optical fibres for in situ monitoring the damage development in composites and the relation with acoustic emission measurements,* Journal of Acoustic Emission 18 (2000) 41-50.

[181] *Olympus Microscopy Resource Center*, Olympus America Inc. Retrieved 2011-11-13.

[182] G. Thursby, B. Sorazu, D. Betz, W. Staszewski and B. Culshaw. *Comparison of point and integrated fiber optic sensing techniques for ultrasound detection and location of damage*. Smart Mater Struct. 13 (2004) Vol. 5384, 287-295.

[183] P. Burgholzer, C. Hofer, G. Paltauf, M. Haltmeier and O. Scherzer, *Thermoacoustic tomography with integrating area and line detectors* IEEE Trans. Ultrason. Ferroelectr. Freq. Control 52 (2005) 1577-1583.

[184] G. Thursby, B. Sorazu, F. Dong and B. Culshaw, *Damage Detection in Structural Materials using Polarimetric Fibre Optic Sensors Smart Structures and Materials*, Proceedings of SPIE 5050 (2003) 61-70.

[185] Mili F. & Necib B. *Impact behavior of cross-ply* laminated *composite* plates *under low velocities*, Composite and Structures, Vol. 51, p. 237-244, 2001.

[186] J. Lee, T. Kim and B. Choi, *Energy Conversion according to Impact loading on Piezoelectric material*, Nanotechnology 2009: Fabrication, Particles Characterization, MEMS, Electronics and Photonics, Vol. 1, p. 488-491.

[187] J. H. Park, S. K. Ha, K. W. Kang, C. W. Kim and H. S. Kim, *Impact damage resistance of sandwich structure subjected to low velocity impact*, Journal of Materials Processing Technology, Vol. 201, Issues 1-3, 26 May 2008, p. 425-430.

[188] L. Iannucci, *Dynamic Delamination Modelling Using Interface Elements*, Computers and Structures, Vol. 84, p. 1029-1048, 2006.

[189] R. K. Mittal and M. S. Jafri, *Influence of fibre content and impactor parameters on transverse impact response of uniaxially reinforced composite plates*, Composites, Vol 26, Issue 12, p. 877, 1995.

[190] N. V. Padaki, R. Alagirusamy and B. L. Deopura, *Low velocity impact behaviour of textile reinforced composites*, Indian Journal of Fibre & Textile Research, Vol. 33, p. 189-202, June 2008.

[191] G. Van Dijck, M. Wevers and M.M. Van Hulle, *Wavelet Packet Decomposition for the Identification of Corrosion Type from Acoustic Emission Signals,* Int. J. Wavelets Multiresolut. Inf. Process. 7 (2009) 513-534.

[192] Lamb H. *Waves in an Elastic Plate*, Proceedings of the Royal Society of London., Containing Papers of a Mathematical and Physical Character, v.93, n.651, 1917, 293-312.

[193] A. H. Nayfeh, *Wave Propagation in Layered Anisotropic Media with Applications to Composites*. v.39, Elsevier, Amsterdam, 1995.

[194] H. Pfeiffer, I. Pitropakis and M. Wevers, *The use of pseudo-defects in validation of ultrasonic structural-health-monitoring techniques,* www.ndt.net, 10th ECNDT Proceedings, Moscow, Aug. 2008.

[195] W. Hillger, *Structural Health Monitoring using Lamb waves and visualization of their propagation in composites*, AISHA European project meeting Leuven, Belgium, 2007.

[196] M. Sale, P. Rizzo and A. Marzani, *Semi-analytical formulation for the guided waves reconstruction of elastic moduli*, Mechanical Systems and Signal Processing, Vol. 25, Issue 6, Aug. 2011, p. 2241-2256.

[197] S.M. Prasad, K. Balasubramaniam and C.V. Krishnamurthy, *Structural Health Monitoring of Composite Structures using Lamb wave tomography* Smart Mater Struct. 13 (2004) N73-N79.

[198] I. Pitropakis, H. Pfeiffer , M. Wevers, *The use of a polarimetric fibre sensor to detect impact damage in aircraft composites*, ISBN 978-0-415-62131-1, 5th International conference on Emerging Technologies in Non-Destructive Testing (ETNDT), Ioannina, Greece, 19-21 September 2011.

[199] Seth S. Kesslera, S. Mark Spearinga and Mauro J. Atallab, *In-Situ Damage Detection of Composites Structures using Lamb Wave Methods*, European Workshop on Structural. Health Monitoring (EWSHM), Cachan 2002.

[200] H. Pfeiffer and M. Wevers, *Pseudo-defects for the Validation and Tuning of Structural Health Monitoring in Plate-like Structures using Lamb Waves,* Aircraft Integrated Safety Health Assessment (AISHA), Leuven, Belgium, June 2007.

[201] V. Giurgiutiu, *Tuned Lamb Wave Excitation and Detection with Piezoelectric Wafer Active Sensors for Structural Health Monitoring*, Journal of Nondestructive Evaluation, Vol. 26, Issue (2-4), 2007, p. 123-134.

[202] S. Markus and H. Siegfried, *Simulation of lamb wave excitation for different elastic properties and acoustic emission source geometries*, Journal of Acoustic Emission, ISSN 07300050, Vol. 28, 2010.

[203] J.W.S. Reyleigh, *The theory of sound*, Macmillan & Co. Publishing, London, 1877.

[204] A. Arnau, *Piezoelectric Transducers and Applications, Springer Publishing,* ISBN-978-3-540-77507-2.

[205] N. Hu, T. Shimomukai, H. Fukunaga and Z. Su, *Damage identification of Metallic Structures Using A_0 Mode of Lamb Waves*, Sage Publications, Structural Health Monitoring 2008, 7: 271 originally published online 1 April 2008.

[206] D. A. Forman P. N. Chang, E. F. Herzberg, A. R. Kelly, N. T. O'Meara and J. C. Tran, *The annual cost of corrosion for navy and marine corps aviation equipment*, LMI Government Consulting, Report MEC70T3, May 2008.

[207] WorkSafeBC, *Confined Space Entry Program – A Reference Manual,* ISBN 1715-4189, 2007.

[208] H. Pfeiffer, P. Heer, I. Pitropakis, G. Pyka, G. Kerckhofs, M. Patitsa, M. Wevers, *Liquid detection in confined aircraft structures based on lyotropic percolation thresholds*, Sensors & Actuators B: Chemical, Vol. 161, Issue 1, January 2012, p. 791-798.

[209] T. F. Zhang, S. Yin and S. G. Wang, *An under-aisle distribution system facilitating humidification of commercial aircraft cabins*, Building Environment, Vol. 45, 2010, p. 907-915.

[210] H. Pfeiffer, I. Pitropakis, M. Patitsa, M. Wevers, *Leakage detection in aircraft by percolation sensors for the prevention of floor beam corrosion and detection of pinhole cracks in hydraulic tubes*, 6th International Conference "Supply on the wings", Frankfurt/M, Germany, 2-4 November 2011.

[211] H. Pfeiffer, P. Heer, H. Sekler, M. Patitsa, I. Pitropakis, M. Wevers, *Structural Health Monitoring in an Operational Airliner: An Intermediate Report on Leakage Monitoring with Percolation Sensors*, Proceedings from 6th European Workshop on Structural Health Monitoring, 3-6 July 2012, Dresden, Germany.

[212] J. F. Young, *Humidity control in the laboratory using salt solutions – a review*, Journal of applied Chemistry, Vol. 17, Issue 9, Sep. 1967, p. 241-245.

[213] E. Traversa, *Ceramic sensors for humidity detection: the state-of-the-art and future developments* ,Sensors and Actuators B, Vol. 23, 1995, p. 135-156.

[214] C. Sriram and A. Haghani, *An optimization model for aircraft maintenance scheduling and re-assignment*, Transport Res. Pt. A-Policy Pract., Vol 37, 2003, p.29-48.

[215] M. Bory et al., *Sonotrode for Ultrasonic Machinig device,* United States Patent 5426341, Issue date: 20 Jun 1995.

[216] N. Krohn, R. Stoessel and G. Busse, *Acoustic non-linearity for defect selective imaging*, Ultrasonics, Vol. 40, Issues 1-8, May 2002, p. 633-637.

[217] R. Hessert, J. Bamberg, W. Satzger and T. Taxer, *Ultrasonic impact treatment for surface hardening of the aero-engine material IN718*, Proceedings from the 10th International Conference on Shot Peening, Tokyo, Japan, 15-18 Sep., 2008.

[218] A. Baranzahi, *C-SAM®...How it works...*, ITN, Campus Norrköping, Linköping University, March 2004.

[219] D. Bates, G. Smith, D. Lu and J. Hewitt, *Rapid thermal non-destructive testing of aircraft components*, Vol. 31, Issue 3, 1 April 2000, p. 175-185.

[220] R. Ruzek, R. Lohonka and J. Jironc, *Ultrasonic C-Scan and shearography NDI techniques evaluation of impact defects identification*, NDT & E International, Vol. 39, Issue 2, March 2006, p. 132-142.

[221] A. Szewieczek, C. Heinze, W. Hillger, D. Schmidt and M. Sinapius, *Analysis Methods of Lamb Wave Propagation in Complex Structures*, 6th European Workshop on Structural Health Monitoring, Dresden, Germany, 6-9 July, 2012.

[222] R. Meza, C. J. Carrasco, R. A. Osegueda, G. James and N. Robinson, *Damage Detection in a DC-9 Fuselage using Laser Doppler Velocimetry*, Proceedings from 15th International Modal Analysis Conference, Orlando, Florida, United States, 3-6 February 1997.

[223] V. K. Sharma, *Laser Doppler Vibrometer for Efficient Structural Health Monitoring*, ProQuest LLC, PhD Dissertation, Georgia Institute of Technology, United States.

[224] P. F. Pai and L. G. Young, *Dynamics-based damage inspection of an aircraft wing panel*, Journal of Intelligent Material Systems and Structures, Vol. 15, Issue 11, 2004, p. 803-821.

[225] W. J. Staszewski, R. Bin Jenal, A. Klepka, M. Szwedo and T. Uhl, *A Review of Laser Doppler Vibrometry for Structural Health Monitoring Applications*, Key Engineering Materials, Vol. 518, 2012, p. 1-15.

[226] P. Sriram, S. Hanagud and J. I. Craig, *Scanning laser Doppler techniques for vibration testing*, Experimental Techniques, 1992, p. 21-26.

[227] A. B. Stanbridge and D.J. Ewins, *Modal testing using a scanning laser Doppler vibrometer*, Mechanical Systems and Signal Process, Vol. 13, Issue 2, 1999, p. 255-270.

[228] B. Sarens, B. Verstraeten, C. Glorieux, G. Kalogiannakis and D. Van Hemelrijck, *Investigation of Contact Acoustic Nonlinearity in Delaminations by Shearographic Imaging, Laser Doppler Vibrometric Scanning and Finite Difference modelling*, IEEE Transactions on Ultrasonics, Ferroelectrics, and Frequency Control, Vol. 57, Issue 6, June 2010.

[229] R. Longo, S. Vanlanduit, J. Vanherzeele and P. Guillaume, *A method for crack sizing using Laser Doppler Vibrometer measurements of Surface Acoustic Waves*, Ultrasonics, Vol. 50, Issue 1, January 2010, p. 76-80.

[230] H. Pfeiffer, M. Bock, I. Pitropakis, A. Szewieczek, W. Hillger, C. Glorieux and M. Wevers, *Identification of impact damage in sandwich composites by acoustic camera detection of leaky Lamb wave mode conversion*, www.ndt.net, April 2013.

[231] P. Sriram, J. I. Craig and S. Hanagud, *A scanning laser vibrometer for modal testing,* International Journal of Analytical and Experimental Modal Analysis (ISSN 0886-9367), vol. 5, July 1990, p. 155-167.

[232] G. M. Sessler and J. E. West, *Electret Transducers: a review*, Journal of Acoustic Society of America, Vol. 53, Issue 6, 1973, p. 1589-1600.

[233] G. K. Miller, *Flexible Electret Transducer*, Journal of the Acoustic Society of America, Vol. 60, Issue 47, 1976.

[234] A. Mast, *An experimental microphone antenna array for measuring aircraft noise*, Master Thesis, Department of Applied Physics, TU Delft, The Netherlands, March 2001.

[235] W. M. Humphreys Jr., D. P. Lockard and M. R. Khorrami, *Airframe noise flight test measurements using an electret condenser microphone array*, Journal of the Acoustic Society of America, Vol. 127, Issue 3, 2010, p. 2009.

[236] G. G. Podboy and C. Horvath, *Phased Array Noise Source Localization Measurements Made on a Williams International FJ44 Engine*, NASA Technical Report, Proceedings from the 15th Aeroacoustics Conference, 11-13 May 2009, Miami, Florida, United States, March 2010.

[237] G.M. Sessler, *Acoustics Sensors*, Sensors and Actuators A: Physical, Volume 26, Issues 1-3, March 1991, p. 323-330.

[238] V. Giurgiutiu and J.J. Bao, *Embedded-ultrasonics Structural Radar for In Situ Structural Health Monitoring of Thin-wall Structures*, Structural Health Monitoring 3, (2004) 121-144.

[239] J. Peña, C.P. Melguizo, R. Martínez-Oña, Y. Gómez Ullate, F. Montero de Espinosa Freijo and G. Kawiecki. Proceedings of the 3rd European Workshop on Structural Health Monitoring, Granada 2006.

Short Curriculum Vitae

Personal information

Full name: Ioannis Pitropakis
Date of birth: March 6th, 1982
Place of birth: Athens, Greece
Nationality: Hellenic (Greek)

Education

2009-2015 **University of Leuven (KU Leuven), Belgium**
Doctor of Engineering Sciences (PhD), Materials Engineering

2013-2014 **University of Pisa, Italy**
Master of Business Administration (MBA)

2006-2007 **University of Stuttgart, Germany**
Master Thesis (MEng) - (2007 Best Project Award from IMechE)

2004-2007 **University of Glasgow, United Kingdom**
Master of Engineering (MEng) in Mechanical Engineering
(5 years full time degree, direct entry in 3rd year)

2000-2004 **Piraeus University of Applied Sciences (TEI of Piraeus), Greece**
Bachelor of Engineering (BEng) in Mechanical Engineering
(4 years full time degree)

Work experience

2015-Present **RECARO Aircraft Seating GmbH & Co. KG, Germany**
Crash Test Engineer
Delethalization and Dynamic Testing on RECARO aircraft seats

2014-2015 **TURBOMED SA, Greece**
Sales Engineer
Turbochargers of large marine vessels (Tankers, Ferries, etc.)

2009-2013 **KU Leuven, Belgium**
Research Engineer
European Commission's FP7 Project "AISHA II"

2008-2009 **Alpha Grissin SA, Greece**
Sales engineer
High Precision Air-Conditioning (HPAC) for large data rooms

2007-2008 **Compulsory Military Training, Greece**
Amphibious Commando (Special Forces)
Battle Vehicle Gunner (Heavy Artillery Unit)
Training locations: Megalo Pefko, Sparta, Chios Island

Publications

Published articles in peer reviewed international journals

1) "Crack detection in aluminium plates for aerospace applications by electromagnetic impedance spectroscopy using flat coil sensors", I. Pitropakis, H. Pfeiffer, M. Wevers, at Sensors & Actuators A: Physical, Vol. 176, April 2012, p. 57-63.

2) "Liquid detection in confined aircraft structures based on lyotropic percolation thresholds", H. Pfeiffer, P. Heer, I. Pitropakis, G. Pyka, G. Kerckhofs, M. Patitsa, M. Wevers, at Sensors & Actuators B: Chemical, Vol. 161, Issue 1, January 2012, p. 791-798.

3) "Leakage monitoring using percolation sensors for revealing structural damage in engineering structures", H. Pfeiffer, P. Heer, M. Winkelmans, W.Taza, I. Pitropakis, M. Wevers, Structural Control and Health Monitoring (International Journal), December 2013.

Published articles in the online journal of Non-Destructive Testing and NDT Database (www.ndt.net)

4) "Impact damage detection in composite materials of aircrafts by optical fibre sensors", I. Pitropakis, H. Pfeiffer, M. Wevers, 10th European Conference for Non-Destructive Testing (ECNDT 2010), Moscow, Russia, 7-11 June 2010.

5) "The use of pseudo-defects in validation of ultrasonic structural-health-monitoring technologies", H. Pfeiffer, I. Pitropakis, M. Wevers, 10th European Conference for Non-Destructive Testing (ECNDT 2010), Moscow, Russia, 7-11 June 2010.

6) "Crack detection in aluminium 2024-T3 plates and in Airbus A320 slat-track using electrical crack gauges", I. Pitropakis, H. Pfeiffer, T. Gesang, S. Janssens, M. Wevers, 18th World Conference for Non-Destructive Testing (WCNDT 2012), Durban, South Africa, 16-20 April 2012.

7) "Identification of impact damage in sandwich composites by acoustic camera detection of leaky Lamb wave mode conversions", H. Pfeiffer, M. Böck, I. Pitropakis, W. Hillger, A. Szewieczek, C. Glorieux, M. Wevers, April 2013.

Other published papers from proceedings of international conferences and workshops

8) "The use of a polarimetric fibre sensor to detect impact damage in aircraft composites", I. Pitropakis, H. Pfeiffer , M. Wevers, ISBN 978-0-415-62131-1, 5th International conference on Emerging Technologies in Non-Destructive Testing (ETNDT), Ioannina, Greece, 19-21 September 2011.

9) "The use of flat coil sensors and impedance spectroscopy for fatigue crack monitoring of Al 2024-T3 plates", I. Pitropakis, H. Pfeiffer , M. Wevers, ISBN 978-0-415-62131-1, 5th International conference on Emerging Technologies in Non-Destructive Testing (ETNDT), Ioannina, Greece, 19-21 September 2011.

10) "Structural Health Monitoring in an operational airliner: results on the implementation of percolation sensors achieved within the European Project: Aircraft Integrated Structural Health Assessment II (AISHAII)", H. Pfeiffer , M. Patitsa, I. Pitropakis, M. Wevers, ISBN 978-0-415-62131-1, 5th International conference on Emerging Technologies in Non-Destructive Testing (ETNDT), Ioannina, Greece, 19-21 September 2011.

11) "Leakage detection in aircraft by percolation sensors for the prevention of floor beam corrosion and detection of pinhole cracks in hydraulic tubes", H. Pfeiffer, I. Pitropakis, M. Patitsa, M. Wevers, 6th International Conference "Supply on the wings", Frankfurt/M, Germany, 2-4 November 2011.

12) "Structural health monitoring in an operational airliner: an intermediate report on leakage monitoring with percolation sensors", H. Pfeiffer, P. Heer, H. Sekler, M. Patitsa, I. Pitropakis, M. Wevers, 6th European Workshop on Structural Health Monitoring, Dresden Germany, 6-12 July 2012.

13) "Fuse-like devices replacing linear sensors – working examples of percolation sensors in operational airliners and chemical installations", H. Pfeiffer, I. Pitropakis, M. Wevers, H. Sekler, M. Schoonacker, 6th International conference on Emerging Technologies in Non-Destructive Testing (ETNDT 2015), Brussels, Belgium, 27-29 May 2015.

Presentations

Presentations at AISHA II international meetings

1) "Eddy current sensor", AISHAI II meeting in Fraunhofer Institute for Manufacturing Technology and Advanced Materials (IFAM), Bremen, Germany, 17-18 September 2009.
2) "Pseudo defects", AISHA II meeting in Fraunhofer Institute for Manufacturing Technology and Advanced Materials (IFAM), Bremen, Germany, 17-18 September 2009.
3) "Damage detection with optical fibres in EC 135 Tailboom", AISHA II meeting in AIRBUS HELICOPTERS (ex. EUROCOPTER), Marignane, France, 27-28 January 2010.
4) "Eddy current sensors in a realistic fatigue experiment", AISHA II meeting in AIRBUS HELICOPTERS (ex. EUROCOPTER), Marignane, France, 27-28 January 2010.
5) "Extended crack propagation gauges - progress achieved by fatigue measurements", AISHA II meeting in AIRBUS HELICOPTERS (ex. EUROCOPTER), Marignane, France, 27-28 January 2010.
6) "Damage detection in EC 135 Helicopter Tailboom", AISHA II meeting in MEGGIT SA, Helsingor, Denmark, 31 May - 1 June 2010.
7) "Fatigue crack detection using implemented crack wires", AISHA II meeting in Aeronautical Technologies Centre (CTA), Vitoria, Spain, 18-19 October 2010.
8) "Imaging of defects using air-coupled Lamb wave detectors", AISHA II meeting in LUFTHANSA TECHNIK, Frankfurt, Germany, 26-27 January 2011.
9) "Fatigue crack determination using painted crack gauges in aluminium sheets", AISHA II meeting in KU LEUVEN, Leuven, Belgium, 27 October 2011.

Presentation at KU Leuven MRC meeting

1) "Dedicated Solutions for Structural Health Monitoring of Aircraft Components", Annual Materials Research Centre (MRC) Meeting, KU Leuven, Leuven, Belgium, 26 February 2015.

Posters and Training

Posters on aircraft SHM

1) "Structural Health Monitoring", I. Pitropakis, H. Pfeiffer, N. Chatziathanasiou, M. Wevers, Participant at the exhibition at the Flemish Aerospace Days, Brabanthal, Leuven, Belgium, 8-10 May 2009.
2) "Structural Health Monitoring based on Optical and Piezoelectric Sensors", I. Pitropakis, H. Pfeiffer, M. Wevers, Open Day KU Leuven, MTM, KU Leuven, Belgium, 1 May, 2010.

Training courses and certificates at KU Leuven

1) "Exploitation of Research – Technology & Knowledge Transfer", Doctoral School Skills Training Course Certificate, KU Leuven Research & Development, Belgium, 2011-2012.
2) "Doctoral Seminars in Materials Engineering", Doctoral School Thematic Research Training Course Certificate, KU Leuven, Department MTM, Belgium, 2011-2012.

"It is not important what happens to you but how you react to it that matters."

Epictetus (55 – 135 A.D.)